University of Sussex

A University of Sussex PhD thesis

Available online via Sussex Research Online:

http://sro.sussex.ac.uk/

Spirooxindoles Derivatives as Novel Inhibitors of the Respiratory Syncytial Virus

UNIVERSITY OF SUSSEX

Michael Paradowski

Supervisor: Prof. Simon E. Ward

This thesis is submitted to the University of Sussex for the degree of Doctor of Philosophy, August 2017

Declaration

This thesis is submitted to the University of Sussex for my application of the degree of Doctor of Philosophy. All research described in this thesis is original material and has not been previously submitted in any other application for any other degree at the University of Sussex or any other institutions.

The work presented in this thesis is the result of my own investigations:

- All the medicinal chemistry ideas have been designed by me from the mining of the scientific literature.
- All the compounds described in this thesis have been prepared by me and the synthetic methodologies are of my own design or adapted from the scientific literature where appropriately cited.

except for the cases outlined below:

- The 2-chloromethyl benzimidazole intermediates **48** and **75** were either prepared within the Sussex Drug Discovery Centre or purchased from commercial sources.

The biological data reported in Chapter 2, 3 and 4 were obtained from the following sources:

- The primary biological RSV Fusion assay was carried out within the Sussex Drug Discovery Centre at the University of Sussex. The data were generated by Mr Gareth Williams and Mr Marcus Hanley.
- The RSV plaque reduction assay and clinical isolates screening were conducted at the University of Queensland, Australia, within the laboratory of Professor Paul Young.
- The *in vitro* DMPK studies were performed at Cyprotex.
- The *in vivo* pharmacokinetic studies in pre-clinical species were conducted at Pharmidex.

Other sources are acknowledged and given explicit references in the appended bibliography.

Michael Paradowski

Acknowledgements

I would like to thank Prof. Simon Ward and Prof. John Atack for giving me the opportunity to do a PhD in their group. Their support, guidance and suggestions over the last few years has been invaluable and greatly appreciated.

I would also like to thank Dr Paul Beswick, Dr Alessandro Mazzacani, Dr Marco Derudas and Dr Lewis Pennicott for all their help in proof reading this thesis and I am grateful for their suggestions.

I would like to thank the members of the RSV team. Dr Irina Chuckowree, Dr Carol Villalonga, Dr Sandra Luengo-Arratta, Mr Graham Lunn and Mr Jose Gascon for providing some useful discussions, synthetic intermediates and who helped me in accomplishing this work. Mr Gareth Williams and Mr Marcus Hanley for the biological evaluation of all the compounds in the RSV fusion assay.

I would like to express my gratitude to Dr Alaa Abdul-Sada for his help in collecting the mass spectrometry data and Dr Iain Day for his help and advice collecting and analysing NMR spectra.

A special thank you to Mr Alex Burns for his continual help with technical services and without who the chemistry labs would not be functioning and this work would not have been accomplished.

Abstract

Respiratory Syncytial Virus (RSV) is an important pathogen that affects the lower respiratory track resulting in hospitalisation in infants and young children and is a significant cause of morbidity and mortality in the elderly and immunocompromised patients. The RSV F protein plays a crucial role in the life cycle of the virus and its entry into the host cells. Once the fusion has been initiated, it causes a series of conformational changes facilitating the fusion of the virus with the host's cellular membranes which eventually leads to releasing viral RNA strands into the host cells. Disruption of the viral envelop and in particular of the RSV F protein by small molecules has been shown to be efficacious in the treatment of RSV infection in rodent models. Small molecule inhibitors of the RSV fusion protein have been reported over the last 15 years and several compounds have progressed into early clinical development but none have reached the market.

RV-39 had previously been reported as a RSV fusion inhibitor, exhibiting excellent *in vitro* antiviral activity in both the fusion and plaque reduction assays. Although **RV-39** showed good stability in rat liver microsomes, the compound showed high clearance in human liver microsomes. Furthermore, **RV-39** showed high plasma clearance and low bioavailability when progressed to a rat pharmacokinetic study.
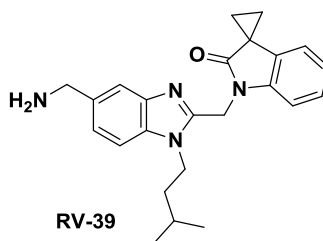
RV-39

In this work, a series of novel 3,3'-spirocyclic oxindoles and aza-oxindoles were designed and synthesised as potential RSV fusion inhibitors, aiming to improve on human liver microsomes and on the pharmacokinetic profile of **RV-39** in rat. Novel chemistry was established to synthesise the spirocyclic oxindoles and aza-oxindoles *via* a palladium catalysed α-arylation of 2-bromo anilides as the key synthetic step. The scope of the reaction was explored, demonstrating that access to spirocyclic oxindoles could be obtained in good to excellent yield from readily available carboxylic acids and 2-bromo anilines. Conditions for the removal of the *para*-methoxybenzyl protecting group were optimised to enable the preparation of a series of analogues with potent antiviral activity against the RSV virus.

The novel compounds prepared demonstrated excellent antiviral potency in both the fusion and the plaque reduction cellular assays and also showed improved metabolic stability in human liver microsomes compared to **RV-39**. A selection of compounds was further profiled in *in vivo* rat pharmacokinetic studies and the preliminary results suggested that whilst the plasma clearance remained high, good half-life and significant improvement in bioavailability compared to **RV-39** could be achieved across this novel series of compounds.

Table of Contents

Abbreviations

Ac	Acetyl
Ad	Adamantyl
ADME	Absorption, distribution, metabolism, excretion
APCI	Atmospheric-pressure chemical ionisation
ATP	Adenosine triphosphate
BCRP	Breast cancer resistance protein
Boc	*tert*-Butyloxycarbonyl
CAN	Ceric (IV) ammonium nitrate
CDI	Carbonyldiimidazole
Cl	Clearance
Cl_p	Clearance in plasma
Cl_{int}	Intrinsic clearance
COPD	Chronic obstructive pulmonary disease
Cy	Cyclohexyl
CYP	Cytochrome P450
DDQ	2,3-Dichloro-5,6-dicyano-1,4-benzoquinone
DMA	Dimethylacetamide
DMAP	4-(Dimethylamino)pyridine
DME	1,2-Dimethoxyethane
DMF	*N,N*-Dimethylformamide
DMSO	Dimethylsulfoxide
DNA	Deoxyribonucleic acid
DTT	Dithiothreitol
EDCI	*N*-(3-Dimethylaminopropyl)-*N'*-ethylcarbodiimide
EDTA	Ethylenediaminetetraacetic acid
ER	Efflux ratio in the MDCK permeability assay
ESI	Electrospray ionisation
Et	Ethyl
F	Oral bioavailability
FBS	Foetal bovine serum
FG	Functional group

GTP	Guanosine triphosphate
HATU	1-[*bis*(Dimethylamino)methylene]-1*H*-1,2,3-triazolo[4,5-*b*]pyridinium 3-oxide hexafluorophosphate
HBA	Hydrogen bond acceptor
HBD	Hydrogen bond donor
HBTU	*N,N,N',N'*-Tetramethyl-O-(1*H*-benzotriazol-1-yl)uronium hexafluorophosphate
hERG	Human ether-a-go-go-related gene
HLM	Human liver microsomes
HMDS	Hexamethyldisilazane
HPLC	High performance liquid chromatography
HRMS	High resolution mass spectrum
IC_{50}	Concentration for inhibition of 50% of the maximal response
^{i}Pr	*iso*-Propyl
iv	Intravenous
LCMS	Liquid chromatography-mass spectrometry
LDA	Lithium diisopropylamide
LiHMDS	Lithium *bis*(trimethylsilyl)amide
LiPE	Lipophilic ligand efficiency
MDCK	Madin Darby canine kidney cell line
Me	Methyl
MLM	Mouse liver microsomes
mol equiv.	Molar equivalent
MS	Mass spectrum
MW	Microwave irradiation
Mwt	Molecular weight
m/z	Mass charge ratio
*n*Bu	n-Butyl
NOESY	Nuclear Overhauser effect spectroscopy
NMP	*N*-Methyl-2-pyrrolidone
NAATs	Nucleic acid amplification tests
*P*app	Apparent permeability rate in MDCK cell assay
PBS	Phosphate Buffered Saline
PFU	Plaque forming unit

PCR	Polymerase chain reaction
PEPPSI	Pyridine-enhanced pre-catalyst preparation stabilization and initiation
Ph	Phenyl
PG	Protecting group
P-gp	P-glycoprotein
PK	Pharmacokinetics
PMB	*para*-Methoxybenzyl
po	*per os* (by mouth), Oral dosing
PPB	Plasma protein binding
ppm	Parts per million
PRA	Plaque reduction assay
RNA	Ribonucleic acid
RSV	Respiratory syncytial virus
RT-PCR	Reverse transcriptase polymerase chain reaction
rt	Room temperature
SAR	Structure-activity relationship
ss	Single strand
SF	Serum free
$T_{1/2}$	Half-life
T_3P	Propylphosphonic anhydride
TBTU	2-(1*H*-Benzotriazole-1-yl)-1,1,3,3-tetramethylaminium tetrafluoroborate
^{t}Bu	*tert*-Butyl
Tf	Trifluoromethanesulfonic (triflic)
TFA	Trifluoroacetic acid
THP	Tetrahydropyran
tPSA	Topological polar surface area
V_d	Volume of distribution
WHO	World Health Organisation

Chapter 1. Fusion Inhibitors for the Treatment of RSV Infections

1.1 Introduction

Respiratory Syncytial Virus (RSV) is the leading cause of acute lower respiratory tract infection in infants, young children and other high-risk populations.[1] The virus was first reported in 1956 in chimpanzees with upper tract respiratory illnesses and later isolated from infants with acute lower respiratory tract diseases.[2,3] RSV is a negative single stranded RNA virus from the *paramyxoviridae* virus family of the order mononegavirales which also includes mumps, measles and parainfluenza viruses (Figure 1.1).[4]
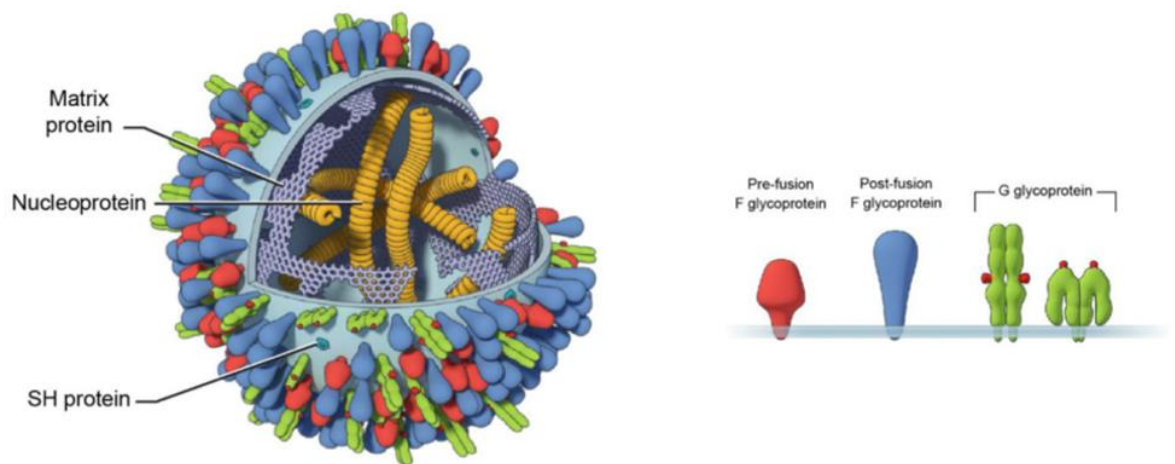
Figure 1.1. Respiratory Syncytial Virus Structure. Reproduced from McLellan *et al.*[5]

Initially considered to be exclusively an airborne paediatric pathogen, RSV is highly contagious and spreads through the respiratory tract, affecting all ages of the population. The virus ranges from mild upper respiratory tract illness in healthy adults to severe and potentially life-threatening infections of the lower respiratory tract in infants, the elderly and patients with an impaired immune system.[6,7] The virus is still recognised as an important cause of morbidity and mortality in these high risk target populations and still remains a major cause of death.[8–10] In infants, the virus remains the most important pathogen causing lower respiratory tract infections.[11–13]

1.2 Disease Burden and Patient Population

Estimates of the total burden of RSV-related respiratory infections across the population vary greatly across studies due in part to the lack of cases reported or incorrect diagnosis of RSV-related illnesses that may appear for example as benign chest colds in healthy adults. Furthermore, routine screening of viral infections in hospital settings are not recommended in developed countries as these are deemed to have no influence on the case management of the disease, meaning that the burden of RSV-related respiratory infections remains difficult to quantify.[14] A summary of a selection of various recent studies is reported below, estimating the impact of RSV-related infections in the high-risk groups.

1.2.1   RSV in Infants and Children

Reports from Nair *et al.* estimate that in 2005 there were 33.8 million new episodes globally of RSV-related acute lower respiratory infections in children younger than 5-year-old and at least 3.4 million of severe lower respiratory infections associated with RSV infection requiring hospitalisation.[1] In the United States alone, RSV-related hospitalisations account for up to 125,000 hospitalisations annually in infants and children.[6] In their research, Nair *et al*. estimated between 66,000 and 199,000 deaths worldwide were related to RSV-related illnesses for children under the age of 5 years, mostly in developing countries. The variability of those data is partly due to the lack of diagnosis and understanding of the diseases in the developing world. Overall, up to 99% of RSV-related deaths in childhood are estimated to be in those developing countries with children up to the age of five vulnerable to RSV-related illnesses. More recent studies from Taylor *et al*. suggest that in the United Kingdom alone, between the period of 1996 and 2009, the burden of GP visits, hospitalisation and death attributed to RSV-related events in children exceeded that of influenza.[15]

It is estimated that RSV-related lower respiratory tract illnesses affect more than 20% of infants in the first year of their life and that up to 2% require hospitalisation.[16,17] Re-infection is a common occurrence; between 30% and 75% of children younger than 2 years of age who had previously been infected by the virus in their infancy (first 15 months of their life) are likely to suffer a second infection of the virus, and most children will have been infected by RSV by the time they are 2 years old.[16] It is believed that most children under the age of 2 years will have contracted at least one RSV infection and a large number will be re-infected often during the same season.[16] Additionally, infants that have been infected by the virus are more likely to be

prone to recurrent wheezing and the development of asthma later in childhood.[18] However, early prevention during infancy may reduce the frequency of post-viral wheezing later in life.[19,20]

1.2.2   RSV in Adults, Elderly and Immunocompromised Patients

In the adult population, RSV is estimated to be second only to the influenza virus and is responsible for serious respiratory tract illnesses causing 14,000 annual deaths in the elderly population in the United States alone. [21] The severity of the infection is age related, owing to a gradual alteration of the immune response with aging and combination of comorbid conditions, explaining in part why the elderly are at a higher risk of RSV-related respiratory disease.[22] A 10 year study by Thompson *et al.* showed that RSV infections were responsible for 175,000 hospitalisations and 11,000 respiratory and circulatory deaths occurring annually among persons aged 65 years or older in the United States.[8] In adults and the elderly with chronic lung or heart disease, RSV-related infections are responsible for 10% of hospitalisations for pneumonia and COPD and 5% of hospitalisation for asthma and congestive heart failure.[21]

However, age alone is not the only determining factor; immunocompromised patients such as those undergoing chemotherapy or organ transplants are at high risk of RSV infections. In the immunocompromised patients, RSV causes between 30% and 50% of life threatening respiratory infections in leukaemia, bone marrow transplant and solid organ transplant.[21] Of all viral infections, RSV has the highest incidence of progression to pneumonia mortality in transplant patients[23] These statistics are supported by Bowden *et al*. where in one study 49% of transplant patients contracted pneumonia following RSV infection.[24]

1.3 Clinical Manifestation and Epidemiology

Although RSV is not readily differentiated from influenza A and other viral infections based on symptoms alone, the initial diagnosis of infections is still based on the presentation of typical respiratory symptoms.[25,26] Chest X-ray and epidemiological studies are used to support the diagnosis in cases of viral uncertainty.[27] However, Nucleic Acid Amplification Tests (NAATs) and rapid antigen detection (direct immunofluorescence and enzyme immunoassays) tests are now available, replacing the viral culture systems usually taking 3 to 5 days which were used as reference standards for many years. In particular, commercially available NAATs detection methods such as Reverse Transcriptase Polymerase Chain Reaction (RT-PCR) and real-time PCR are the new reference standard offering highly sensitive measurements of the viral load in RSV-infected patients. The viral load quantification by real-time PCR remains the biomarker of choice for monitoring the severity and progression of the infection.[28–31] However, since there are no treatments for the virus, RSV testing is not performed routinely in the adult and the elderly population in outpatient settings due mainly to cost and screening availability. Infection treatments in those population often remains supportive.[31,32]

Immune protection against RSV is limited in time and symptomatic recurrence of re-infection is common throughout an individual's life. Previous infections do not protect from re-infection.[33] This re-infection is in part due to the presence of homologous strains which have been shown to co-exist and circulate in any given regions and seasons that can re-infect persons of all ages. [16,34] Although the virus is able to evade innate immunity and adaptive immune responses, most RSV re-infections, generally symptomatic and limited to the upper respiratory tract, have been linked to a decreased risk of re-infection over the lifetime of individuals.[35,36]

RSV infections across populations also vary with the seasons and often coincide with the flu epidemics.[16,37–39] In Northern America and Europe, epidemic outbreaks occur during the winter season, whilst in tropical countries, RSV outbreaks are linked to the rainy seasons and can have multiple recurrences during the year.[40–42]

Although highly contagious, the clinical manifestation of RSV infection depends on the age of the patients and their health situation. In healthy children and adults, a RSV infection is self-limiting and usually responds to supportive care without any health issues.[27] Upper respiratory tract events commonly precede those in the lower respiratory tract by a few days.
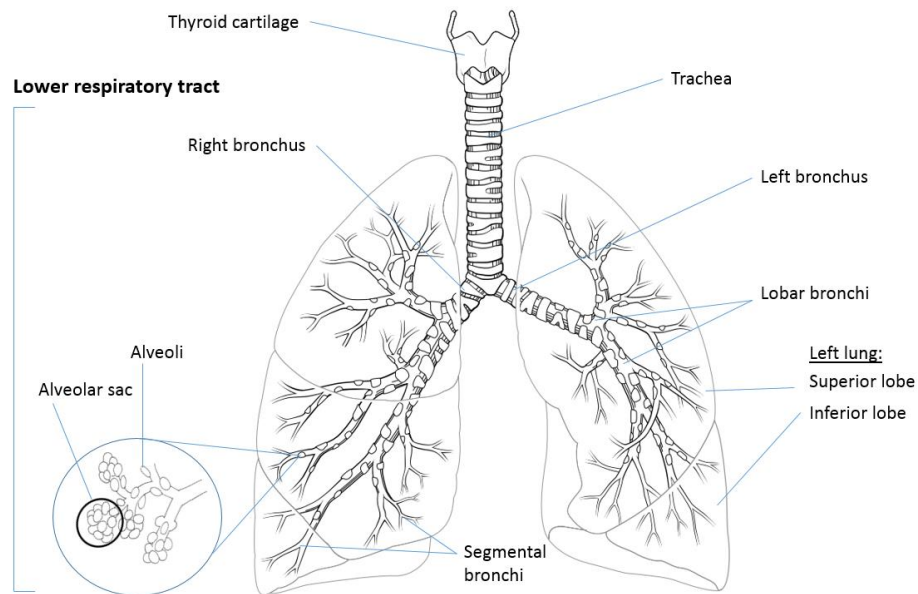
Figure 1.2. Schematic of the lower respiratory tract. Adapted from Medscape, anatomical line drawings.[43]

In infants and young children, RSV infection most commonly manifests itself by acute lower respiratory tract infections such as obstructive small airway disease (bronchiolitis) and restrictive pattern (pneumonia), often accompanied by fevers, wheezing, hyperinflation and atelectasis, a collapse of the lungs in the absence of gas exchange (Figure 1.2).[14,27] In the early stages, the virus will only infect ciliated epithelial cells of the small bronchioles and alveolar epithelium.[44] The subsequent immune response results in an increased shedding of the infected epithelium and an accumulation of epithelial cell debris mixed with inflammatory fibrins, mucus and oedema in the narrow lumens of the bronchiolar airways leading to pulmonary obstructions. Such contributing factors partially explain the increased outcome and pre-disposition of infants, who have reduced respiratory airways, to more frequent and severe acute inflammation of the small bronchiolar airways.[45] According to Pickles *et al.*, the accumulation of mucus and epithelial debris due to narrow airway in infants, combined with a loss of mechanical clearing of the airway contributes to an increase of both of the inflammation and of the disease symptoms.

In the older adult population, RSV infection manifests itself as bronchitis, pneumonia as well as exacerbation of chronic obstructive lung disease (COPD) and can lead to acute deterioration for those with cardiac disease and congestive heart failure. The pathogenesis of the disease has been well described for infants but remains less well known in the adult population, often wrongly diagnosed, owing to the milder symptoms, and occasionally asymptomatic, of the viral infection.

1.4 Prevention and Current Treatments

The management of RSV-related lower respiratory tract infections requiring hospitalisation is primarily through supportive care such as oxygen supplement, antipyretics, intravenous fluids and nasal suctions.[32] Bronchodilators and corticosteroids are also used for COPD patients and those with pre-existing respiratory conditions but the impact of such treatments on the course of the viral infection and evidence of their meaningful effects are lacking.[46]

The only recommended drug indicated for the prevention of lower respiratory tract infections caused by RSV is palivizumab (Synagis), a humanised monoclonal antibody targeting the antigenic site II of the RSV fusion protein that mediates the entry of the virus into the host cells. Used prophylactically from the start of the seasonal viral prevalence, palivizumab has been shown to be safe and effective for the prevention of RSV-related illnesses.[47] It is however only recommended for paediatric patients at the greatest risk of infections such as children younger than 2 years with chronic lung diseases or heart diseases and for the first year of life for prematurely born infants.[48] According to the IMpactRSV study group, palivizumab administered prophylactically reduced the rate of RSV hospitalisation by 55%.[49] Other studies have confirmed similar efficacy following prophylactic treatment prior to the viral infective season.[50–52] Unfortunately, due to its high cost, multiple studies have shown that palivizumab is only cost effective in a restricted paediatric patient population.[53–55] The cost of immunoprophylaxis with the drug is far greater than the economic benefit of preventing hospitalisation following on RSV infections.

RSV-IVIG (RespiGam) is an immune globulin indicated as a prophylactic treatment for the prevention of RSV in infants less than 24 months or prematurely born. It was developed as a natural immune response from pooled human plasma with a high concentration of antibodies. RSV-IVIG was shown to reduce RSV-associated hospitalisation by over 40% but lacked efficacy in infants with congenital heart disease or bronchopulmonary dysplasia.[56,57] However the lack of cost effectiveness, efficacy and monthly injection regimen led to its withdrawal and replacement by palivizumab.[58]

Ribavirin is a broad-spectrum nucleoside antiviral drug against both RNA and DNA viruses. Although the mechanism of action of Ribavirin is still not clear, it is believed to act by mutagenic incorporation into the RNA viral genome, competing with ATP and GTP for viral RNA-dependent

RNA polymerase, the main enzymatic complex in viral replication and transcription.[59,60] Ribavirin has been approved since 1986 in the US and administered as an aerosol to infants and children with severe bronchiolitis.[14] Financial and safety concerns have overshadowed the potential benefits of the drug and multiple clinical trials have led to conflicting results proving inconclusive in confirming the effectiveness of Ribavirin on the course of RSV infections.[61] The drug is currently not recommended for routine use in case of bronchiolitis by the American Academy of Pediatrics (AAP) guidelines.[56]

1.5 RSV Molecular Virology

RSV is an enveloped negative-sense single-stranded non-segmented RNA virus ((-)ssRNA) of approximately 15,000 nucleotides from the *Pneumovirus* genus, *Pneumovirinae* subfamily of the *paramyxoviridae* family and mononegavirales order. The virus requires attachment and fusion of its membrane to the host cells to deliver its genome and initiate viral replication.[62] The virus is a single serotype classified in two distinct antigenic groups A and B, whereby the genotyping was established based on the variation in reactivity against a panel of monoclonal antibodies of the heterogeneous attachment glycoprotein (G).[63] The main differences among the antigenic groups were found on the attachment glycoprotein G and believed to have evolved separately over time.[64] Both groups co-exist and co-circulate at any one time during the infectious seasons. RSV subtype A has been associated with more severe infections across all types of the population.[65,66] The different clinical and epidemiologic characteristics of these subtypes are supported by *in vitro* studies that have shown that subgroup A isolates induced an increased activation of the NF-κB complex, responsible for the release of pro-inflammatory receptors.[67]

In contrast to most other members of the *paramyxovirinae* family that typically have 6-7 mRNA encoding for 7-9 different proteins, RSV is a more complex virus.[68] The RSV genome consists of 10 genes which encode for 11 proteins.[68–71] This includes five structural proteins, the large (L) protein, nucleoprotein (N), phosphoprotein (P), matrix (M and M2) and two non-structural proteins (NS1 and NS2) (Figure 1.3). The viral envelope consists of three transmembrane proteins, the glycoprotein (G), fusion (F) glycoprotein and small hydrophobic (SH) protein.
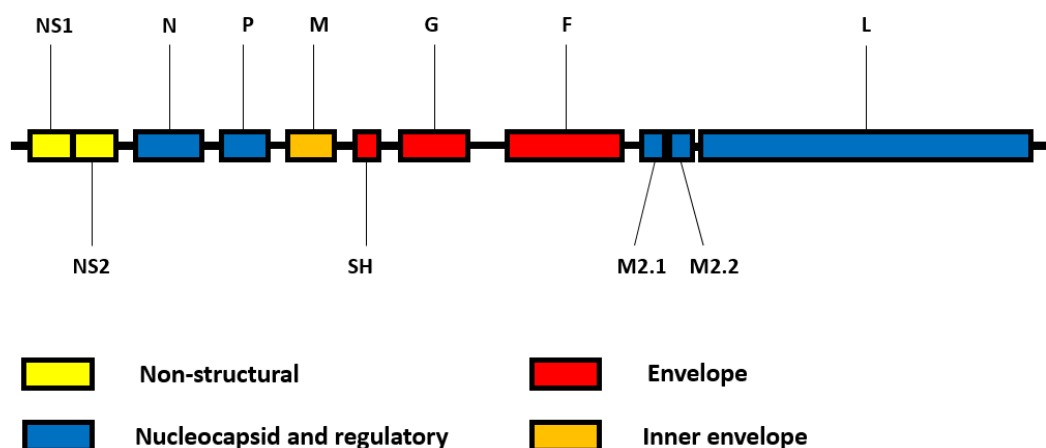

Figure 1.3. Schematic of the human RSV Genome. 10 genes encoding for 11 proteins.

RSV infection is initiated when a virion interacts with a cellular receptor on the surface of ciliated epithelial cells *via* the attachment (G) protein and the fusion (F) protein, fusing its envelope with the host (Figure 1.4).[35,72,73] This fusion process mediates the release of the nucleocapsids consisting of the nucleoprotein (N), that encapsidates the genomic RNA in the cytoplasm, along with the RNA-dependent polymerase complex consisting of the large (L) polymerase protein, cofactor (P) phosphoprotein and transcription factor (M2-1).[17,74,75] Once the viral nucleocapsid has entered the cell cytoplasm, the RNA-dependent RNA polymerase complex transcribes the viral mRNA in a stop-start type mechanism to synthesise the viral proteins (Figure 1.4. The RNA-dependent RNA polymerase is also responsible for the replication of the genome to generate a positive-sense RNA intermediate (the antigenome) (Figure 1.4, b). This antigenome serves in turn as a template for further synthesis of negative single-stranded progeny genomes for further introduction in new virions. The newly formed genomes are encapsidated by the N protein as they are synthesised to create a RNase-resistant nucleocapsid. The viral assembly is a key step in the replication of the virus and all the viral structural proteins are associated in the plasma membrane with new nucleocapsids, forming new virions released by budding through the plasma membrane of the host cell. The process of replication of negative-sense single-stranded RNA viruses, and RSV in particular, has been extensively reviewed.[17,68,74–77]
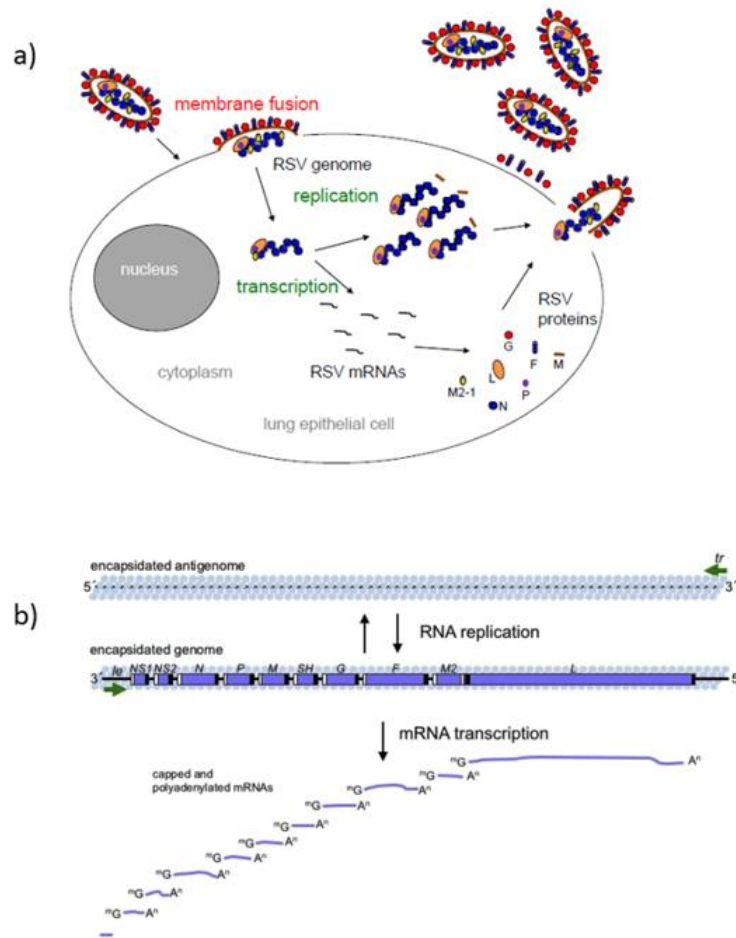
Figure 1.4. a) Schematic representation of the RSV replication cycle. b) Replication and transcription representation of –ssRNA into its proteins and antigenome. Adapted from Fearns *et al*.[78]

The large (L) protein is the main protein sub-unit of the viral RNA-dependant RNA polymerase complex which comprises four viral proteins (L, P, M2-1 and N). The protein is 2,165-amino acids long and contains the catalytic domains associated with the enzymatic reactions in transcription of mRNA, capping of mRNA and viral genome replication.[68,79] Similarly, the 241-amino acid phosphoprotein (P) is an homotetramer and an essential cofactor in the viral polymerase, believed to be responsible in part for transcription elongation activities.[80,81] Additionally, P has been shown to bind to N, L and M2-1. The binding with the nucleoprotein N, *via* its C-terminal region, is believed to prevent N from self-aggregation and binding to non-viral RNA.[82] The phosphoprotein (P) also plays a role in the dissociation of the matrix M from the nucleocapsid during the uncoating to initiate host's infection.[83] The transcription factor protein M2-1 is a zinc-binding anti-terminator binding to mRNA and essential for the efficient synthesis of full-length mRNA.[84,85] M2-1 is also believed to bind to the protein M and facilitate its interaction with the

nucleocapsid.[86] Deletion of the M2-1 protein results in the translation terminating non-specifically and in a reduced expression of the non-structural proteins NS1 and NS2.[87] Although not essential and expressed at low levels in the infected cells, the factor protein (M2-2) is believed to regulate the balance between transcription and RNA replication.[68] In *in vitro* cell culture studies, M2-2 knockout mutations reduced viral growth by 10,000 fold but increased gene replication.[88] The matrix (M) protein lines the inner viral envelope. Although little is known about the function of the RSV M protein, Meanger *et al.* have shown that the matrix has a double role of regulating the assembly of the virion by interacting with the nucleoprotein N, P and M2-1 proteins and the envelope proteins and of inhibiting the transcriptase activity of the nucleocapsid prior to encapsidation.[86] The two non-structural proteins NS1 and NS2 are non-essential proteins believed to play a role in modulating or evading the innate immune response of the host cells and pre-existing immune responses, including interferon induction and signaling.[89–91] Further studies suggest that NS1 and NS2 inhibit premature apoptosis during infection.[92,93]

The 298-amino acid glycoprotein (G) plays a major role in the attachment of the virus to the host cell membrane and facilitate the F-mediated membrane fusion. Although the receptors on the host cells have not been clearly identified, the RSV G protein has been shown to bind to annexin II, intercellular adhesion molecules (ICAM)-1, CXCR1 and CX3CR1 chemokine receptors, glycosaminoglycans, and TLR4 receptors.[94–99] Furthermore, the ectodomain of G is highly glycosylated with O-linked oligosaccharides and N-linked sugars, thought to reduce the virus' immunity recognition.[100] Surprisingly, this attachment G protein is not essential and the virus remains viable, albeit attenuated, after its deletion, suggesting that the F protein can bind independently as well as mediate the fusion to the host cells.[101,102] Similarly to the G protein, the 64-amino acid transmembrane small hydrophobic (SH) viral envelop protein is not essential. It has a pentameric pore-like structure with ion channel-like properties and its role in the viral replication and pathogenesis is not fully understood but is believed to alter the membrane permeability.[68,103] Collins *et al*. showed that RSV could grow more efficiently in cell lines where the SH protein had been deleted (RSVΔSH) than in the wild-type recombinant virus.[104] In mouse studies, when inoculated intranasally, RSVΔSH could replicate as well as wild-type virus in the lower respiratory tract but replication was restricted 10-fold in the upper respiratory tract. Similarly, studies by Karron *et al*. have demonstrated that the RSV cp- 52 mutant, missing most of the coding sequence for the small hydrophobic SH and attachment G proteins was still infectious and able to replicate in cell culture.[105] The RSV F protein is responsible for fusion of the viral envelop to the cellular host and syncytium formation (budding from cell to cell) and

shares general structural features with other viruses from the *Paramyxoviridae* family, suggesting a similar fusion mechanism. In contrast to those studies where SH and G proteins have been shown to be dispensable, at least in cell cultures and animal models, mutant RSV proteins with deletion of the F protein (hRSVΔF) are not able to infect cells on their own, suggesting the fusion is an essential mechanism for the viral entry to the host cells.[106,107] Although the F protein is the only membrane glycoprotein necessary for cell-cell fusion, the efficiency of the virus to replicate is attenuated when the attachment glycoprotein has been deleted.[105] The fusion protein has been found to bind to TLR-4 receptors, intercellular adhesion molecule (ICAM-1) expressed on the cell surface and nucleolin, a multifunctional phosphoprotein distributed mainly in the nucleus but also found in the cytoplasm and at the surface of atypical cells.[70,108] The later target has raised the possibility of drug repositioning from anti-cancer aptamer therapy as a novel approach.[30,109]

Every step in the replication of the virus is a potential target for novel antivirals and vaccines. Multiple approaches have been investigated and validated in preclinical studies as potential antiviral targets, including small-interfering RNA (siRNA) gene silencing and the nucleoprotein (N).[110–112] However, the RSV F protein and the RNA polymerase complex have been the targets of choice for many drug discovery programs inhibiting the entry of the virus or interfering with the replication and translation pathways respectively. Comprehensive reviews on the novel antiviral approaches targeting the RSV RNA polymerase have been reported by both Fearns and Simoes.[30,78]

The rest of this chapter will focus exclusively on the strategies and challenges to reduce the severity of the infection by blocking the fusion glycoprotein to the cellular host and will review the various small molecules that have been published in the literature since 2000.

1.6 RSV Fusion

The RSV F protein belongs to the class I of viral fusion proteins, which includes among others HIV, Ebola and influenza, due to their similarities in structure and function .[113] These fusion proteins all require an initial proteolytic cleavage from a metastable pre-fusion form, including, among others, a fusion peptide at or near the N-terminus and an α-helical coiled-coil structure post fusion.[114] The F protein is a transmembrane surface protein that is synthesised in an inactivated precursor form called F0 at the surface of the virus and comprises of 574 amino acids (Figure 1.5).
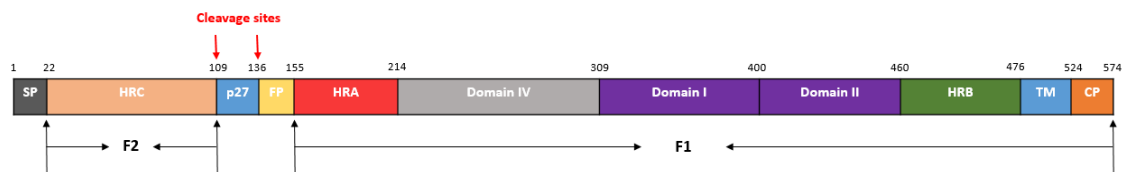

Figure 1.5. Schematic representation of the RSV F protein structure, denoting the signal peptide (SP), heptad-repeat C (HRC), 27-mer fragment (p27), putative fusion peptide (FP), heptad-repeat A (HRA), domain I, II and IV, heptad-repeat B (HRB), transmembrane (TM) and cytoplasm (CP). The proteolytic cleavages of the precursor F0 to generate the F1 and F2 subunits are represented by red arrows.

Similar to other viral membrane fusion, the F protein has no fusion activity unless the F0 protein precursor is cleaved into two F1 and F2 trimeric subunits, from the C- and N-terminus respectively, remaining covalently linked *via* disulphide bridges.[114–116] The F1 subunit consists of the heptad-repeat A (HRA), domains I, II and IV, the heptad-repeat B (HRB), a transmembrane domain (TM) and a cytoplasm protein (CP) whilst the F2 subunit only consists of the heptad-repeat C (HRC).[117,118]

In its pre-fusion form, the F0 protein folds to a metastable homotrimeric structure. The pre-fusion protein has a globular head containing the heptad-repeats HRA and HRC and is anchored to the viral transmembrane region through a trimeric HRB stalk (Figure 1.6a). Following triggering by binding to the receptor host cells in a pH-independent fashion, the F protein is activated into 2 subunits F1 and F2 by the cleavage of F0 at two polybasic sites by furin-like proteases, releasing the p27 peptide and initiating the fusion between the viral and cell membranes.[119,120]
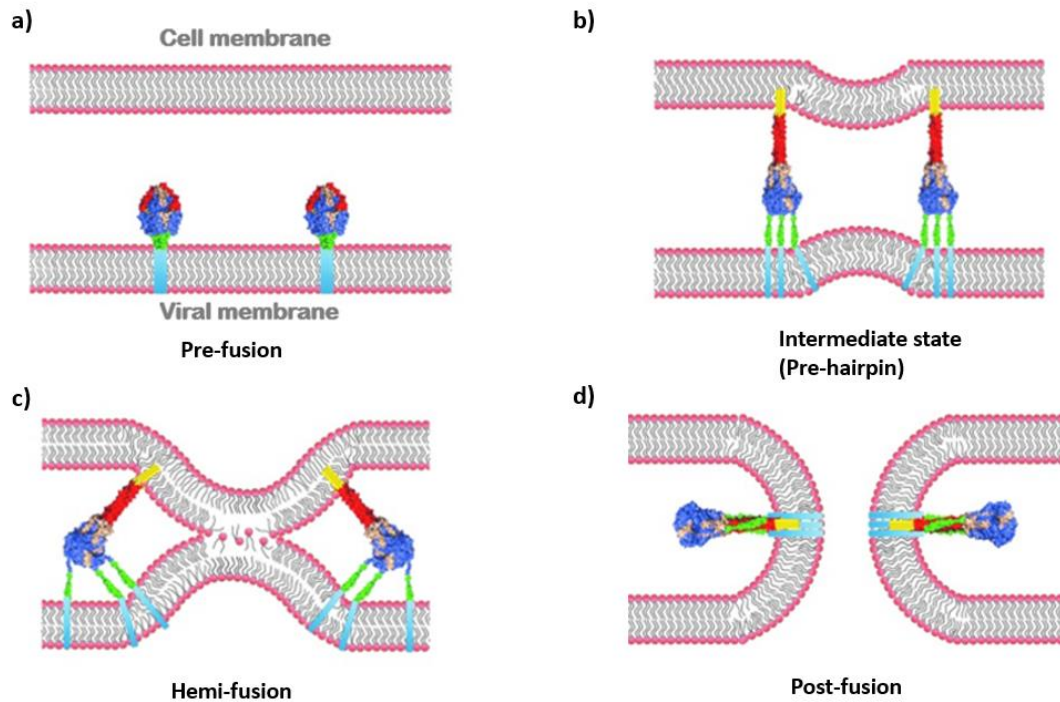
Figure 1.6. The respiratory syncytial virus membrane fusion. (a) Inactivated pre-fusion protein with its globular head linked to the viral transmembrane by HRB (green). (b) Upon activation, a conformation change where the HRA (red) undergoes an α-helical transition and the N-terminal fusion protein (yellow) inserts into the cell membrane. (c) hemi-fusion state with collapse of the intermediate forcing the membranes in close proximity. (d) Assembly of a stable 6-helix bundle (6-HB) formed by coiled-coil HRA and HRB, leading to the formation of a fusion pore. Adapted from Plemper *et al.*[33]

The protein undergoes a series of conformational changes whereby the N-terminal HRA α-helices refold along a trimeric coil, inserting the post-cleavage hydrophobic fusion peptide of each subunits into the host cell membrane, forming a pre-hairpin intermediate (Figure 1.6b).[33] Subsequently, the unstable intermediate collapses to a more stable hemifusion structure whereby the C-terminal HRB, attached to the viral membrane, undergoes an α-helical conformational change running alongside HRA (Figure 1.6c and 1.6d). In the post-fusion form, the assembly of the so-called 6-helix bundle (6-HB) formed by three HRA α-helices coiled-coil surrounded by three antiparallel coiled-coil HRB results in both inner and outer leaflets of the cell and viral membranes mixing (Figures 1.6d and 1.7). The completion of the 6-helix bundle assembly leads to the formation of a fusion pore, enabling the nucleocapsid to enter the cell cytoplasm.

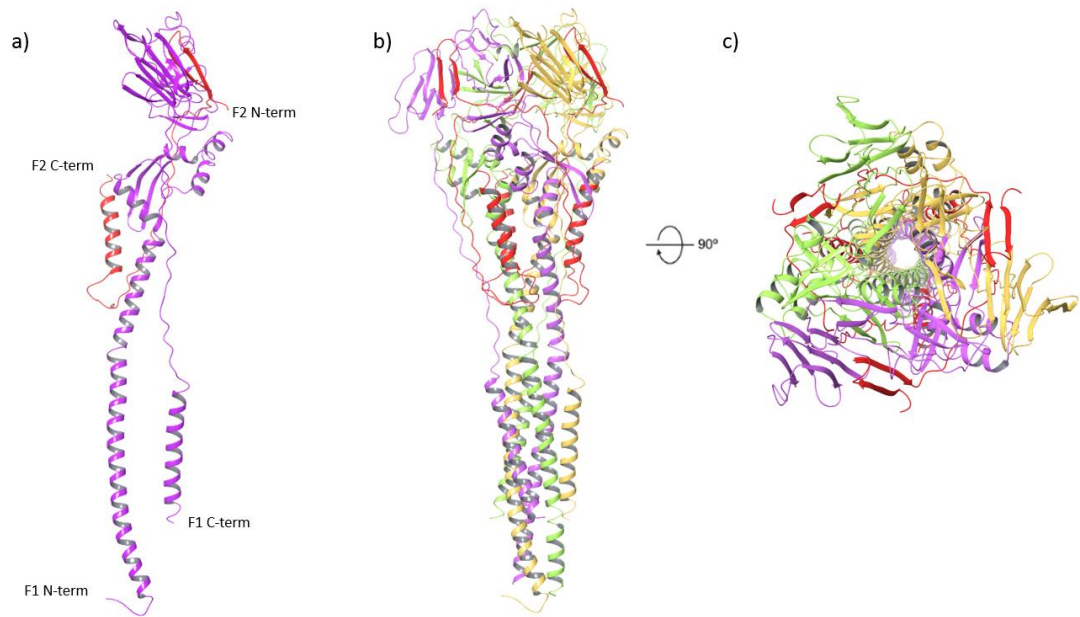**Figure 1.7.** Structure of the RSV F protein in the post-fusion conformation (PDB ID: 4RRR and reprocessed with Schrödinger Maestro 11 software) (a) Ribbon representing a F1/F2 monomer. F1 (in purple) with the α-helices F1 C-terminal refold along a trimeric coiled-coil F1 N-terminal. (b) Post-fusion six-helix bundle of N- and C-terminal helices with each F1 monomer a different colour. (c) Rotation 90° of the post-fusion 6-helix bundle.

1.7 Mechanism of Activity of Small-Molecules Entry Inhibitors

Early studies by photoaffinity labelling with [^{125}I], targeting the binding pockets of known small molecules entry inhibitors **BMS-433771** and **TMC-353121** (described in section 1.8), suggested these inhibitors interfered with the zippering of the post-fusion six-helix bundle formed by the HRA and HRB heptad-repeats essential for the membrane fusion (Figure 1.6).[121,122] Furthermore, following the co-crystallisation of **TMC-353121** with the six-helix bundle construct, Roymans suggested that **TMC- 353121** inhibits the RSV fusion to the host cell membrane by binding to a hydrophobic pocket of the HRA trimeric coiled-coil, stabilising the HRA and HRB heptad repeats in a different and somewhat distorted conformation to the one required for the fusion process (Figure 1.8).[122]
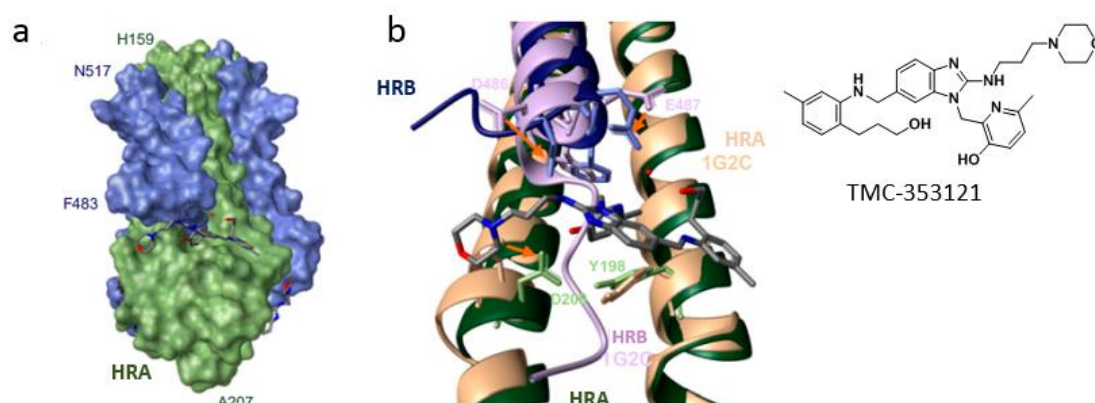
Figure 1.8. (a) **TMC-353121** bound to the 6-helix bundle with trimeric HRA helices (green surfaces surrounded by the HRB helices (blue surfaces). (b) Superimposition of the **TMC-353121** co-crystal structure (dark green and blue ribbons) with the 6HB (purple and tan ribbons) shows a change in the conformation of the 6HB.[122]

However, recent biophysical and structural studies by McLellan *et al*. suggests that some of these early pre-clinical RSV fusion inhibitors **BMS-433771**, **JNJ-2408068, BTA-9881** and **TMC-353121** (the compounds are described in section 1.8) all bind to a central binding site within the pre-fusion conformation of the RSV F protein.[123] Indeed, McLellan showed that the different chemotypes all bind with high affinity to a stabilised pre-fusion RSV F protein following isothermal titration calorimetry (ITC) experiments. When tested against the post-fusion 6-helix bundle state of the F protein, the compounds did not show any binding to the fusion protein. Furthermore, the recent structural elucidations of the pre-fusion RSV structure in the presence of these fusion inhibitors highlighted a central cavity pocket with two binding modes for the

inhibitors (Figure 1.9). It is believed that the inhibitors may stabilise the pre-fusion conformation by acting as a tether between the fusion peptide (FP) at the N terminus of the F1 subunit and the heptad repeat B (HRB) located at the C terminus of the F1 subunit, preventing a refold of the fusion protein during the rearrangement process leading to the fusion between the viral membrane and the host membrane as described in Figure 1.6.
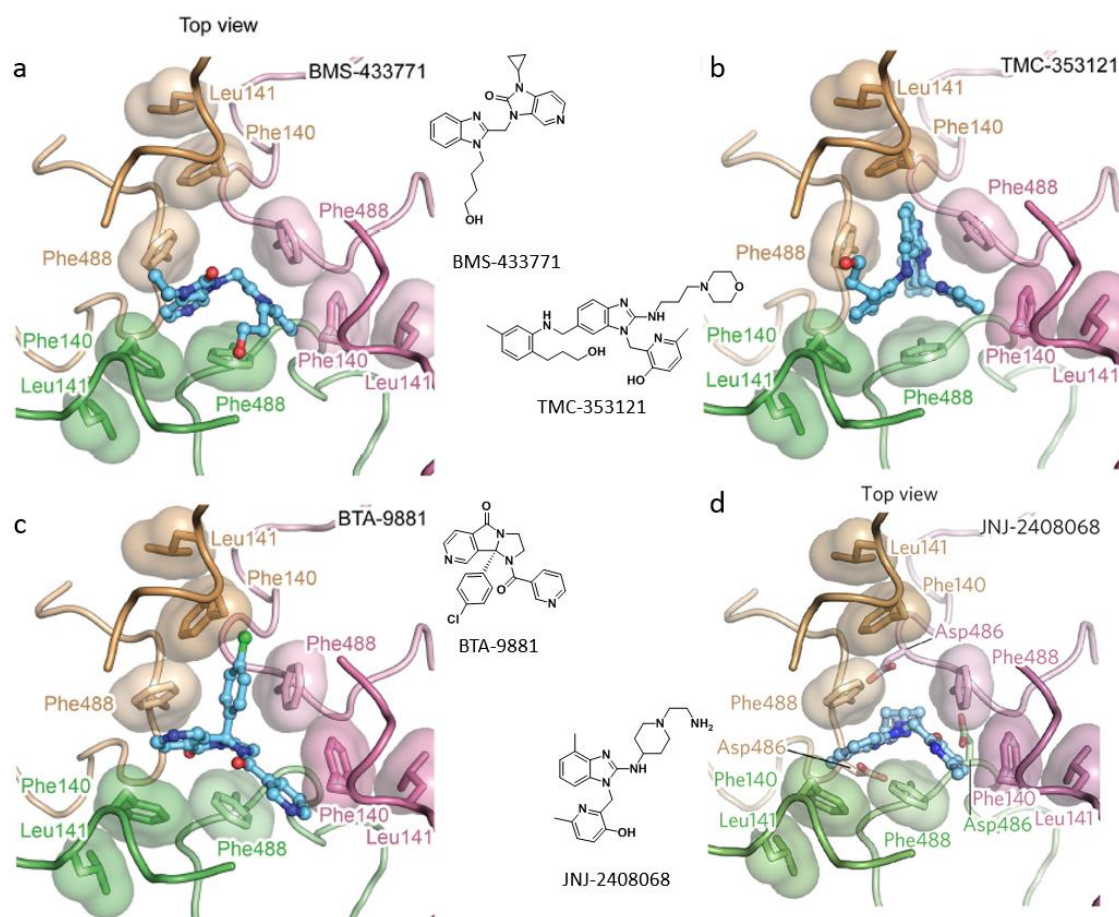
Figure 1.9. Inhibitors **BMS-43771** (a), **TMC-353121** (b), **BTA-9881** (c) and **JNJ-2408068** (d) tethered within the fusion peptide and heptad repeat B in the pre-fusion metastable state of the RSV F protein.[123]

Other recent studies from Samuel *et al*. also support a pre-fusion binding of the RSV fusion inhibitor clinical candidate **GS-5806** (Section 1.8.2, Table 1.2, Compound **9**) and preventing the pre- to post-triggered conformational change.[124] Triggering of the metastable pre-fusion to the post-fusion conformational states can be achieved by changes in temperature or in concentration of buffer ion strength (HEPES buffer). Under the modification of the ionic-strength buffer, a pre-fusion truncated extracellular domain of the RSV F protein showed no conformational change in a dose-dependent effect of **GS-5806** compared to a DMSO control and

inactive analogue of **GS-5806**, thus preventing the formation of the post-fusion state of the protein.

Despite conflicting results in the understanding of the molecular mechanisms of RSV fusion inhibitors, it is clear that known RSV fusion inhibitors of the F protein do interfere with the conformational change of the protein from a pre-fusion metastable state to a post-fusion form, thus preventing a refolding of the F1 subunit and blocking the fusion of the viral F protein to the host cell membrane.

1.8 Current Development and Clinical Landscape of Small-Molecule RSV Fusion Inhibitors

For the purpose of this section, peer-reviewed publications as well as World, EP and US patents filed from companies and universities between January 2000 and March 2017 related to small-molecule RSV fusion inhibitors have been considered. The data are selected from the SciFinder database of Chemical Abstracts.

A significant number of patents for small molecules targeting RSV have been filed since 2000 and Table 1 summarises the increase in interest in this area. Although the targets of some of those patents are not explicit, a large proportion of these patents have been targeting the viral fusion protein. A number of observations can be made from the data presented in Figure 1.10. Firstly, after the initial wave of patent filings in the 2000 to 2006 period, the interest in the RSV area significantly dropped in the subsequent 5-year period. The reason for this decline is not clear but may be a consequence of the failure of some of the initial clinical candidates from the early filings. Secondly, from 2012, a significant number of the patents have been filed by biotech companies, suggesting the interest, and rewards, for successful on-going development in novel RSV therapies is still high.
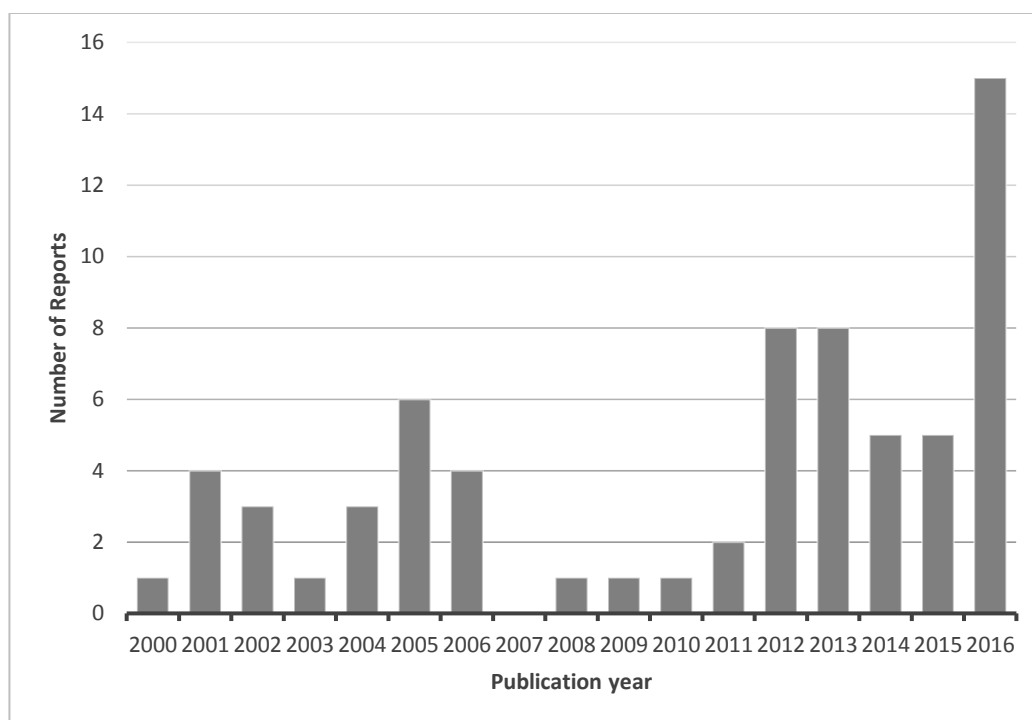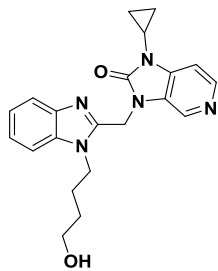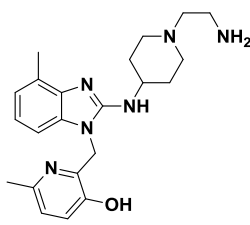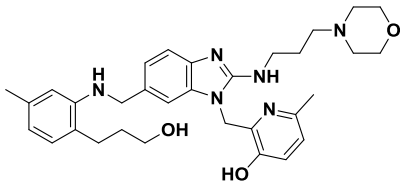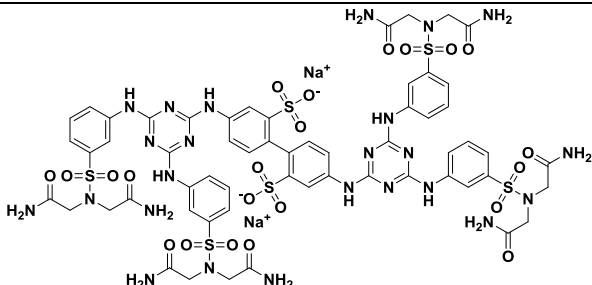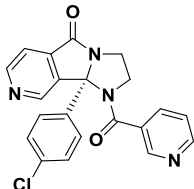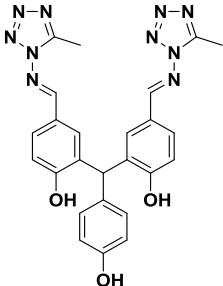

Figure 1.10. RSV patents covering the 2000-2016 period.

1.8.1 Summary of Small-Molecules Fusion Inhibitors Reported in the Literature During the 2000-2009 Period

As mentioned in the previous section, the fusion protein responsible for viral entry has been a target of choice for the development of antiviral drugs. Bristol-Meyers-Squibb (BMS) filed a number of patents during 2000 to 2004 covering a novel class of fusion inhibitors of RSV.[125–128] All the patents had a fairly narrow scope centred around a benzimidazol-2-one chemotype and BMS have published more detailed information and extensive structure-activity relationships in the benzimidazole part of this series which led to the identification of **BMS-433771** (Table 1.1).[129–135] **BMS-433771** was shown to be a potent RSV inhibitor *in vitro* and demonstrated efficacy following oral dosing in *in vivo* animal models. In the BALB/c mouse model of RSV infection, the compound was active against multiple strains of the virus and clinical isolates for both antigenic groups A and B with an average EC_{50} of approximately 20 nM.[136] Further studies showed that prophylactic oral dosing of **BMS-433771** at doses of ≥ 5 mg/kg led to > 1.0 $\log_{10}$ reduction in viral load in the BALB/c mouse, but doses of ≥ 50 mg/kg were required at 1 hour pre-infection to achieve a similar level the viral load reduction in the cotton rat.[136] The compound was however discontinued following a strategic portfolio realignment by BMS.

Table 1.1. Key reported RSV fusion inhibitors during 2000 – 2009.

Research Institute	Identifier	Structures
Bristol-Myers-Squibb	**BMS-433771**	
Johnson & Johnson	**JNJ-2408068**	

Research Institute	Identifier	Structures
Johnson & Johnson	TMC-353121	
Wyeth-Ayerst	RFI-641	
Biota Holdings Ltd	BTA-9881	
Teva	MDT-637 (VP-14637)	

Johnson & Johnson filed a series of patents on a benzimidazole chemotype as potential RSV inhibitors.[137–139] From these filings came **JNJ-2408068**, a fusion inhibitor and a candidate for clinical evaluation which was later described in the scientific literature.[140–142] The compound had a reported activity of EC_{50} = 0.16 nM and in cotton rat studies showed significant reduced levels of the lung viral titres after 0.39 mg/kg aerosol administration against both RSV A and B sub-types. **JNJ-2408068** was able to inhibit both virus-cell fusion and cell-cell syncytia at the end of the replication process, as well as the release of pro-inflammatory cytokines. However, the compound was shown to have a poor pharmacokinetic profile; in particular long lung retention in rat, dog and monkey species.[141] The aminoethyl-piperidine moiety of the molecule was

associated with the extended long retention time in tissues and a subsequent SAR optimisation to remove this cause of concern led to the discovery of **TMC-353121** as a back-up candidate for **JNJ-2408068**.[143]

TMC-353121 retained a high activity (EC_{50} = 0.12 nM) and low cytotoxicity whilst presenting a much reduced half-life in the lungs ($T_{1/2}$ = 25.1 h).[143] In the cotton rat model of the disease, **TMC-353121** demonstrated *in vivo* efficacy by intravenous (10 mg/kg), oral (40 mg/kg) and inhaled (5 mg/kg) routes of administration and led to significant viral load reduction against a range of clinical isolates from both A and B sub-types.[143] More recent studies from Olszewska *et al*. suggest that **TMC-353121**, administered either prophylactically or acutely shortly after infection, reduced both viral load and virus-induced inflammation in the BALB/C mouse model of the disease.[144] In 2011, **TMC-353121** was still reported to be undergoing further investigation. However, there are limited data available on this compound which has so far not reached any clinical development and further details of this compound have yet to publish in the literature.

RFI-641 was identified from an antiviral high-throughput screen by Wyeth.[145] The compound showed both *in vitro* and *in vivo* activity against RSV and was active against clinical isolates of the RSV sub-families A and B but had no other effect on any other viruses. Further studies by Wyeth demonstrated that **RFI-641** was a specific inhibitor of the fusion protein.[146] After prophylactic intranasal administration at 1.3 mg/kg, 2 hours prior to inoculation, **RFI-641** reduced the viral titres $\geq$ 1.5 $\log_{10}$ in the mouse models. Similar viral load reductions were observed with intranasal administration in the cotton rat model with doses up to 10 mg/kg which showed viral load reduction by 3.2 $\log_{10}$ units.[147] Furthermore, in the human primate infection model of the disease developed in the African green monkey, both prophylactic and therapeutic administration of **RFI-641** at 6 mg doses showed efficacy in reducing nasal viral load > 3.4 $\log_{10}$ units over a 10 day period.[148] **RFI-641** entered Phase II clinical trials in 2000 but was later discontinued.
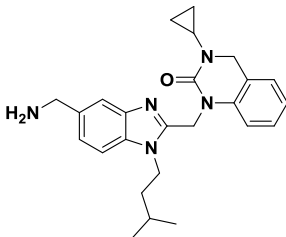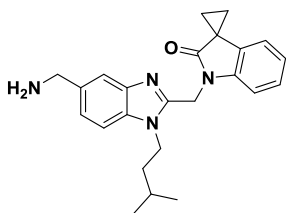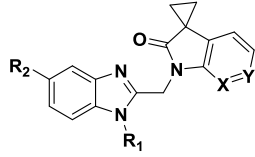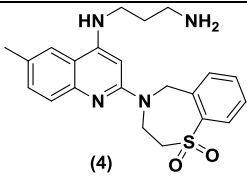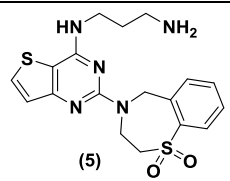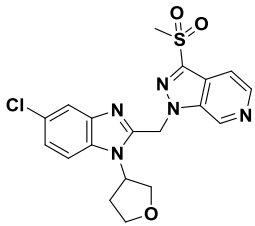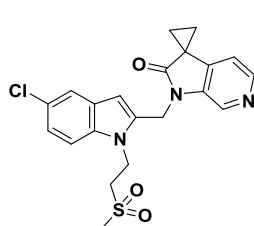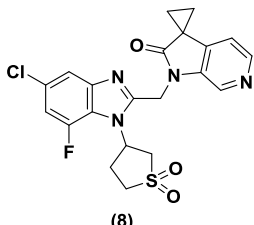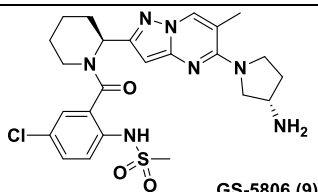
In 2005, Biota holdings Ltd filed a patent on a new class of imidazoisoindolone as a new class of RSV fusion inhibitors.[149] Extensive SAR studies on this new class of compounds led to **BTA-9881** that was selected as candidate for pre-clinical development. There has been very little biological data reported on this series and a medicinal chemistry publication has only been recently published.[150] **BTA-9881** displayed good oral pharmacokinetics in the rat ($T_{1/2}$ = 4.5 h, F ~100%) and was progressed into Phase I clinical studies but was discontinued in 2009 following safety concerns.
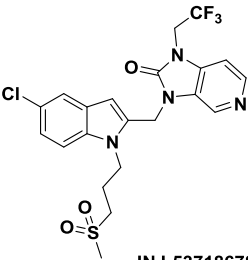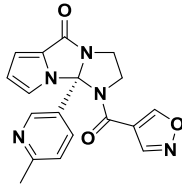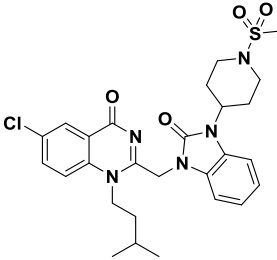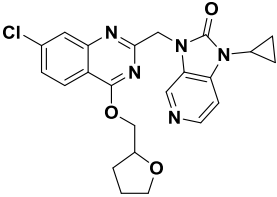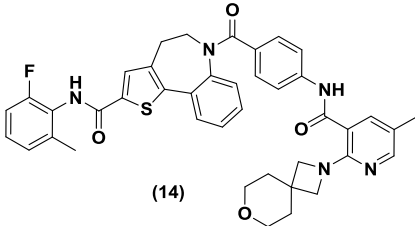
The *bis*-tetrazole benzhydrylphenol **MDT-637** was initially developed by Viropharma Inc. and has demonstrated *in vitro* antiviral efficacy against RSV (EC_{50} = 1 nM) and reduction of lower pulmonary RSV titres in *in vivo* studies in the cotton rat after 0.126 mg/kg administration post infection in either RSV A or B sub-types.[151,152] The compound was acquired and reformulated by MicroDose Therapeutx (now part of Teva) as a dry powder inhaled drug following issues with poor oral bioavailability in clinical studies.[153,154]

1.8.2 Summary of Small-Molecules Fusion Inhibitors Reported in the Patent Literature During the 2010-2016 Period

The number of patent filings targeting RSV, and in particular the fusion protein, has significantly increased since 2011 as described in Figure 1.10, not only within the large pharmaceutical companies but also in small biotech companies and university groups. The reasons for this significant increase is not clear, but it may be a consequence of the failure of the early RSV fusion compounds and suggesting that the interest in RSV small-molecule treatments remains high due to the significant unmet medical needs. Furthermore, the volume of data gathered on those initial development candidates has validated the fusion protein both in pre-clinical and early clinical studies as a target of choice. The next section focuses exclusively on the developments of fusion inhibitors in the patent literature since 2010 (Table 1.2).

Table 1.2. Patents covering RSV fusion inhibitors published between 2010 and 2016.

Research Institute	Chemotype	Representative structures
Astra-Zeneca	Benzimidazole quinazolin-2-one	AZD-4316 (1)
ReViral	Benzimidazole oxindoles	RV-39 (2) RV-521 (3)
Roche		(4) (5) (6) (7) (8)
Gilead	Pyrazolo[1,5-*a*]pyrimidine	GS-5806 (9)

Research Institute	Chemotype	Representative structures
Johnson & Johnson	Indole quinazolin-2-one	JNJ-53718678 (10)
Biota Holdings Ltd (Aviragen Therapeutics)	Imidazo [1,2-*a*]pyrrolo[1,2-*d*]pyrazinone	BTA-585 (11)
Medivir	Quinolinone and quinazoline	(12) (13)
Pulmocide Ltd	Benzo[*b*] thieno-[2,3-*d*] azepine	(14)

The chemistry efforts over the last 6 years have partly focused on developing new fusion inhibitors with novel chemotypes such as the pyrazolo[1,5-*a*]pyrimidine from Gilead (Table 1.2, example **9**) but also building on optimising older benzimidazole chemotypes such as the benzimidazole series initially developed by Bristol-Meyers-Squibb (Table 1.2, examples **1**-**3**, **6**-**8** and **10**).

In 2010, Astra-Zeneca published a patent on RSV, following on the work from Arrow Ltd which they acquired in 2007 (Table 1.2).[155] From this came an aminomethylene benzimidazole series (Table 1.2, example **1**) designed using the pharmacophore derived from the **BMS-433771** series, replacing the benzimidazol-2-one moiety with a novel quinazolin-2-one. There are no pre-clinical data available in this series but **AZD-4316** (**1**) entered Phase I studies to determine its safety, tolerability and pharmacokinetics in healthy volunteers. There are however no further data regarding the development status of this compound.

ReViral published one patent in 2013, claiming analogues of the aminomethylene benzimidazole chemotype previously exemplified by Astra-Zeneca and focused on replacing the quinazolin-2-one with spirocyclic oxindoles and quinoline-2-ones (Table 1.2, example **2**).[156] The patent has a relatively narrow scope exemplified only by cyclopropyl, cyclobutyl and cyclopentyl spirocycles and **RV-39** (**2**) was progressed as a pre-clinical development compound but was not advanced any further due to a poor pharmacokinetic profile. *In vitro* efficacy and *in vivo* pharmacokinetic data for **RV-39** were published in a 2016 follow-up filing with a very narrow scope and limited exclusively to cyclopropyl oxindole analogues.[157] This later filing led to **RV-521** (**3**), which entered Phase I clinical studies in October 2016 and for which the structure remains undisclosed. ReViral have disclosed data showing that **RV-521** is a potent RSV inhibitor with EC_{50} = 3.47 nM in the sub-type A of the disease and EC_{50} = 1.20 nM in the sub-type B. In pre-clinical *in vivo* studies, the compound was shown to be bioavailable in rat, mouse and dog (greater than 40% across species).[158] Efficacy of the compound was also demonstrated in the BALB/C mouse and human airway epithelial cell (HAE) models of the infection after prophylactic administration at 50 mg/kg. In April 2017, ReViral announced that **RV-521** had achieved positive results in pharmacokinetics and safety profile following from the Phase I clinical studies.[159]

Roche published 6 patents between 2013 and 2015. Initially, Roche explored a series of benzothiazepines coupled to quinolones or thienopyrimidine as exemplified by (**4**) and (**5**) respectively (Table 1.2).[160,161] These compounds have been described for the 'treatment and prophylaxis of RSV disease' but there is no evidence that these chemotypes are RSV fusion inhibitors. However, in 2016, Roche published some similar quinazoline cores containing a piperazine rather than a benzothiazepine in the scientific literature suggesting that these quinazoline chemotypes could indeed be targeting the viral fusion protein.[162] In the later patents filed between 2014 and 2015, Roche described a series of fusion protein chemotypes.[163–166] The first 2 patents covered benzimidazoles coupled to indazoles as represented by (**6**) as well as indole and aza-indole analogues as replacements to the benzimidazole chemotype, represented

by example (**7**). The following patents filed in 2015 were a combination of the benzimidazole moiety combined with the cyclopropyl aza-oxindole with extensive exploration of the pendant substituents on the *N*-benzimidazole as depicted by (**8**). *In vitro* antiviral data is given on key examples across these patents. In 2014, Roche licensed their RSV fusion inhibitor **AK-0529** to Ark Biosciences. The structure of this compound has however not been disclosed to date.

Gilead have filed a series of patents between 2011 and 2013 which exemplified a novel chemotype based on pyrazolo[1,5-*a*]pyrimidine analogues.[167–169] Representative activity against RSV-induced cytopathic effect was reported for key compounds across these patents. The initial patents have a very broad scope focusing on SAR explorations around the common pyrazolo[1,5-*a*]pyrimidine core. The later 2013 patent has a much narrower scope focusing on amide analogues around **GS-5806** (**9**) which was developed as Gilead's clinical candidate (Table 1.2). Gilead have published more detailed information in the scientific literature on **GS-5806** which will be described in the following section.[170–172]

Johnson & Johnson have filed extensively during this period with 12 patents covering the development of new RSV fusion inhibitors. In the early patents covering the period of interest, Johnson & Johnson have exemplified structures very similar to **BMS-433771** and described replacement of the benzimidazole moiety by chemotypes including indoles, aza-benzimidazoles and imidazopyridines (Table 1.2, example **10**).[173–176] Further filings in 2013 explored variations on the benzimidazol-2-one moiety, followed by a further filling replacing the benzimidazole-2-one by an extended range of spirocyclic oxindole analogues in a similar fashion to compounds (**2**) and (**3**) from ReViral.[177–179] From this series of claims, compound (**10**) is believed to be the development candidate **JNJ-53718678**.[174] Recent studies in neonatal lambs showed that **JNJ-53718678** is efficacious against RSV infection following prophylactic and therapeutic administration.[180] Furthermore, **JNJ-53718678** also demonstrated significant viral load reduction in healthy adults following intranasal inoculation with RSV (sub-type A) prior to therapeutic treatment.[180]

Following on from their initial clinical candidate **BTA-9881**, Biota Holdings Ltd, now renamed as Aviragen Therapeutics, have filed a series of 3 new patents between 2011 and 2013 and a further one later in 2016 (Table 1.1).[181–184] All the patents are based on a similar core of fused 5- and 6-membered rings containing a substituted carbonyl oxazole as depicted by **BTA-585** (Table 1.2, example **11**) that is believed to be Biota Holdings Ltd's clinical candidate. There are no pre-clinical data available in this series but in 2015, **BTA-585** was reported to have

successfully completed phase I studies in healthy volunteers with no serious adverse events reported.
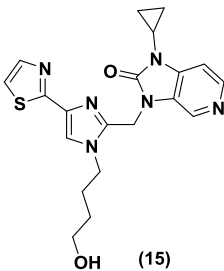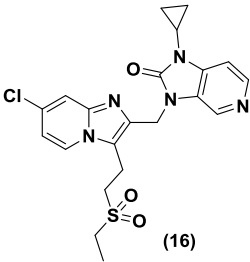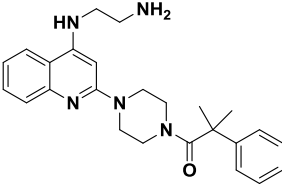
Medivir have filed two patents in 2015 for the treatment of RSV exploring substituted quinazolinone and quinazoline cores coupled to benzimidazol-2-one and quinazolin-2-one chemotypes very similar in structure to previously reported fusion inhibitors (Examples **12** and **13**, Table 1.2).[185,186] The scope of the patents is very broad, being based on substitutions across both of the quinazoline and quinazolinone templates. *In vitro* antiviral activity is reported on key examples. Medivir nominated **MIV-323**, in-licensed from Boehringer Ingelheim, as a pre-clinical RSV fusion inhibitor candidate in late 2016.[187] However, it remains unclear if the chemotypes described in the series of patents mentioned above are related to the structure of **MIV-323**.

Pulmocide Ltd have published two patents in 2016, covering a benzothieno[2,3-a]azepine series with a very broad scope.[188,189] However, one of the patents claims a single structure (Table 1.2, example **14**), including data on the inhibition of the fusion protein (IC_{50} = 0.17 nM against RSV A2 F protein strain), *in vitro* virus titres data in human lung epithelium and *in vivo* antiviral activity in mice and cotton rats. In both animal models, example **14** demonstrated potent dose-dependent inhibition of the viral titre in lung homogenates.[189] There is however no further information on the development of this series.

1.8.3 Summary of Recent Journal Development for Small-Molecules Fusion Inhibitors

In contrast to the volume of patents filed over the last 6 years, there has only been a limited amount of publications in the scientific literature, in part explained by the competitiveness of the area and commercial potential of any novel inhibitors reaching the market.

Table 1.3. Chemotypes described in the scientific literature between 2010 and 2016.

Research Institute	Representative structures
Pfizer	
Roche	

In a 2013 publication, Pfizer described a novel non-benzimidazole chemotype based around an imidazole core that gave good *in vitro* antiviral potency (Example **15**, Table 1.3).[190] Despite issues with *in vitro* permeability in this series, compound (**15**) was further profiled in *in vivo* pharmacokinetic studies and shown to be bioavailable in the rat (F = 34%). The series has not been progressed further following the reorganisation of Pfizer's antiviral activities.

Roche have published two papers describing the identification of imidazopyridine derivatives and piperazinyl quinoline derivatives as fusion inhibitors (Table 1.3, examples **16** and **17**).[162,191] In the first paper, the imidazopyridine analogues as exemplified by (**16**) are closely related to their 2014 and 2015 patent filings, although this published imidazopyridine series was not part of the initial patent claims. Several compounds in this series were identified with low nanomolar *in vitro* antiviral activity. However, no further *in vivo* pharmacology data are provided. In the

second publication, a similarity-based virtual screening approach led to the identification of piperazinyl quinolines as a novel chemotype of RSV fusion inhibitors (Table 1.3, example **17**). The basic side-chain of this series was shown to be essential for antiviral activity. Compound (**17**) showed an antiviral activity of EC_{50} = 28 nM in the cytopathic effect reduction assay (CPE) and was confirmed as a fusion inhibitor. The CPE reduction assay assesses the effect of an antiviral agent on cell viability following on viral infection.[112] In *in vivo* studies, compound **(17)** had good bioavailability (F = 57%) and half-life ($T_{1/2}$ = 3 hours) in the rat despite high plasma clearance.

Gilead have published details of their clinical candidate **GS-5806** (Table 1.2, example **9**), a potent fusion inhibitor against a wide range of clinical isolates from both A and B sub-types, with reported EC_{50} = 0.43 nM and dose-dependent efficacy in the cotton rat model of the disease.[170] The pharmacokinetic profile across species (rat, dog and non-human primate) is predictive of once daily oral administration in infants and adults. Furthermore, **GS-5806** has achieved proof of concept in human RSV challenge studies in healthy adult volunteers and showed significant viral load reduction by 1.8 $\log_{10}$ compared to the placebo treatment. The compound is currently being evaluated in the clinic.

1.8.4   Summary of Key Small-Molecule Fusion Inhibitors in Clinical Evaluation

Whilst a number of small molecule fusion inhibitors are under development, only few have reached clinical trials and none have yet entered wider population Phase III studies. Many of the compounds described previously have failed to pass pre-clinical studies or failed in Phase I safety studies. A summary of compounds still reported to be currently in clinical trials is shown in table 1.4.

Table 1.4. Recent development fusion inhibitors in clinical trials for RSV therapy. Data extracted from http://clinicaltrials.gov.

Molecule	Trial	Status
GS-5806	Studies in hospitalized adults, lung transplant, hematopoietic cell transplant recipients with RSV infection	Phase II (200 patients)
	Safety and efficacy study of **GS-5806** in healthy volunteers infected with RSV	Phase II (140 patients completed)
	Evaluation of the pharmacokinetics, metabolism and excretion of **GS-5806**	Phase I (8 patients completed)
JNJ-53718678	Safety and tolerability of **JNJ-53718678** in infants hospitalized with RSV infection	Phase II (42 patients)
	Evaluation of the antiviral effect of repeated oral dosing of **JNJ 53718678** in healthy adult inoculated with RSV-A (Memphis 37b strain)	Phase II (66 patients completed)
RV-521	Safety, tolerability and pharmacokinetics of single-ascending and multiple-ascending oral doses of **RV521** in addition to the impact of food on drug absorption	Phase I (110 patients completed)
BTA-585	Safety, pharmacokinetics and antiviral activity of orally dosed **BTA585** in healthy volunteers challenged intranasally with RSV	Phase II
AK-0529	Safety, tolerability, pharmacokinetics and antiviral effect of **AK-0529** in hospitalized infants with RSV infection	Phase II (78 patients – Recruiting)
	Safety, tolerability and PK Study of **AK0529**	Phase I (74 patients completed)
MDT-637	Safety, tolerability and pharmacokinetics of **MDT-637**	Phase I (48 patients completed)

GS-5806 is the most advanced RSV fusion inhibitor in the clinic.[192] The compound has showed promise in early phase clinical trials and is now advancing in both RSV-infected hospitalised adults and immunocompromised patients (ClinicalTrials.gov studies: NCT02254421, NCT02254408, NCT02534350 and NCT02135614). Similarly, **JNJ-53718678** has been registered for both phase I and phase II clinical studies. After entering Phase I clinical trial in October 2016, ReViral announced in April 2017 that **RV-521** had achieved positive results in tolerability at all dose levels (175, 250 and 350 mg) and no significant treatment-related adverse events in healthy volunteers dosed orally twice a day for five consecutive days.[159] Following positive data from Phase I clinical studies for **AK-0529** in which the drug was well tolerated and safe, Ark Biosciences have initiated Phase II studies in infants hospitalised with RSV infection which should complete in 2017.[193] However, **BTA-585** which was progressed into Phase II by Aviragen Therapeutics failed to achieve its primary endpoint by reporting non-significant reduction in viral load in adult volunteers infected intranasally with RSV.[194] Following a lengthy development and

reformulation for aerosol delivery, **MDT-637** was progressed into Phase I clinical evaluation. There are, however, no further details on the progress of **MDT-637** and the compound no longer appears in Teva's development portfolio.

1.9 Non Small-Molecules Treatment of RSV Infections

There have been extensive reviews on the vaccine and antibody developments over the recent years and the intention of this section is merely to highlight the alternatives and opportunities to small molecule RSV development.[115,195–198]

1.9.1 Vaccine Development

Despite over half a century of research, there is currently no vaccine available for the treatment of RSV infections. Following vaccine-related adverse events and deaths in the 1960s after administration of formalin-inactivated RSV vaccine (FI-RSV), there have been significant hurdles in developing safe and effective novel vaccines. Indeed, the lack of understanding of the cause of these vaccine-related adverse events has raised concerns over the development of any future vaccines, in particular in the infant population.[196,199] Furthermore, the disparity in the target populations (infants, children, pregnant women, and the elderly) renders the development of a single safe and effective vaccine very difficult and potentially requires more than one type of vaccine to suit each of these populations.[197] The development of RSV-specific vaccines is faced with multiple challenges that are unique to the virus: first, the young age of the main patient population, second the legacy of adverse events in the early development of formalin-inactivated RSV vaccine and third the many mechanisms by which RSV is able to evade the host's innate immunity.[200] Despite these difficulties, the requirement for a vaccine still remains an important approach in the treatment of the viral infection. Figure 1.11 illustrates some of the main vaccine strategies currently pursued and provides a snapshot of the 2016 vaccine landscape.

A number of live attenuated vaccines are in development both in pre-clinical and phase I clinical studies. However, the development of such vaccines has so far been hampered by achieving the right balance between safety and efficacy with viruses sufficiently attenuated to avoid significant disease but still able to replicate to generate a protective antigen exposure.[197] As mentioned previously, the outcome of adverse events resulting in formalin-inactivated RSV vaccine has hindered to fields for such strategy, which is reflected by the lack of vaccines currently in development. With the advance of genomics, nanoparticle-based vaccines, consisting of a self-assembled viral envelope but lacking the viral RNA, have received much attention as exemplified in Table 1.9 by the number of particle-based vaccines in pre-clinical and clinical development.[201,202] However, this remains a risky strategy as demonstrated by the recent failure

of Novavax's RSV F protein recombinant nanoparticle vaccine in Phase III clinical trials failing to meet its efficacy endpoint.

Although less likely to induce long lasting immunity, subunits vaccines using both the fusion (F) and attachment (G) proteins are advancing very rapidly into clinical studies. These vaccines circumvent the safety issues related to live or attenuated vaccination.[203] Several other approaches such as gene-based vectors are also in development where genetically engineered RSV encoding viral vector can provide protective immunity against RSV. These vaccines aim at mimicking the antigen during RSV infection and stimulating an immune response without the risk of being insufficiently attenuated, whilst avoiding the problems of pre-existing immunity and viral evasion from the host's innate immunity.[197]

1.9.2   Next Generation Antibodies

Since the commercialisation of palivizumab, there has been little development in novel monoclonal antibodies. Motavizumab, a promising successor to palivizumab, has completed Phase III clinical trials achieving a 26% reduction in hospitalisation compared to palivizumab and showed non-inferiority.[204] However, in 2010, the FDA did not recommend motavizumab for licensure.

A further two monoclonal antibodies are currently in clinical evaluation. **REGN2222** from Regeneron is currently in Phase III clinical studies in infants born no more than 35 weeks gestational age and who are no more than 6 months of age (ClinicalTrials.gov studies: NCT02325791). **MEDI8897** has reached Phase II clinical studies as a monoclonal antibody binding the pre-fusion conformation of the RSV fusion (F) protein. It is being pursued for the prophylactic treatment of RSV of all infants entering their first RSV season and children with chronic lung disease or congenital heart disease.
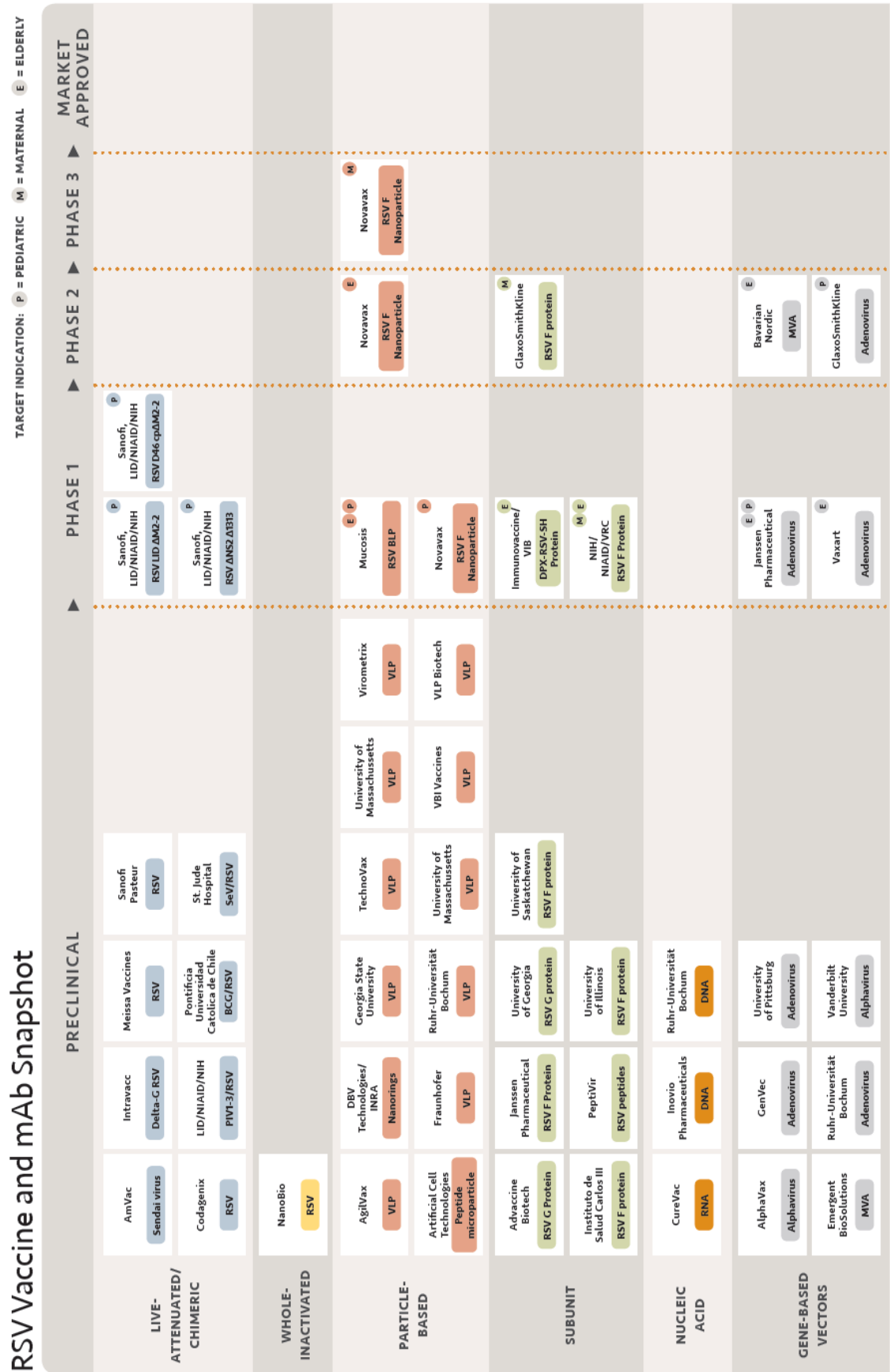
Figure 1.11. 2016 RSV vaccine candidates in development (Adapted from PATH RSV Vaccine Snapshot).

1.10 RSV Market Opportunities

Until recently, RSV had attracted only sporadic interest from the pharmaceutical industry, focusing on larger antiviral markets such as hepatitis C virus and HIV. The sections above have shown there is an increased commitment in developing new small-molecule antiviral treatments and vaccines against RSV. The last few years have led to a better understanding of the disease and a recognised patient population which is not only restricted to infants as previously believed. There are very few reports of the size of the RSV market. In 2010, Charron *et al*. estimated that global RSV sales would reach over $2 billion by 2014 (Figure 1.12).[205]
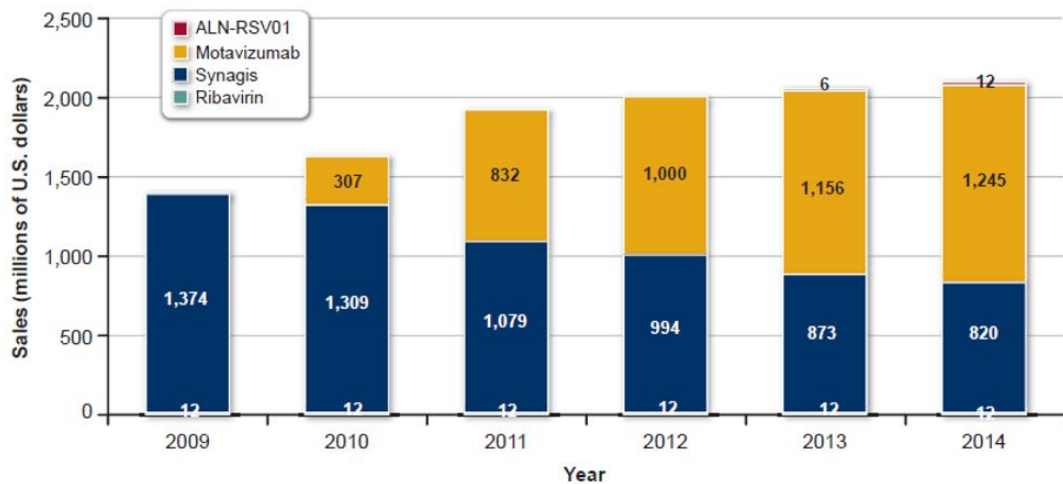
Figure 1.12. Projected global RSV drug sales, 2009-2014 (million of 2009 U.S. dollars). Adapted from Charron *et al*.[205]

However, further market projections analysis by GlobalData in 2016 showed that the RSV global market was estimated to only be approximately $640 million in 2014 across the seven major markets (US, France, Germany, Italy, Spain, UK and Japan) but with projected sales greater than $2 billion by 2024, with a 62% market share for the US alone.[206] The 2016 data are falling short of the predictions from only half a decade ago. Additionally, these market estimates may in part be made on the back of anticipated launches of novel drugs such as the highly anticipated monoclonal antibody Motavizumab failing to reach the market in 2010 and the RNAi ALN-RSV01 failing to achieve its primary endpoint in Phase IIb in 2012. These late stage failures could explain the shortfall in the 2010 market estimates from Charron *et al.* who anticipated sales of Motavizumab exceeding $1 billion from 2012.[205] Similarly, the recent failure of the Novavax's RSV-F vaccine may significantly reduce the RSV market's prospect from the anticipated growth

that was predicted by the 2016 GlobalData forecast. Such uncertainty and variability in the RSV market forecast compared to other drug markets may in part explain the lack of commitment from the pharmaceutical industry in developing novel RSV treatments.

Chapter 2. Project Background – Rationale for a Novel RSV Fusion Inhibitor

2.1 Project Objectives

The initial aim of the project was to identify a novel, potent and selective inhibitor of the RSV F protein for the treatment Respiratory Syncytial Virus (RSV) infection. The novel oral treatment (prophylactic or therapeutic) would primarily prevent RSV infection in the high risk immunocompromised patients. Additional patient populations would include infants and young children as well as patients with underlying chronic respiratory disease (COPD and asthma) who are considered at greater risk of severe viral infections and consequently at higher risk of morbidity and mortality (See Chapter 1 for the disease prevalence).[205,207,208]

We were interested in exploring novel structural modifications which improved antiviral potency and enhanced the pharmacokinetic profile of previously reported benzimidazole-related RSV F protein inhibitors and would allow for further progression into animal studies, safety pharmacology in man and eventually lead to a novel therapeutic agent against the Respiratory Syncytial Virus.

2.2 Preliminary Data and SAR

The RSV F protein has been the subject of intense research over the last two decades as described in Chapter 1 and a large number of the reported small molecule inhibitors of the RSV fusion protein are based on a common benzimidazole core template. Some of the most advanced molecules in this series have shown good antiviral potency, oral bioavailability (Figure 2.1, A) and demonstrated viral load reduction (Figure 2.1, B) such as **BMS-433771,** one of the first benzimidazole-containing compounds developed for RSV treatment.[129,131,132,136,209]

However, many of the small molecules related to **BMS-433771** chemotype targeting the RSV F protein were either halted due to toxicity issues or project realignment (See section 1.8 for

discussion on the development and clinical landscape of small-molecule RSV fusion inhibitors).[210]
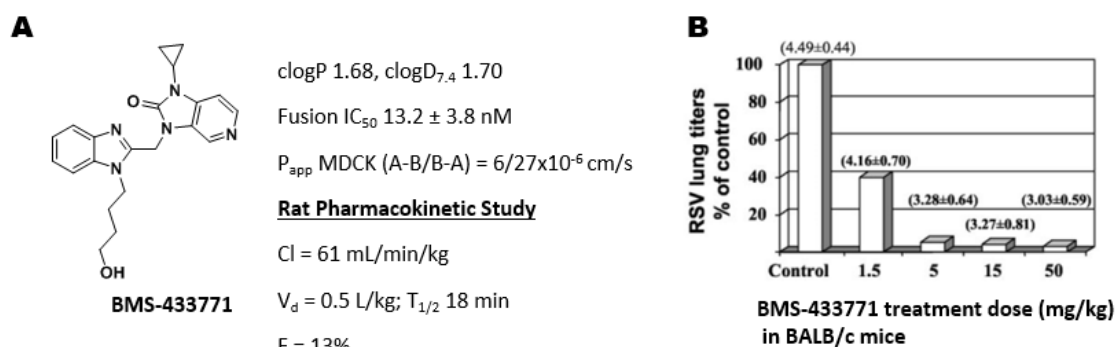
Figure 2.1. (A) **BMS-433771** RSV inhibitor; (B) Single oral dose titration of **BMS-433771** in BALB/c mice 1h prior to intranasal inoculation of RSV long strain.[136]

Initial structure-activity relationship data based on the published literature gives a better understanding of the functionalities tolerated to maintain antiviral activity. A summary of the key modifications is described in figure 2.2.
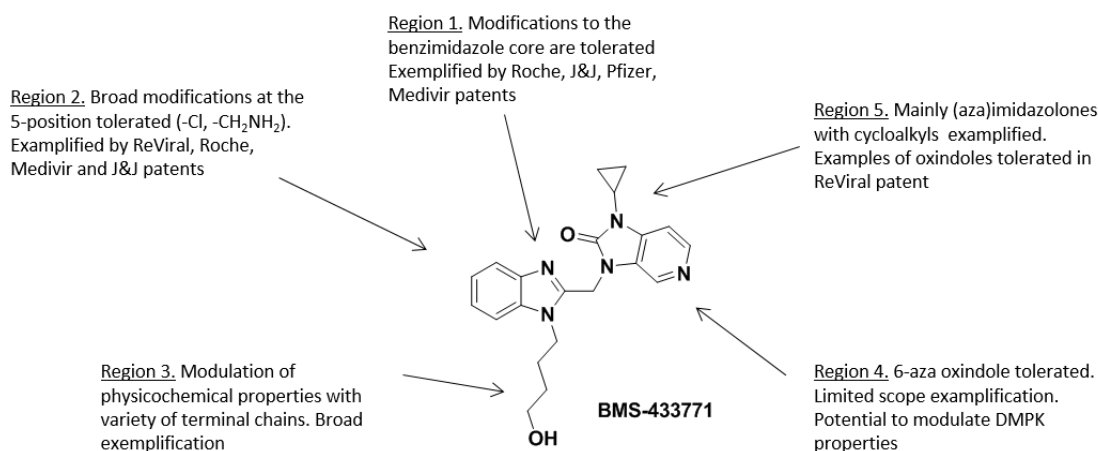
Figure 2.2. Summary of key SARs by regions.

Region 1: The benzimidazole moiety and SAR around the ring have been described extensively mainly by Bristol-Myers Squibb, Johnson & Johnson (J&J), Roche and Trimeris.[129,130,132–134,143,173,174] Recently, several bioisosteres of the benzimidazole region have been explored (aza-benzimidazole, indazole, isoxazole, imidazopyridine).[162,175–178] Among those, the imidazopyridine replacement described by Roche was found to retain good potency and physicochemical properties.[162] The data published by Pfizer explore more significant changes

with the SAR leading to a truncation of the benzimidazole ring to aryl-substituted imidazoles and indazoles.[190]

Region 2: Exploration of the substitutions around the aryl ring have also been extensively described, revealing the 5- position as the preferred substitution pattern and tolerating a broad range of modifications. Addition of substituents, mainly chloro and aminomethylene moieties, exhibited a trend toward an improvement in antiviral potency compared to **BMS-433771.**[156,162,177,178]
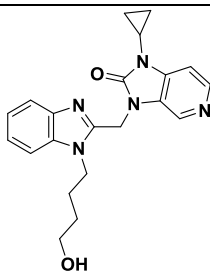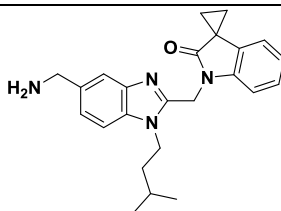
Region 3: Based on the published data and proposed docking models for **BMS-433771**, it could be speculated that the alkyl side-chain may be exposed to an open surface of the pocket with no specific polar interactions.[133,162] The wide range of tolerated side-chains reported in the scientific literature suggests that these side chains may only modulate the physicochemical properties of the overall molecule, thus helping to mitigate the potential increase in lipophilicity elsewhere in the molecule. The scope explored in this area is very large but the preference is for C_3 to C_5 carbon chains with terminal hydroxy, sulfone, trifluoromethyl and *iso*-butyl moieties.[156,161,165,173–175,177,178,190,211]

Region 4: The investigation of the aromatic region 4 remains very limited. Examples of aza-imidazolones (**BMS-433771**), isatins and aza-oxindoles have been reported and the data published show that modifications in this area are tolerated.[134,156,165,166,209]

Region 5: There are very limited data available in this region. Various alkyl imidazolones have been reported but most of the exploration has been exemplified with retention of the cyclopropyl aza-imidazolone as initially reported with **BMS-433771**. ReViral exemplified a small subset of spirooxindoles as potent replacement to the imidazolones.[156] Further examples of spirooxindoles were recently disclosed with the description of a series of spirooxindoles as potential replacement of the cyclopropyl imidazolone core.[179]

Following on the data publically available for **BMS-433771** and access to unpublished *in vivo* data from a collaboration with ReViral, **RV-39 (2)** was considered as a potential starting point for the identification of novel RSV fusion inhibitors (Table 2.1).[129,131,132,134,135,209]

Table 2.1. Profile summary of **BMS-433771** and **RV-39**.

	BMS-433771		RV-39 (2)	
Physicochemical properties				
Molecular weight	377.4		388.5	
clogP^a/logD$_{7.4}$	1.68/1.7^b		3.62/1.75^c	
Solubility, pH$_{7.4}$ buffer (μM)	NA		156	
Primary pharmacology				
RSV Fusion IC$_{50}$ (nM)^d	13.2 ± 3.8		0.5 ± 0.2	
RSV PRA IC$_{50}$ (nM)^e	2 – 40^f		2.2 (n = 1)	
P$_{app}$ MDCK (A-B/B-A) (x 10^{-6} m/s)	6/27		0.42/49.1	
	Rat	**Human**	**Rat**	**Human**
Intrinsic Clearance (Liver microsomes, μL/min/mg)^g	65	<8	20.7	120

^{a}cLogP was calculated using ChemAxon; ^{b}measured logD at pH 7.4 in octanol/neutral buffer; ^{c}calculated clogD at pH 7.4 using ChemAxon calculator plugins; ^{d}RSV Fusion assay (nM). Determinations ± standard deviation from mean of n = two or more determinations; ^{e}RSV Plaque Reduction Assay (nM). Data obtained from a single determination; ^{f}Plaque reduction assay from published data for the long strain RSV in Hep-2 cells[9]; ^{g}Intrinsic clearance from liver microsomal stability assay; NA not available.

RV-39 (**2**) is part of a small compound set exemplified in patent WO2013/068769 with novel 5-aminomethyl benzimidazole and spirooxindole motifs.[156] The unpublished data highlighted in Table 2.1 suggest that **RV-39** exhibits excellent *in vitro* antiviral activity in both the fusion and plaque reduction assays against the RSV A2 strain. **RV-39** is also >25 fold more potent than **BMS-433771** in the primary fusion assay (IC$_{50}$ = 0.5 nM for **RV-39** compared to IC$_{50}$ = 13.2 nM for **BMS-433771**). Surprisingly, **BMS-433771** showed no activity in the plaque reduction assay against the RSV A2 strain of the virus (IC$_{50}$ > 10,000 nM). However, **RV-39** suffers from poor cell permeability (P$_{app}$ A-B 0.42 x 10^{-6} m/s) with a high efflux ratio of about 100-fold in the MDCK permeability assay. Although **RV-39** showed reasonable stability in the rat liver microsomes (Cl$_{int}$ = 20.7 μL/min/mg), in human liver microsomes, the turnover was significant (Cl$_{int}$ = 120 μL/min/mg). To understand the lack of microsomal stability in liver microsomes, **RV-39** was further profiled in a metabolite identification study (Figure 2.3).

RV-39 was incubated at 10 µM for 2 hours in either rat or human liver microsomes. As expected, the results from this metabolite identification suggest that the isobutyl chain showed some level of oxidation, mainly in the rat microsomes (Figure 2.3, metabolite M1). Evidence of metabolism at the aminomethylene moiety (M4 metabolites) was also observed for both rat and human microsomes. However, most of the microsomal metabolism, across both species, results from hydroxylation of the cyclopropane oxindole moiety (Figure 2.3, metabolites M2, M3, M5 and M6), either on the oxindole itself or the cyclopropane ring.
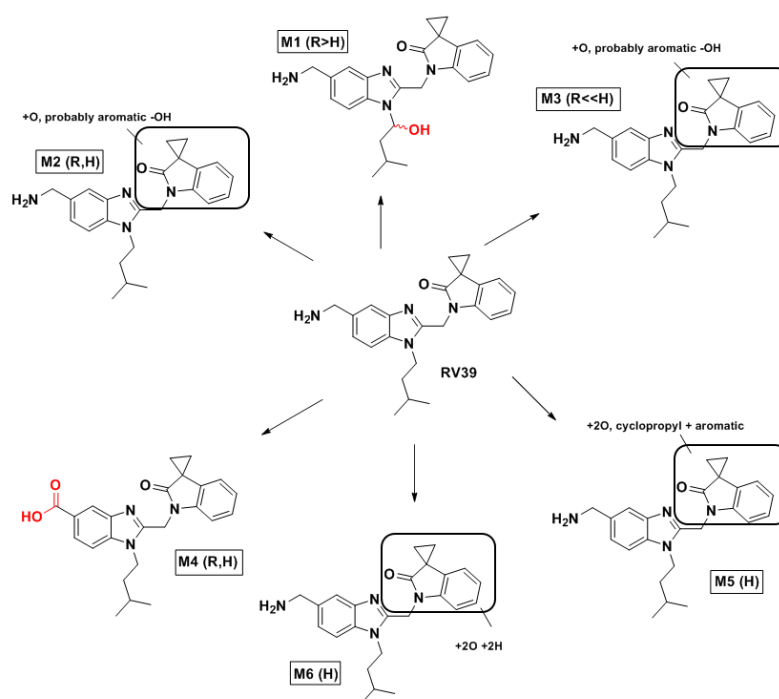
Figure 2.3. Metabolite profiling and identification on **RV-39** in human (H) and rat (R) liver microsomes. The metabolite profiling was performed by Cyprotex on Waters Xevo G2-S QTof.

RV-39 was further progressed to a rat pharmacokinetic study, where the compound was dosed orally as a suspension at 5 mg/kg and iv at 1 mg/kg (Figure 2.4). The rat pharmacokinetic study revealed high plasma clearance of 98 mL/min/kg and a moderate half-life ($T_{1/2}$) of 3.3 hours (Table 2.2). However, **RV-39** showed very low bioavailability (F = 4%) presumably resulting from a combination of both high first pass clearance by the liver and low permeability. This low bioavailability is consistent with the low A-B membrane permeability (P_{app} 0.42 x 10^{-6} m/s) and high efflux ratio (E_R = 116) observed in the *in vitro* MDR1-MDCK assay as reported in table 2.1. Unfortunately, the low metabolic turnover observed from the rat liver microsomal data for **RV-39** did not translate to a low clearance in the rat PK study where high systemic clearance was observed. The discrepancy in the data between *in vitro* and *in vivo* may suggest that **RV-39** could

be potentially cleared from systemic circulation *via* non-oxidative mechanisms such as renal excretion, biliary excretion or phase II metabolism *via* conjugation. However, no further data were available from ReViral to explain the mismatch between *in vitro* intrinsic clearance and *in vivo* clearance. In particular, it may have been informative to have performed a detailed metabolite identification study both in the rat liver microsomes and the blood samples from the rat pharmacokinetic study which could have explained the mismatch between low *in vitro* turnover and the *in vivo* data obtained.
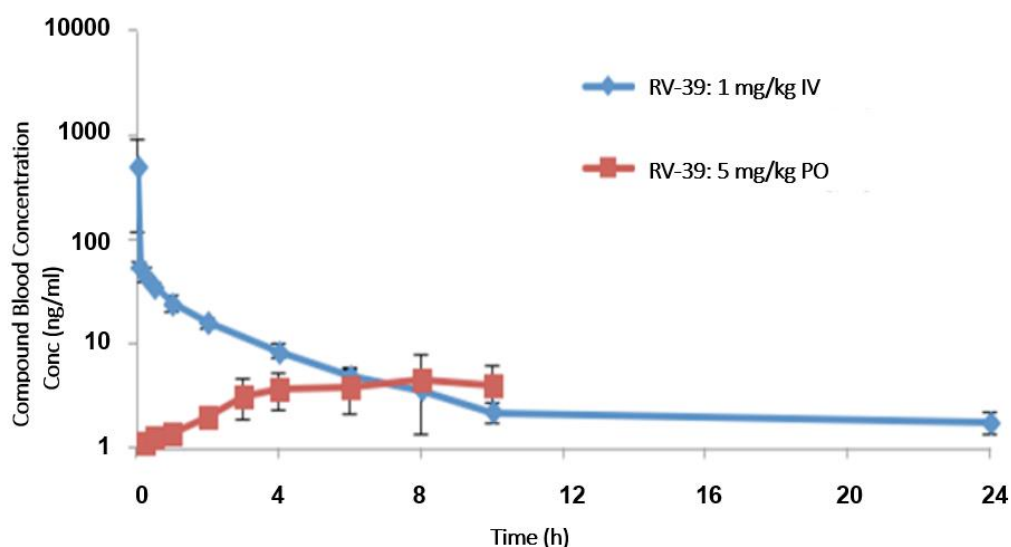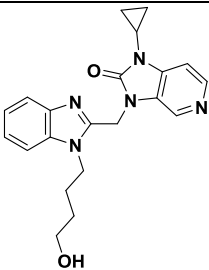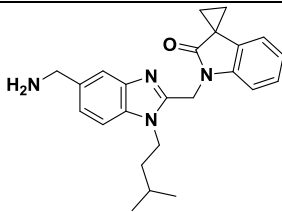
Figure 2.4. Pharmacokinetic study of **RV-39** dosed in Sprague-Dawley male rats; iv dose at 1 mg/kg as a solution in and po at 5 mg/kg.

The pharmacokinetic data obtained from ReViral suggest that the *in vivo* profile of **RV-39** is not better than **BMS-433771** (Table 2.2). **RV-39** has an improved half-life ($T_{1/2}$ = 3.3 h) compared to **BMS-433771** ($T_{1/2}$ = 0.3 h), owing to the large volume of distribution conferred by the basic aminomethylene moiety but both compounds are highly cleared by the liver in the rat and both are poorly absorbed orally.

Table 2.2. Rat pharmacokinetic summary of **BMS-433771** and **RV-39**.

	BMS-433771	RV-39
Rat Pharmacokinetics		
Cl (mL/min/kg)[a]	61	98
V_d (L/Kg)	0.5	34
$T_{1/2}$ (h)	0.3	3.3
F (%)[b]	13	4

[a] iv clearance determined from a 1 mg/kg dose in Sprague-Dawley male rats (n = 3); [b]Bioavailability following oral administration of 5 mg/kg in Sprague-Dawley male rats (n = 3).

2.3 Chemistry Strategy for Improving RV-39

The preliminary *in vitro* and *in vivo* data suggest that **RV-39** is a tractable starting point and it is hoped that modulation of the physicochemical profile would lead to the identification of compounds with an improved pharmacokinetic profile and *in vivo* efficacy whilst retaining the antiviral potency observed for **RV-39**. Indeed, the modification of the physicochemical parameters such as clogP, pKa and molecular weight have been shown to have a profound effect on absorption (solubility, permeability, bioavailability), distribution (volume of distribution, CNS penetration, P-gp efflux, plasma protein binding), metabolism (*in vivo* clearance) and toxicity (hERG inhibition, cytochrome P450 inhibition).[212–215] Such examples of how key molecular properties impact a range of ADME parameters has been clearly illustrated by Gleeson (Figure 2.5).[213]

Neutral molecules

Neutral molecules	Mwt < 400 and clogP < 4	Mwt > 400 and/or clogP > 4
Solubility	Average	Lower
Permeability*	Higher	Average/higher
Bioavailability	Average	Lower
Volume of distribution**	Average	Average
Plasma protein binding	Average	Higher
CNS penetration***	Higher/average	Average/lower
Brain tissue binding	Lower	Higher
P-gp efflux	Average	Higher/average
In vivo clearance	Average	Average
hERG inhibition	Lower	Lower
P450 inhibition***	Lower 2C9, 2C19, 2D6 & 3A4 inhibition	Higher 2C9, 2C19 & 3A4 inhibition
P450 inhibition***	Higher 1A2 inhibition	Lower 1A2 inhibition
P450 inhibition***		Average 2D6 inhibition

Basic molecules

Basic molecules	Mwt < 400 and clogP < 4	Mwt > 400 and/or clogP > 4
Solubility	Higher/average	Lower/average
Permeability*	Higher/average	Average
Bioavailability	Average	Lower
Volume of distribution**	Higher/average	Higher
Plasma protein binding	Lower	Average
CNS penetration***	Higher/average	Average/lower
Brain tissue binding	Lower	Higher
P-gp efflux	Average	Higher/average
In vivo clearance	Average	Higher/average
hERG inhibition	Average/higher	Higher
P450 inhibition***	Lower 1A2, 2C9 & 2C19 inhibition	Lower 1A2 inhibition
P450 inhibition***	Average 2D6 & 3A4 inhibition	Average 2C9, 2C19 inhibition
P450 inhibition***		Higher 2D6 & 3A4 inhibition

Acidic molecules

Acidic molecules	Mwt < 400 and clogP < 4	Mwt > 400 and/or clogP > 4
Solubility	Higher	Average/higher
Permeability*	Lower	Average/higher
Bioavailability	Average	Average
Volume of distribution**	Lower	Lower
Plasma protein binding	Average/higher	Higher
CNS penetration***	Lower	Lower
Brain tissue binding	Lower	Higher
P-gp efflux	Lower	Lower
In vivo clearance	Lower/average	Average
hERG inhibition	Lower	Lower
P450 inhibition***	Lower 1A2, 2C9, 2C19, 2D6 & 3A4 inhibition	Lower 1A2, 2C19, 2D6 & 3A4 inhibition
P450 inhibition***		Higher 2C9 inhibition

Zwitterionic molecules

Zwitterionic molecules	Mwt < 400 and clogP < 4	Mwt > 400 and/or clogP > 4
Solubility	Higher	Average/higher
Permeability*	Lower	Lower/average
Bioavailability	Lower	Lower
Volume of distribution**	Lower	Average/lower
Plasma protein binding	Average/higher	Higher
CNS penetration***	Average/higher	Lower
Brain tissue binding	Lower	Higher
P-gp efflux	Average	Average
In vivo clearance	Average	Average
hERG inhibition	Lower	Average/lower
P450 inhibition***	Lower 1A2, 2C9, 2C19, 2D6 & 3A4 inhibition	Lower 1A2, 2C19 & 3A4 inhibition
P450 inhibition***		Average 2C9, 2D6 inhibition

Figure 2.5. Effect of key molecular properties on ADME parameters. Adapted from Gleeson.[213] Mwt and clogP cut-offs of 400 and 4, respectively, are used. * Optimum clogP bin is 3–5 with respect to permeability. ** Average to high volumes rather than high, low, or average generally considered optimum. *** Low CNS considered optimum, although for targets in the brain, this will be reversed. **** Some isoforms show a nonlinear relationship with clogP and/or Mwt.

2.3.1 Improving on Lipophilicity – Impact of Lipophilic Efficiency

Lipophilic efficiency (LiPE), also referred as Lipophilic Ligand Efficiency (LLE), was introduced by Springthorpe and Leeson as a metric in drug design to ascertain the 'drug-likeness' and potency gains across compounds in lead optimisation and drug candidates.[216–219] Defined as the difference between the negative logarithm of a potency measurement (pIC_{50}, pEC_{50} or pKi) and the clogP (or logD) of a particular compound (LiPE = pIC_{50} - clogP), LiPE captures in a single parameter how efficiently hydrophobic groups are utilised for a given affinity. LiPE has been used as a parameter to improve on structure – efficiency relationships rather than just on potency alone and as a means to control affinity driven solely by increase of lipophilicity and recognised as a key strategic component utilised during late stage optimisation projects.[218,220–222] Indeed, multiple studies and assessments of medicinal chemistry projects leading to drug candidates have shown that high LiPE values (greater than 5 units) have been associated with

greater chances of achieving good efficacy *in vivo* through a combination of high potency and good pharmacokinetics.[218,219,223,224] For example, Shultz demonstrated how a novel class of highly potent and selective Tankyrase inhibitors were designed *via* efficiency-driven optimisation based on LiPE and how potency alone cannot be used as a driver in a multi-dimensional medicinal chemistry approach where physicochemical and ADME parameters need careful consideration.[225] Whilst LiPE values are only relevant when comparing compounds against a specific target, it is widely recognised that an average oral drug candidate with clogP ranging from 2 to 3 and potency in the range of 1 nM to 10 nM leads to LiPE values of 5 to 7 units or greater.[216,217] Compounds with lower LiPE are usually a compromise between increased lipophilicity (clogP > 4) and reduced potency, potentially leading to high doses in humans and compound-related toxicity.[226,227]

The lipophilic efficiency for a selection of key inhibitors of the RSV fusion protein is presented in table 2.3 and an analysis of these inhibitors is reported in Figure 2.6 which shows a plot of clogP against pIC_{50} (see Chapter 1 for reported RSV fusion inhibitors when the structure is known). The antiviral potency measured in the RSV fusion assay was obtained from published data or from the preparation of competitor compounds within the group. Although the antiviral potency values are highly dependent on different experimental methods and the RSV strains used by each research group, Figure 2.6 confirms that values where LiPE is greater than 5 are achievable for this target. In particular, differentiated chemotypes such as the Roche compound **16** and Gilead's compound **9** with clogP ~ 1 and high antiviral affinity (pIC_{50} > 8.5) both exhibit LiPE > 7. However, there is an obvious disparity among the representative compounds reported in this graph with **AZD-4316** (**1**) and **TMC-353121** having LiPE values lower than 5, owing to a compromise between reduced potency and high clogP.

Table 2.3. Lipophilic efficiency for reported RSV F protein inhibitors.

Compound ID	Structure	clogP[a]	pIC$_{50}$[b]	LiPE[c]
RV-39		3.62	8.95	5.34
BMS-433771		1.68	7.89	6.21
15		1.34	7.24	5.89
9		1.28	9.43	8.15
JNJ-2408068		1.33	8.02	6.69
TMC-353121		3.59	8.44	4.85
1		3.45	8.05	4.60
16		0.77	8.52	7.75

[a]Calculated from ChemAxon calculator plugins; [b]pIC$_{50}$ = -log IC$_{50}$ expressed in M. Uncorrected from values reported in the literature; [c]LiPE = pIC$_{50}$ − clogP.

Of the published RSV F protein inhibitors, only a few reported compounds are within the top left quadrant highlighted in blue (Figure 2.6), owing for a balanced clogP and high antiviral potency. As discussed previously, compounds fitting within this top left quadrant are more likely to

achieve reasonable *in vivo* pharmacokinetic.[215–218,223] Indeed, targeting compounds with clogP between 0 and 2, whilst maintaining an antiviral activity similar to **RV-39** (IC$_{50}$ < 10 nM, pIC$_{50}$ > 8) in the RSV fusion assay would seem a good starting range to optimise **RV-39**, contributing to an increased chance of obtaining balanced physicochemical and ADME properties. Such a reduction of the lipophilicity whilst retaining the antiviral potency in the fusion assay is schematised by the red arrow in figure 2.6, leading to compounds of higher lipophilic ligand efficiency.
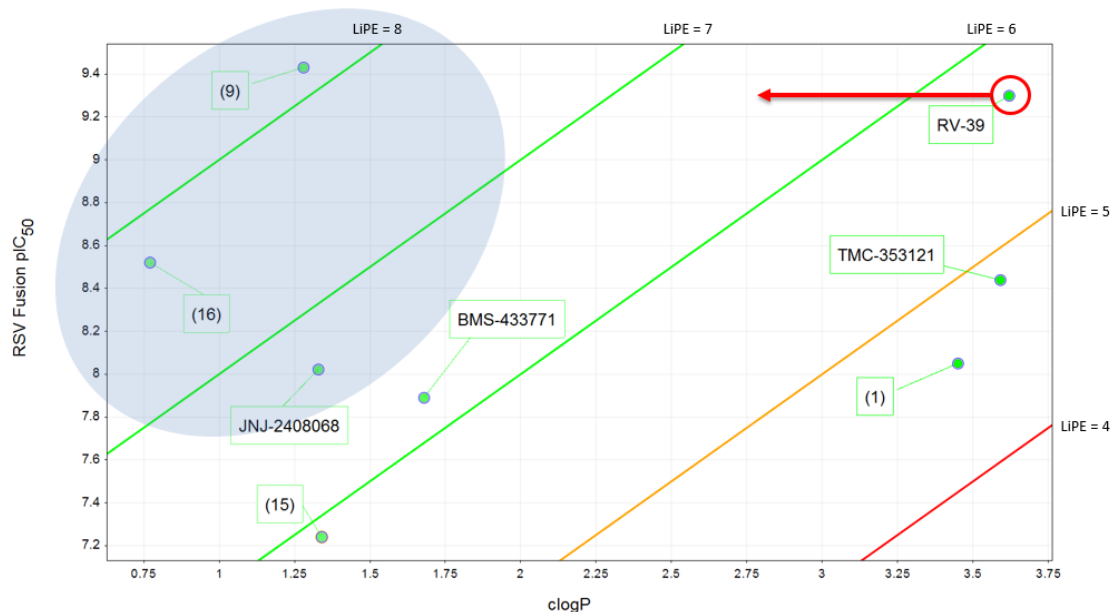
Figure 2.6. Analysis of LiPE for reported RSV fusion inhibitors. The blue area highlights the compounds exhibiting high values of lipophilic ligand efficiency.

Therefore, a key consideration in designing novel inhibitors of the F protein with improved lipophilic efficiency over **RV-39** is the awareness for a careful balance between changes in antiviral potency and any potential tendency to increase lipophilicity.

2.3.2 Improving on Metabolic Stability

The results from the metabolite identification from the rat and human liver microsome studies highlighted the cyclopropane oxindole of **RV-39** as one of the major metabolically vulnerable site. Blocking the potential sites of metabolism, whilst retaining or improving on the antiviral activity, would potentially mitigate the human cytochrome P450 oxidation, addressing the high clearance observed in the human liver microsome studies and hopefully improving on the rat *in vivo* exposure (high clearance and low bioavailability). In particular, the introduction of substituents such as fluorine atoms on the aryl ring would potentially reduce the phase I oxidative metabolism highlighted by the metabolic identification. Similarly, the incorporation of

nitrogen atoms in the electron rich oxindole moiety (aza-oxindoles) would have a similar effect of mitigating the overall electron density of the oxindole moiety whilst reducing the lipophilicity and potentially addressing the metabolic instability in human liver microsomes observed with **RV-39**.

2.3.3 Improving on Permeability – pKa Modulation

Various reports have shown that the benzimidazole region (Figure 2.2, regions 1 and 2) can tolerate some structural modifications as exemplified by **7**, **10** and **16**. However, key issues observed with **RV-39** were the lack of oral bioavailability due to a combination of poor permeability as observed in the *in vitro* MDCK assay, high efflux ratio and high plasma clearance in the rat pharmacokinetic study, along with potential metabolic instability of the aminomethylene moiety. A modulation of the pKa to reduce the ionisation state of aminomethylene moiety present in **RV-39** was considered as a potential way to improve the permeability of the novel compounds prepared.[213] To support this hypothesis, the mining of the patent fillings from Johnson & Johnson revealed that chlorine has been used extensively as an alternative to the aminomethylene moiety present in **RV-39**.[173–178] The introduction of the chlorine atom instead of the aminomethylene moiety as present in **RV-39** was used in a selection of compounds prepared to remove the ionisable nature of the basic aminomethylene fragment.

The exploration of alternative benzimidazole chemotypes and replacement of either the aminomethylene (Figure 2.2, region 2) and benzimidazole side-chains (Figure 2.2, region 3) was not investigated as part of the work reported in this thesis and was the focus of other members of the group.

2.3.4 Development Criteria for RSV F Protein Optimisation

The objective of the work reported in this thesis was to design novel inhibitors of the RSV F protein with an improved pharmacokinetic profile over **RV-39** in rat (improved clearance and bioavailability). The target product profile of the desired criteria identified for an improved pre-clinical candidate over **RV-39** is outlined in Table 2.4. As previously mentioned, the initial effort endeavoured to improve on the physicochemical properties, and in particular reducing the lipophilicity of **RV-39**, whilst improving on the microsomal stability and permeability measured in the *MDR1*-MDCK assay and retaining a similar level of antiviral potency against both the fusion assay and the plaque reduction assay.

Table 2.4. Typical target product profile for a pre-clinical candidate in the RSV project.

Category	Parameters		RV39	Candidate profile
Physicochemical Properties	Molecular weight (MW)		388.5	< 450
	clogP		3.62	< 3.5
	logD (pH 7.4)		1.75	< 1.5
Primary Pharmacology	Fusion IC_{50} (nM)		0.5 ± 0.2	< 5
	Plaque Reduction Assay IC_{50} (nM)		2.2 (n= 1)	< 10
	LiPE (pIC_{50} - clogP)		5.68	> 5
	hERG IC_{50} (μM)		ND	> 10
In Vitro ADME	Solubility, pH 7.4 buffer (μM)		156	> 100
	Rat liver microsome clearance (μL/min/mg)		20.7	< 50
	Human liver microsome clearance (μL/min/mg)		120	< 50
	MDCK A-B P_{app} ($\times 10^{-6}$ cm/s) / Efflux ratio		0.42/117	> 5 / < 2
	Cytochrome P450: CYP1A2, CYP2C9, CYP2C19, CYP2D6, CYP3A4 (μM)		ND	> 10
DMPK[a]	IV	Cl (mL/min/kg)	98	< 30
		V_d (L/Kg)	34	> 1
		$T_{1/2}$ (h)	3.3	> 2
	PO	F (%)	4	> 30

[a]In rat; ND: Not determined

2.3.5   Patent Publication from Johnson & Johnson

At the time of initiating the work reported in this thesis, none of the chemistry or any biological data had been published on any of the compounds that are described in the next chapters.

The publication of a patent from Johnson & Johnson which covered part of the spirocyclic oxindole series (Figure 2.7) did not influence any of the chemistry and synthetic steps described in the following chapters.[179] The chemical strategy to prepare the spirooxindoles and spirocyclic-aza-oxindoles described in chapter 3 had already been designed and the key palladium-catalysed α-arylation step had been optimised prior to the patent publication date.
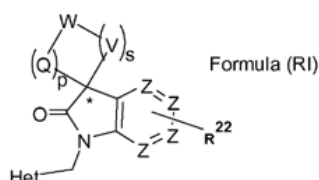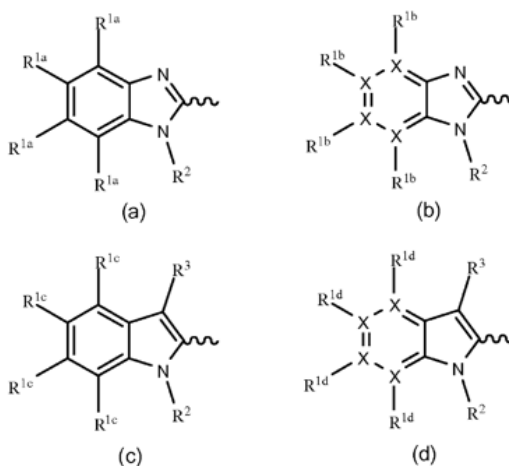
Figure 2.7. Markush structure for patent WO2014/060411.

Chapter 3. Development of Novel RSV Fusion Inhibitors

3.1 Objective: Exploration of the Spirooxindole Chemotype

Following on the project's objectives to identify a novel inhibitor of the RSV F protein with an improved pharmacokinetic profile over **RV-39**, and in particular to improve on the high lipophilicity and poor permeability of **RV-39** as well as metabolic instability of the cyclopropyl oxindole moiety observed in the metabolic identification, four specific objectives were determined which would become the focus of this work:

1. Explore 3,3'-spirooxindoles as potential replacement to the cyclopropyl moiety (Figure 3.1, Objective 1). Establish a synthetic route amenable to the preparation of a range of substituted oxindoles bearing a 3,3'-heterocyclic motif.

2. Block the potential site of metabolism on the spirooxindole moiety (Figure 3.1, Objective 2). One common approach relying on structural modification to block the metabolic vulnerability is by the addition of fluorine atoms at the labile sites.[227] Of possible blockers, the addition of fluorine atoms seems to have the least effect on the size of the modified molecules.

3. In a similar fashion to objective 2 (Figure 3.1), explore novel 3-3'-aza-spirooxindoles that would reduce the electronic density of the electron rich oxindole moiety (Figure 3.1, objective 3).

4. Combine the prepared spirooxindoles and spiro-aza-oxindoles with either the aminomethylene or chloro benzimidazole moieties (Figure 3.1, objective 4). The choice of side-chains on the benzimidazole moiety would be guided by the modulation of the correct physicochemical properties, mainly driven by clogP calculations and 'rule of five'

characteristics of the overall compounds as defined by the target product profile (Chapter 2, table 2.4). In this work, the compounds prepared were limited to previously reported fragments and as exemplified in figure 3.1 ($–CH_2^iBu$, $–(CH_2)_3SO_2CH_3$, $–(CH_2)_3CF_3$ and $–(CH_2)_4OH$).
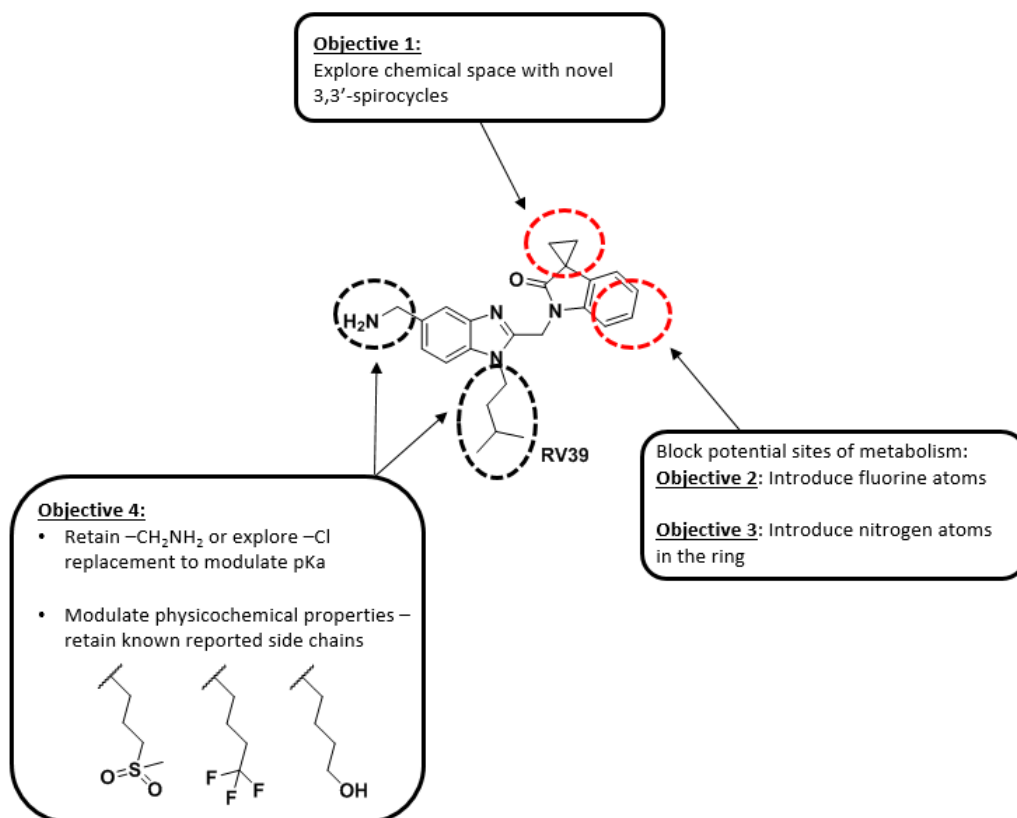
Figure 3.1. Chemistry aims for improving **RV-39**. Areas circled in red are key areas of modification addressed in this work. Area circled in black have been the focus of previous work (reported in Chapters 1 and 2).

3.2 RSV Inhibitors Incorporating Spirooxindole Chemotypes

3.2.1   Spirooxindole Scaffolds

Oxindoles containing a quaternary stereogenic centre at the C(3) position are commonly occurring scaffolds in many natural products and pharmacologically active molecules. For example, **SSR-149,415** is a selective vasopressin receptor antagonist selective for the V1b subtype developed by Abbott and entered clinical trials for the treatment of anxiety (Figure 3.2).[228] Not surprisingly, due to their prevalence in nature, C(3) quaternary oxindoles have emerged as attractive synthetic scaffolds and have been the subject of many total syntheses and development of synthetic methodologies, in part due to their challenging structures.[229–232]
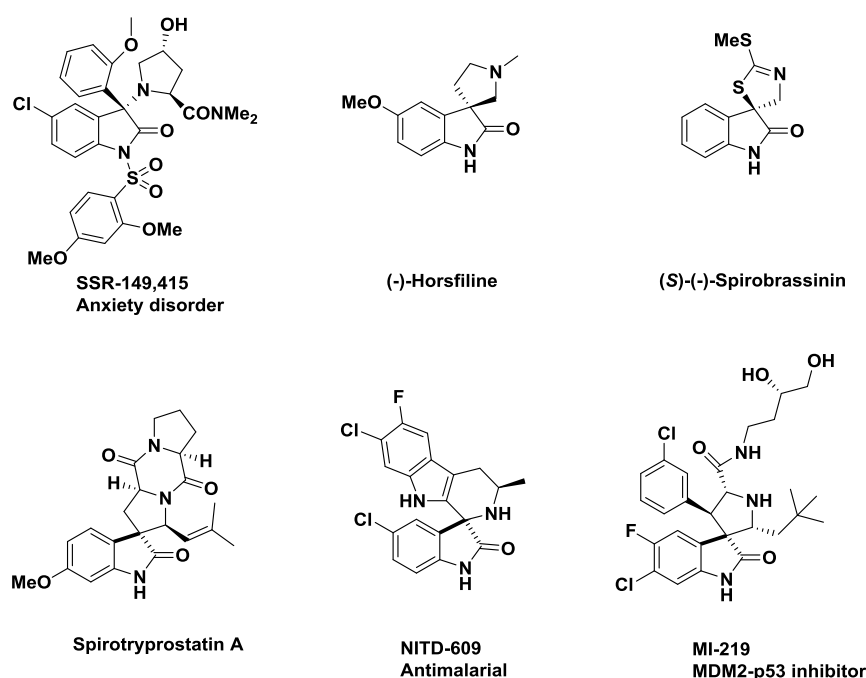
Figure 3.2. Examples of natural products and pharmaceutical lead compounds containing a 3,3'-substituted oxindole core.[233–238]

Spirooxindoles have the key structural characteristic of an oxindole-containing fused spiro ring at the C(3) position with a variety of heterocyclic motifs (Figure 3.3). Many spirooxindole-containing natural products have been associated with a broad range of biological activities. For instance, the alkaloid (-)-horsfiline isolated from medicinal plants *Horsfildea Superba (Myristicaceae)* was shown to possess analgesic properties.[233] (*S*)-(-)-Spirobrassinin, isolated from Japanese radish (*Raphanus sativus*) is part of a class of spirooxindoles reported to exhibit antimicrobial and antitumor activities.[234] In addition, the alkaloid Spirotryprostatin A was

isolated from the *Aspergillus fumigatus* fungus as having anti-mitotic properties by inhibiting the mammalian G2/M cell cycle.[235]
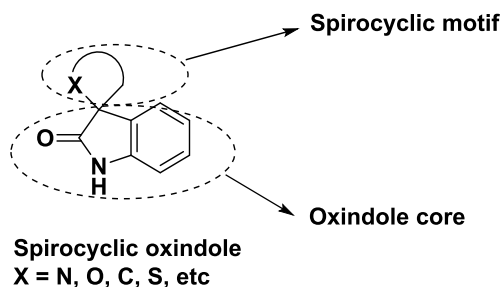
Figure 3.3. Spirooxindole motif.

From a medicinal chemistry design perspective, the introduction of a restriction of structural conformation imposed by the incorporation of a fused spirocyclic moiety is a widely used strategy to induce a reduction of conformational entropy upon binding to proteins.[232] As such, spirooxindoles have emerged as attractive scaffolds and synthetic targets across a wide range of therapeutic areas and have been shown to confer a broad range of biological activities. For example, **NITD-609** was developed as a potent antimalarial compound by the Novartis Institute for Tropical Diseases and rapidly inhibits protein synthesis in *Plasmodium falciparum* (Figure 3.2).[236] In addition, the MDM2 inhibitor **MI-219** was reported to disrupt p53-MDM2 binding, leading to p53 activation and suppression of tumour cell growth in human malignant B-cell lymphomas (Figure 3.2).[237,238]

Despite the increasing interest in recent years in the preparation of spirooxindoles, efforts in novel synthetic methodologies have been slower than those published for the preparation of 3,3'-disubstituted oxindoles, owing to the synthetic challenges of such complex polycyclic oxindole motifs. A publication analysis by Franz *et al*. in 2012 shows that the number of reports for the preparation of spirooxindoles has drastically increased over the last decade and with a significant increase in 2010-2011 (Figure 3.4).[239]

Furthermore, the recent increase in reviews and different approaches for the efficient synthesis of spirooxindoles, both enantioselective and non-enantioselective, clearly highlight the ongoing synthetic challenges with such scaffolds and requirements for novel synthetic strategies. [232,239–243]
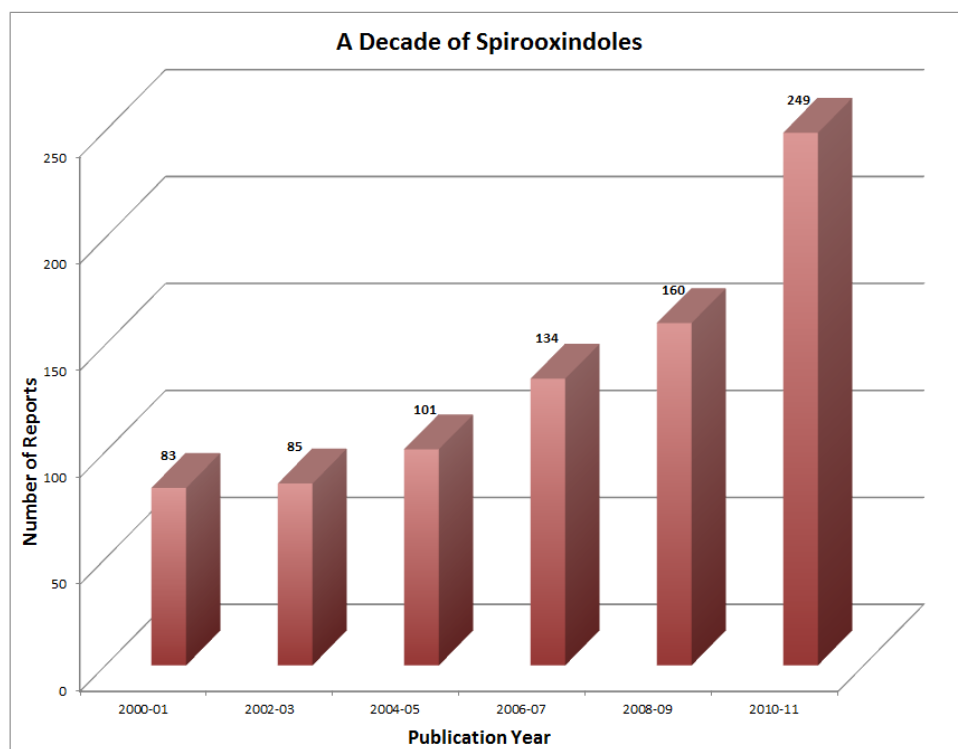
Figure 3.4. Publication rate for spirocyclic oxindoles for the 2000 – 2011 period. Reproduced from Franz *et al.*[239]

3.2.2   Retrosynthetic Analysis

The retrosynthetic approaches considered for the preparation of spirooxindole scaffold **18** (Figure 3.5) are described in Figure 3.6. The first two initial disconnections considered (Figure 3.6, route 1 and route 2) relied on starting from protected oxindoles or isatins since both of these can be readily purchased or easily prepared. It was envisaged that either of these two synthetic routes would allow the preparation of a range of simple spirooxindoles as represented by the general structure **18** where n = n' = 1 and X = S (thietane), O (oxetane) or N (azetidine) and these chemotypes would serve as an initial synthetic model for the preparation of more complex spirooxindoles.
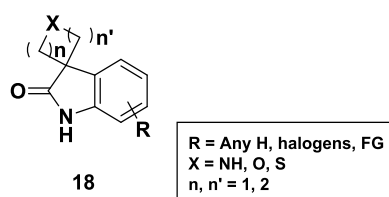
Figure 3.5. Spirooxindole motif.

In a similar fashion to the preparation of **RV-39**, that was obtained *via* the *bis*-alkylation of a protected oxindole **19** (R = H, R' = PMB) with 1,2-dibromoethane, the oxindoles of general structure **19** could be *bis*-alkylated to form the required spirooxindole **18** (Figure 3.6, route 1). Deprotonation of *N*-protected oxindole **19** with a base such as K_2CO_3, LiHMDS, NaH or nBuLi followed by the subsequent trapping of the formed anion with a range of alkyl *bis*-halides should indeed allow access to the spirocyclic targets (Figure 3.6, route 1).[244,245] However, this methodology suffers from the need to prepare and use highly toxic *bis*-alkylating agents. Sulfur mustard reagents (n = n' = 2, X = S, Y = Cl) for example have very powerful vesicant effects and are mutagenic and carcinogenic agents. As a consequence, the preparation of spirooxindoles **18** *via* this methodology was not considered as an attractive synthetic route to explore a diverse range of spirooxindoles.
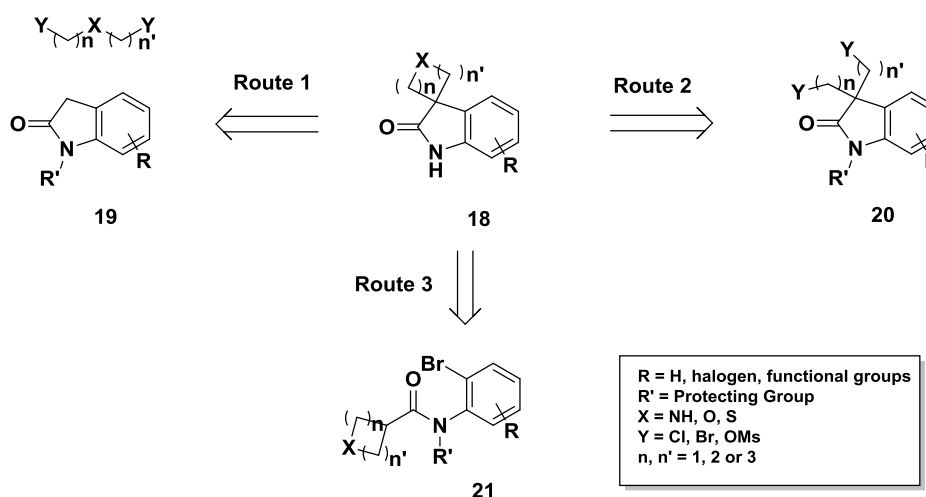
Figure 3.6. Retrosynthetic approach to spirooxindoles.

The formation of oxetane, azetidine and thietane has been reported on a range of very diverse templates, including the preparation of 3,3'-spirocyclic oxindoles.[246–254] Nucleophilic displacement of a 1,3-*bis*-electrophilic synthon **20** (1,3-dimethyl sulfonates or 1,3-dihaloalkanes for example) with either an oxygen, sulfur or ammonia nucleophile equivalent (Figure 3.6, route 2) would allow for late stage formation of the spirocyclic oxetane, thietane and azetidine rings respectively (n = n' = 1). Similarly to route 1, this approach also relies on a pre-existing oxindole precursor for the formation of the key quaternary C(3) centre at a late stage of the synthesis, making it an attractive route for the rapid generation of a small array of compounds. The second approach (Figure 3.6, route 2) is discussed in section 3.2.3 where late stage ring closures to form the required spirooxindoles were attempted.

Palladium catalysed cyclisation represents another powerful and more contemporary approach for the formation of 3,3'-*bis*-substituted oxindoles as initially reported by Hartwig *et al*.[255] Using a similar strategy to the one described by Hartwig *et al*., 3,3'-spirooxindoles could also be prepared *via* a palladium-catalysed intramolecular α-arylation of 2-halo amides **21** (Figure 3.6, route 3). Although introduced very early in the synthesis, the spirooxindoles could be prepared from a wide range of commercially available carboxylic acids and 2-bromo anilines or prepared with limited efforts for more complex templates. The palladium-catalysed intramolecular α-arylation would avoid the synthesis of the oxindole precursors as suggested in Figure 3.6, routes 1 and 2. The synthesis of spirocyclic oxindoles *via* this approach is extensively discussed in section 3.2.4.

3.2.3 Synthesis of Spirooxindoles *via bis*-Electrophilic Displacement

As discussed in the previous section, the initial synthetic strategy (Figure 3.6, route 2) envisaged the formation of the spirocycles **22a-c** (Figure 3.7) *via* a nucleophilic displacement of a 1,3-*bis*-electrophilic synthon **20** at a late stage of the synthesis, allowing for a convergent preparation of all 3 spirocyclic rings **22a**, **22b** and **22c**.

22a X = O
22b X = N-R
22c X = S
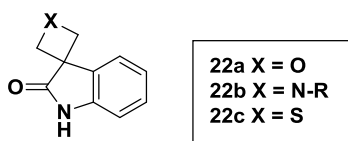
Figure 3.7. Spirocyclic oxindoles initial targets.

Gonzalez-Lopez de Turiso *et al.* reported a similar strategy for the preparation of a spiro[indoline-3,3'-thietane]-2-one derivatives where sodium sulfide was used as a nucleophilic source of sulfur.[251] The *para*-methoxybenzyl protected oxindole **25** was obtained in 2 steps from the commercially available isatin **23** *via N*-alkylation with PMB-Cl using sodium hydride as a base (Scheme 3.1). The protected isatin **24** intermediate was reduced under Wolff-Kishner conditions, by pre-forming the hydrazone in the presence of hydrazine hydrate in n-butanol, followed by addition of triethylamine to promote the solvent-induced proton abstraction to give oxindole **25**, obtained in 96% yield over the 2 steps (Scheme 3.1). Treatment of oxindole **25** with an excess of paraformaldehyde in the presence of K_2CO_3 gave the *bis*-alkylated intermediate **26** which upon reaction with methanesulfonyl chloride led to the formation of the key 1,3-*bis*-mesylated oxindole intermediate **27** in 42% yield over the 2 steps. However, when **27** was heated with sodium sulfide in DMF as described by Gonzalez-Lopez de Turiso *et al*., none of the

desired product **28c** was formed and the unreacted 1,3-*bis*-mesylate **27** was recovered despite lengthy reaction times and elevated temperature (100 °C under conventional heating and 160 °C under microwave irradiation).[251] Similar results were observed when potassium thioacetate was used as an alternative sulphur source instead of sodium sulfide as reported by De Carvalho *et al.*[256]

Scheme 3.1.
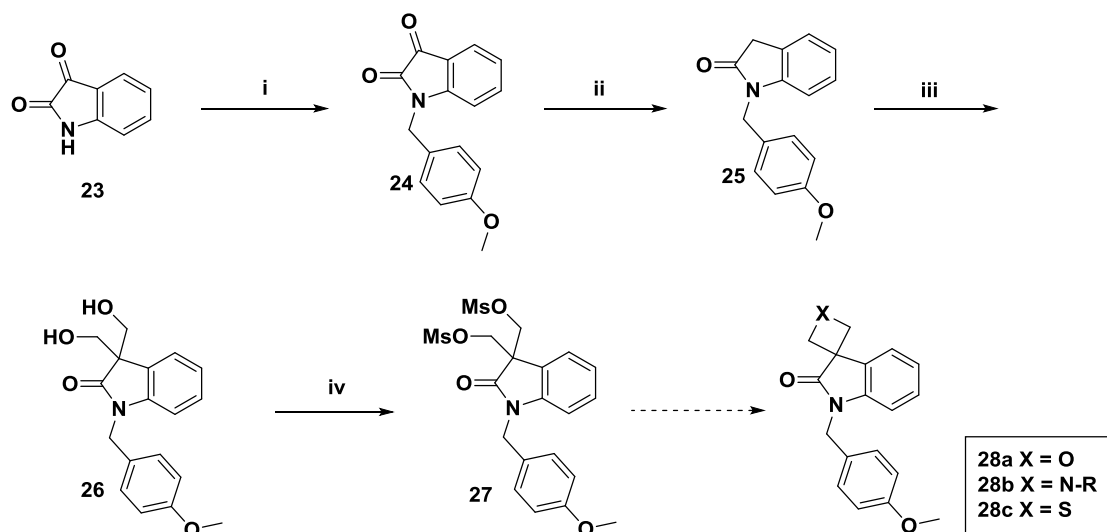
Reagents and conditions: (i) NaH, PMB-Cl, DMF, 0 °C to 70 °C, 4 h, 100%; (ii) Hydrazine hydrate, *n*BuOH, 80 °C, 3 h then Et₃N, 100 °C, 48 h, 96%; (iii) paraformaldehyde, K₂CO₃, THF, rt, 16 h, 52%; (iv) MeSO₂Cl, Et₃N, CH₂Cl₂, rt, 4 d, 82%.

Further precedents for the formation of spironucleosides resulting from the displacement of 1,3-*bis* electrophilic moiety with benzylamine have also been reported.[250,253] However, when applying a similar methodology and heating **27** with benzylamine at 110 °C in THF or under microwave irradiation at 160 °C in neat benzylamine, none of the product **28b** could be detected.

Mandal *et al.* reported that oxetanes could also be formed from 1,3-*bis*-mesylate glucofuranose intermediates **29** which upon treatment with sodium hydride would undergo an addition-elimination process, providing the oxetane **30** upon hydrolytic work up (Scheme 3.2).[253] When **27** was heated with sodium hydride in DMF at 100 °C, no oxetane product **28a** was observed and the unreacted 1,3-*bis*- mesylate **27** was recovered.

The closest precedent for the preparation of **28a** was described by Lindsley *et al.*, reporting the formation of spirooxetane, albeit in very low yield (6% yield) *via* mono triflation of a 1,3-*bis*-diol

and nucleophilic displacement. Although these exact conditions were not tried (Tf$_2$O, lutidine, CH$_2$Cl$_2$, -78 °C to rt), the low yield reported by Lindsey *et al*. and overall failed attempts described above to access any spirooxindoles only reinforced the need for an alternative strategy that would be more amenable to a robust synthesis delivering a diverse range of novel spirocyclic analogues in sufficient quantities.[252]

Scheme 3.2. Proposed mechanism for the formation of oxetane from 1,3-*bis* mesylate under sodium hydride conditions.[253]
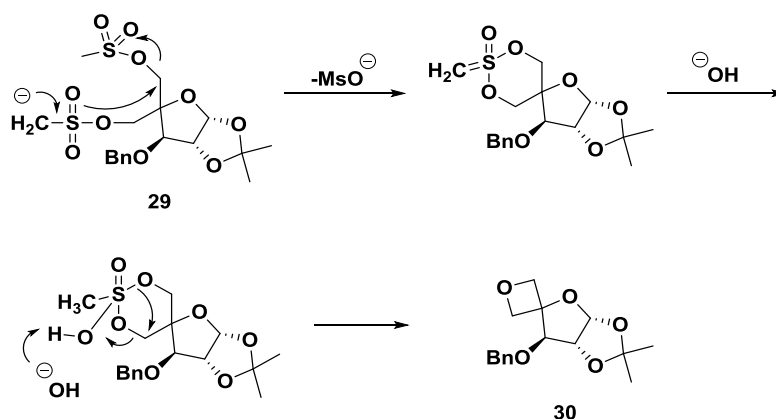
3.2.4 Synthesis of Spirooxindoles *via* α-Arylation

Following on from the initial difficulties encountered in attempting to form the spirooxindoles such as **28a-c**, the third strategy (Figure 3.6, route 3), previously mentioned in section 3.2.2 was envisaged.

Whilst the α-arylation or CH activation (both terminologies will be used interchangeably in the remainder of this chapter) has been the subject of numerous reviews over the past two decades, the predominant focus has been on the formation of C(sp^2)-C(sp^2) bonds between aryl halides and 'activated' C(sp^2)-H bonds.[250,257–260] The formation of C(sp^3)-H C(sp^2) bonds *via* a transition metal catalyst however has received far less attention but the reported examples have allowed access to the formation of complex centres without the requirement of any organometallics, involving extra synthetic steps, which can be difficult and costly to prepare.[261–268]

Initially reported by Hartwig in 2001, the α-arylation of 2-halo anilides under palladium-catalysed conditions allowed the intramolecular cyclisation of 3-mono substituted oxindoles but

more encouragingly the preparation of 3,3'-*bis*-substituted oxindoles under mild conditions (Scheme 3.3, equation A).[255]

Scheme 3.3. Formation of oxindoles from 2-haloanilides according to Hartwig *et al.* (equations A and B) and Maison *et al.* (equation C).[255,269]
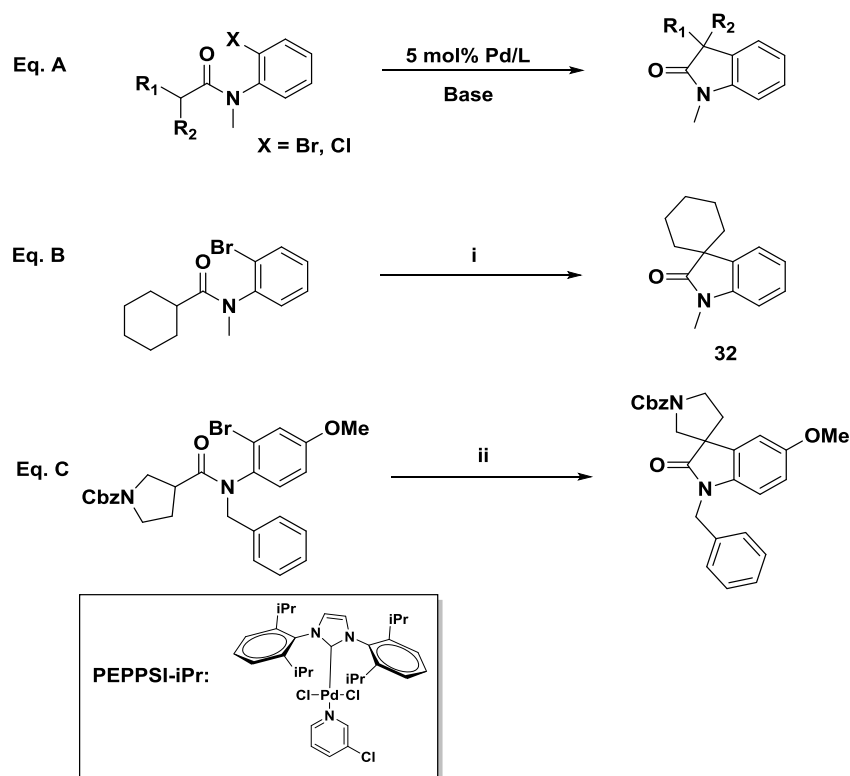
Reagents and conditions: (i) Pd(OAc)$_2$ (5 mol %), PCy$_3$ (5 mol %), NaO^{t}Bu, 1,4-dioxane, 24 h, 50 °C, 93%; (ii) PEPPSI™-iPr, NaO^{t}Bu, toluene, 110 °C, 81%.

The effect of the ligands, palladium, base solvent and temperature were investigated. Pd(OAc)$_2$ used as the palladium source, PCy$_3$ as the ligand and sodium *tert*-butoxide as the base in 1,4-dioxane used as solvent were found to be the best conditions for this cyclisation reaction. Under these conditions, a small number of templates were exemplified bearing C(3) aliphatic spirooxindoles such as **32** which was obtained in high yield (Scheme 3.3, equation B). Surprisingly, this intramolecular α-arylation synthetic strategy has had very limited use until recently when Maison *et al.* in 2010 explored the scope and optimisation of the reaction (palladium, ligands, reaction temperature and potential *N*-anilide protecting groups) specifically for the formation of spirooxindoles (Scheme 3.3, equation C).[269] Under the conditions that were evaluated on a small subset of 2-bromo anilides, Maison *et al.* concluded that, although the conditions reported by Hartwig *et al.* worked well, the best results for the formation of spirooxindoles were obtained when using PEPPSI™-iPr as a catalyst in toluene at 110 °C.[269,270]

The efficiency of this palladium-catalysed intramolecular cyclisation methodology for the preparation of spirooxindoles was demonstrated in the racemic synthesis of the natural product Horsfiline (Figure 3.2).[269]

Despite the lack of mechanistic studies for this palladium-catalysed arylation, it is presumed that the α-arylation of 2-halo anilides is facilitated by the pseudo sp^2 nature of the α-(sp^3)-H from the anilide and its increased acidity, resulting in facilitated palladium insertion.[263,266] The mechanism of the cyclisation presumably involves an oxidative addition of palladium into the aryl bromide bond (Figure 3.8, intermediate A), followed by a six-membered palladacycle (Figure 3.8, intermediate B) which can undergo a reductive elimination to regenerate Pd(0) and give the product (Figure 3.8, product C) (Figure 3.8). Hartwig *et al.* initially suggested that the reaction mechanism proceeded *via* an enolate pathway although there was no evidence to support this mechanism pathway.[255]
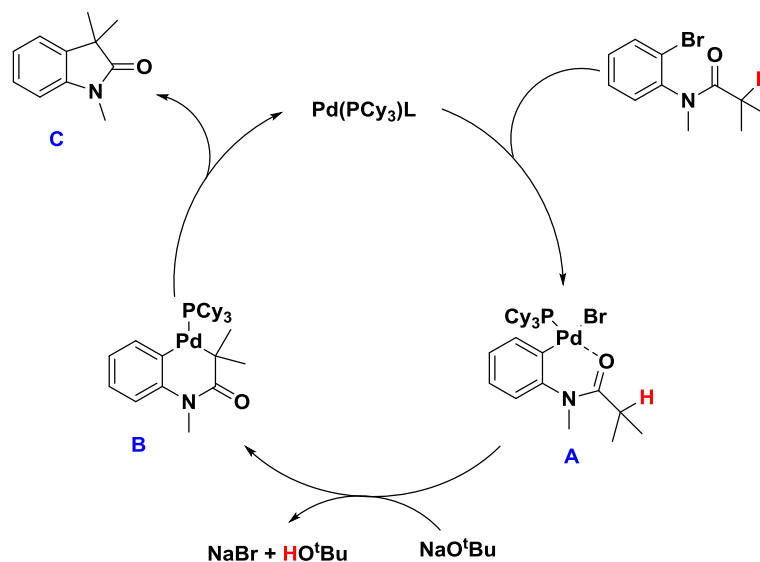
Figure 3.8. Proposed mechanism pathway for α-arylation of 2-bromo anilides proposed by Hartwig *et al.*[255]

More recently, Charette *et al.* have developed a silver-promoted, palladium catalysed arylation of cyclopropanes which is claimed to proceed *via* a direct metalation-deprotonation pathway involving the irreversible formation of a palladacycle and facilitated by K_2CO_3 used as a base (Figure 3.9).[263] Under the proposed mechanism proposed by Charette *et al.*, the silver salts are used to abstract the halide, generating a reactive cationic palladium species (Figure 3.9, intermediate B) that can further proceed to 6-membered palladacycle in the presence of CO_3^{2-} (Figure 3.9, intermediate D).

To further confirm the proposed mechanism pathway, Charette *et al*. performed the silver-promoted arylation with enantio-enriched cyclopropane amides that proceeded with no notable epimerisation, refuting the enolate mechanism pathway, at least under those silver-promoted reaction conditions.
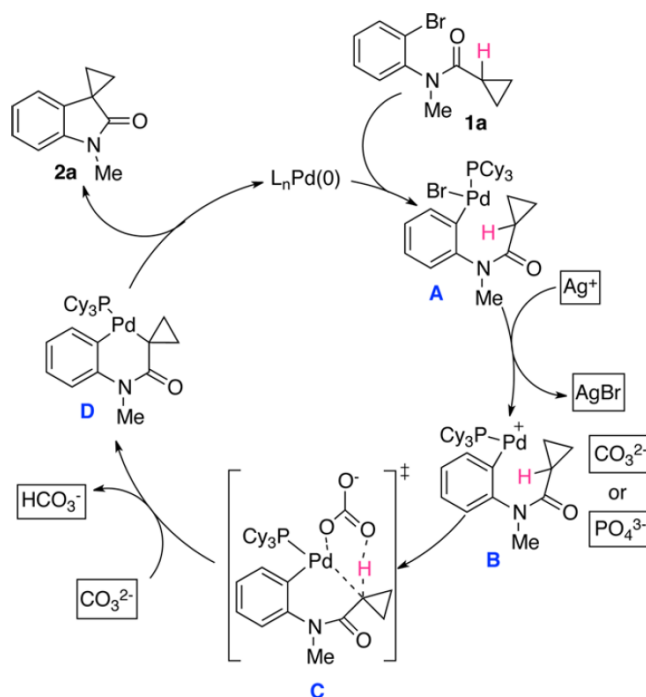
Figure 3.9. Silver-mediated direct metalation-deprotonation pathway proposed by Charette.[263]

There is however not enough evidence to confidently determine the mechanistic pathway of the palladium-catalysed α-arylation reaction under the conditions reported by Hartwig and Maison.

An initial model was envisaged where the 3,3'-azetidine oxindole **22b** (Figure 3.7, R = Boc) would be prepared using the conditions reported by both Hartwig and Maison, and would serve as an initial strategy to allow the rapid exploration of spirooxindoles.

The requisite protected amide **35** could be easily prepared from 2-bromo aniline and the protected azetidine carboxylic acid as shown in Scheme 3.4. Thus, commercially available 1-*tert*-butoxycarbonylazetidine-3-carboxylic acid was coupled with 2-bromo aniline **33** under standard amide formation, producing amide **34** which was subsequently protected *via* alkylation with *para*-methoxybenzyl chloride in the presence of sodium hydride to give the intermediate **35** in good yield (64% yield over 2 steps).

Scheme 3.4.
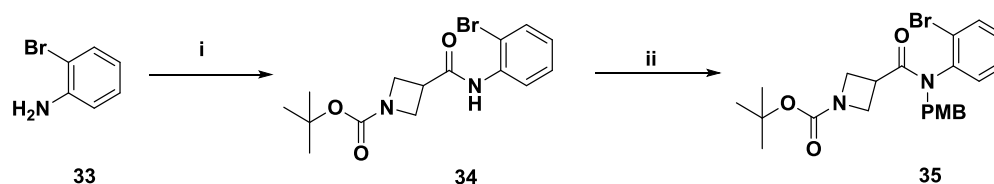
Reagents and conditions: (i) 1-*tert*-butoxycarbonylazetidine-3-carboxylic acid, DMAP, EDCI.HCl, CH$_2$Cl$_2$, rt, 4 d, 80%; (ii) NaH, PMB-Cl, DMF, 0 °C to rt, 16 h, 80%.

Interestingly, for compound **35**, the two –CH$_2$ protons (H-1') of the *para* methoxybenzyl group form a very characteristic pair of enantiotopic protons at δ 5.55 ppm (doublet) and δ 3.98 ppm (doublet) in CDCl$_3$, presumably due to hindered rotation of the PMB moiety, leaving the two protons in very different environments, hence the difference in chemical shifts (Figure 3.10). Furthermore, the azetidine protons H-9 and H-10 all appear to be in a different environment, leading to 4 different broad signals observed at δ 4.28 ppm, δ 3.98 ppm, δ 3.70 ppm and δ 3.56 ppm. However, neither homonuclear correlation (COSY) nor through-space correlations (NOESY) allowed to unambiguously conclude on the identification of each of the 4 signals seen for H-9 and H-10 (Figure 3.10).
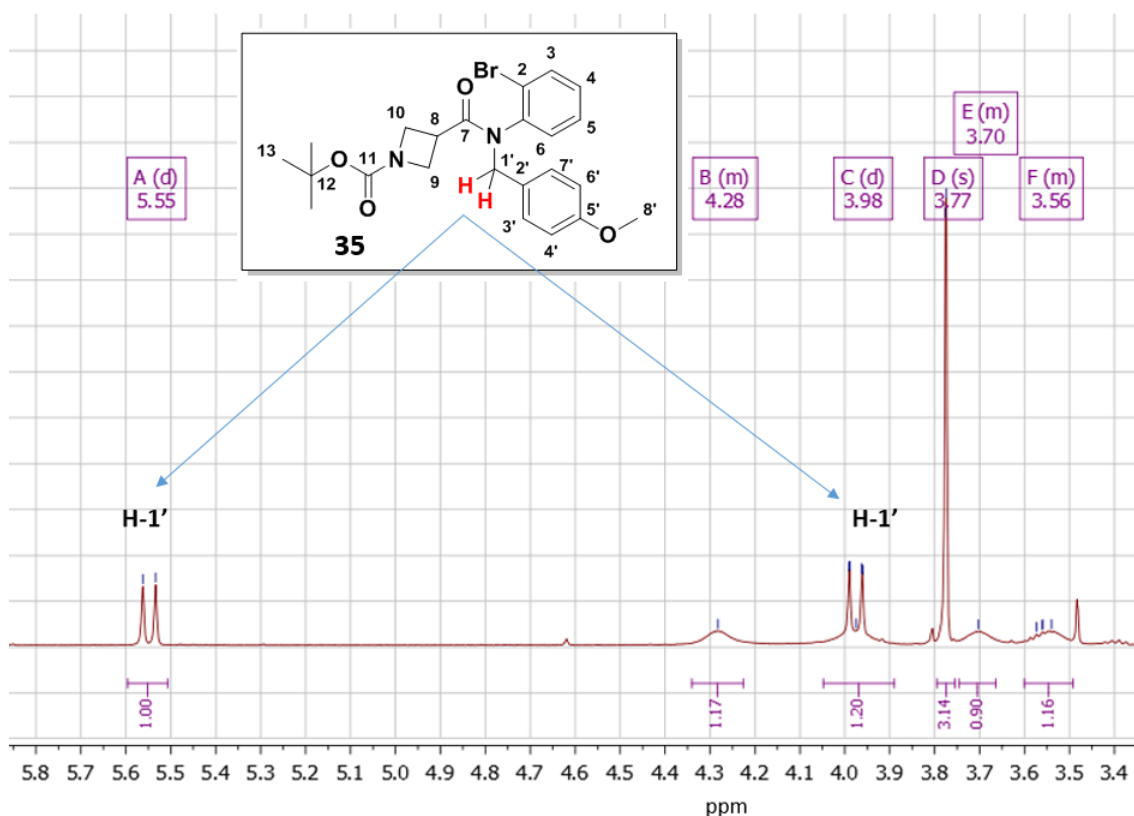
Figure 3.10. Enantiotopic protons formed from PMB restricted rotation for **35**.

The initial palladium-catalysed cyclisation of the amide **35**, using the conditions reported by Hartwig *et al*., in 1,4-dioxane in the presence of sodium *tert*-butoxide (1.5 equiv.) and catalytic amount of both Pd(OAc)$_2$ (10 mol%) and PCy$_3$.HBF$_4$ (10 mol%) at 80 °C over 5 hours, proceeded smoothly and gave the desired spirooxindole **36** in good yield (78%) and no significant level of any by-products were detected (Scheme 3.5).

Scheme 3.5. Palladium-catalysed α-arylation attempt.
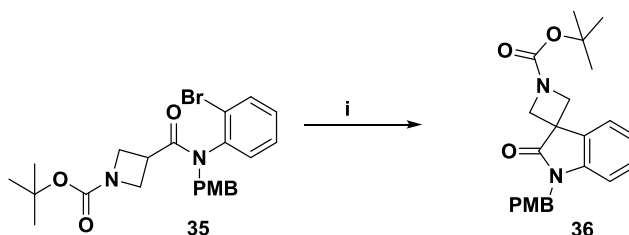
Reagents and conditions: (i) Pd(OAc)$_2$, PCy$_3$.HBF$_4$, NaO^{t}Bu, 1,4-dioxane, 80 °C, 5 h, 78%.

The formation of the spirooxindole **36** could be in part confirmed by ^{1}H-NMR spectroscopy, where the azetidine proton α to the amide which was previously identified as a multiplet at δ 3.06 ppm in CDCl$_3$ for the intermediate **35**, had clearly disappeared (Figure 3.11). Also, the enantiotopic protons (H-1') observed for **35** as two doublets have now collapsed to a singlet at δ 4.83 ppm in CDCl$_3$ for **36** and presumably linked to a more constrained system, enabling free rotation of the *para*-methoxybenzyl moiety.
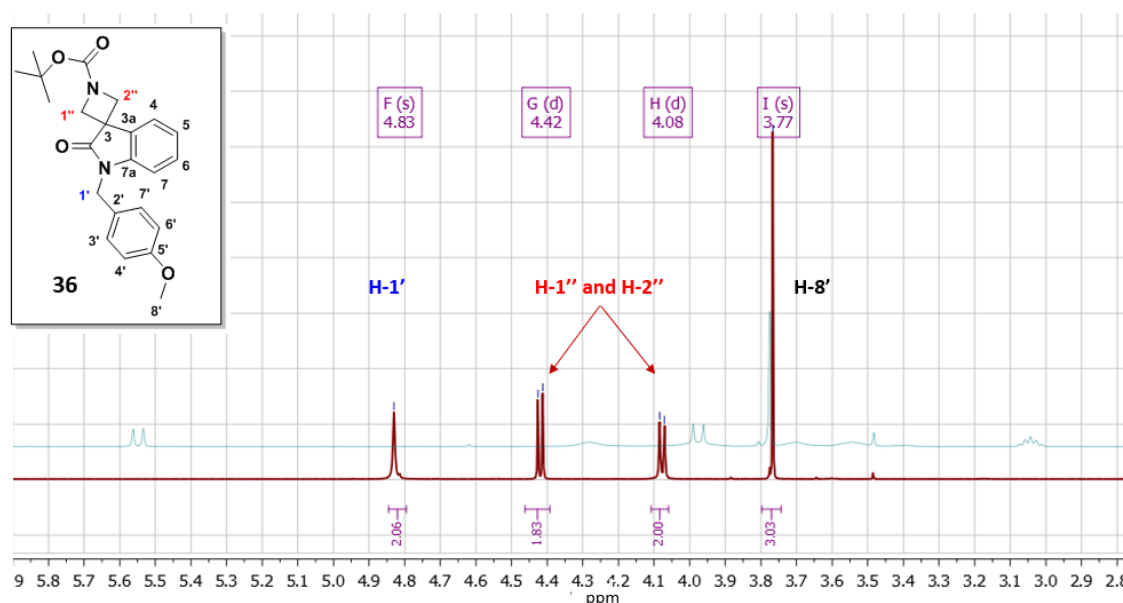
Figure 3.11. ^{1}H-NMR in CDCl$_3$ of compound **36** (red spectrum). The spectrum of compound **35** previously described in Figure 3.10 is superimposed (blue spectrum).

Furthermore, heteronuclear multiple-bond correlation spectroscopy (HMBC) could also confirm the formation of the C(3) quaternary centre. Indeed, a long range correlation between the C-3 carbon at δ 42.4 ppm and the H-4 proton at δ 7.55 ppm as well as correlations between the C-3a carbon at δ 130.5 ppm and both protons H-5 at δ 7.11 ppm and H-7 at δ 6.78 ppm could be observed, confirming unambiguously the formation of the spirooxindole **36** by intramolecular arylation (Figure 3.12).
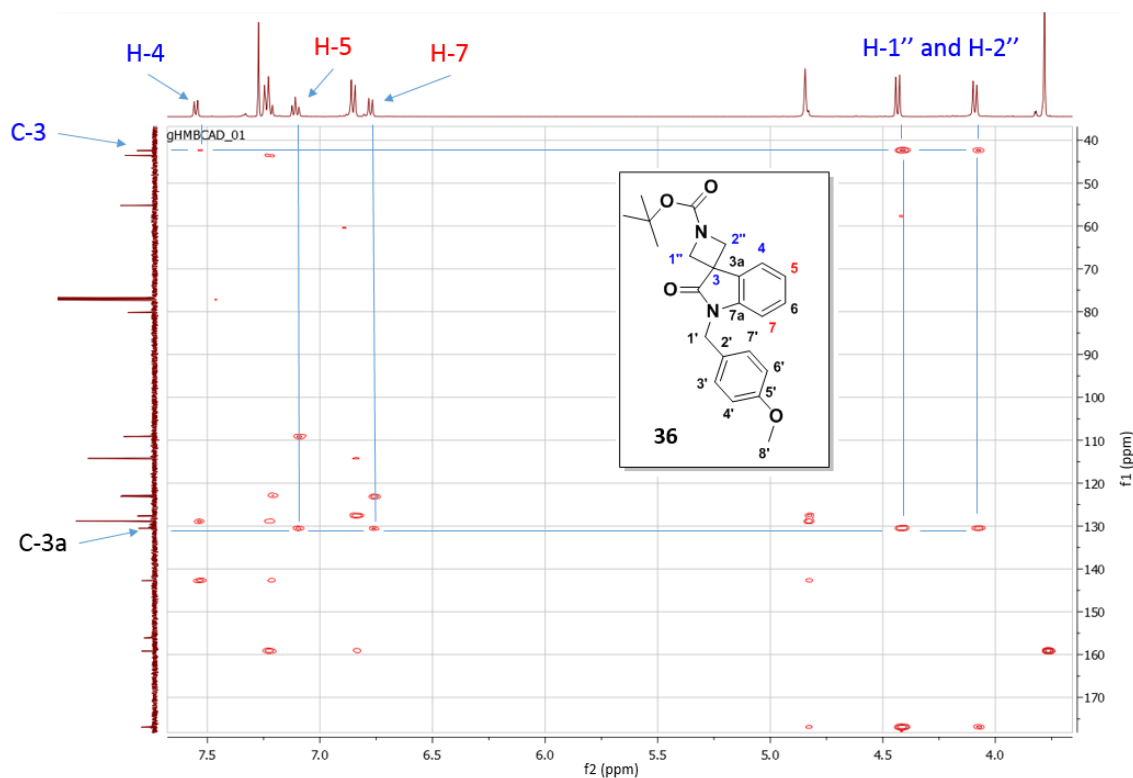
Figure 3.12. Heteronuclear multiple-bond correlation spectroscopy (HMBC) of compound **36** in CDCl$_3$. The blue lines represent the HMBC correlations observed between the carbons and protons. Long range correlation between the C-3 (δ 42.4 ppm) and the H-4 proton (δ 7.55 ppm) and correlations between the C-3a (δ 130.5 ppm) and the protons H-5 (δ 7.11 ppm) and H-7 (δ 6.78 ppm).

To eliminate any possibility of the arylation undergoing a palladium-free pathway, the reaction was performed in the absence of any palladium and ligands. Heating intermediate **35** in the presence of sodium *tert*-butoxide (1.5 equiv.) initially at 80 °C for 5 hours and then to 130 °C for 16 hours only led to unreacted amide **35**, supporting the palladium-catalysed reaction pathway. Furthermore, in an attempt to circumvent the use of any amide protecting group, the non-protected amide **34** was also subjected to the same palladium arylation reaction conditions as reported in Scheme 3.5 but unfortunately failed to generate any cyclised oxindole. Increasing

the temperature of the reaction up to 150 °C only led to reagent degradation, suggesting that the nitrogen of the unprotected amide may interfere with the reaction conditions and potentially coordinate to the palladium or may be deprotonated under the basic conditions used, becoming unreactive as a sodium salt. Additionally, increasing the amount of base from 1.5 equivalents to 2.5 equivalents led to the same unsuccessful results, supporting the requirement a nitrogen protecting group.

On scaling up the reaction to 18 mmol and under the same reaction conditions, a mixture of product **36** and des-brominated by-product **36a** was obtained in a 3:7 ratio (Scheme 3.6). The outcome of the isolated by-product **36a** is described in Scheme 3.9.

Scheme 3.6. α−Arylation scale up.
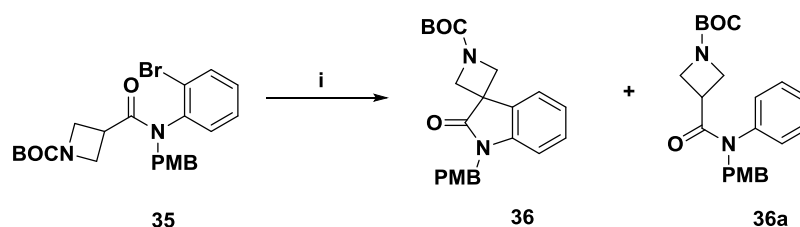
Reagents and conditions: (i) Pd(OAc)$_2$, PCy$_3$.HBF$_4$, NaO^{t}Bu, 1,4-dioxane, 80 °C, 16 h, 68% overall.

Treatment of the spirooxindole **36** with trifluoroacetic acid in dichloromethane at 0 °C cleanly cleaved the Boc protecting group without removal of the *para*-methoxybenzyl moiety in 65% yield (Scheme 3.7). The subsequent acylation of the azetidine **37** with acetyl chloride in the presence of triethylamine gave **38** in an excellent 95% yield.

Scheme 3.7. Spirocyclic azetidine oxindole BOC deprotection and acylation.
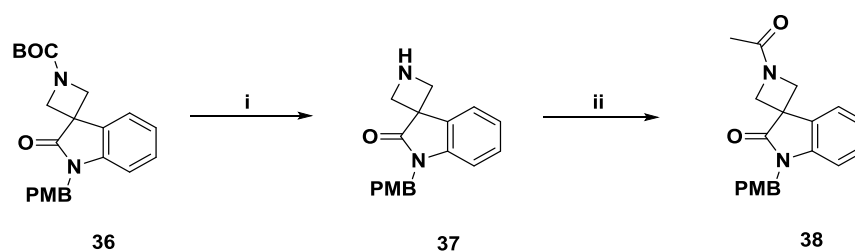
Reagents and conditions: (i) TFA, CH$_2$Cl$_2$, 0 °C, 2 h, 65%; (ii) AcCl, Et$_3$N, CH$_2$Cl$_2$, rt, 16 h, 95%.

However, removal of the PMB protecting group of intermediate **38** proved more difficult than anticipated and required some optimisation (Scheme 3.8). The introduction of the *para*-methoxybenzyl protecting group was initially selected based on reported literature precedents as a widely used protecting group for oxindoles.

Scheme 3.8. PMB deprotection.

38   39
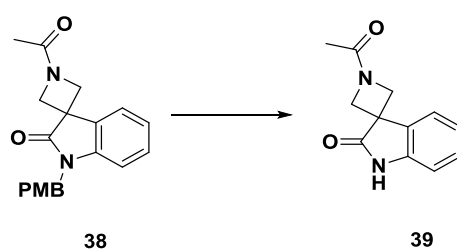
Initially, oxidative cleavage in conditions such as ceric (IV) ammonium nitrate (CAN) in acetonitrile and water at room temperature or 2,3-dichloro-5,6-dicyano-1,4-benzoquinone (DDQ) in dichloromethane and water at room temperature both led mainly to decomposition of **38** and no desired product could be isolated cleanly (Table 3.5, entries 1 and 2 respectively).[271,272] Under protolytic conditions with trifluoromethanesulfonic acid (Table 3.5, entry 3) at room temperature, the cleavage of the *para*-methoxybenzyl group also proved unsuccessful despite lengthy reaction times and led to compound degradation.[273] Heating the intermediate **38** in trifluoroacetic acid in the presence of methoxybenzene (anisole) failed to deliver any product when heating to 60 °C and 80 °C (Table 3.5, entries 4 and 5 respectively). However, refluxing the protected spirooxindole **38** in trifluoroacetic acid in the presence of anisole led to the cleavage of the PMB group in a moderate 38% yield but only after extended reaction time (Table 3.5, entry 6, 4 days at reflux). Pleasingly, rapid cleavage of the PMB could be obtained by heating the reaction mixture under microwave irradiation at 150 °C (Table 3.5, entry 7), delivering the spirooxindole **39** in a moderate 46% yield but which could be reproduced consistently over multiple attempts. Anisole has been reported to be acting as a scavenger and source of proton wherein the *para*-methoxybenzyl group is transferred from the *N*-oxindole to the *para* position of anisole.[274–276]

Table 3.5. PMB cleavage for the preparation of intermediate **39**.

Entry	Reagents	Temperature	Time	Yield
1	CAN	20 °C	2 to 24 hours	Degradation
2	DDQ	20 °C	2 to 24 hours	Degradation
3	CF₃SO₃H	20 °C	2 days	Degradation
4	TFA/anisole	60 °C	24 hours	No reaction[b]
5	TFA/anisole	80 °C	24 hours	No reaction[b]
6	TFA/anisole	100 °C	4 days	38%[a]
7	TFA/anisole	150 °C	2.5 hours	46%[a,c]

[a]Isolated yield; [b]Unreacted starting material; [c]Under microwave irradiation.

With the harsh conditions required to remove the *para*-methoxybenzyl protecting moiety and moderate yields obtained, a series of alternative protecting groups were examined. Unfortunately, the best results were obtained when using *para*-methoxybenzyl chloride and, although precedented, any attempts to protect intermediate **34** (Scheme 3.4) with an acetate, methyl carbamate or *tert*-butyl carbamate led to unsatisfactory results with either no reaction or decomposition of the starting materials.[277–280] However, the examples of palladium-mediated α-arylation reported by both Hartwig and Maison contained oxindoles bearing either a *N*-methyl or *N*-benzyl moiety. The introduction of a carbamate or acetyl protecting groups may have led to a different reactivity profile with regards to the formation of the spirooxindoles. Since excellent results were obtained for the key palladium-catalysed α−arylation step with the *para*-methoxybenzyl protecting group, no further investigation of any alternative protecting groups was sought.

Compound **36a** which was isolated as a by-product during the α−arylation scale up (Scheme 3.6) was further converted to the acylated amine **41** in 3 steps, following similar conditions to those described for the preparation of **39** (Scheme 3.9). Compound **36a** was BOC deprotected by treatment with trifluoroacetic acid in dichloromethane at room temperature, followed by acylation with acetyl chloride in dichloromethane in the presence of triethylamine. The intermediate was isolated in high yield over the 2 steps. Following on the conditions optimised for the PMB deprotection of intermediate **38**, the amide **41** was obtained in 55% yield after treatment with trifluoroacetic acid at 150 °C under microwave irradiation (Scheme 3.9). The

amide **41** was further functionalised as a potential novel RSV inhibitor in section 3.2.5 and its antiviral activity against RSV compared directly to the azetidine spirooxindole **39** in Chapter 4.

Scheme 3.9.
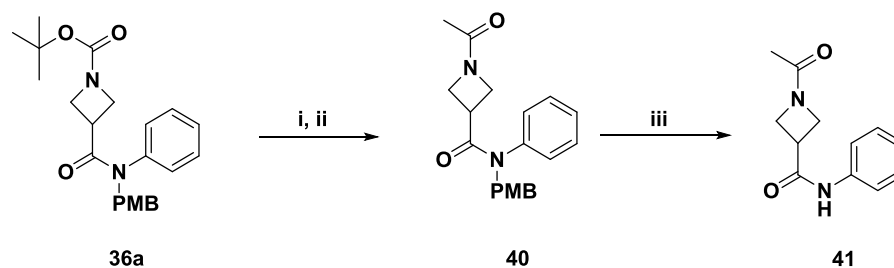
Reagents and conditions: (i) TFA, CH$_2$Cl$_2$, rt, 16 h, 97%; (ii) AcCl, Et$_3$N, CH$_2$Cl$_2$, rt, 16 h, 99%; (iii) TFA, anisole, MW 150 ^{o}C, 2.5 h, 55%.

Having established a robust route for the preparation of azetidine spirooxindoles, a small set of compounds was prepared to explore the scope of the palladium-catalysed α-arylation reaction and the Structure-Activity Relationship (SAR) within the spirocyclic oxindoles series. All the amides **42a-e** could be obtained from the commercially available carboxylic acids and anilines (Scheme 3.10). Tetrahydrofuran-3-carboxylic acid leading to the preparation of **42b** was purchased as a racemic mixture rather than both single enantiomers, mainly due to cost and availability of each enantiomer.

Scheme 3.10.

Compound	42	Yield	Compound	43	Yield
42a		86%	43a		74%
42b		63%	43b		85%
42c		88%	43c		71%
42d		45%	43d		79%
42e		98%	43e		89%
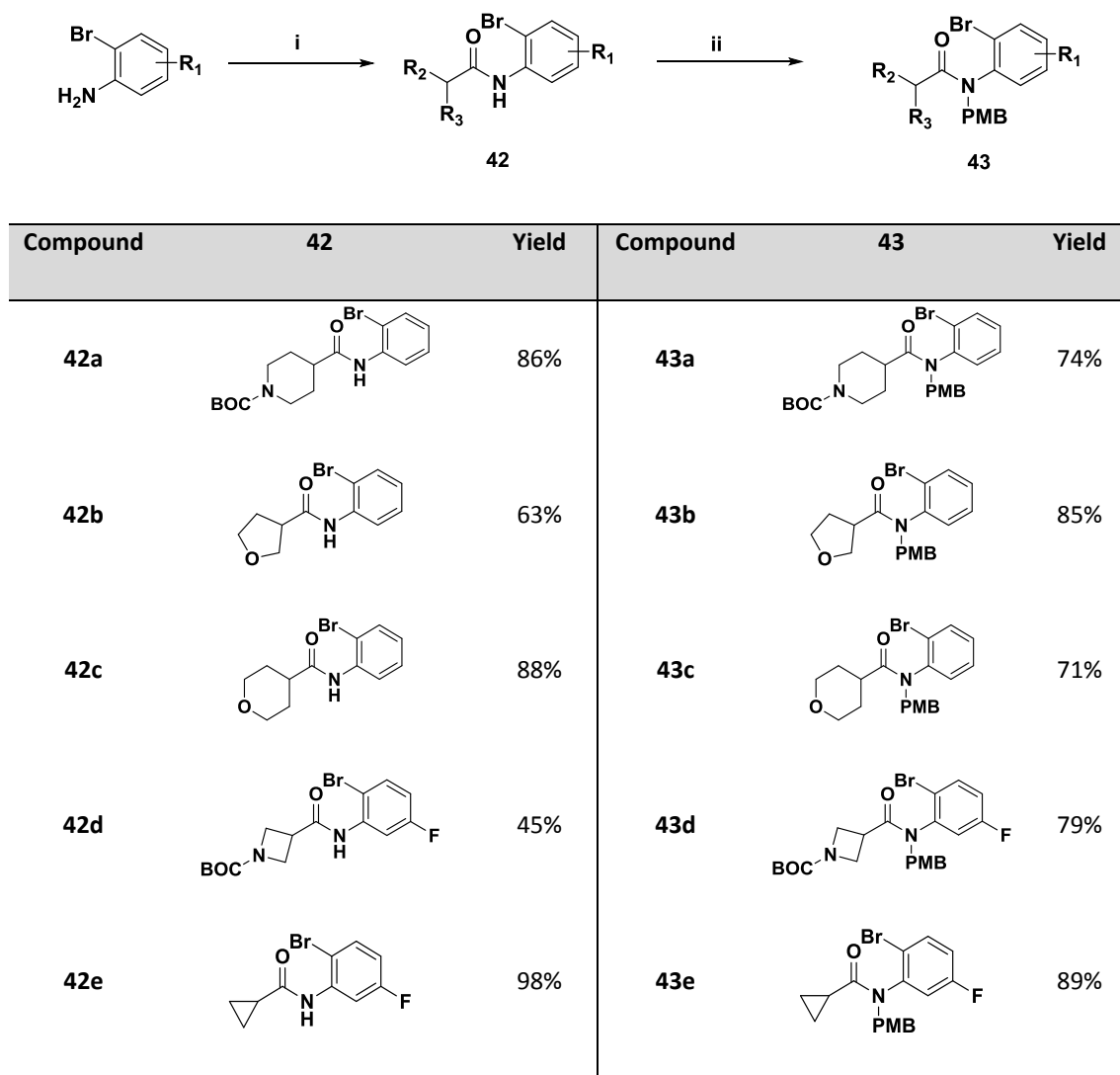
Reagents and conditions: (i) Carboxylic acid, DMAP, EDCI.HCl, CH$_2$Cl$_2$, rt, 16 h to 4 days (**42a**, **42b** and **42d**) or T$_3$P, pyridine, EtOAc (**42c** and **42e**); (ii) NaH, PMB-Cl, DMF, 0 °C to rt, 16 h.

Initially, **42a**, **42b** and **42d** were prepared from either 2-bromo aniline or 2-bromo-5-fluoro aniline and the corresponding carboxylic acid *via* a *N*-(3-dimethylaminopropyl)-*N'*-ethylcarbodiimide hydrochloride-mediated coupling (EDCI.HCl) in the presence of DMAP in dichloromethane (Scheme 3.10). Surprisingly a disparity of yields was obtained under these conditions ranging from 45% for **42d** to 86% for **42a** and slow reaction times where **42b** was obtained in good yields but after 4 days of reaction time. Under the same coupling conditions, **42e** could only be isolated in poor yield (<20% yield) even after an extended reaction time. Alternative coupling agents were tried but all the activated esters tested (HBTU, HATU, TBTU) led to similar poor yields (Figure 3.13). However, propylphosphonic anhydride (T$_3$P®), a trimeric form of phosphoric acid commonly used as a dehydrating agent and as a mild peptide coupling

agent led to near quantitative yields for the formation of the amides **42c** and **42e** without any need for purification (Figure 3.13).[281]
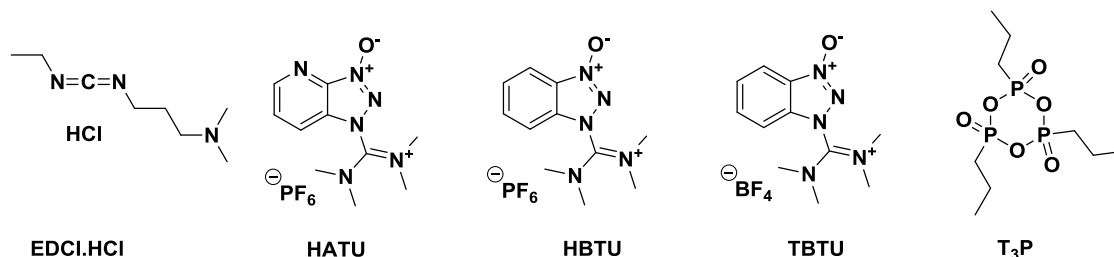
Figure 3.13. Coupling agents tried for the formation of amides **42c** and **42e**.

The amides **42a-e** were subsequently protected with the PMB moiety using *para*-methoxybenzyl chloride and sodium hydride as a base in DMF to provide **43a-e** in good to excellent yields ranging from 71% to 89%. Similarly to what was observed for compound **35**, alkylation of the amides **42a-e** with the *para*-methoxybenzyl protecting group introduces a restriction of rotation around the PMB-CH$_2$, inducing very different environments for those 2 enantiotopic CH$_2$ protons, leading to a significant difference in the chemical shifts from the ^{1}H-NMR spectrum, independent of the solvents used (CDCl$_3$, methanol-d_4 and DMSO-d_6). From the range of carboxylic acids used in the analogues exemplified in Scheme 3.10, even the smallest cyclopropyl amide **43e** induced a change of environment around the PMB-CH$_2$ moiety as depicted in Figure 3.14.
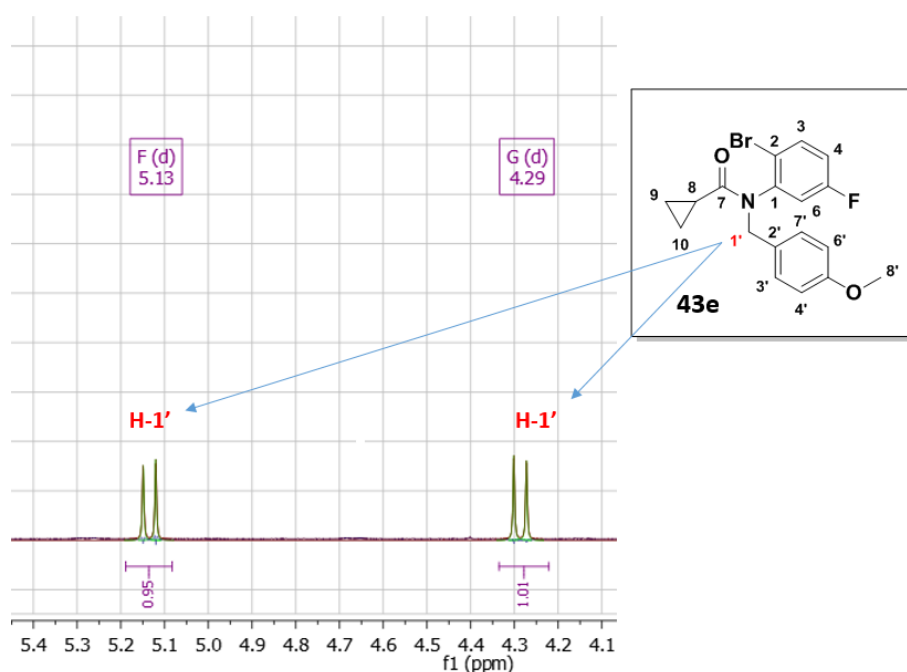
Figure 3.14. ^{1}H-NMR (DMSO-d_6) of PMB protected analogue **43e**.

Following on the conditions developed previously for the preparation of the spirooxindole **36**, the palladium-mediated α-arylation of the PMB-protected 2-bromo amides **43a-e** proceeded smoothly and gave the desired spirooxindoles **44a-c** and **44e** in moderate to good yields under thermal heating between 80 °C and 90 °C (Scheme 3.11, entries 1-3 and 5). As previously observed for the preparation of the spirooxindole **36**, the only detectable by-products were the result of the de-halogenated anilides. When the PMB-protected amide **43d** was subjected to the same reaction conditions but heating under microwave irradiation at 130 °C instead of conventional thermal heating, the spirooxindole **44d** was isolated in 87% yield, significantly reducing the reaction time and the reaction was complete after 4 minutes (Scheme 3.11, entry 4).

Scheme 3.11. Palladium-mediated α-arylation cyclisation.
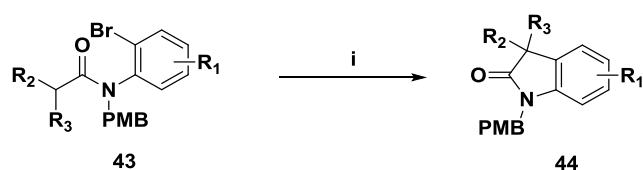
Entry	Compound	Structure	Temperature	Time	Yield
1	**44a**		80 °C	16 hours	51%
2	**44b**		90 °C	16 hours	80%
3	**44c**		90 °C	16 hours	65%
4	**44d**		130 °C	4 min[a]	87%
5	**44e**		90 °C	16 hours	69%

Reagents and conditions: (i) Pd(OAc)$_2$, PCy$_3$.HBF$_4$, NaO^{t}Bu, 1,4-dioxane; [a]microwave irradiation.

Although strategies have been reported in the scientific literature to generate asymmetric and spirocyclic C(3) quaternary stereocentres, we did not anticipate any stereogenic enrichment of the tetrahydrofuran spirooxindole **44b** under the conditions used.[282–285] As such, the tetrahydrofuran spirooxindole **44b** was treated as a racemic compound and the chiral resolution of the RSV inhibitor prepared from this intermediate is discussed in a later section. Furthermore, following on the silver-promoted palladium-catalysed arylation conditions described by Charette *et al.* (Pd(OAc)$_2$, PCy$_3$, K$_2$CO$_3$, Ag$_3$PO$_4$ in toluene at 130 °C), it may have been possible to obtain both enantiomers of **44b** starting from chirally pure (*R*) and (*S*)-tetrahydrofuran-3-

carboxylic acids. However, as described previously, the cost of each enantiomer led to the use of the racemic tetrahydrofuran-3-carboxylic acid.[263]

Pleasingly, the cyclopropyl spirooxindole **44e** (Scheme 3.11, entry 5) also proceeded smoothly under these palladium-catalysed α-arylation conditions and was obtained in 69% yield. This methodology to access cyclopropyl spirooxindoles has only been reported recently by Charette *et al.* under a silver-promoted palladium-catalysed arylation as described above and in probing the mechanistic pathway of the reaction (Figure 3.9).[263] Of particular interest, this synthetic route circumvents the alkylation of 2-oxindoles with carcinogenic and toxic 1,2-dibromoethane or 1,2-chloroethane reagents (Figure 3.15, route A) and as initially described in the retrosynthetic analysis section (Chapter 3, section 3.2.2). The only other reported methods to prepare these cyclopropyl spirooxindoles have involved Rh(II)-catalysed cyclopropanation of diazo intermediates, obtained from isatin but involving hazardous reagents for their preparation (Figure 3.15, route B).[286–288] Recently, cyclopropanation with sulfur ylides has also been reported (Figure 3.15, route C).[289] However neither of the routes B or C allow for the preparation of non-substituted 1,3-cyclopropyl spirooxindoles, further highlighting the efficiency of the palladium-catalysed α-arylation reaction from readily and cheap commercial reagents.
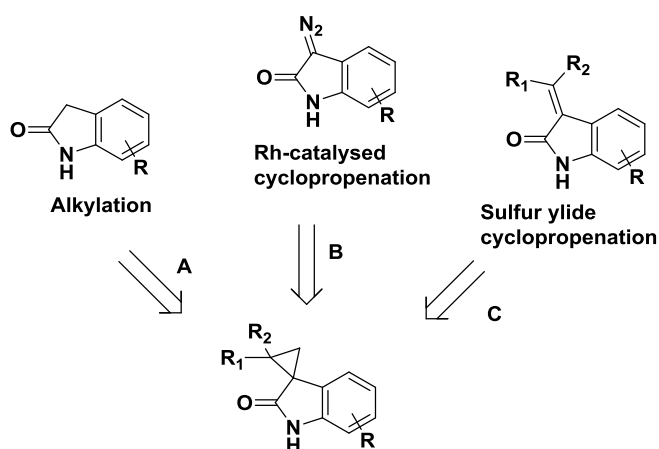
Figure 3.15. Alternative routes to 1,3-cyclopropyl spirooxindole.

In a similar fashion to the preparation of compound **36**, the spirooxindole analogues **44a-e** all showed formation of the expected cyclised product as determined by ^{1}H-NMR spectroscopy with the disappearance of the proton α to the amide. For example, in the case of the analogue **44a** (Figure 3.16), the disappearance of the multiplet at δ 2.05 ppm in CDCl$_3$ of the non-cyclised analogue **43a** supports the formation of the expected spirooxindole.
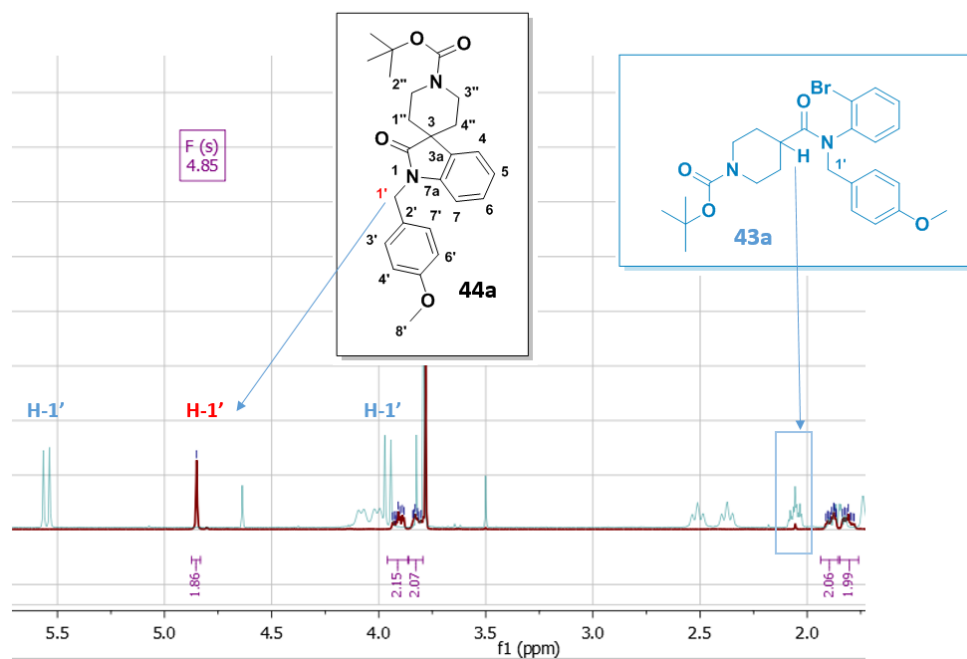
Figure 3.16. ^{1}H-NMR in CDCl$_3$ of compound **44a** (red spectrum). The spectrum of precursor intermediate **43a** is superimposed (blue spectrum), highlighting the disappearance of the multiplet at δ 2.05 ppm.

The palladium-catalysed α-arylation conversion of the amides **43a-e** to the spirooxindoles **44a-e** was further supported by mass spectrometry with the disappearance of the bromine atom present in the 2-bromo amides **43a-e** and long range ^{1}H – ^{13}C HMBC correlations for the spirooxindoles **44a-e**. For example, the ^{1}H – ^{13}C HMBC correlations for the spirooxindole **44a** showed a long range correlation between the C-3 carbon at δ 45.0 ppm and the H-4 proton at δ 7.29 ppm as well as a correlation between the C-3a carbon at δ 133.6 ppm and the H-5 and H-7 protons at δ 7.03 ppm and δ 6.77 ppm respectively could be observed, confirming unambiguously the formation of the spirooxindole **44a** by intramolecular cyclisation (Figure 3.17).
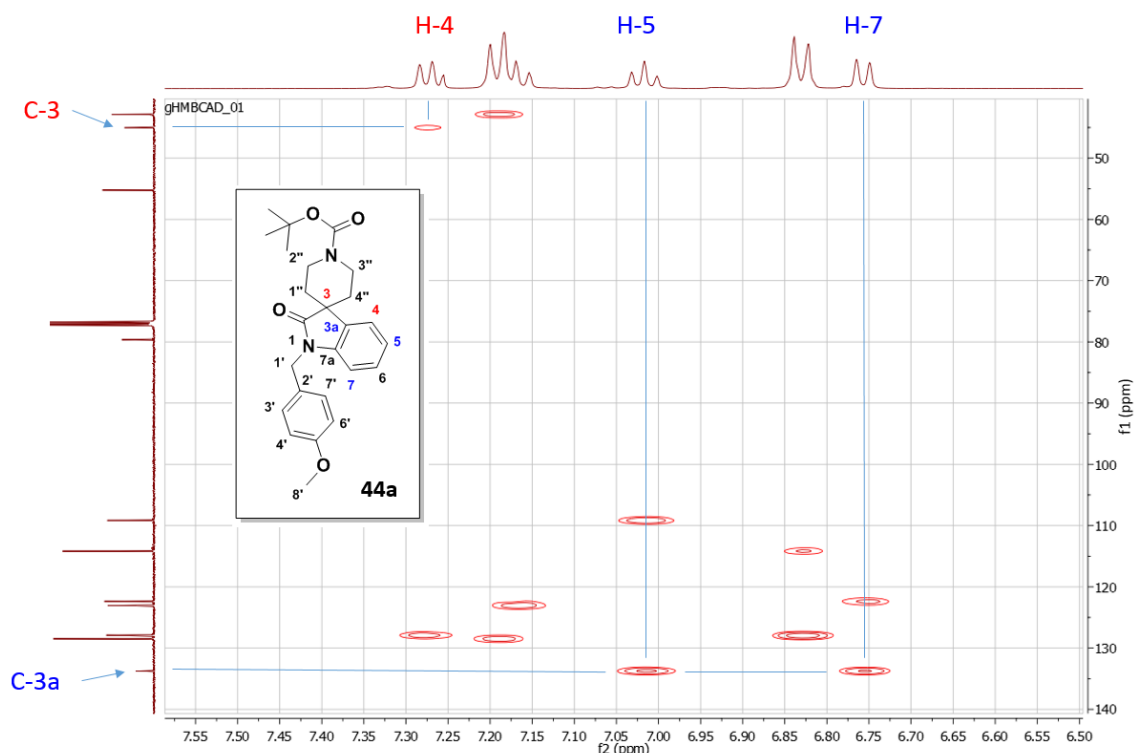
Figure 3.17. Heteronuclear multiple-bond correlation spectroscopy (HMBC) of compound **44a** in CDCl₃. The blue lines represent the HMBC correlations observed between the carbons and protons. Long range correlation between the C-3 carbon (δ 45.0 ppm) and the H-4 proton (δ 7.29 ppm) and between the C-3a (δ 133.6 ppm) and the H-5 (δ 7.03 ppm) and H-7 protons (δ 6.77 ppm).

Cleavage of the *para*-methoxybenzyl moiety was achieved as previously reported using trifluoroacetic acid in the presence of anisole at 150 °C under microwave irradiation, apart for analogue **45d** where alternative conditions were used (Scheme 3.12). All the spirooxindoles **45a-e** were obtained in good to excellent yield. In the case of the analogues **45a** and **45d**, and as expected, the Boc protecting group was cleaved simultaneously under the acidic reaction conditions. When attempting to cleave the PMB from the tetrahydropyran spirooxindole **44b**, the reaction proved more difficult and the deprotected product **45b** was obtained after 4 hours of heating at 150 °C in trifluoroacetic acid under microwave irradiation instead of 2 hours as for the analogues **45a**, **45c** and **45e**. Despite this extended reaction time, the yield obtained for the deprotected THP spirooxindole **45b** was consistent with the yield obtained for the other analogues prepared.

Scheme 3.12. PMB cleavage under acidic conditions.
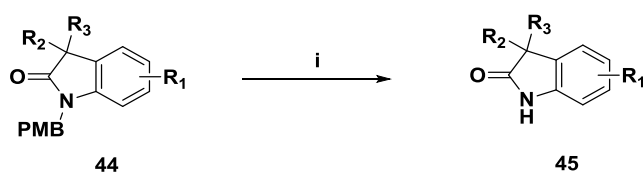
Compound	Structure	Conditions	Temperature	Time	Yield
45a		TFA/anisole	150 °C	2 hours	100%
45b		TFA/anisole	150 °C	4 hours	79%
45c		TFA/anisole	150 °C	2 hours	95%
45d		TFA/CF$_3$SO$_3$H	rt	16 hours	72%
45e		TFA/anisole	150 °C	2 hours	87%

Reagents and conditions: (i) TFA, anisole, MW or CF$_3$SO$_3$H, TFA, rt.

Trost *et al.* recently reported similar difficulties in removing *para*-methoxybenzyl protecting groups from *N*-protected oxindoles and succeeded in achieving mild cleavage using trifluoromethanesulfonic acid (3 equiv.) in trifluoroacetic acid at room temperature.[290] The conditions such as those reported by Trost allowed the clean deprotection of **44d** by removing both the Boc and PMB protecting groups at room temperature and led to **45d** in good yield (72%). Interestingly, when using trifluoromethanesulfonic acid as solvent for the preparation of the azetidine spirooxindole **39** (Table 3.5, entry 3), no clean *para*-methoxybenzyl cleavage could be achieved. However, an excess of trifluoromethanesulfonic acid with trifluoroacetic acid as solvent allows for clean PMB cleavage at room temperature. Similar results have been reported by Guillaumet *et al.* where PMB deprotection of oxindoles could only be achieved cleanly by

using 10 equiv. of trifluoromethanesulfonic acid in a mixture of trifluoroacetic acid and dichloromethane at room temperature, further highlighting the lack of a reliable and generic methodology for the cleavage of *para*-methoxybenzyl moiety from oxindoles.[291]

The analogue **45c** has previously been reported by Hsieh *et al*. and was prepared *via* a copper-catalysed domino coupling reaction as described in Scheme 3.13.[292] The preparation of compound **45c** by an alternative synthetic method and analysis of both the ^{1}H-NMR and ^{13}C- NMR reported by Hsieh *et al*. is a further unambiguous confirmation of the formation of the spirooxindole analogues accessed *via* palladium-catalysed α-arylation.

Scheme 3.13. Spirooxindoles *via* copper-catalysed coupling reaction as reported by Hsieh *et al*.[292]
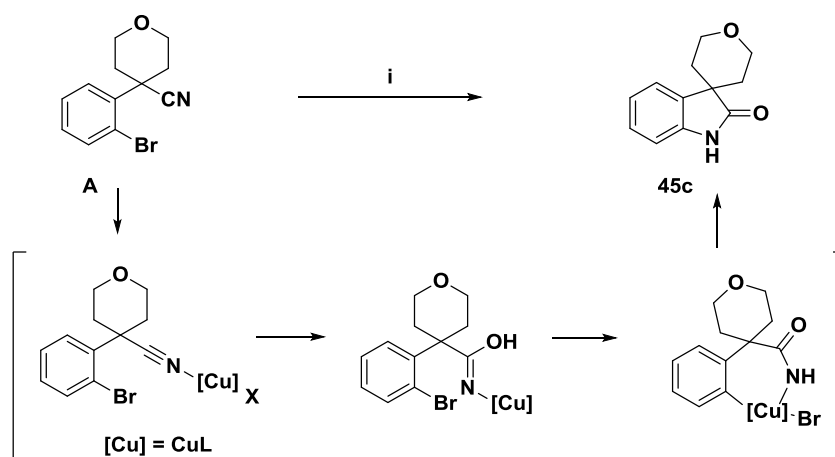
Reagents and conditions: (i) CuI (3.0 mol %), *N*-acetylglycine (6.0 mol%), NaOH, ᵗBuOH, 80 °C, 12 h.

The *bis*-deprotected spirooxindoles **45a** and **45d** were further functionalised (Scheme 3.14). In order to allow late stage diversification once coupled to the benzimidazole moiety, the piperidine spirooxindole **45a** was re-protected with a Boc group under standard conditions to give the intermediate **46** in good yield (78%), whilst the preparation of acetyl azetidine spirooxindole **47** was achieved *via* acetylation of **45d** with acetyl chloride in dichloromethane, in the presence of triethylamine.

Scheme 3.14. Amine functionalisation.
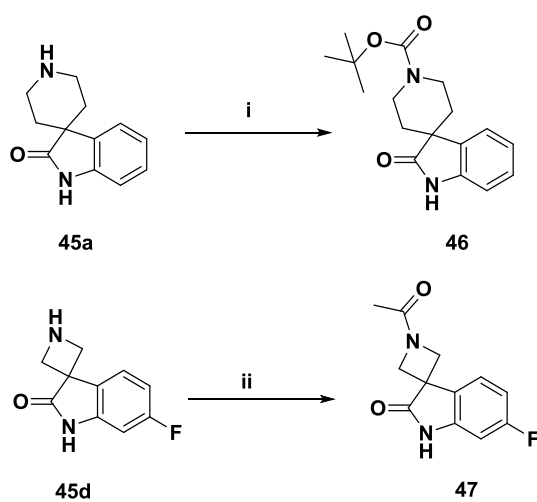
Reagents and conditions: (i) (Boc)₂O, CH₂Cl₂, rt, 16 h, 78%; (ii) AcCl, Et₃N, CH₂Cl₂, 0 °C to rt, 16 h, 63%.

3.2.5   Synthesis of Novel RSV Inhibitors Incorporating Spirocyclic Oxindoles

2-Chloromethyl benzimidazoles of generic structure **48** (Scheme 3.15) have been previously reported and were all obtained commercially (Onyx Scientific) or prepared by other members of the group following literature methods.[155,156,173,293,294] A succinct preparation of these 2-chloromethyl benzimidazoles is presented in Scheme 3.17.

Scheme 3.15.

R₁ = H, F
R₂, R₃ = Spirocycles
R₄ = Cl, -CH₂NHBOC
R₅ = -CH₂SO₂Me, -CH₂CF₃, -iPr, -CH₂CH₂OH
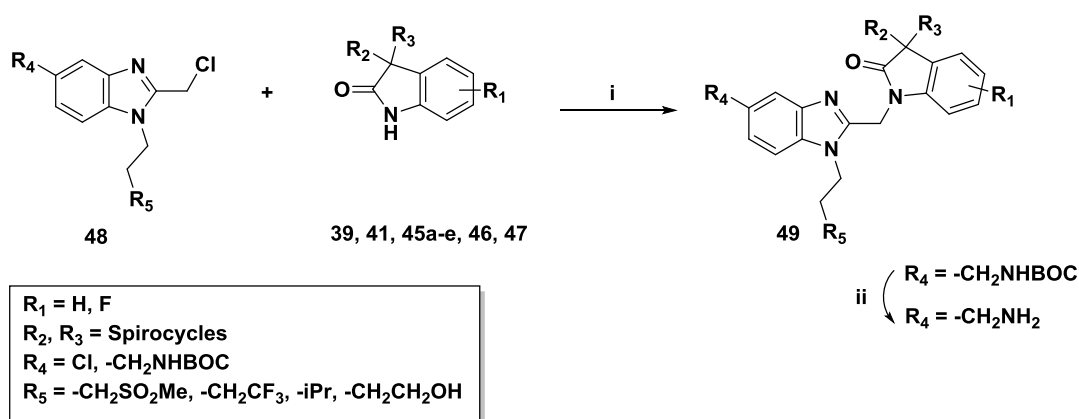
Reagents and conditions: (i) NaH, DMF, 0 °C to rt, 16 h to 48 h or K₂CO₃, MeCN, 80 °C, 16 h; (ii) 1 M HCl, Et₂O, rt, 16 h (for the preparation of **49b**); TFA, CH₂Cl₂, rt (for the preparation of **49c**, **49g** and **49i-k**).

Completing the synthesis of the target compounds **49**, the previously described spirooxindoles **39**, **41**, **45a- c, 45e**, **46** and **47** were alkylated with 2-chloromethyl benzimidazole **48** in the presence of sodium hydride in *N,N*-dimethylformamide (Scheme 3.15). When 2-chloromethyl benzimidazole **48** bearing an unprotected hydroxy moiety was used (R₅ = -CH₂CH₂OH), the alkylation could be achieved in the presence of potassium carbonate as a base in acetonitrile heated to 80 °C. Under these conditions, the free hydroxy at the R₅ position (R₅ = -CH₂CH₂OH) did not require any protection. When a Boc-protected aminomethyl moiety was present (**48**, R₄ = -CH₂NHBOC), subsequent deprotection was achieved under acidic conditions to give the aminomethyl moiety using either trifluoroacetic acid in dichloromethane (**49c**, **49g** and **49i-k**) or 1 M HCl in diethyl ether (**49b**). A summary of the compounds prepared is presented in Table 3.6.

Table 3.6. Summary of compounds prepared.

Compound	Structure	Yield	Compound	Structure	Yield
49a		78%	**49h**		72%[b]
49b		5%[a]	**49i**		59%
49c		48%[a]	**49j**		61%
49d		52%	**49k**		56%

Compound	Structure	Yield	Compound	Structure	Yield
49e		47%	**49l**		75%
49f		80%	**49m**		74%
49g		61%[a]			

[a]Over 2 steps; [b]racemic mixture.

Except for **49b** where poor yields were obtained (5% yield) due to purification issues, all the compounds were obtained in moderate to good yields, ranging from 47% to 80%. Compound **49h** was separated into its enantiomers **49n** and **49o** by supercritical fluid chromatography (SFC) on a chiral column (Chiralpak AD) to establish the effect of the chiral centre on the biological activity and both enantiomers were obtained in high enantiomeric excess (100% and 99.2% ee respectively) (Figure 3.18).

Compounds	49n	49o
	Isomer 1	Isomer 2
ee (%)	100%	99.2%
UV Purity at 220 nm	93.9%	97.9%

Figure 3.18. Chiral separation of compound **49h** by SFC on Daicel Chiralpak AD column.

Compound **49g** was amenable to further functionalisation and converted to the sulfonamide **49p** and acetamide **49q** under standard conditions (Scheme 3.16). Treatment of **49g** with methanesulfonyl chloride in the presence of triethylamine in dichloromethane gave the sulfonamide **49p** in good yield (84%). The acetamide **49q** was obtained under similar conditions using acetyl chloride and isolated in a moderate 54% yield.

Scheme 3.16.
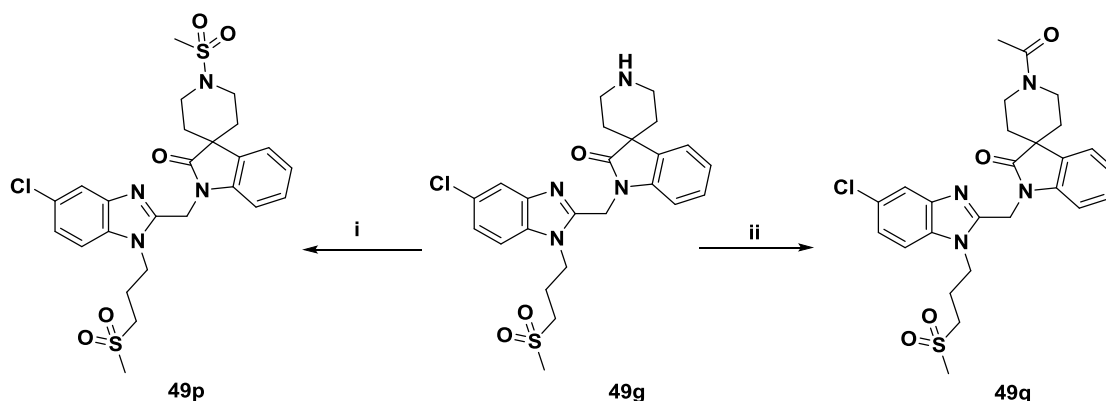
Reagents and conditions: (i) MeSO$_2$Cl, Et$_3$N, CH$_2$Cl$_2$, rt, 16 h, 84%; (ii) AcCl, Et$_3$N, CH$_2$Cl$_2$, rt, 24 h, 54%.

As previously mentioned, the 2-chloromethyl benzimidazoles **48** were either obtained commercially or prepared within the group independently from the work reported in this thesis, following literature precedents.[129,156,173,177,293–295] A short synthesis is presented in Scheme 3.17. The 2-chloro benzimidazole **52** was obtained from the displacement of 5-chloro-2-fluoronitrobenzene **50** with the required primary amine, using K$_2$CO$_3$ as a base in acetonitrile at 50 °C. The benzimidazole **52** was obtained by condensation of the *bis*-1,2-aniline intermediate, obtained by hydrogenation of **51** at atmospheric pressure of hydrogen, with 2-chloroacetyl chloride in concentrated hydrochloric acid heated at 50 °C. The benzimidazole **57** was obtained in seven steps from commercially available 4-chloro-3-nitrobenzonitrile. In a similar fashion to

the preparation of intermediate **51**, compound **54** was obtained *via* nucleophilic displacement of 4-chloro-3-nitrobenzonitrile **53** with the required alkyl amine. Nitro reduction under hydrogenation at atmospheric pressure of hydrogen in the presence of 10% palladium on carbon, followed by imidazole ring cyclisation with acetoxyacetyl chloride and acetic acid and subsequent acetal protecting group removal under basic conditions gave the 2-hydroxy benzimidazole **55**. The nitrile moiety of the benzimidazole intermediate **55** was further reduced by hydrogenation at atmospheric pressure of hydrogen to the aminomethylene benzimidazole in the presence of 10% $Pd(OH)_2$ on carbon, followed by *N*-BOC protection and chlorination of the hydroxy methylene using methanesulfonyl chloride to give the 2-chloro benzimidazole **57**. When the hydroxy side-chain was used (R_5 = -CH_2CH_2OH), a silyl protecting group was used on the hydroxy moiety that was removed at the last step with a fluoride source such as tetrabutylammonium fluoride.

Scheme 3.17. Preparation of 2-chloromethyl benzimidazole intermediates **48**.
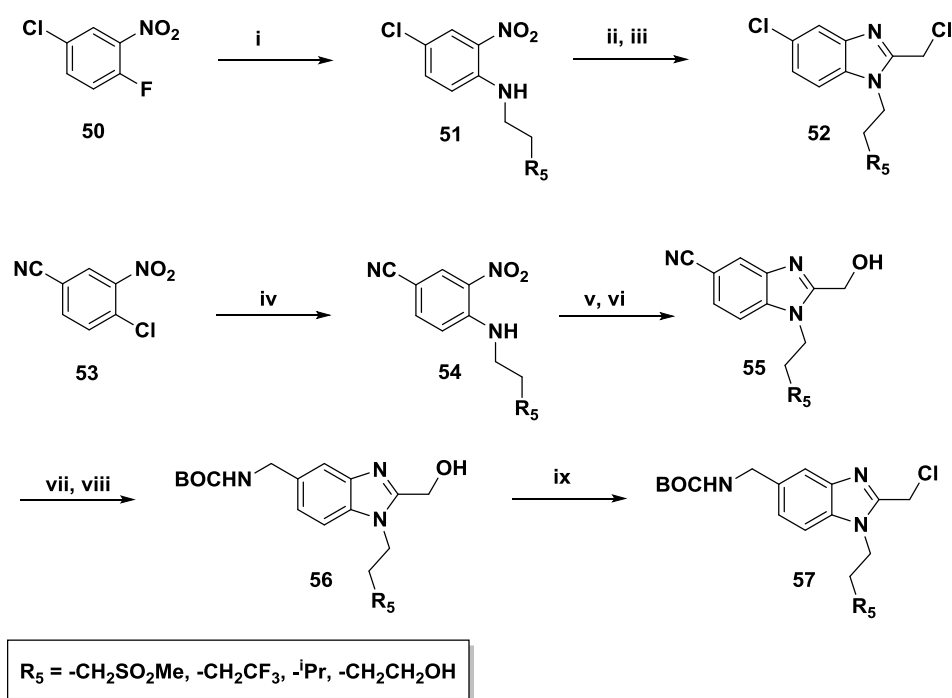
Reagents and conditions: (i) K_2CO_3, MeCN, 50 °C, 16 h, 80 - 96%; (ii) H_2 (14 psi), 10% Pd/C, MeOH, rt, 16 h, 52 – 90% ; (iii) 2-chloroacetyl chloride, conc. HCl, 50 °C, 4 h, 23 – 82%; (iv) K_2CO_3, MeCN, rt, 16 h, 85 – 95%; (v) H_2 (14 psi), 10% Pd/C, MeOH, rt, 16 h, 70 – 96%; (vi) (a) acetoxyacetyl chloride, Et_3N, CH_2Cl_2, rt, 2 h, (b) AcOH, 80 °C, 16 h then K_2CO_3, MeOH, rt, 2 h, 62 - 75% over 2 steps; (vii) H_2 (14 psi), 10% $Pd(OH)_2$/C, conc. HCl, MeOH: THF (2:1), rt, 16 h, 39 – 100%; (viii) *tert*-butoxycarbonyl *tert*-butyl carbonate, $^iPr_2NEt$, CH_2Cl_2, rt, 2 h, 51 – 83%; (ix) $MeSO_2Cl$, $^iPr_2NEt$, THF, rt, 2 h to 16 h, 90 – 99%.

3.3 RSV Inhibitors Incorporating Aza-Spirooxindoles

3.3.1 Rationale

As discussed in Chapter 2, the metabolic identification study for **RV-39** revealed that metabolic instability may occur from the oxindole part of the molecule. To investigate the potential reduction of metabolic instability, the replacement of the oxindole moiety by an aza-oxindole was envisaged as initially set in the objectives for this work (section 3.1, Figure 3.1, objective 3). The introduction of a nitrogen would lower the overall clogP of the oxindole moiety. In particular, the introduction of a nitrogen at either the 5- or 6- position would reduce the clogP by 1.2 $\log_{10}$ unit compared to the equivalent oxindole, potentially blocking the site of metabolism by reducing the electron density of the oxindole moiety (Figure 3.19).

	Oxindole	4-Aza-oxindole	5-Aza-oxindole	6-Aza-oxindole	7-Aza-oxindole
Structure					
clogP[a]	1.71	0.88	0.49	0.49	1.08
ΔclogP[b]	--	-0.83	-1.22	-1.22	-0.63

[a]clogP calculated with ChemAxon calculator plugin; [b]reduction in clogP compared to the oxindole.

Figure 3.19. clogP comparison between oxindole and aza-oxindole templates

Initially, the preparation of both the 5-aza-spirooxindole (**58**) and 6-aza-spirooxindole (**59**) was envisaged (Figure 3.20).

5-aza-spirooxindole

58

6-aza-spirooxindole

59

X = N, O, C, S
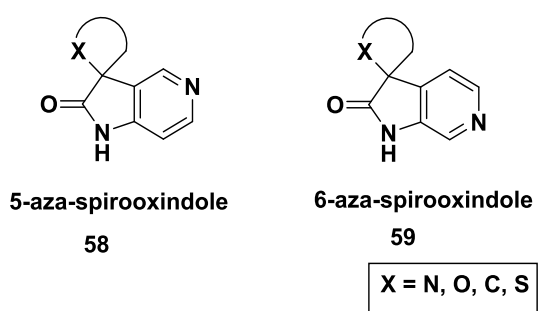
Figure 3.20. 5-Aza-spirooxindole and 6-aza-spirooxindole structures.

3.3.2 Synthesis of RSV Inhibitors Incorporating Aza-Spirooxindole Motifs

Several synthetic approaches have been reported for the preparation of aza-oxindole, including oxidative couplings,[296] radical cyclisations,[297] Pauson-Khand type cycloadditions and cyclisation of aminopyridine acetic acids.[298,299] However, reports for the formation of 3,3'-spirocyclic aza-oxindoles are very limited, and in particular, the preparation of spirocyclic 5-aza and 6-aza-oxindoles has only ever been reported a few times over the last decade (Figure 3.21).
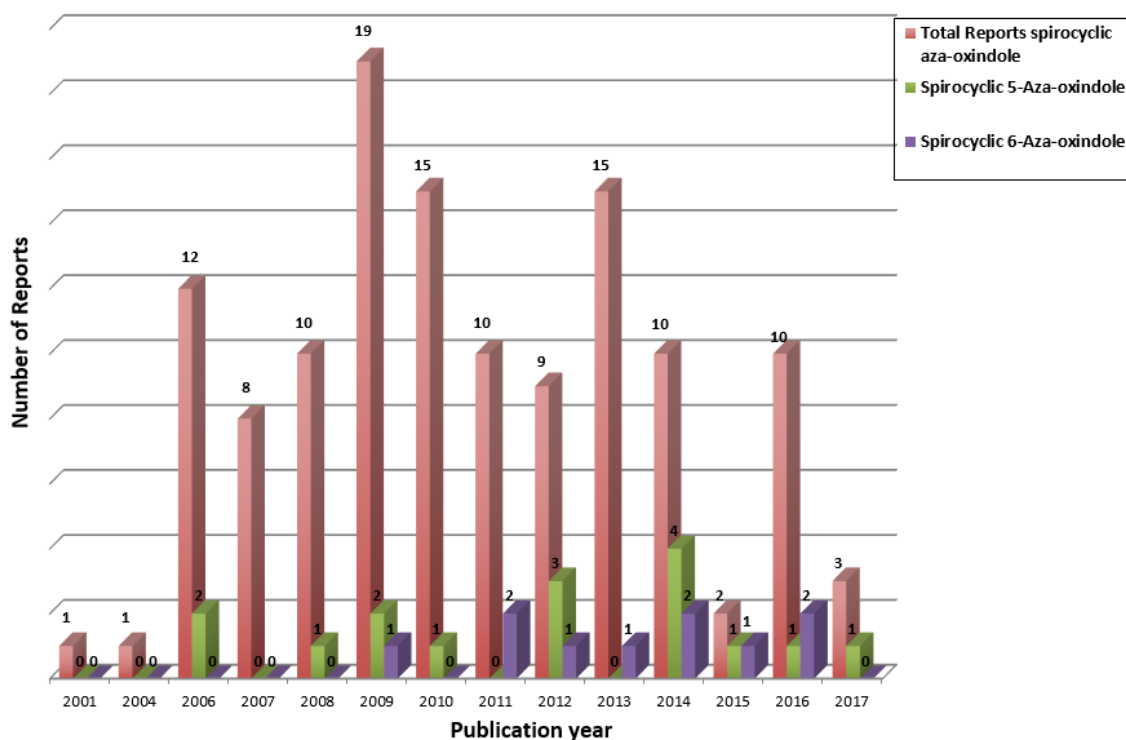
Figure 3.21. Spirocyclic aza-oxindoles reported in the scientific literature and patent literature from January 2001 to July 2017. Data generated from the SciFinder® database of Chemical Abstracts.

An initial strategy that would make use of the palladium-catalysed α-arylation methodology as described in section 3.2.4 would potentially provide an easy access to novel spirocyclic 5-aza-oxindoles and 6-aza-oxindoles. Independent reports from Kündig and Ackermann suggest that the α-arylation may indeed be a viable strategy for the preparation of these spirocyclic aza-oxindoles.[300,301] Both groups report the preparation of 3,3'-substituted 4-aza-oxindoles and 3,3'-substituted 7-aza-oxindoles *via* intramolecular palladium catalysed methodologies.

Based on the report from Ackermann, the 3,3'-disubstituted-4-aza-oxindoles **61** were prepared *via* palladium-catalysed α-arylation of 2-chloro pyridines **60** under similar conditions to those described in section 3.2.4 and as described in Scheme 3.18. Ackermann only reports three examples derived from 2-chloro pyridines using a sterically hindered adamantyl-substituted secondary phosphine oxide ligand. However, the 2-chloro pyridines described by Ackermann are prone to undergo facile palladium insertion and subsequent intramolecular arylation similarly to the arylation described in section 3.2.4 but unfortunately there was no report of any 5-aza and 6-aza-oxindoles prepared *via* this methodology.

Scheme 3.18. Palladium-catalysed α-arylation with chloroarenes as reported by Ackermann.[300]
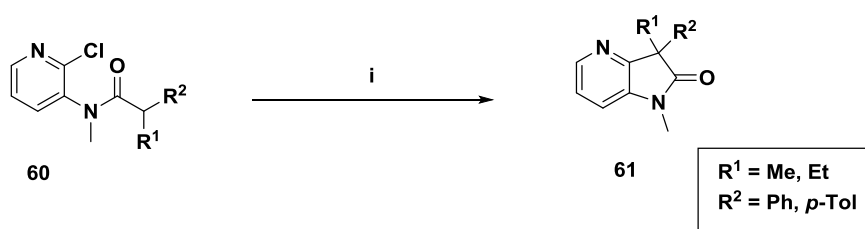
Reagents and conditions: (i) NaO^tBu, Pd(OAc)$_2$, (1-Ad)$_2$P(O)H, 1,4-dioxane, 100 °C, 18 h.

More intriguing however was the report from Kündig *et al*. suggesting that under palladium-catalysed α-arylation of 3-bromo-2-anilide-pyridine **62**, a mixture of the expected 7-aza-oxindole **63** and the 4-aza-oxindole **64** regioisomer was obtained in a 44:56 ratio (Scheme 3.19, equation A). Furthermore, in the same report, additional examples from Kündig *et al*. illustrated the exclusive formation of 6-aza-oxindoles **66** obtained in good to excellent yields (66% to 99% yield) from 3-bromo-4-anilide pyridines **65** when palladium was not present under the reaction conditions used (Scheme 3.19, equation B). According to the report, the 6-regioisomer product (**66**) could be formed exclusively *via* a relatively unknown Truce-Smiles rearrangement and proceeded through a bicyclic reaction intermediate in an addition-elimination S$_N$Ar pathway (Scheme 3.19, equation C).[302–305] The reaction has been reported to proceed *via* the base-mediated formation of a putative 4-membered ring spirocyclic anionic σ-adduct **65b**, known as a Meisenheimer adduct (Figure 3.19, equation C).[305] The carbanion nucleophile is formed usually from deprotonation of a C-H bond, stabilised by an electron withdrawing group α to the carbanion such as nitrile or carbonyl moiety.[305] There are very few reports of the Truce-Smiles rearrangement on pyridyl rings and reports from Wood *et al*. suggest that a strong-electron withdrawing substituent in the *ortho-* or *para-*positions of the substrate aryl ring may favour such rearrangement.[304,306]

Scheme 3.19. Competition between Truce-Smiles rearrangement and Pd-catalysed α−arylation.[301]
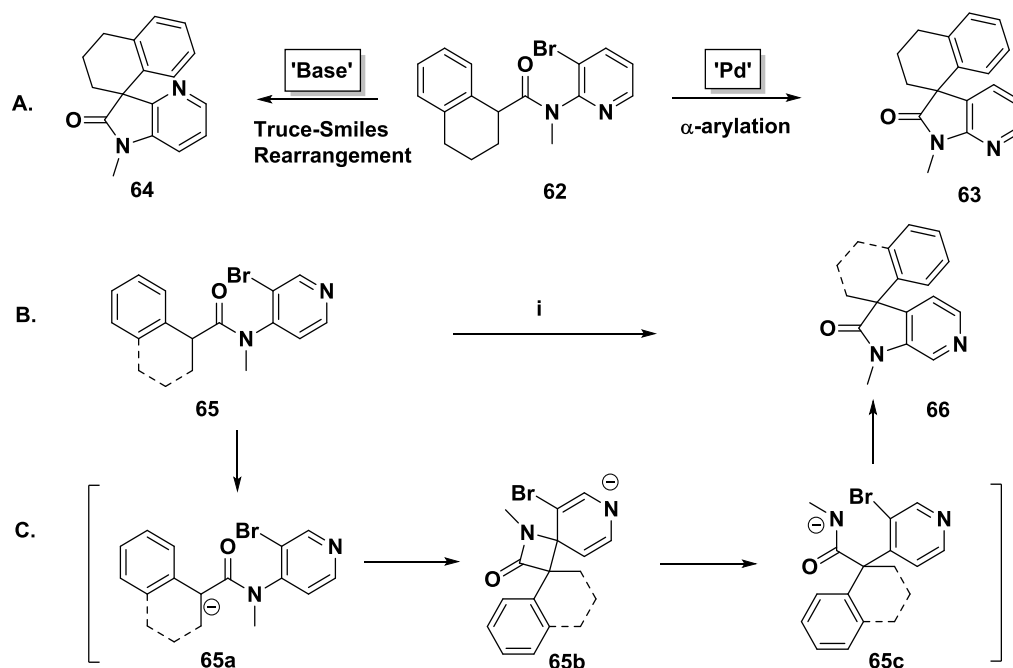
Reagents and conditions: (i) NaO^{t}Bu (2.1 equiv.), DME (0.05 M), 50 °C.

Capitalising on the work from Kündig *et al.*, it was anticipated that both the 5-aza-spirooxindole and 6-aza-spirooxindole could be obtained as a mixture of regioisomers from a single reaction. Indeed, under the conditions initially described for the preparation of the spirooxindoles from section 3.2.4, the product from the Truce-Smiles rearrangement could be formed and would compete with the product expected from the Pd-catalysed α-arylation.

As an initial model to validate this palladium-catalysed α-arylation strategy for the synthesis of the 5-aza-spirooxindole and 6-aza-spirooxindole series, the preparation of the tetrahydropyran-amide **67** intermediate was envisaged. Based on the report from Kündig *et al.*, the conversion of the PMB-protected amide **67** should generate a mixture of the aza-spirooxindole regioisomers **68** and **69** under the palladium-catalysed α-arylation in the presence of sodium *tert*-butoxide as the base was reported to compete with the palladium-mediated α-arylation as previously described (Scheme 3.20, equation A). However, when using sodium *tert*-butoxide as a base in 1,2-dimethoxyethane, the amide intermediate **67** may only undergo a Truce-Smiles rearrangement to the 6-aza-spirooxindole **69** as a single regioisomer (Scheme 3.20, equation B).

Scheme 3.20. Approach to 5-aza and 6-aza-spirooxindoles.
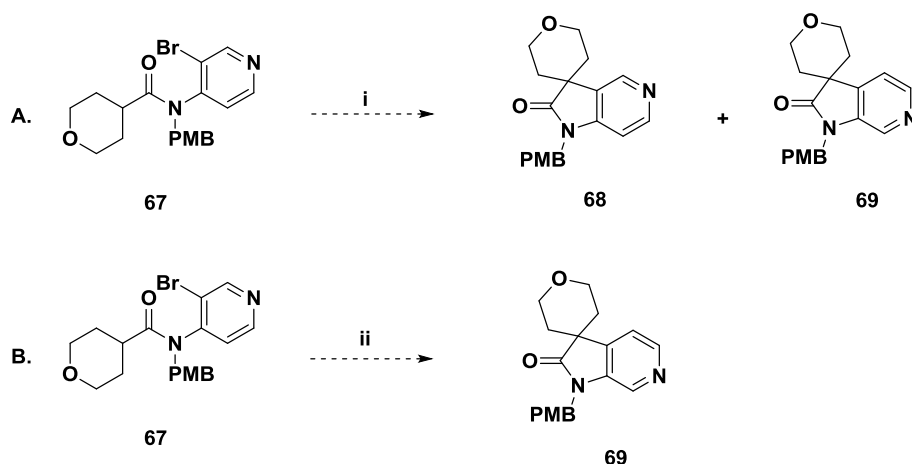
Reagents and conditions: (i) Pd(OAc)$_2$, PCy$_3$.HBF$_4$, NaO^{t}Bu, 1,4-dioxane, 80 - 130 °C; (ii) NaO^{t}Bu, DME, 50 °C.

The preparation of the PMB-protected amide **67** proved to be a significant challenge. Initially, acylation of 4-amino pyridine **70** with tetrahydropyran-4-carbonyl chloride obtained from the corresponding carboxylic acid gave the amide **71** in good yield (Scheme 3.21). However, subsequent alkylation with *para*-methoxybenzyl chloride in the presence of sodium hydride gave the PMB-protected amide **67** in very low but consistent yield (16% yield) despite multiple attempts at the alkylation reaction. In such case, the nitrogen of the pyridyl amide **71** is much less nucleophilic than the nitrogen from the phenyl amide equivalent. Instead, the main product formed seemed to result from quaternisation of the pyridyl ring.

Scheme 3.21.
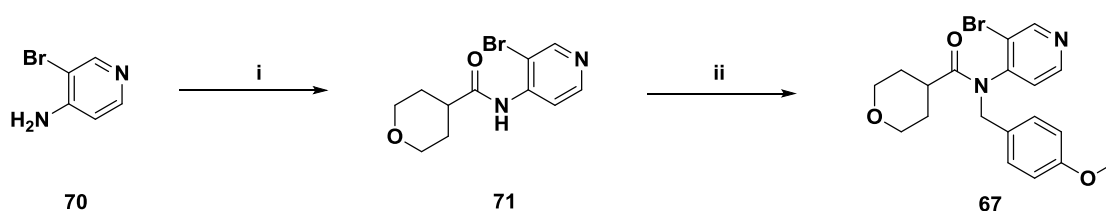
Reagents and conditions: (i) Tetrahydropyran-4-carbonyl chloride, Et$_3$N, CH$_2$Cl$_2$, 0 °C to rt, 16 h, 76%; (ii) NaH, PMB-Cl, DMF, 0 °C to rt, 16 h, 16%.

In an attempt to improve the yields for the formation of the key intermediate **67**, alternative conditions were considered but changing both the solvent and the base failed to affect the reaction outcome. Replacing *N,N*-dimethylformamide as a solvent with tetrahydrofuran (Table 3.28, entry 2) or heating the reaction mixture to 60 °C in tetrahydrofuran (Table 3.28,

entry 3) led to no reaction whilst carrying out the reaction with potassium carbonate as a base in acetonitrile at 90 °C also led to unreacted starting material **71**. The lack of success for this transformation was re-enforced by the limited number of references in the scientific literature.

Table 3.28. Alkylation with *para*-methoxybenzyl chloride for the preparation of amide **67**.

Entry	Base/Reagents	Solvent	Temperature	Yield
1	NaH	DMF	0 °C to rt	16%
2	NaH	THF	0 °C to rt	No reaction[a]
3	NaH	THF	60 °C	No reaction[a]
4	K$_2$CO$_3$	MeCN	90 °C	No reaction[a]

[a]Unreacted starting material

To overcome the *para*-methoxybenzyl alkylation problem, the order of the synthetic sequence was reversed (Scheme 3.22). Treatment of the 3-bromo-4-chloro pyridine **72** with *para*-methoxybenzyl amine in *N*-methyl-2-pyrrolidinone in the presence of triethylamine at 150 °C did not lead to the formation of any product. However, the aniline **73** could be obtained in high yields (98% yield) under harsher conditions by heating the reaction at 220 °C for 2 hours under microwave irradiation.

Scheme 3.22.
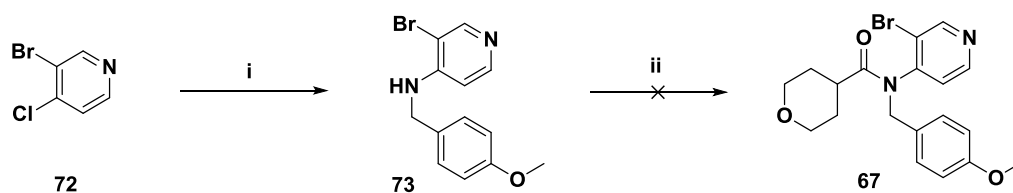
Reagents and conditions: (i) PMB-NH$_2$, Et$_3$N, NMP, MW, 220 °C, 2 h, 98%; (ii) Tetrahydropyran-4-carbonyl chloride or tetrahydropyran-4-carboxylic acid (conditions Table 3.29).

Unfortunately, any attempts at the acylation of intermediate **73** with either tetrahydropyran-4-carbonyl chloride or tetrahydropyran-4-carboxylic acid were unsuccessful (Table 3.29). When using tetrahydropyran-4-carbonyl chloride in either dichloromethane at 20 °C (Table 3.29, entry 1) or *N,N*-dimethylformamide at 60 °C (Table 3.29, entry 2), no conversion was observed. Similar results were obtained when using standard coupling agent such as HATU or EDCI.HCl

(Table 3.29, entries 3 and 4 respectively) or the more activated propylphosphonic anhydride in *N,N*-dimethylformamide at 60 °C (Table 3.29, entry 5).

Table 3.29. Condition attempts for the acylation of compound **73** with tetrahydropyran-4-carbonyl chloride or tetrahydropyran-4-carboxylic acid.

Entry	Reagents	Temperature
1	Acid chloride, Et$_3$N, CH$_2$Cl$_2$	20 °C
2	Acid chloride, Et$_3$N, DMF	60 °C
3	Carboxylic acid, HATU, Et$_3$N, DMF	20 °C
4	Carboxylic acid, EDCI.HCl, DMAP, CH$_2$Cl$_2$	20 °C
5	Carboxylic acid, T$_3$P, DMF	60 °C

No further attempts were tried to optimise the preparation of the amide **67** and instead, the material obtained in low yield as described in Scheme 3.21 was used to validate the key intramolecular arylation reaction. An initial attempt at the palladium-catalysed α-arylation using Pd(OAc)$_2$, PCy$_3$.HBF$_4$, and sodium *tert*-butoxide in 1,4-dioxane heated at 90 °C as previously described for the preparation of the spirooxindoles **36** and **44a-e** only gave unreacted starting material (Scheme 3.23). Encouragingly, when the reaction temperature was raised to 130 °C, partial formation of the 5-aza-spirooxindole **68** was observed. However, increasing the temperature to 150 °C and heating under microwave irradiation for 4 hours led to the clean formation of the 5-aza-spirooxindole **68** in 62% yield. Surprisingly the 6-aza-spirooxindole regioisomer **69,** expected to be a main component of the reaction, could not be detected from the reaction mixture.

Scheme 3.23. Probing the Truce-Smiles rearrangement hypothesis.
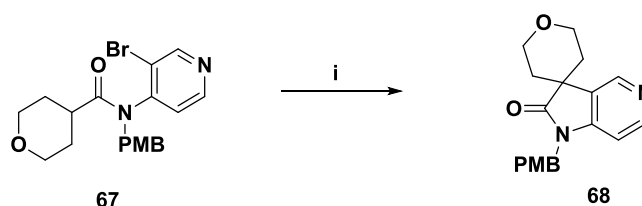
Reagents and conditions: (i) Pd(OAc)$_2$, PCy$_3$.HBF$_4$, NaO^{t}Bu, 1,4-dioxane, 150 °C, 4 h, 62%.

The regiochemistry of the 5-aza-spirooxindole **68** was confirmed by through-space NMR correlation experiment (Nuclear Overhauser effect spectroscopy – NOESY) (Figure 3.22). Irradiation of the singlet H-4 proton at δ 8.56 ppm showed a strong enhancement for the THP moiety at δ 1.82 ppm for the H-1'' and H-4'' protons and δ 3.92 ppm for the H-2'' and H-3'' protons (Figure 3.22). Furthermore, irradiation of the H-7 proton at δ 6.73 ppm showed a strong enhancement for the singlet PMB-CH$_2$ (H-1') at δ 4.81 ppm, confirming unambiguously the regiochemistry of the isolated product **68**. Additionally, following on the work published by Abraham *et al.* on the chemical shifts of THP, the irradiation of the H-4 proton suggested an enhancement that could be attributed to the equatorial H-1'' and H-4'' protons at δ 1.82 ppm as well as the axial H-2'' and H-3'' protons at δ 3.92 ppm.[307]
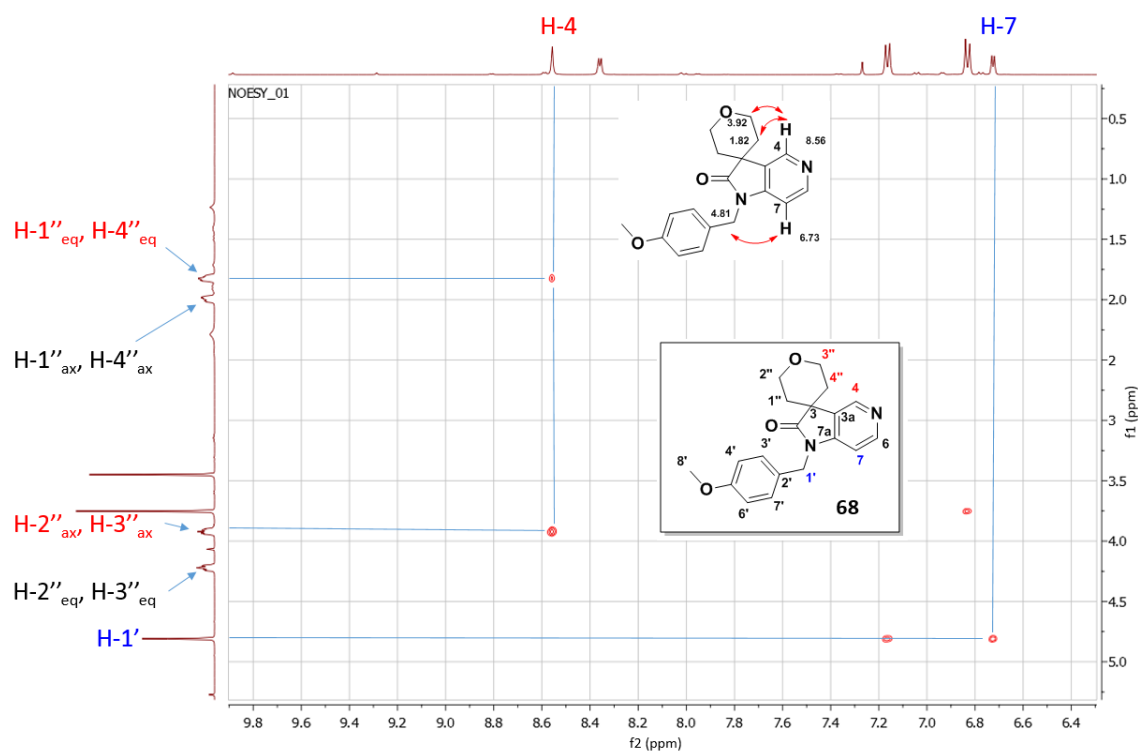
Figure 3.22. NOESY confirmation of the 5-aza-spirooxindole **68** in CDCl$_3$. Irradiation of H-4 (δ 8.56 ppm) showed an enhancement for H-1'' and H-4'' (δ 1.82 ppm) and H-2'' and H-3'' (δ 3.92 ppm). Irradiation of H-7 (δ 6.73 ppm) showed an enhancement for H-1' (δ 4.81 ppm).

Based on the precedents from Kündig *et al.*, the results obtained in Scheme 3.23 for the preparation of the 5-aza-spirooxindole **68** were unexpected as no regioisomer 6-aza-spirooxindole **69** could be detected during the reaction. Although surprising, these excellent results obtained for the formation of the regioisomer **68** are however consistent with the preparation of the spirooxindoles described previously in section 3.2.4 and are the first report

of the use of intramolecular palladium-catalysed α-arylation for the selective preparation of 5-aza-spirooxindoles.

It may be envisaged that in Kündig *et al.*'s report, the rate of reaction of the Truce-Smiles rearrangement is faster at 50 °C than the palladium-catalysed ring cyclisation. A further explanation for the lack of rearranged product **69** may reside in the decreased stability of the carbanion formed compared to the benzylic examples **65a** reported by Kündig *et al.* (Scheme 3.19, equation C). Non-benzylic substrates undergoing a Truce-Smiles rearrangement have been described in the literature, albeit not in a substituted pyridine substrate.[230,306,308]

To confirm Kündig's rearrangement theory, the anilide **67** was heated at 50 °C with 2.1 equivalents of sodium *tert*-butoxide in 1,2-dimethoxyethane (0.05 M) and in the absence of any palladium catalyst. Interestingly, none of the expected Truce-Smiles rearranged 6-aza-spirooxindole **69** could be observed, even after prolonged heating time. Increasing the temperature to 150 °C and under microwave irradiation for 4 hours, none of the 6-aza-spirooxindole **69** could be detected either. Although a different anilide and protecting group (*para*-methoxybenzyl instead of methyl) were used compared to the anilides reported by Kündig, it is interesting that none of the Truce-Smiles rearranged isomer **69** could be detected during neither the palladium-catalysed nor the base-mediated conditions reported. These results further suggest that a more stable carbanion may be required to undergo a Truce-Smiles rearrangement. As a consequence, an alternative to the preparation of the 6-aza-spirooxindole **69** is reported in a later part of this chapter.

Removal of the *para*-methoxybenzyl protecting group from the intermediate **68** proved significantly more problematic than anticipated. Following on the mild conditions identified for the removal of the PMB protecting group from the cyclopropyl oxindole **44d** (Scheme 3.12), the intermediate **68** was treated with an excess of trifluoromethanesulfonic acid (3.0 equiv) in trifluoroacetic acid (Scheme 3.24, entry 1) at room temperature. Unfortunately, under these conditions, no cleavage of the PMB was observed. Raising the reaction temperature to 100 °C led to a complex mixture, suggesting some decomposition of the aza-oxindole moiety (Scheme 3.24, entry 2). Similarly, when using trifluoromethanesulfonic acid at room temperature, no deprotection of the PMB could be observed (Scheme 3.24, entry 3). Reverting to the oxidative cleavage conditions previously attempted with ceric (IV) ammonium nitrate (Scheme 3.24, entry 4) proved not to be compatible with the aza-oxindole template and led to rapid compound decomposition.

The harsh trifluoroacetic acid conditions initially developed for the cleavage of the *para*-methoxybenzyl moiety were therefore reconsidered. Using trifluoroacetic acid at 150 °C under microwave irradiation for 90 minutes (Scheme 3.24, entry 5) was unsuccessful and only the starting material was recovered. Increasing the temperature to 170 °C and extending the reaction time to 3 hours also proved unsuccessful but surprisingly, no material decomposition could be observed by LCMS (Scheme 3.24, entry 6). Encouragingly, further temperature increase to 200 °C for 1 hour led to some partial PMB protecting group cleavage (Scheme 3.24, entry 7). An acceptable conversion to the required deprotected product could be observed (60% conversion monitored by LCMS) but only after extended heating time at 200 °C (Scheme 3.24, entry 8). However, despite the apparent clean conversion profile observed by LCMS, the desired 5-aza-spirooxindole **74** could only be isolated in a disappointing 11% yield.

Scheme 3.24. PMB deprotection attempts of intermediate **68**.
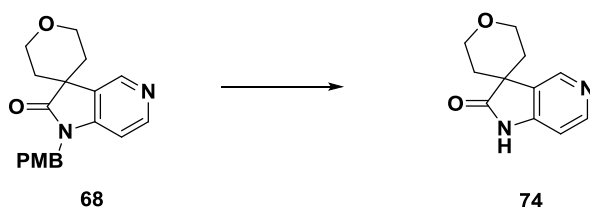
Entry	Conditions	Temperature	Time	Conversion[b]
1	CF$_3$SO$_3$H/TFA	20 °C	16 hours	No reaction
2	CF$_3$SO$_3$H/TFA	100 °C	4 hours	Partial decomposition
3	CF$_3$SO$_3$H	20 °C	2 hours	No reaction
4	Ce(NH$_4$)$_2$(NO$_3$)$_6$/H$_2$O/MeCN	20 °C	16 hours	Decomposition
5	TFA/anisole[a]	150 °C	90 minutes	No reaction
6	TFA/anisole[a]	170 °C	3 hours	No reaction
7	TFA/anisole[a]	200 °C	1 hour	Trace of product
8	TFA/anisole[a]	200 °C	4.5 hours	11%[c]

[a]Microwave irradiation; [b]monitored by LCMS; [c]Isolated yield.

Although the appropriate instrument safety enclosure and shutdown procedures were in place, the same reaction conditions were not repeated to generate any further material. Heating trifluoroacetic acid at 200 °C in a sealed vessel under microwave irradiation whilst generating 20 bars of pressure was deemed unsafe for any potential scale up.

However, with a limited amount of 5-aza-spirooxindole **74** in hand, alkylation with 2-chloromethyl benzimidazole **75** in *N,N*-dimethylformamide in the presence of sodium hydride gave the final derivative **76** in a moderate 35% yield (Scheme 3.25).

Scheme 3.25.
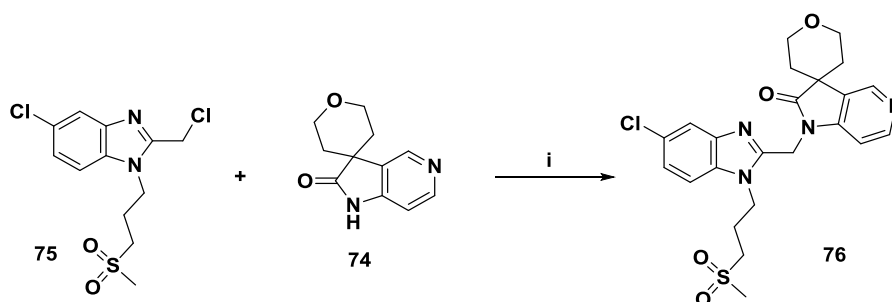
Reagents and conditions: (i) NaH, DMF, 0 °C to rt, 16 h, 35%.

Following on the successful preparation of the 5-aza-spirooxindole **74** *via* palladium-mediated arylation, it was envisaged that 6-aza-spirooxindoles could be obtained in a similar fashion. However, the significant issues that led to the removal of the *para*-methoxybenzyl protecting group and in particular the safety concerns with the PMB deprotection in trifluoroacetic acid at high temperature and high pressure led to consider an alternative synthetic strategy for the preparation of 6-aza-spirooxindoles. Furthermore, following on the encouraging biological data obtained for cyclopropyl spirooxindoles **49j-m** (see SAR tables and discussion in Chapter 4), the synthesis of the cyclopropyl-6-aza-oxindole **77** was investigated (Figure 3.23). Bakke *et al*. have previously reported the synthesis of the 6-aza-oxindole **78**. It was envisaged that upon preparation of the intermediate **78**, the 6-aza-spirooxindole **77** could be obtained *via* a double alkylation with 1,2-dihaloethane in the presence of a base.
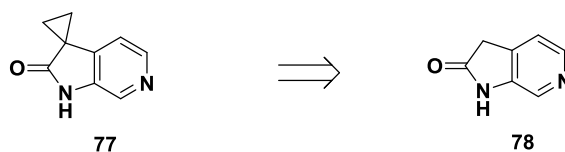
Figure 3.23. Preparation of the 6-aza-spirooxindole regioisomer.

Following on independent reports from Jończyk and Bakke, ethyl chloro acetate could undergo a base-mediated vicarious nucleophilic substitution with 3-nitro pyridine **79** in THF using potassium *tert*-butoxide (10 equiv.) as a base (Scheme 3.26).[309,310] During the vicarious nucleophilic substitution, the nitro group acts as an electron withdrawing and activating group whereby initially the ethyl chloro acetate reacts with potassium *tert*-butoxide, producing a nucleophile attacking the electrophilic 3-nitro pyridine **79** either at the *ortho* or *para* position of the nitro group. The adduct formed can further undergo an elimination of HCl under the basic conditions, which on protonation gives the product **80**. Similar to the report from Bakke, from the three isomers possible under the reaction mechanism with 3-nitro pyridine, the 4-isomer **80** was the only product isolated and both the 2- and 6- isomers were not detected. Although the 4-ethoxycarbomethyl-3-nitropyridine **80** was not obtained in yields as high as those from Bakke, the compound could be isolated in modest but reproducible 50% yield.

Scheme 3.26. Vicarious Nucleophilic Substitution.
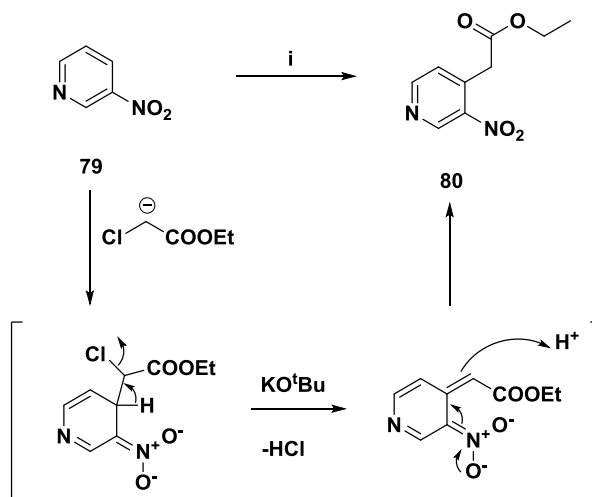
Reagents and conditions: (i) ClCH₂COOEt, KOᵗBu, THF, 0 °C, 2 h then rt, 1 h, 50%

Catalytic hydrogenation at atmospheric pressure of the nitropyridine **80** in presence of Pd/C, followed by intramolecular cyclisation under acidic conditions at room temperature led to the isolation of the 6-aza-oxindole **82** isolated as its HCl salt without any need for purification in 77% yield over 2 steps (Scheme 3.27).[299]

Scheme 3.27. 6-Aza-oxindole formation.
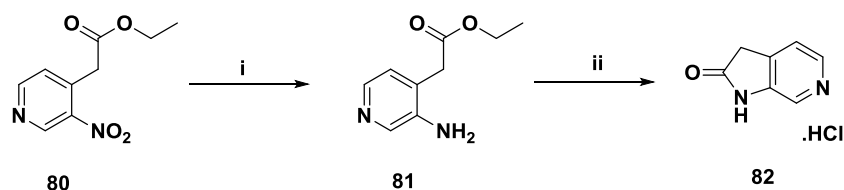
Reagents and conditions: (i) H$_2$ (1atm), 10% Pd/C, MeOH, rt, 24 h, 94%; (ii) HCl (1.4 M), Et$_2$O, rt, 16 h, 82%.

However, 3,3'-*bis*-alkylation of the non-protected 6-aza-oxindole **82** proved more challenging than the standard alkylation procedures reported for the preparation of **RV-39** and its analogues.[156] Woolford *et al*. have reported the double methylation on a closely related *N*-boc-5-methoxy-6-aza-oxindole intermediate **83** using potassium carbonate as a base but no yields were given for that reaction (Scheme 3.28, equation A).[311] Bakke *et al.* also reported the *bis*-alkylation transformation similar to Woolford *et al.* in a non-protected 5-methoxy-6-aza-oxindole template **85** and using sodium hydride and iodomethane as the alkylating agent to yield 3,3'-dimethyl-5-methoxy-6-aza-oxindole **86** (Scheme 3.28, equation B).[299]

Scheme 3.28. Reported literature precedents of the alkylation of the 6-aza-oxindole template.
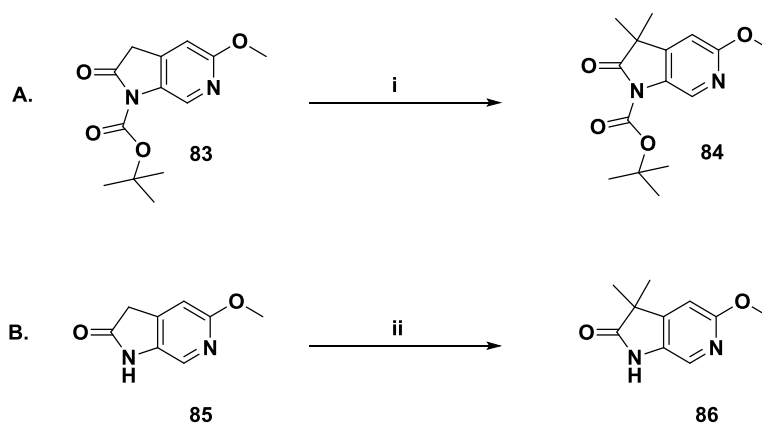
Reagents and conditions: (i) K$_2$CO$_3$, iodomethane, acetone, rt; (ii) NaH, iodomethane, DMF, 0 °C to rt, 48 h, 30%.[299,311]

There are however no precedents for the cyclopropanation of 6-aza-oxindoles, or more generally for the formation of 3,3'-spirocyclic 6-aza-oxindoles reported in the literature. Capitalising on the alkylation reports from Bakke and Woolford, the treatment of the 6-aza-oxindole **82** with potassium carbonate in acetonitrile either at room temperature or 80 °C did not lead to the formation of any product (Scheme 3.29, entry 1 and 2). Similar results were

obtained when using sodium hydride (4 equivalents) as a base at 0 °C and only led to a very complex mixture from which no product could be detected (Scheme 3.29, entry 3). Alternative bases were also attempted and the reaction with either LiHMDS or LDA were not successful either and no product could be detected (Scheme 3.29, entry 4 and 5 respectively). However, when using lithium diisopropylamide (4 equivalents) as a base formed *in situ* in the reaction proved successful. Indeed, the addition of n-butyl lithium to a solution of the 6-aza-oxindole **82** and diisopropylamine in tetrahydrofuran at -40 °C and subsequent slow addition of the 1,2-dibromoethane alkylating reagent led to the formation of the 3,3'-cyclopropane-6-aza-oxindole **77**, albeit in very low yield (11% yield) (Scheme 3.29, entry 6). These conditions led to a complex mixture but from which the 3,3'-cyclopropane-6-aza-oxindole **77** could be isolated.

Scheme 3.29. Cyclopropyl alkylation of 6-aza-spirooxindole.
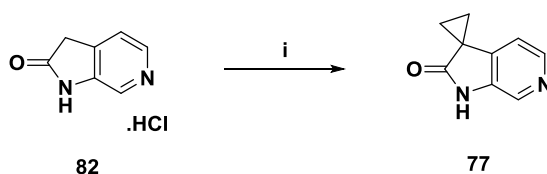
Reagents and conditions: (i) base, 1,2-dibromoethane

Entry	Base	Solvent	Temperature	Conversion
1	K$_2$CO$_3$ (4 equiv.)	MeCN	0 °C to 20 °C	No reaction
2	K$_2$CO$_3$ (4 equiv.)	MeCN	20 °C to 80 °C	No reaction
3	NaH (4 equiv.)	DMF	0 °C to 20 °C	Complex mixture
4	LiHMDS (4 equiv.)	THF	-78 °C to 20 °C	No reaction
5	LDA (4 equiv.)[a]	THF	-40 °C to 20 °C	No reaction
6	LDA (4 equiv.)[b]	THF	-40 °C to 20 °C	11%[c]

[a]Preformed LDA solution; [b]Formed *in situ*; [c]Isolated yield.

Unfortunately, the reaction proved difficult to reproduce and the cyclopropyl aza-oxindole product **77** could not be isolated in better yield, mainly due to the complex mixture resulting from the reaction. It is unclear why the 3,3'-cyclopropyl 6-aza-oxindole **77** was obtained in such a low yield as no other by-products could be easily isolated and characterised. It can be assumed that if the cyclopropanation is not fast enough, a multitude of mono and *bis*-alkylated by-products as well as alkylation on the pyridyl nitrogen and dimers may be formed. However, none

of these by-products could be isolated. The poor yield obtained for this *bis*-alkylation reaction further reinforce the initial strategy set for this work to avoid such a synthetic methodology. Access to the 6-aza-spirooxindole **77** proved to be less than optimal with an overall 4% yield over 4 steps from commercial starting materials but did not involve the use of any protecting groups that have been demonstrated to be difficult to remove on such oxindole and aza-oxindole templates. Despite the low yield obtained during the cyclopropanation reaction, the 3,3'-cyclopropyl-6-aza-oxindole **77** was further alkylated with 2-chloromethyl benzimidazole **48** (R_4 = -CH_2NHBoc, R_5 = - ^{i}Pr or -CH_2CF_3) using sodium hydride as a base in *N,N*-dimethylformamide and subsequently Boc deprotected under trifluoroacetic acid conditions (Scheme 3.30). The desired products **87a** and **87b** were isolated in 18% and 24% yield respectively over the 2 steps and are summarised in Table 3.30.

Scheme 3.30.
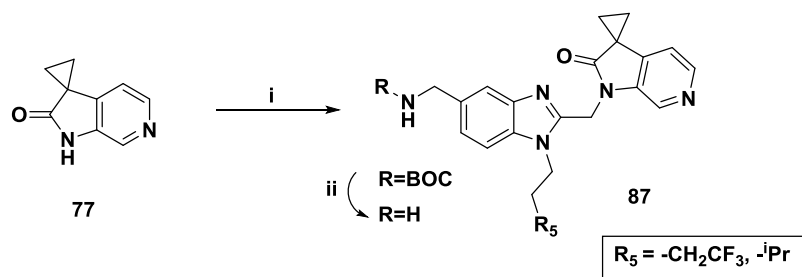
Reagents and conditions: (i) NaH, **48**, DMF, 0 °C to rt, 16 h; (ii) TFA, CH_2Cl_2, rt, 2 h.

Table 3.30. Summary of spirocyclic 6-aza-oxindole derivatives prepared.

Compound	Structure	Yield[a]
87a		18%
87b		24%

[a]Isolated yield over 2 steps

3.3.3 Summary

Despite some precedents in the literature for the preparation of spirooxindoles, very few methodologies allowed for the preparation of a broad range of derivatives. Many of the synthetic strategies that have been reported have focussed on the preparation of very specific spirooxindole alkaloids, often requiring complex starting materials and precursors to install the spirooxindoles.[312] Unfortunately, the initial method reported in this work *via bis*-alkylation of oxindoles did not allow for the preparation of the planned oxetane, azetidine and thiethane spirocyclic oxindoles **22a-c**. The lack of reactivity of the *bis*-mesylate intermediate **27** led to consider an alternative synthetic strategy.

A very efficient synthetic route *via* palladium-catalysed α-arylation has however enabled the preparation of various 3,3'-spirooxindole derivatives in moderate to good yield. The key intermediates **35** and **42a-e** could be prepared from commercially available carboxylic acids and substituted 2-bromo-anilines. Under the thermal condition initially identified (80 °C to 90 °C), the spirocyclic oxindoles **36**, **44a-c** and **44e** could be obtained *via* palladium-catalysed α-arylation over 16 hours. However, the reaction conditions were further optimised and the spirooxindole **44d** could be prepared in high yield in 4 minutes under microwave irradiation at 130 °C. The subsequent removal of the *para*-methoxybenzyl protecting group proved more difficult and was achieved by treatment of the protected spirooxindoles with trifluoroacetic acid at 150 °C for 2 hours to 4 hours. The deprotection step was further optimised and the *para*-methoxybenzyl protecting group could be removed at room temperature in the presence of an excess of trifluoromethanesulfonic acid in trifluoroacetic acid to give the spirooxindole **45d** in good yield.

All the spirooxindoles prepared were subsequently *N*-alkylated with 2-chloromethyl benzimidazole **48**. The obtained final compounds were evaluated as potential RSV inhibitors.

Following on the optimisation of the reaction conditions leading to the preparation of the spirooxindoles **39**, **41**, **45a-e**, **46** and **47**, and in particular the mild PMB deprotection step, it is anticipated that the synthetic sequence presented in this work should be amenable to the scale up of any spirooxindoles of interest.

The preparation of 5-aza-spirooxindoles and 6-aza-spirooxindoles was also envisaged. Acylation and PMB-alkylation of the 3-bromo-4-amino pyridine **70** were not fully optimised but allowed the preparation of the key arylation precursor **67**. The palladium-catalysed α-arylation,

previously described, allowed for the preparation of the 5-aza-spirooxindole **68** in good yield, despite the need to increase the reaction temperature to 150 $^{\circ}$C. The PMB deprotection could only be achieved under high temperature and pressure in the presence of trifluoroacetic acid. Following on from the *para*-methoxybenzyl deprotection issues for the preparation of the 5-aza-spirooxindole **68**, an alternative synthetic strategy was used to prepare the cyclopropyl 6-aza-oxindole **77**. Indeed, this example was prepared *via* a *bis*-alkylation methodology instead, albeit in very low yield.

Chapter 4. SAR and Biological Evaluation

4.1 RSV Project Screening Cascade

The compounds prepared in chapter 3 were progressed according to the screening cascade presented in figure 4.1. The compounds were initially profiled in a RSV fusion assay, measuring the ability of a cell line expressing the F protein from the A2 strain of the RSV subtype A to fuse to adjacent cells (Section 4.1.1). Compounds with encouraging *in vitro* potency (IC_{50} < 100 nM) were progressed in the plaque reduction assay, a titration of the viruses on Vero cells (Section 4.1.2), as well as through a panel of *in vitro* DMPK screens: rat, dog and human liver microsomes to assess metabolic turnover and a MDCK permeability assay (Section 4.1.3) that would inform further progression into *in vivo* PK studies in the rat. Selected key compounds were also evaluated in thermodynamic solubility and hERG safety assays (Section 4.1.3) as well as cytotoxicity assay (Section 4.1.4).
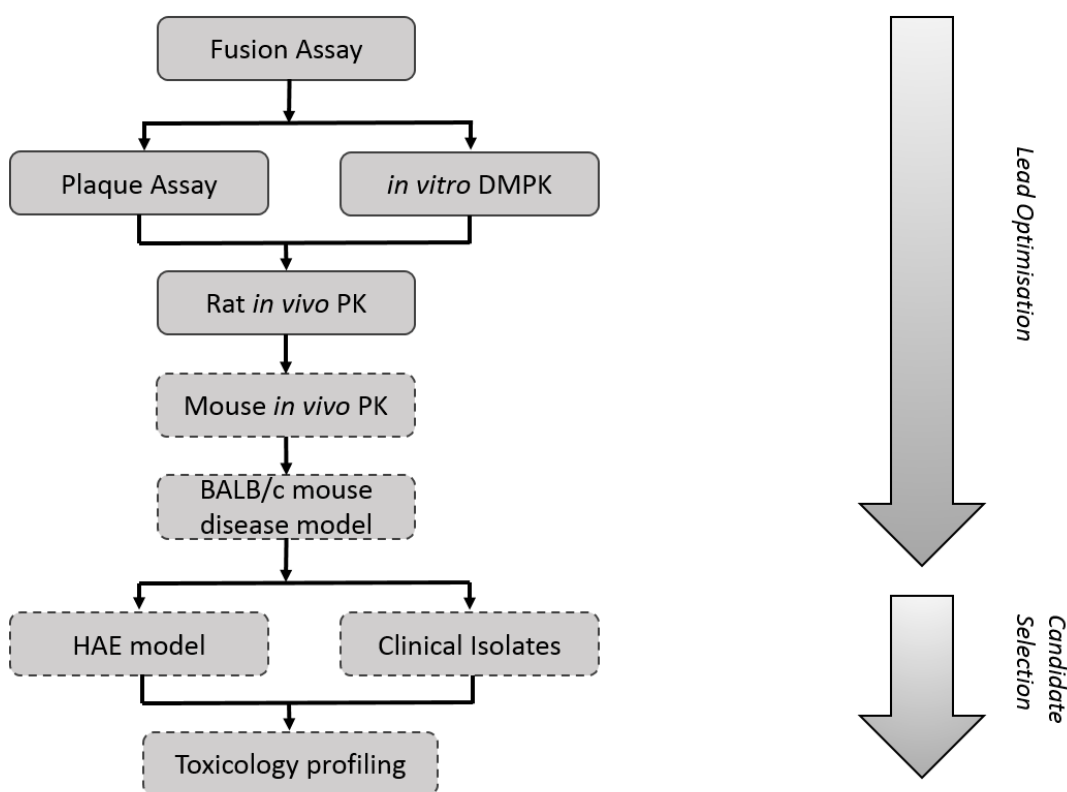

Figure 4.1. RSV screening cascade. Assays represented in dashed cells were not performed on any of the compounds described in this thesis.

Compounds meeting the rat pharmacokinetic desired criteria of the target product profile described in Chapter 2, table 2.4 ($T_{1/2}$ > 2 hours, F > 30%) were progressed in a mouse pharmacokinetic study and the BALB/c mouse model of the disease, assessing the effects *in vivo* on infection of the virus. The compounds were subsequently evaluated in both the Human Airway Epithelial (HAE) model, a measure of the ability of a compound to block viral infection and spreading, and a clinical isolates assay, measuring the antiviral activity of a compound against a broad panel of clinical isolates.

The assays used to generate the antiviral data and *in vitro* DMPK data presented in this chapter were carried out within the biology department of the Sussex Drug Discovery Centre (*in vitro* cellular pharmacology and cell viability), at the University of Queensland, Australia (plaque reduction assay) or at Cyprotex (*in vitro* ADME assays) and are described succinctly below. A comprehensive description of the *in vitro* cell-cell fusion, cell viability and plaque reduction assay is presented in the appendix section.

4.1.1 *In vitro* Cellular Pharmacology and Cell Viability

This assay assesses both the concentration at which test compounds are able to inhibit cell-cell fusion in cells transfected with an optimised gene construct of the RSV F protein and cell viability.[123,157] Cell-cell fusion can be initiated *in vitro* by transfecting cells with a codon optimised gene construct of the RSV fusion protein.[313] This assay is based on the mixing of two HEK 293T/17 cell populations, one co-transfected with luciferase reporter (pFR-Luc vector) and RSV F plasmids and the other transfected with a plasmid containing a transcriptional activator (pBD-NFκB vector) (Figure 4.2a). The transfected cell populations were mixed to allow cell-cell fusion, mediated by the RSV F protein and were exposed to serial dilutions in the presence of the compounds of interest.

a. *In vitro* Cell Based Assay

The cells were lysed and the luciferase reporter gene activity was monitored by light emission at the end of the assay by the addition of a luciferin substrate. The inhibition of cell-cell fusion by a test compound was measured by a reduction in the luminescence signal. A standard non-linear regression analysis (four parameter logistic regression) of the data obtained from each compound was used to calculate the IC_{50} cell-cell inhibition (Figure 4.2b). Cells transfected with the luciferase reporter alone were used as a control.
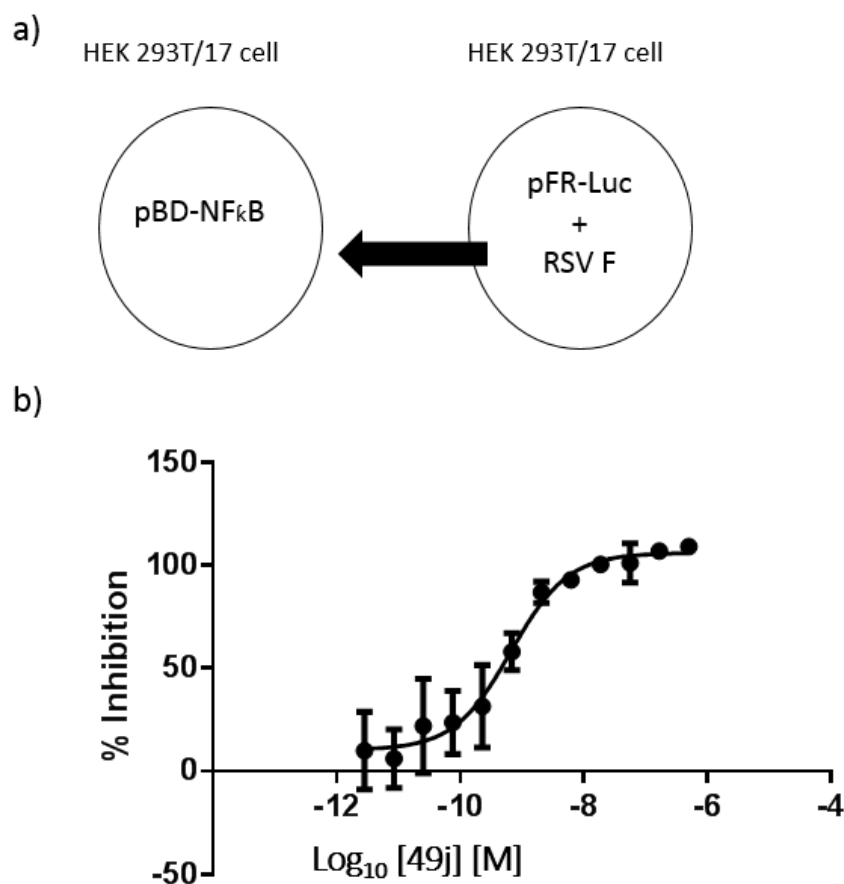
Figure 4.2. (a) Schematic of the RSV cell-cell fusion assay; (b) Example of IC_{50} determination by *in vitro* cell-based fusion assay for compound **49j**.

b. Cell Viability

The cell viability was also assessed from the same assay. Cell viable with active metabolism can reduce resazurin, a cell permeable redox indicator, into resofurin. The cells were treated with CellTiter-Blue® (resazurin cell viability kit) and incubated at 37 °C for 2 hours. The fluorescence of resofurin, proportional to the number of viable cells, was measured at 590 nm and a standard non-linear regression analysis of the data obtained was used to calculate the cell toxicity of each test compound of interest (Figure 4.3).[157]
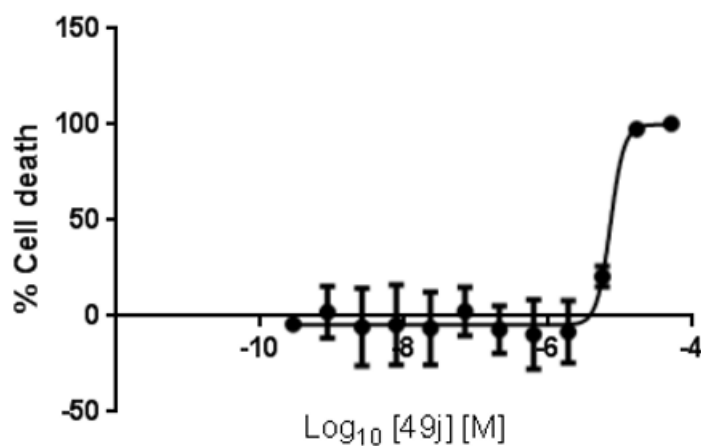
Figure 4.3. Cell viability example for compound **49j**. The dose response curve represents an increase in cell death with an increase concentration of compound **49j**.

4.1.2 RSV Plaque Reduction Assay

A plaque reduction neutralisation assay (PRNT) was used to quantify RSV infection on Vero cells (isolated from the kidney of an African green monkey) in the presence of the test compounds of interest through the counting of discrete plaques in cell culture.[157,314] Vero cells into 96 well plates were treated with a solution of the compound of interest and the RSV A2 strain and incubated for 48 hours. After fixing and staining the infected cellular monolayer, the plaques were visualised and counted to determine titre viral stock present. EC_{50} values for the compounds were derived from the dose response curves (Figure 4.4).
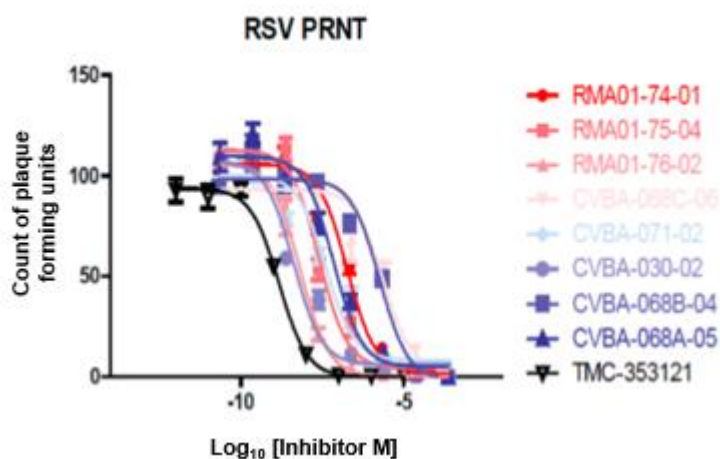
Figure 4.4. RSV plaque reduction neutralisation assay (PRNT) dose response curves across a selection of compounds. Each dose response curve represents a reduction in the number of RSV plaque forming units as the concentration of the fusion inhibitor increases.

4.1.3   *In vitro* DMPK assays

The assays used to assess the *in vitro* pharmacokinetics properties of each compound were outsourced to an experienced contract research organisation, namely Cyprotex, and are summarised in Table 4.1.

Table 4.1. Summary of outsourced *in vitro* ADME assays used for the RSV project optimisation.[315,316]

Assay	Description
Liver microsome metabolic turnover	A measure of the vulnerability of a compound to be metabolised by membrane-bound cytochromes P450 enzymes across various species (human, rat, mouse and dog). Data are quoted as intrinsic clearance (Clint) expressed as a flow in µL/min/mg with lower values representing lesser liability to enzymatic metabolism.[317–319]
Hepatocyte metabolic turnover	A more comprehensive measure of compound vulnerability to be metabolised by an ensemble of liver enzymes of both phase 1 (oxidation and reduction) and phase 2 (conjugation) metabolic processes, measured using intact liver cells.[319] The hepatocytes carry the metabolizing enzymes of all isoforms along with co-factors, uptake and efflux transporters and represent a metabolism environment similar to *in vivo* conditions.
Membrane permeability	The measure of permeability of a compound across the lipophilic cell membrane of a particular cell line. More specifically, the compound permeability was measured in the *Madin Darby canine kidney* (MDCK) cell line expressing the *MDR1* gene, the gene encoding for the P-glycoprotein (P-gp) efflux protein. Apparent permeability values (P_{app}(A-B), quoted in units of 10^{-6} cm/s) are determined from apical (A) layer to basolateral (B) layer. Efflux ratio P_{app}(B-A)/ P_{app}(A-B) greater than 2 are indicative of compounds P-gp substrates actively transported for efflux.[227]
Aqueous solubility	The assessment of the thermodynamic solubility was achieved the equilibrium shake flask method by the addition of an aqueous buffer to a solid compound. After shaking the mixture

for 24 hours, the measure of the solubility at the equilibrium was determined by MS/MS quantification. Compounds with solubility between 1 µM and 100 µM are considered to be moderately soluble, and above 100 µM to have high solubility.
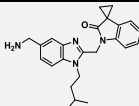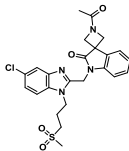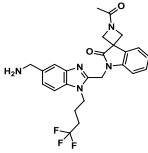
hERG inhibition	The human ether-a-go-go related gene (hERG) encodes a voltage gated potassium channel linked to cardiac repolarisation and inhibition may lead to life-threatening 'Torsades de Pointes' arrhythmia. The hERG channel inhibition, reported as an IC_{50} determination, was measured *via* a high-throughput patch clamp cell-based electrophysiology assay from Chinese hamster ovary cells transfected with the hERG gene (CHO-hERG).[315] A significant safety window over the hERG channel (hERG $IC_{50}/C_{max, unbound}$ > 30) is necessary to mitigate the risks of cardiac events.[227]

4.2 Physicochemical Properties and Inhibitory Activity

A summary of the physicochemical properties of the compounds prepared in Chapter 3 is presented in Table 4.2. All the compounds prepared have an increased molecular weight compared to **RV-39**. This is in part resulting from the exploration of the spirooxindole moiety, increasing the ring size from a cyclopropyl up to a piperidine and also from the modification of the pendant alkyl chain of the benzimidazole with the introduction of both the sulfone and trifluoro chains. However, apart from **49j, 49k and 49l**, all the compounds have a clogP lower than **RV-39**, owing to the introduction of more polar pendant alkyl chains in particular the sulfone chain. Introduction of the aminomethylene linker on the C-5 position of the benzimidazole reduces the clogD$_{7.4}$ significantly compared to the compounds bearing a chloro on this position. The aminomethylene moiety has an estimated pKa of 9.1, and therefore expected to be completely protonated under physiological conditions.

To understand the impact of a basic centre in the 5-chloro benzimidazole sub-series, the piperidine spirooxindole **49g** was also prepared with an estimated pKa of 9.8, thereby significantly reducing the clogD$_{7.4}$ (-0.79) compared to **RV-39**. All of these modifications were made to establish further SAR whilst understanding the impact of lipophilicity (clogP and clogD$_{7.4}$) on metabolic stability and permeability (See Chapter 2, section 2.3 Chemistry strategy for optimising **RV-39**).

Table 4.2. Structures and physicochemical properties of the prepared compounds.

Compound	Structure	Mwt	clogP[a]	clogD[b]
RV-39		388	3.62	1.75
49a		501	0.58	0.58
49b		485	1.88	0.01

Compound	Structure	Mwt	clogP[a]	clogD[b]
49c		446	1.97	0.11
49d		453	1.73	1.73
49e		503	0.86	0.86
49g		487	1.55	-0.79
49h (49n & 49o as single enantiomers)		474	1.58	1.58
49i		433	3.26	1.39
49j		446	3.66	2.00/1.54[c]
49k		406	3.76	1.90
49l		452	5.14	5.14
49m		414	3.51	3.51

Compound	Structure	Mwt	clogP[a]	clogD[b]
49p		565	0.65	0.65
49q		529	1.16	1.16
76		489	0.66	0.65
87a		389	2.40	0.54
87b		429	2.30	0.44
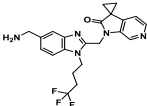
[a]cLogP was calculated using ChemAxon; [b]Calculated clogD at pH 7.4 octanol/neutral buffer using ChemAxon; [c]Measured logD at pH 7.4 in octanol/neutral buffer.

A summary of the initial antiviral activity data for the compounds prepared is reported in Table 4.3. The antiviral activity was evaluated initially in the RSV fusion assay and subsequently in the plaque reduction assay as described in the screening cascade paragraph (Figure 4.1).

Table 4.3. Antiviral activity of selected compounds.

Compound	Structure	Fusion IC$_{50}$[a] (nM)	PRA IC$_{50}$[b] (nM)	LiPE[c]
RV-39		0.5 ± 0.2	2.2	5.34
49a		1.7 ± 0.2	>2,000	8.19
49b		2.7 ± 1.0	50.3 ± 68.0	6.69
49c		1.1 ± 0.4	2.2 (n = 1)	6.99
49d		0.3 (n = 1)	>2,000	7.80
49e		256.8 ± 121.1	>2,000	5.73
49g		2.8 ± 0.8	>2,000	7.01
49h		ND	>2,000	ND

Compound	Structure	Fusion IC$_{50}$[a] (nM)	PRA IC$_{50}$[b] (nM)	LiPE[c]
49i		0.7 ± 0.3	3.4 ± 3.2	5.90
49j		0.8 ± 0.3	3.2 ± 3.6	5.44
49k		0.6 ± 0.2	4.6 ± 5.2	5.46
49l		6.2 ± 2.5	132.3 ± 22.9	3.07
49m		3.4 ± 1.7	185.2 (n = 1)	4.96
49n		2.7 ± 0.6	>2,000 (n = 1)	6.99
49o		1.6 ± 0.6	>2,000 (n = 1)	7.22
49p		1.2 ± 0.2	ND	8.27
49q		1.7 ± 0.4	1178.9 ± 1403.6	7.61
87a		0.9 ± 0.1	1.8 (n = 1)	6.65

Compound	Structure	Fusion IC$_{50}$[a] (nM)	PRA IC$_{50}$[b] (nM)	LiPE[c]
87b		0.8 ± 0.2	0.8 ± 0.4	6.80

[a]RSV Fusion assay (nM). Determinations ± standard deviation from mean of n = two or more determinations unless otherwise specified; [b]Plaque Reduction Assay (nM). Determinations ± standard deviation from mean of n = two or more determinations unless otherwise specified; [c]LiPE = pIC$_{50}$ – clogP calculated against the RSV Fusion assay.

Overall, expanding the ring size of the spirooxindole from a cyclopropyl up to a piperidine is tolerated and all the compounds tested in the RSV fusion assay retain sub-10nM antiviral activity with most compounds having similar antiviral activity to **RV-39**. Surprisingly, even the bulkier acetyl piperidine **49q** and sulfonamide piperidine **49p** remain extremely potent in this assay (IC$_{50}$ = 1.12 and 1.7 nM respectively). The data from the RSV fusion assay suggest that the C(3)-position of the oxindole can tolerate a broad range of modifications whilst retaining potency and all compounds, apart from **49e**, are very potent RSV inhibitors in the fusion assay. Compounds **49a**, **49c-d**, **49i-k**, **49o-q**, **87a** and **87b** are within 3-fold of the antiviral activity of **RV-39** (Fusion IC$_{50}$ = 0.5 nM). Compounds **49g** and **49l- n** also remain very potent, within 6 to 12-fold of the antiviral potency of **RV-39**. Additionally, it is evident from the data that the open chain amide **49e** is not tolerated and showed a significant drop in potency with a 150-fold activity loss compared to the corresponding azetidine spirooxindole **49a**. The restricted conformation conferred by the oxindole appears to be essential and responsible to a large degree for the antiviral activity observed in this series.

The direct replacement of the cyclopropyl with either the acetyl azetidine (**49c**) or the morpholine (**49i**) moieties led to similar antiviral activity to **RV-39** in both the RSV fusion and the plaque reduction assays. Similarly, increasing the ring size from the azetidine **49a** to the piperidine **49q** led to compounds exhibiting similar levels of activity. Capping of the free piperidine **49g** (clogD$_{7.4}$ = -0.79) to the sulfonamide **49p** (clogD$_{7.4}$ = 0.65) or acetyl **49q** (clogD$_{7.4}$ = 1.16) had little influence on the potency in the fusion assay. Expanding the ring size from the acetyl azetidine **49a** to the single enantiomer tetrahydropyrans **49n** and **49o** resulted in similar levels of potency in the fusion assay.

Encouragingly, blocking the putative site of metabolism of the oxindole with a fluorine at the C-6 position (compounds **49j** and **49k**) had no detrimental effect on the antiviral activity. Indeed, both compounds exhibited excellent antiviral activity, with IC$_{50}$ values below 5 nM in both the RSV fusion and PRA assays. Similarly, introduction of the 6-aza spirooxindole moiety (**87a** and

87b) did not impact on the antiviral potency and both compounds showed a similar antiviral activity to **RV-39** in both the fusion and the plaque reduction assays, irrespectively of the pendant side chain on the benzimidazole. Both compounds have a reduced lipophilicity compared to **RV-39**, owing to the introduction of the nitrogen, thus leading to an increase in the lipophilic ligand efficiency (LiPE = 6.65 for **87a** and LiPE = 6.80 for **87b**, compared to LipE = 5.34 for **RV-39**).

With the exception of compounds **49l** and **49m** (clogP > 3.5), all the spirooxindole compounds showed an excellent retention of antiviral activity in the fusion assay, which combined with a reduction of lipophilicity led to a series of compounds with an improved lipophilic ligand efficiency compared to **RV-39** (Table 4.3).

Overall, there appears to be a trend whereby the compounds bearing an aminomethylene moiety on the benzimidazole (Figure 4.5, green dots) appear more potent in the RSV fusion assay than the compounds bearing a chloro in this position (Figure 4.5, red dots). This drop in antiviral potency is illustrated by the matched pair prepared across the two sub-series with the replacement of the aminomethylene moiety **49j** by the chlorine atom in **49l** that led to an 8-fold potency drop in the primary RSV fusion assay (Figure 4.5).

As described in Chapter 2, it was expected that the side chains would allow to adjust the physicochemical properties and reduce the lipophilicity of the compounds prepared compared to **RV-39** rather than having an impact on the antiviral activity. The data in Table 4.3 reveal that modification of the *N*-alkyl side chain on the benzimidazole showed little differences in antiviral activity in the fusion assay between all the side chains investigated. For example, both the analogues **49j** and **49k** with the -CF_3 and -isoamyl pendant chains are equipotent to **RV-39**.
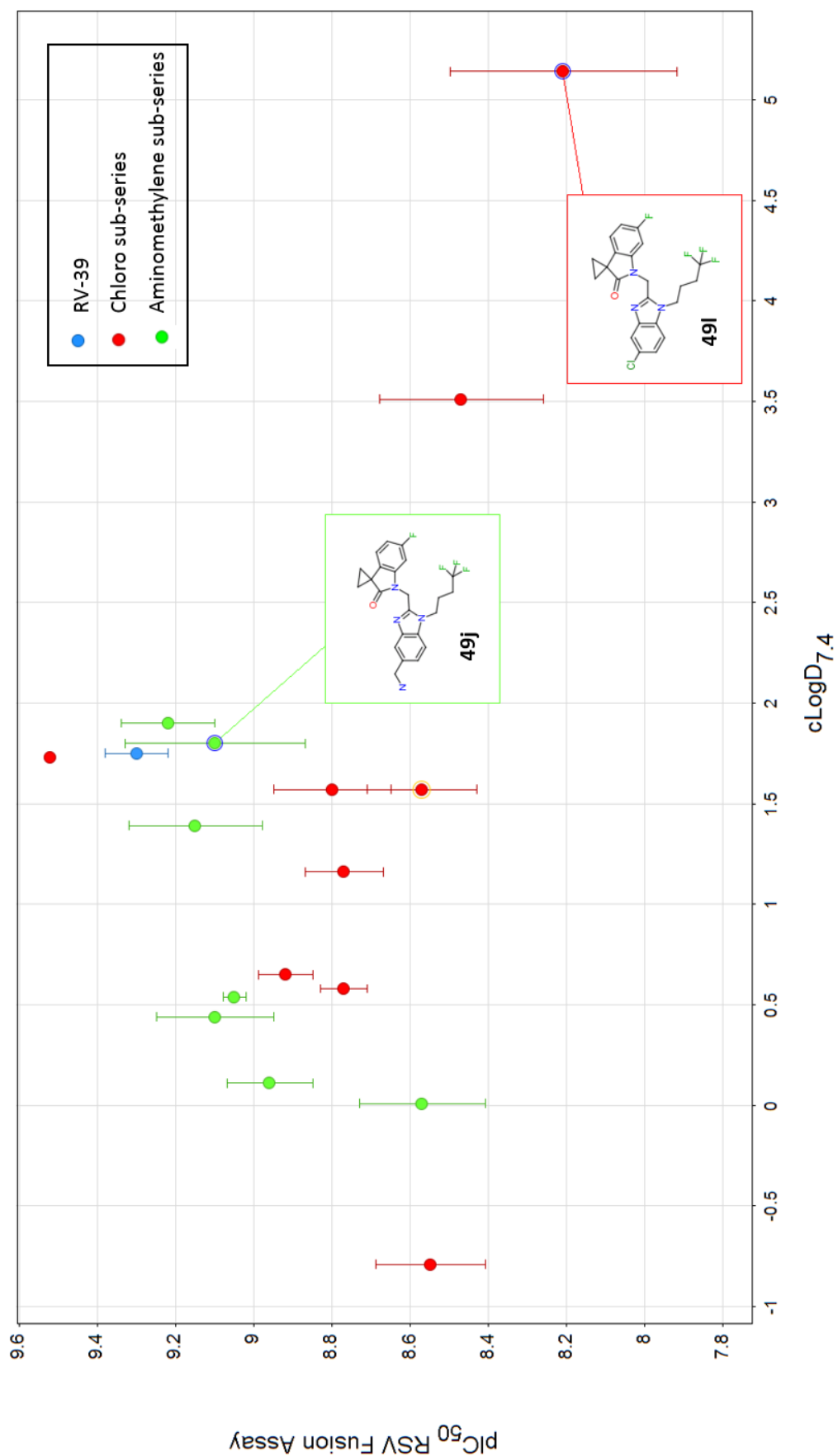
Figure 4.5. Correlation between pIC$_{50}$ (-log IC$_{50}$) in the fusion assay and clogD$_{7.4}$.

However, in the plaque reduction assay, all the compounds bearing a chloro substituent at the 5-position of the benzimidazole showed reduced antiviral potency compared to the aminomethylene derivatives (Table 4.3). Most compounds from the chloro sub-series exhibited antiviral potency with IC_{50} of greater than 2 μM, compared with IC_{50} generally below 10 nM for the aminomethylene compounds. A plot of such a difference in antiviral potency in the PRA assay for the two sub-series is depicted in Figure 4.6. For example, the cyclopropyl spirooxindole matched pair **49j** and **49l** prepared across the two sub-series demonstrated a 40-fold loss in activity in the PRA assay by replacing the aminomethylene by the chlorine atom (Figure 4.6).

For the compounds bearing an aminomethylene moiety (Figure 4.7, green circles), the data obtained from the primary fusion assay correlated with the data from the plaque reduction assay and was in line with the data obtained for **RV-39** (Figure 4.7, blue circle). As already commented, in the chloro benzimidazole sub-series, a significant discrepancy was observed between the data obtained in the RSV fusion assay and the plaque reduction assay (Figure 4.7, red circles), with potent nanomolar compounds in the RSV fusion assay having micromolar antiviral activity in the PRA assay.

These unexpected results were not predicted by the RSV fusion assay data. The loss of antiviral activity in the plaque reduction assay is particularly interesting as compounds bearing a 5-chloro benzimidazole chemotype as exemplified by structures **6** and **8** (Chapter 1, table 1.2) have been previously reported in the patent literature.[166] The antiviral activity of such chloro benzimidazole compounds was reported in a viral cytopathic effect assay, measuring cell viability following genetically engineered viral infection. It remains however unclear if such compounds were profiled in a phenotypic assay such as the plaque reduction assay. The fusion assay uses a luciferase reporter not normally expressed in mammalian cells which may potentially give rise to false positives and over-estimate compound potency in the chloro sub-series of compounds. Alternatively, the plaque reduction assay has a much longer incubation time (5 days) with the compounds tested in a whole cell system and may result in cell toxicity over a longer period of time. Cell toxicity was not measured in the plaque reduction assay but may also explain some of the discrepancy observed between the two assays and in particular with the chloro benzimidazole sub-series.
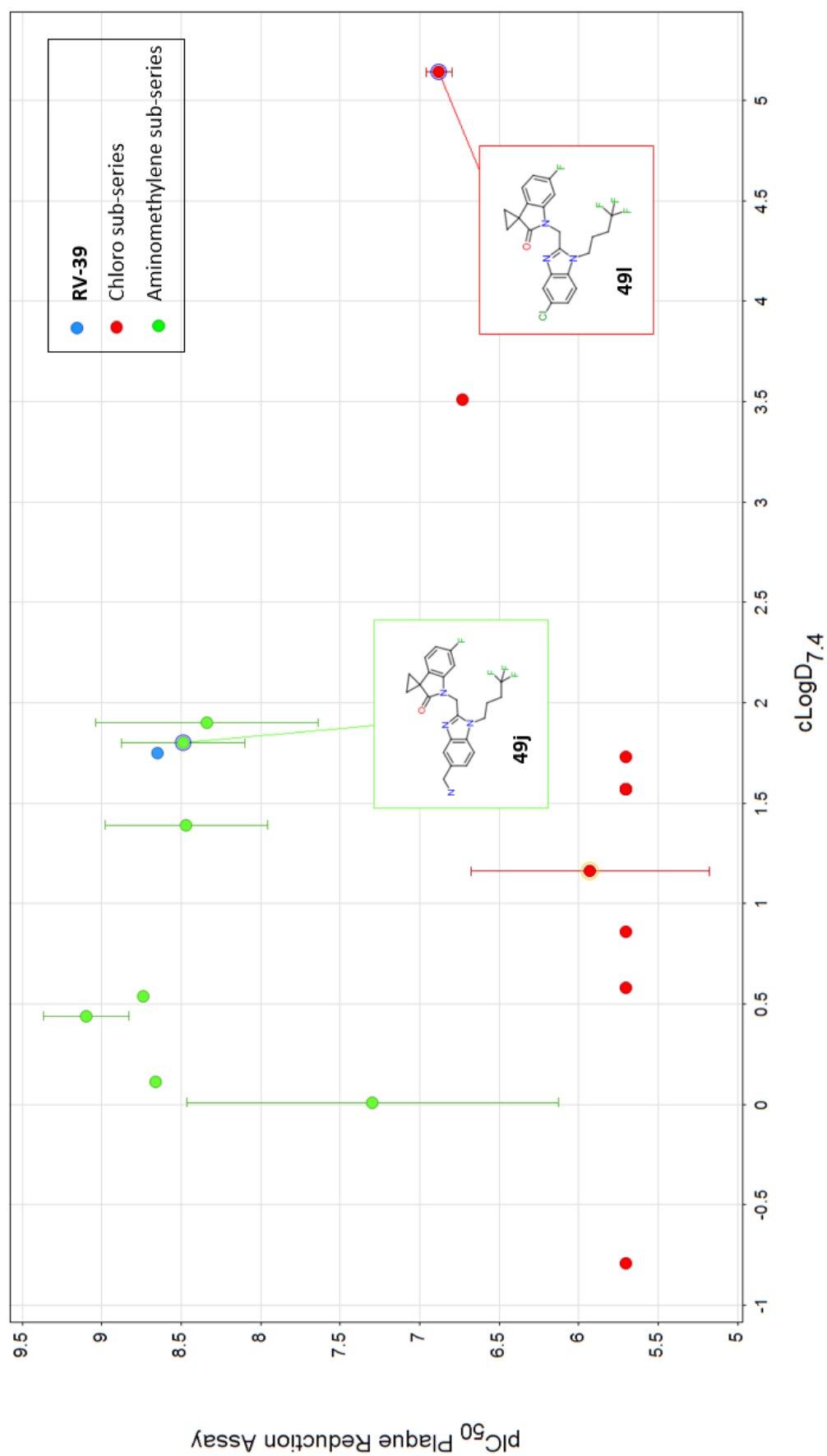
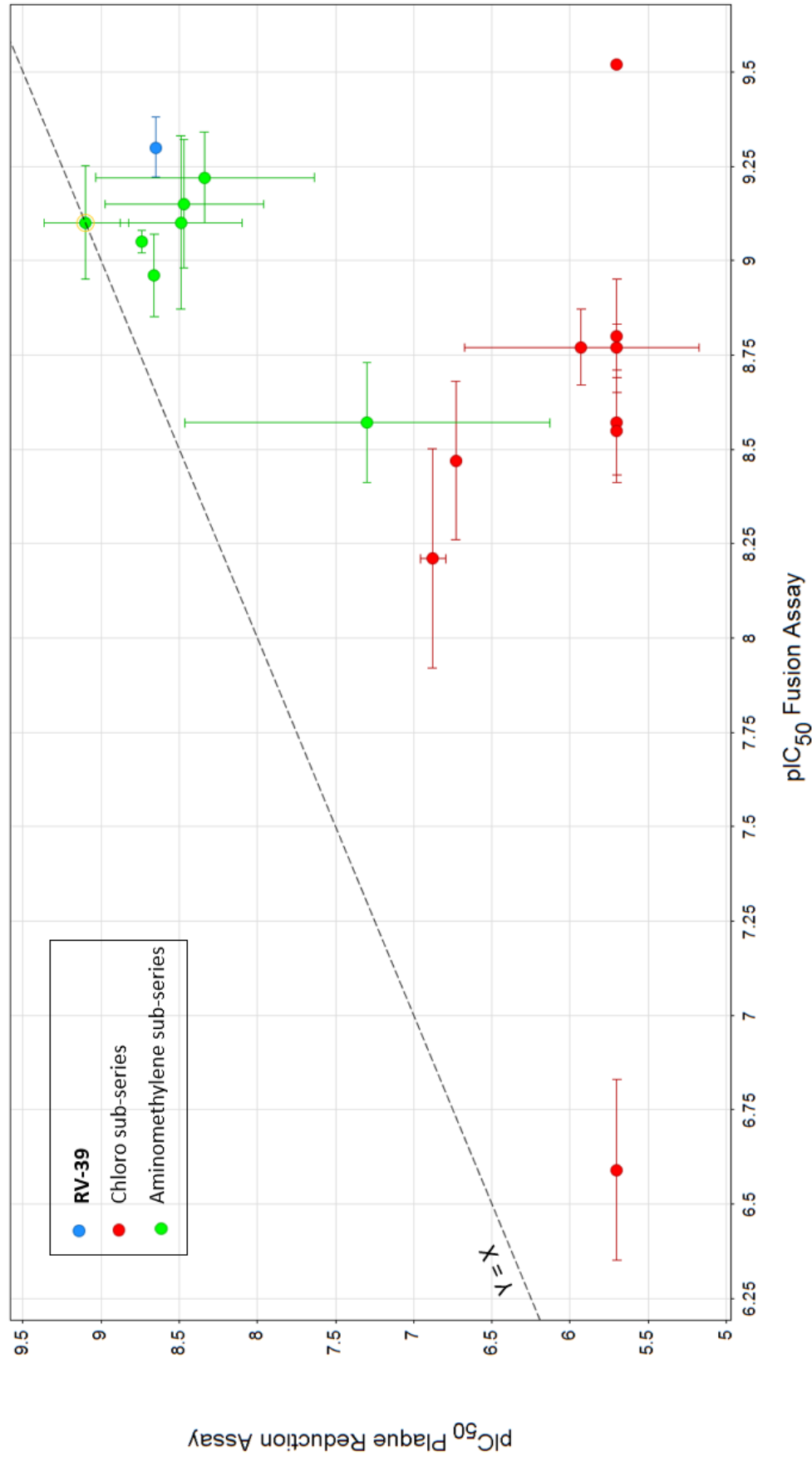**Figure 4.6.** Correlation between pIC_{50} (Plaque Reduction Assay) and $clogD_{7.4}$.

Figure 4.7. Disparity between RSV Fusion and Plaque Reduction Assays.

Following on the loss of antiviral activity in the plaque reduction assay, it was evident that compounds from the chloro sub-series were difficult to progress any further. All the compounds where nonetheless profiled in *in vitro* ADME studies, performed in parallel to the plaque reduction assay, as depicted by the screening cascade (Figure 4.1) due in part to the slow turnaround of the PRA for which the results were only obtained at an advanced stage of the project.

A selection of compounds was also evaluated in the resazurin cell viability assay described in section 4.1.3 (Table 4.4). The compounds bearing an aminomethylene moiety evaluated in this assay (**49i**, **49j** and **49k**) demonstrated measurable levels of cell toxicity at concentrations less than 20 µM toward the HEK 293T/17 cell line. However, the cell toxicity was not significant in the case of the aminomethylene aza-oxindole compound **87b**. The high therapeutic index of these compounds (defined as the ratio of the cytotoxicity CC_{50} over IC_{50}) associated with the low nanomolar antiviral activity did not warrant any safety concerns in this series, at least in this preliminary cell viability assay.[227]

Table 4.4. Cytotoxicity data on selected examples.

Compound	CC_{50}^a (µM)	TI^b	Compound	CC_{50}^a (µM)	TI^b
RV-39	>100	>200,000	**49j**	7.0	>8,700
49a	>100	>59,000	**49k**	15.4	>25,000
49i	19.2	>27,000	**87b**	>50	>62,000

aCytotoxicity expressed as CC_{50} (µM). n = one determination; bTherapeutic index defined as CC_{50}/IC_{50} where IC_{50} was obtained from the fusion assay.

Selected compounds were profiled into a thermodynamic solubility assay (Table 4.5). Pleasingly, reducing the lipophilicity led to an increase in aqueous solubility. Compounds with $clogD_{7.4} > 1.3$ were some of the lesser soluble compounds and in particular compounds such as the chloro-substituted analogue **49d** exhibited sub-optimal solubility. The very high solubility conferred by the aminomethylene moiety is clearly an attractive feature for future drug development and in line with the target product profile for this series. Similarly, compounds profiled in the hERG safety assay did not present any particular concerns with all IC_{50} values greater than 15µM, despite the presence of a basic amine in all the compounds screened (**49c**, **49i-k**), commonly associated with inhibition of the hERG channel.[227]

Table 4.5. Solubility and hERG data on selected examples.

Compound	Thermodynamic solubility (µM)	hERG IC$_{50}$ (µM)[a]	Compound	Thermodynamic solubility (µM)	hERG IC$_{50}$ (µM)[a]
49c	6000	49.9	**49j**	417	20.7
49d	29	ND	**49k**	172	15.7
49g	754	ND	**87b**	490	ND
49i	300	30			

[a]Compounds were tested to a maximum concentration of 100 µM; ND: Non determined.

4.2.1 ADME data
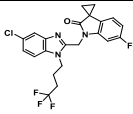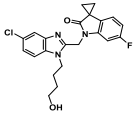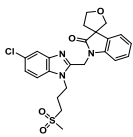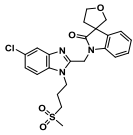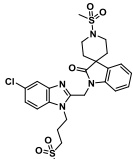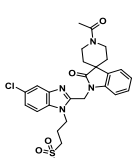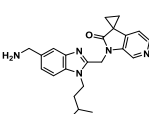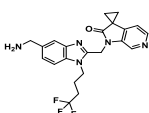
Most of the compounds prepared were progressed to *in vitro* ADME profiling to establish an understanding of the metabolism, permeability and efflux properties.[226,227,320] In particular, *in vitro* metabolism was initially assessed in liver microsome enzymes that are responsible for the metabolism of over 90% of marketed drugs.[227,319]

c. *Microsomal intrinsic clearance*

The initial azetidine oxindole analogues prepared (**49a-c**) demonstrated significantly reduced microsomal clearance compared to **RV- 39**, potentially due to the introduction of polarity and reducing the overall clogD$_{7.4}$ (Table 4.6). With the exception of a few compounds (**49i**, **49l**, **49m** and **49n-o**, **49i**), all the subsequent analogues prepared had low to moderate intrinsic clearance in the rat, dog and human liver microsomes, as categorised by the intrinsic clearance classification depicted in Table 4.7. Oxindoles bearing an oxygen-containing 3,3'-spirocycle (**49i**, **49n** and **49o**) appeared to have species-dependent microsomal turnover and were all highly cleared in both the rat and human liver microsomes.

Table 4.6. Microsomal intrinsic clearance for selected compounds.

Cpd	Structure	Cl$_{int}$ (µL/min/mg)[a]		
		Rat	Dog	Human
RV-39		20.7	11.8	120
49a		3.2	<LLOQ	<LLOQ
49b		<LLOQ	2.8	6.9
49c		3.1	3.9	3.4
49d		<LLOQ	<LLOQ	<LLOQ
49g		15.0	<LLOQ	8.2
49i		46.1	4.9	180
49j		17.4	2.6	43.5
49k		45.1	6.2	50.7

Cpd	Structure	Cl$_{int}$ (μL/min/mg)[a]		
		Rat	Dog	Human
49l		328	71.3	177
49m		315	23.1	39.4
49n		419	36.2	263
49o		487	40.2	245
49p		<LLOQ	1.7	<LLOQ
49q		7.8	2.8	6.5
87a		11.1	1.2	6.1
87b		<LLOQ	0.6	<LLOQ

[a]Cl$_{int}$ intrinsic clearance measure in microsomes; [b]<LLOQ below limit of quantification.

Table 4.7. Microsomal intrinsic clearance classification bands typically used for categorising compounds.[227,315]

Clearance category	Microsomal Intrinsic Clearance Clint (µL/min/mg)		
	Rat	Dog	Human
Low	< 13.2	< 5.3	< 8.6
High	> 71.9	> 28.9	> 47.0

As expected, the intrinsic clearance appeared to be linked to an increase in lipophilicity (Figure 4.8). Compounds with clogP < 2.5 showed a much lower intrinsic clearance than compounds where clog P > 2.5. In particular, in the chloro sub-series, high lipophilicity had a detrimental effect on the microsome stability (**49l** and **49m**, clogP 5.15 and 3.51 respectively). In the aminomethylene sub-series, the increase of lipophilicity did translate to more moderate increase in intrinsic instability with compounds where clog P > 2.5 showed medium levels of microsomal clearance in both the rat and human (**49j** and **49k**).[321]

It was hypothesised that the introduction of the 6-fluoro oxindole would have a positive influence on the microsomal stability. Unfortunately, this was not the case and all of the analogues bearing a 6-fluoro moiety did not exhibit any significant improvement in microsomal stability over **RV-39**. In particular, the analogue **49k** showed a medium level of *in vitro* microsomal clearance in the rat compared to **RV-39** and within 3-fold in the human liver microsomes. The reduction of the electron density on the oxindole was also investigated. Indeed, introduction of an aza-oxindole as represented by **87a** and **87b** did appear to have a clear impact on reducing the microsomal turnover observed in both the rat and human compared to the 6-fluoro analogues (**49j** and **49k**) and **RV-39**. In particular, the analogue **87b** showed no significant levels of microsomal turnover across species. The aza-oxindole **87a** showed a 4-fold reduction in the rat liver microsomes and 8-fold in the human liver microsomes compared to the 6-fluoro analogue **49k**.

Overall, apart from the oxindoles bearing an oxygen-containing 3,3'-spirocycle (**49i**, **49n** and **49o**), all the analogues prepared showed a 2 to 40-fold improvement in human microsomal stability compared to **RV-39**. This was particularly evident in the amino sub-series where introduction of polarity on the oxindole moiety showed a significant drop in the intrinsic clearance (Figure 4.8). Also the replacement of the cyclopropyl moiety of **RV-39** by a more polar acetyl azetidine moiety (**49a-d**) showed a significant reduction of the microsomal turnover in rat.
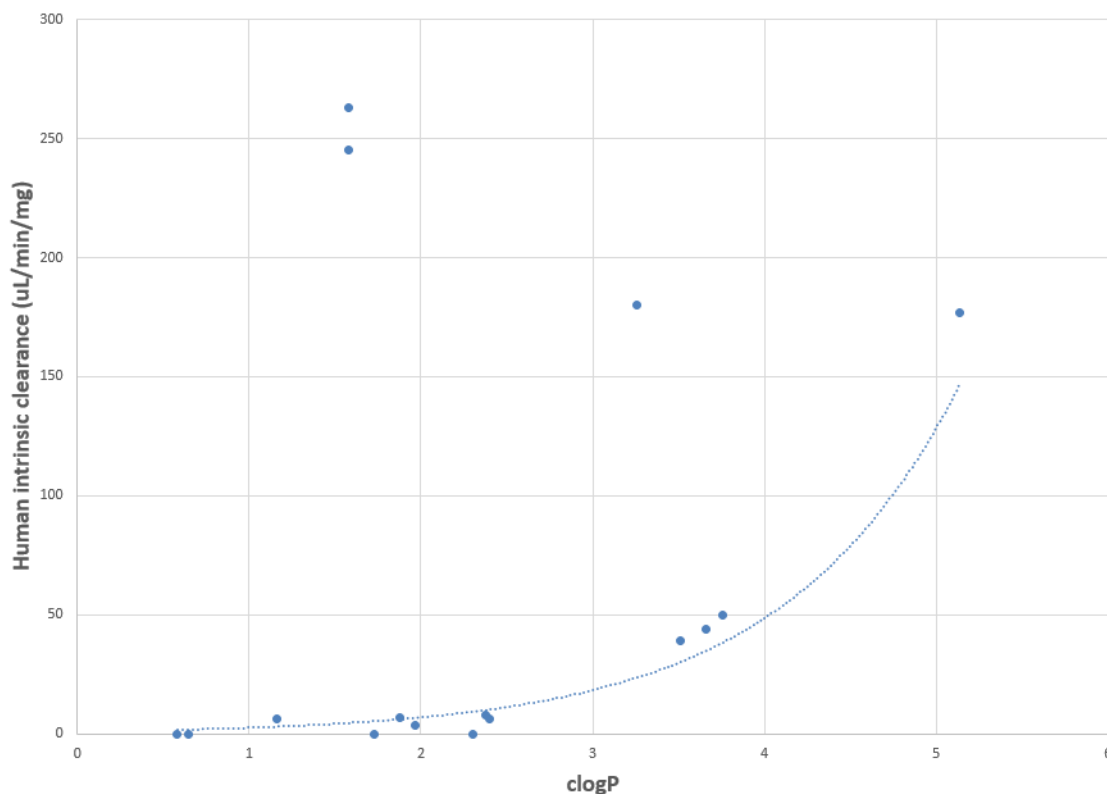
Figure 4.8. Relationship between human liver microsomal stability and lipophilicity across the series of compounds prepared. The dotted line represents the trend toward an increased intrinsic clearance with an increase of clogP.

d. *Membrane permeability*

Of the many processes regulating the absorption of a drug through the intestine, passive absorption and efflux have been identified as predominant factors that affect the pharmacology of a drug both in *in vivo* and *in vitro* experiments.

A range of molecular properties and structural modification strategies have been identified to control and improve on passive permeability by the transcellular route. Compounds satisfying the Lipinski's rule of 5 and a tPSA below 140 Å^2 have been associated with good passive absorption.[322,323] An increase in lipophilicity, resulting in higher affinity with the luminal lipid bilayer membranes, improves permeability. A decrease in hydrogen bonding is also associated with an increase in passive diffusion permeability. A study from SmithKline Beecham Pharmaceuticals showed that replacing ionisable groups by less polar and non-ionisable groups improved both *in vitro* permeability and *in vivo* oral bioavailability.[324] The ionisation state of a

compound has a significant impact on its rate of absorption across membranes. The passive permeability of acid compounds tends to increase at low pH where a large percentage of the compounds is neutral but is reduced as the pH increases, owing to an increased concentration in ionic species. Basic compounds tend to be protonated in the gastrointestinal tract, resulting in increased polarity, thus limiting passive permeability across membranes.[325]

P-glycoprotein (P-gp) and breast cancer resistance protein (BCRP) are two important efflux proteins of the ATP-binding cassette family of transporters and play a predominant role in transporting substrate compounds out of the cells. The efflux proteins can reduce the permeability and overall affect the ADME characteristics for some compounds at certain membranes.[326] In particular, P-gp is the most widely known efflux transporter but the molecular properties that are responsible for the efflux still remain poorly understood.[327] High levels of P-gp expression have been observed in many tissues of the body such as the liver, pancreas, kidney, colon, jejunum and in particular in the endothelial cells of the blood-brain barrier and on the luminal surface of the gastrointestinal epithelial cells.[328] The P-gp substrate specificity is very broad and able to transport a vast diversity of aromatic and non-aromatic compounds. The P-gp substrates can be basic, zwitterionic or uncharged with unrelated structural motifs and of great range of molecular weight.[328] The correlations between lipophilicity and P-gp substrate affinity has proved more difficult and has raised contradictory opinions.[327,329,330]

Seelig has developed an empirical model defining two types of hydrogen bond acceptors patterns that are more likely to be observed in P-gp substrates (Figure 4.9).[328] Type I units where the pattern formed by electron donor pairs with spatial separation of 2.5 ± 0.3 Å (Figure 4.9, a) and type II where the pattern is formed either by three electron donor groups with the largest separation being 4.6 ± 0.6 Å or two electron pair donors with a spatial separation of 4.6 ± 0.6 Å (Figure 4.9, b) have all been classified as possible substrate for recognition by P-gp. In another study analysing over 1000 compounds, Didziapetris *et al*. have described a 'rule of 4' to classify P-gp substrate specificity whereby compounds with (N+O) ≥ 8, Mwt > 400 and acid with pKa > 4 are likely to be P-gp substrates, whereas compounds with (N+O) ≤ 4, Mwt < 400 and base with pKa < 8 are likely to be P-gp non-substrates (Figure 4.9, c).[331]
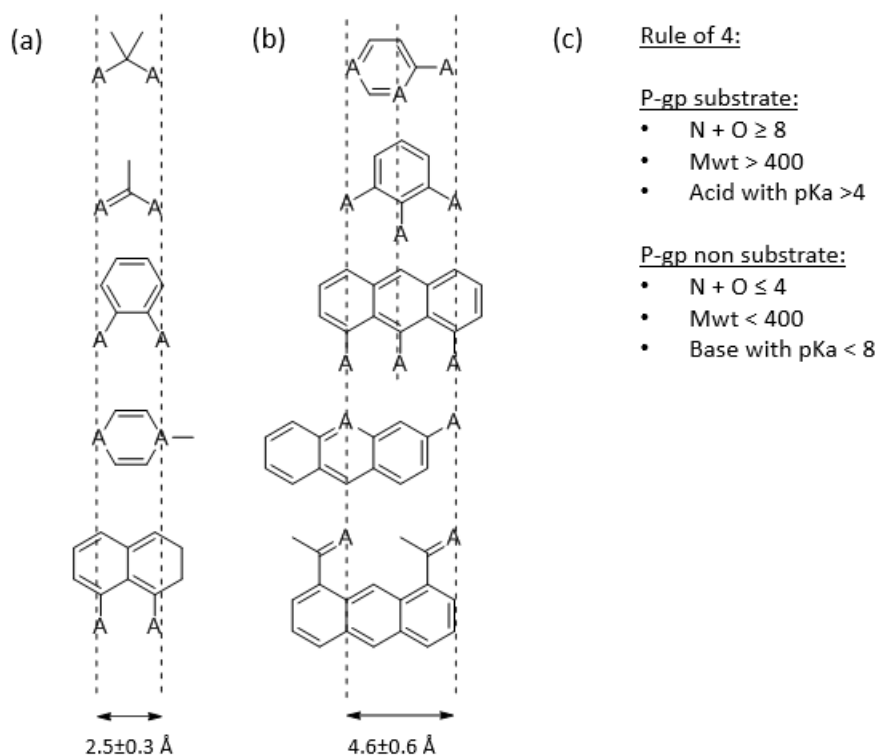
Figure 4.9. (a) and (b) represent the empirical model from Seelig with A denoting a hydrogen bond acceptor. (a) Pattern formed by electron donor pairs with spatial separation of 2.5 ± 0.3 Å. (b) Pattern formed either by three electron donor groups with the largest separation being 4.6 ± 0.6 Å or two electron pair donors with a spatial separation of 4.6±0.6 Å. (c) Rule of 4 for P-gp substrates.[328,331]

Relatively modest structural modifications have been successful in reducing P-gp liability. Indeed, reducing the number of hydrogen bond donors, maintaining tPSA below 90 Å^2 and introducing steric hindrance have been shown to improve chances to evade P-gp recognition.[327] Such strategies have been successfully demonstrated by Blagg *et al.* where a careful analysis of the physicochemical properties (tPSA, clogP, HBD and HBA) within a kinase CDK8 series prone to high P-gp efflux led to an understanding of the parameters contributing to P-gp recognition.[332]

A selection of the compounds prepared were profiled in the *MDR1*-MDCK cell monolayer permeability assay, expressing high levels of P-gp. Similarly to the results obtained with **RV-39**, all the polar compounds were found to have low permeability (Table 4.8).

Table 4.8. *In vitro* MDR1-MDCK Permeability assay for selected compounds.

Cpd	Structure	P_{app} (A-B) (x10⁻⁶ cm/s)[a]	Recovery (%)	P_{app} (B-A) (x10⁻⁶ cm/s)[a]	Recovery (%)	ER[b]
RV-39		0.42 ± 0.01	64	49.1 ± 7.41	71	117.2
49a		0.22 ± 0.09	82	10.6 ± 0.02	93	49.0
49b		0.04 ± 0.01	96	0.48 ± 0.11	104	12.3
49c		0.13 ± 0.02	73	2.12 ± 0.48	99	16.1
49d		0.39 ± 0.05	88	31.5 ± 1.38	91	80.3
49g		0.24 ± 0.01	92	1.26 ± 0.19	88	5.2
49i		0.27 ± 0.02	78	55.5 ± 1.37	83	207.1
49j		0.50 ± 0.06	83	73.1 ± 2.01	92	146.5
49k		0.75 ± 0.02	62	65.6 ± 5.73	77	87.6
		P_{app} (A-B) (x10⁻⁶ cm/s)[a]	Recovery (%)	P_{app} (B-A) (x10⁻⁶ cm/s)[a]	Recovery (%)	

Cpd	Structure	P_{app} (A-B) (x10^{-6} cm/s)[a]	Recovery (%)	P_{app} (B-A) (x10^{-6} cm/s)[a]	Recovery (%)	ER[b]
49l		NC	39	0.13 ± 0.03	57	--
49m		4.33 ± 1.34	50	26.6 ± 3.35	79	5.9
49p		0.14 ± 0.01	77	33.8 ± 2.86	80	233.1
49q		0.25 ± 0.08	80	44.7 ± 3.35	96	178.1
87b		0.30 ± 0.03	89	5.25 ± 0.01	91	17.4

[a]MDR1-MDCK permeability: permeability (P_{app}) determined at 10 μM as the results of two independent experiments. A-B represents the apical to basolateral direction and B-A the basolateral to apical direction; [b]ER: Efflux ratio. Efflux ratio is P_{app}(B-A)/P_{app}(A-B); NC Non conclusive. Compound not detected in compartments A-B due to solubility or binding issues.

All the compounds selected have a clogD$_{7.4}$ lower than 2 (except **49m**) and as anticipated, increasing the lipophilicity improved the apparent permeability but also led to less metabolically stable compounds with high turnover observed in rat microsomes. This is exemplified by **49m** with clog D$_{7.4}$ = 3.51 having the highest permeability in this series (P_{app}(A-B) 4.33 x 10^{-6} cm/s) and a high microsomal turnover in rat (Cl$_{int}$ = 315 μL/min/mg). This poor cellular permeability across the series could limit oral absorption and exposure in *in vivo* studies.

Additionally, most compounds showed an undesirable high efflux ratio (ER) ranging from 5.2 to greater than 200, suggesting these analogues are all substrates for transporter proteins (ER greater than 3 suggests a compound is likely to be actively transported for efflux) (Table 4.8).[226,227,320,333,334]

Variations of the 3,3′-spirocyles, side chain modification or substituents at the 5-benzimidazole position had little influence in interfering with P-gp transporter recognition and reducing the

efflux ratio. Modification of the compound polarity, reduction of the number of nitrogens and oxygens (cyclopropyl oxindole instead of azetidine oxindole for example) and overall basicity of the compounds (chloro benzimidazole sub-series instead of aminomethylene sub-series) similarly had no consistent impact on transporter recognition as all the compounds exhibited a high efflux ratio in the *MDR1*-MDCK assay. In the context of the 'rule of 4' described by Didziapetris *et al.* (Figure 4.9, c) all the compounds prepared, not surprisingly, indicated a reasonable chance to be P-gp substrates with a molecular weight greater than 400 and pKa greater than 9 for all the compounds from the aminomethylene sub-series (**49b-c**, **49i-k**, **87b**). The neutral compound **49m**, with one of the lowest efflux ratio (ER = 5.9) across the series of compounds prepared, showed a better fit to the 'rule of 4' with the heteroatom count (N + O) = 5 and a molecular weight of 414 to mitigate P-gp recognition. However, more interestingly, compounds **49b** and **49g** violated the 'rule of 4' with a high heteroatom count (N + O = 7), a molecular weight > 480 and relatively high basicity with a pKa > 9 for both compounds whilst also having some of the lowest efflux ratio (ER = 12.3 and 5.2 respectively), concluding that the 'rule of 4' may not be a good predictor of P-gp recognition in this series, at least with the limited number of compounds prepared.

To understand the potential contribution of the physicochemical parameters (clogP, tPSA, HBA and HBD) to the efflux ratio, a more detailed analysis was performed and is represented in Figures 4.10, 4.11, 4.12, 4.13 and 4.14. A lower lipophilicity was not indicative of lower efflux across the range of compounds prepared as no correlation between clogP and P-gp efflux ratio could be observed (Figure 4.10). A higher proportion of compounds with tPSA between 75 Å^2 and 95 Å^2 had a lower efflux but a larger set of compounds would have been required to confirm a trend toward reduced P-gp efflux (Figure 4.11). Unfortunately, no trends could be observed in the series where reduction of either the number of hydrogen bond donors (HBD) or hydrogen bond acceptors (HBA) would reduce the efflux ratio (Figures 4.12 and 4.13). Although still prominent, Figure 4.14 shows that compounds with $\text{clogD}_{7.4} < 1$ did marginally reduced the efflux ratio compared to compound with $\text{clogD}_{7.4} > 1$. In conclusion, the probability of compounds in this series to exhibit a low efflux ratio by further improving on the physicochemical properties was unlikely.
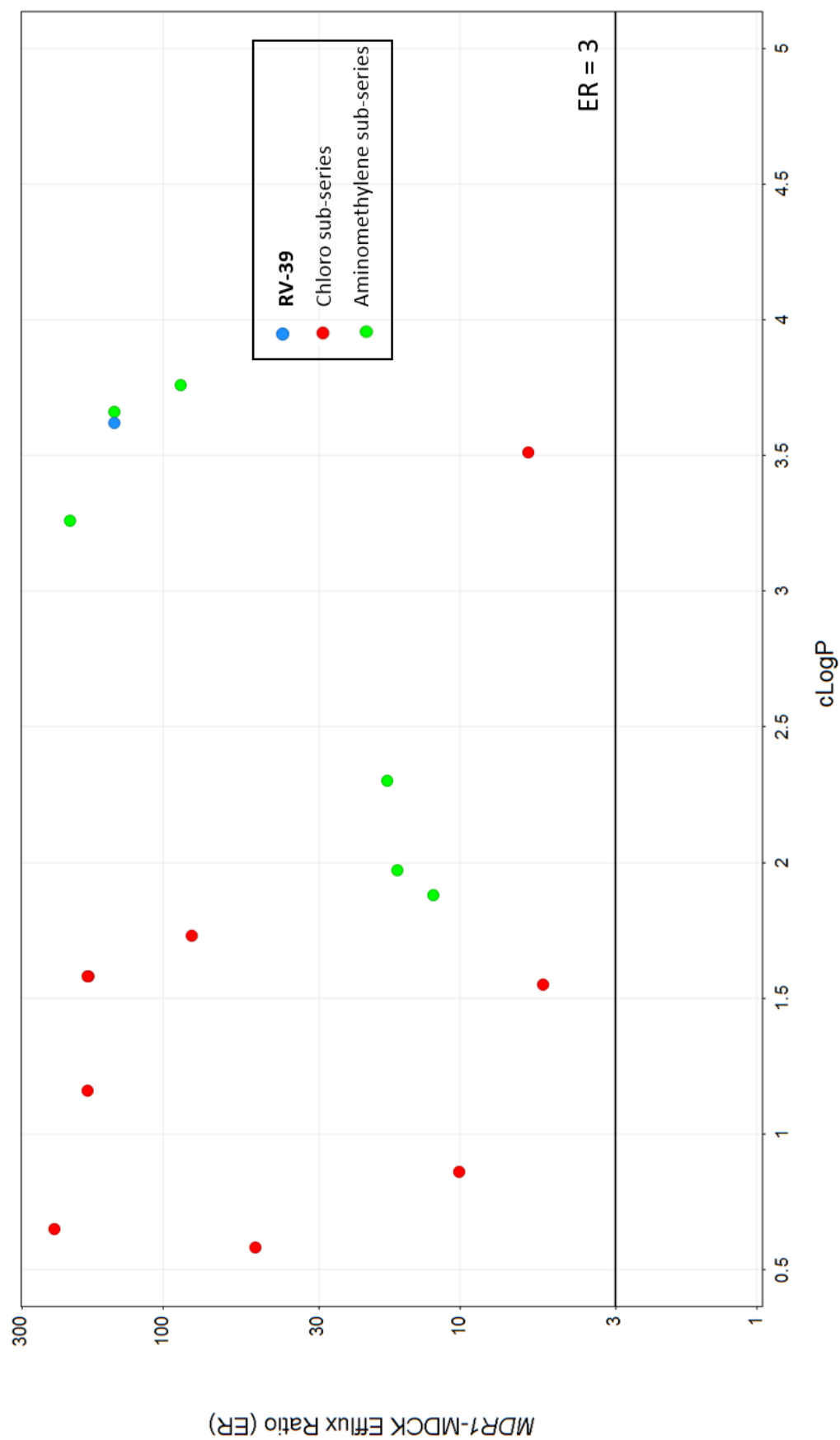
Figure 4.10. Efflux ratio analysis (MDCK permeability) against clogP.
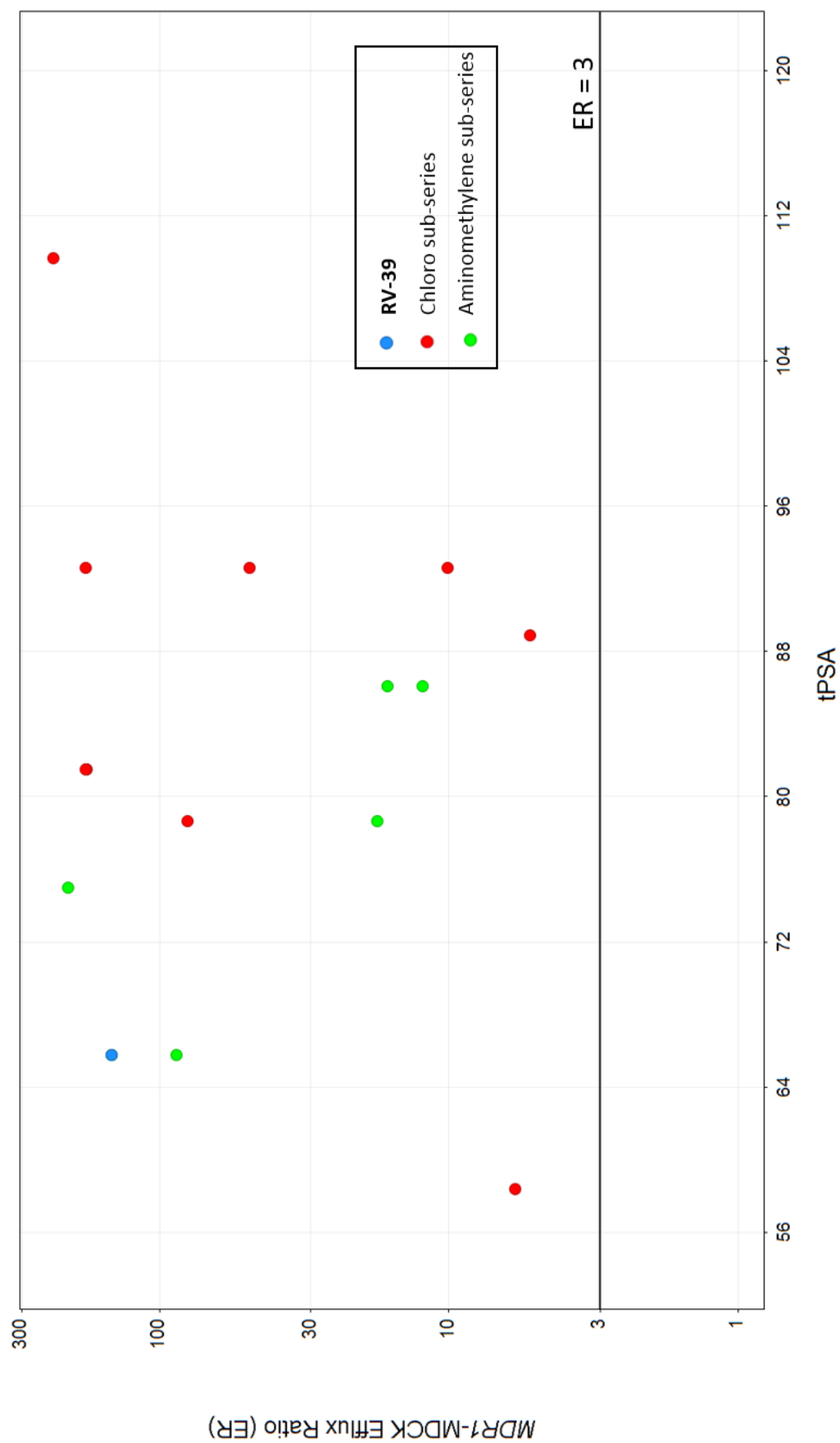
Figure 4.11. Efflux ratio analysis (MDCK permeability) against tPSA.
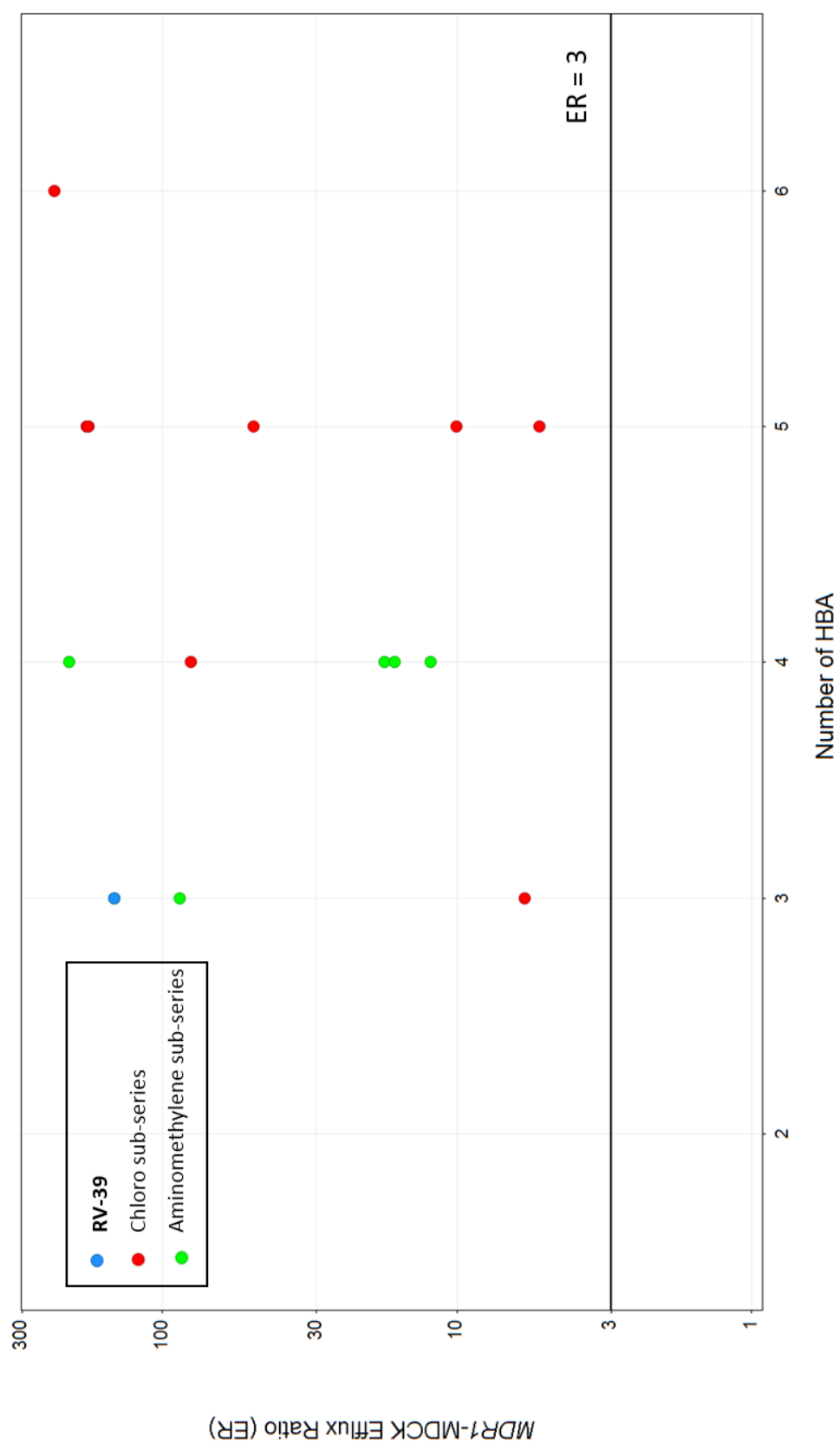
Figure 4.12. Efflux ratio analysis (MDCK permeability) against the number of hydrogen bond acceptors.
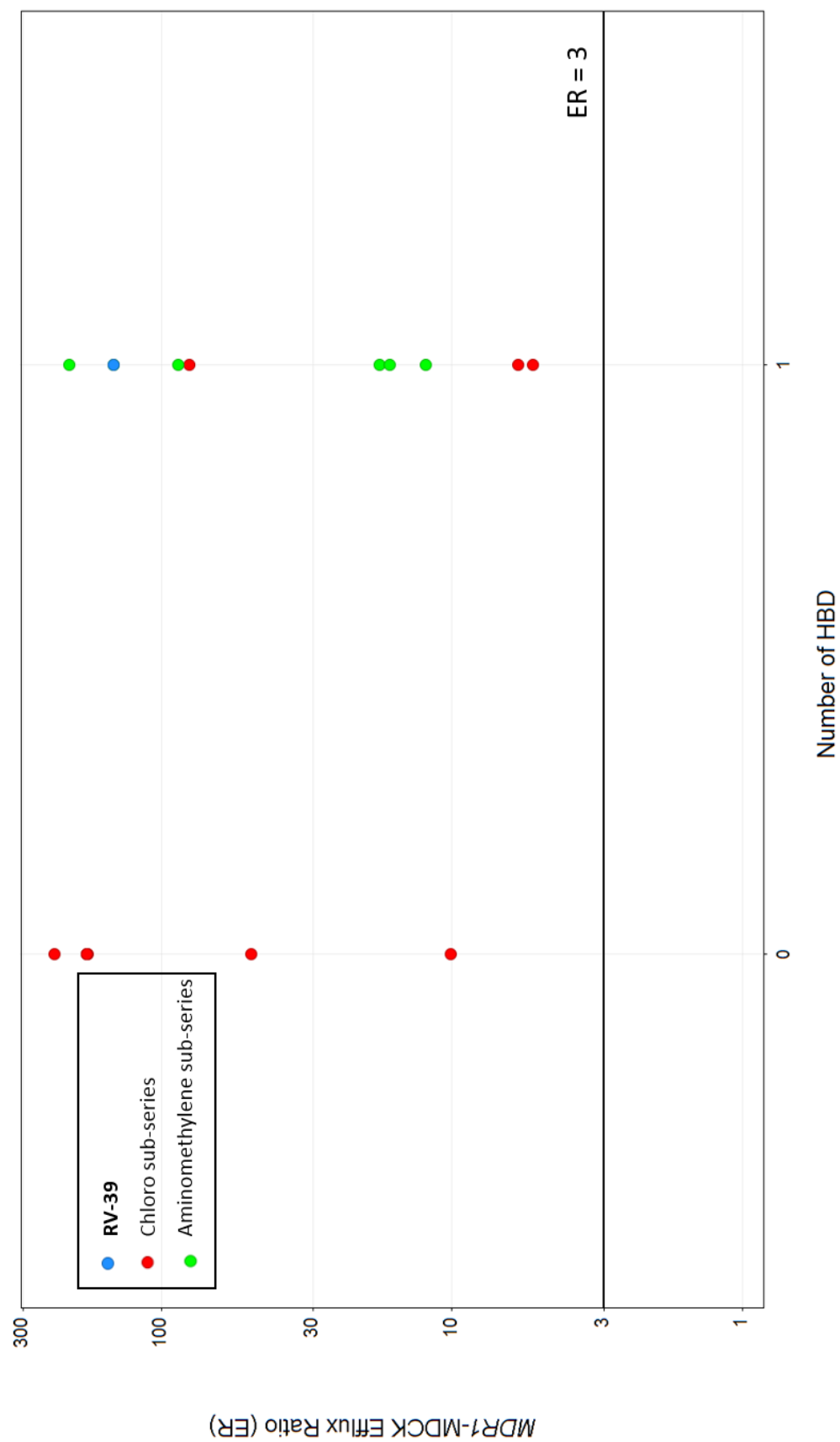
Figure 4.13. Efflux ratio analysis (MDCK permeability) against the number of hydrogen bond donors.
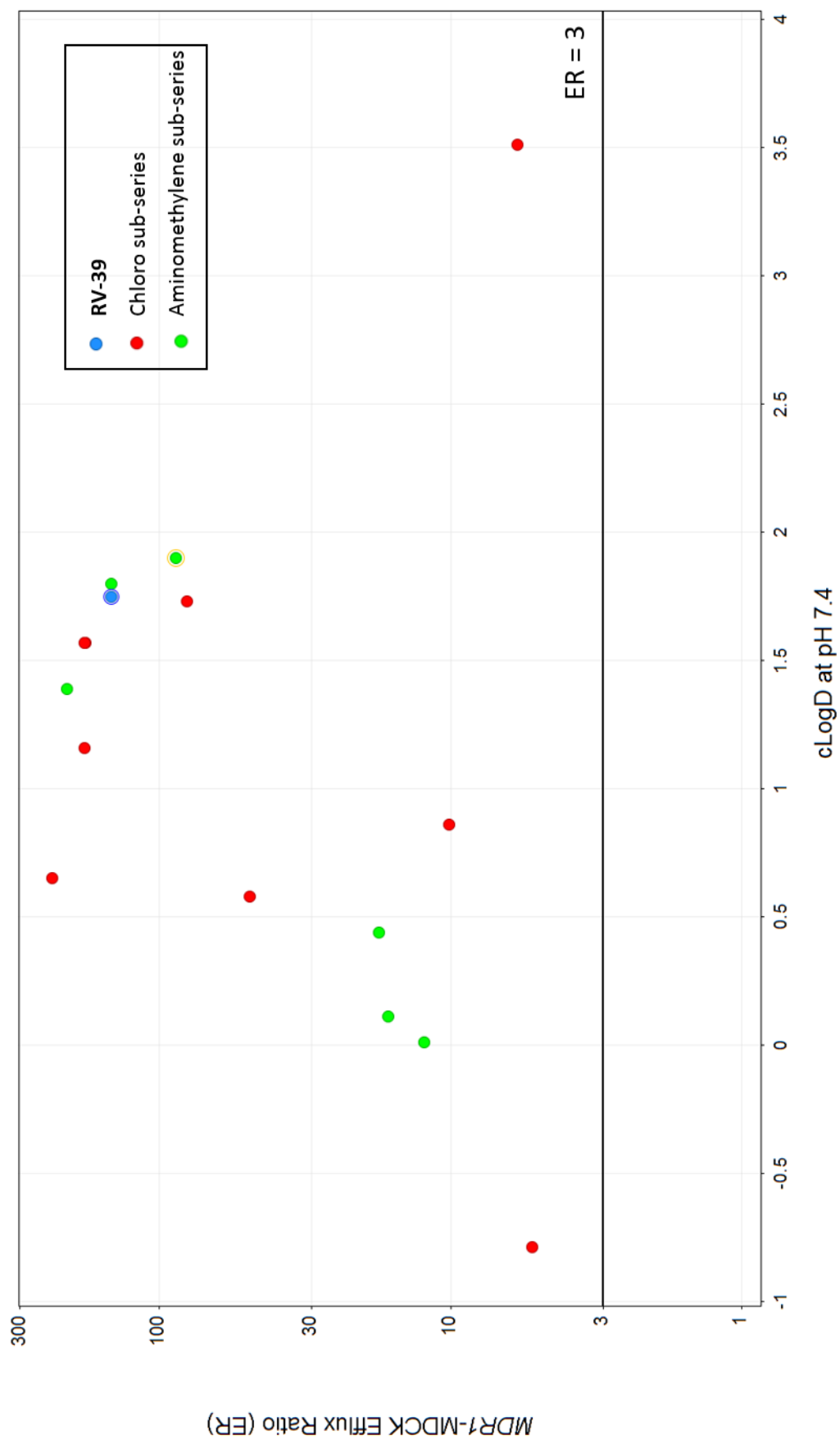
Figure 4.14. Efflux ratio analysis (MDCK permeability) against clogD$_{7.4}$.

e.   *Mismatch between metabolic stability and membrane permeability*

The relationship between the human liver microsome data and apical to basolateral permeability P_{app}(A-B) with $cLogD_{7.4}$ is shown in Figure 4.15. The graph illustrates clearly that compounds with $clogD_{7.4}$ below 1.5 showed consistently low permeability ($P_{app} < 0.6 \times 10^{-6}$ cm/s) but have improved human metabolic stability ($Cl_{int} < 10$ μL/min/mg). Although there are no examples in the set of compounds that retain good human metabolic stability when $cLogD_{7.4}$ is above 2, there is a clear trend toward improved permeability when $cLogD_{7.4}$ increases, unfortunately also leading to a detrimental P-gp efflux ratio increase as depicted in Figure 4.14.
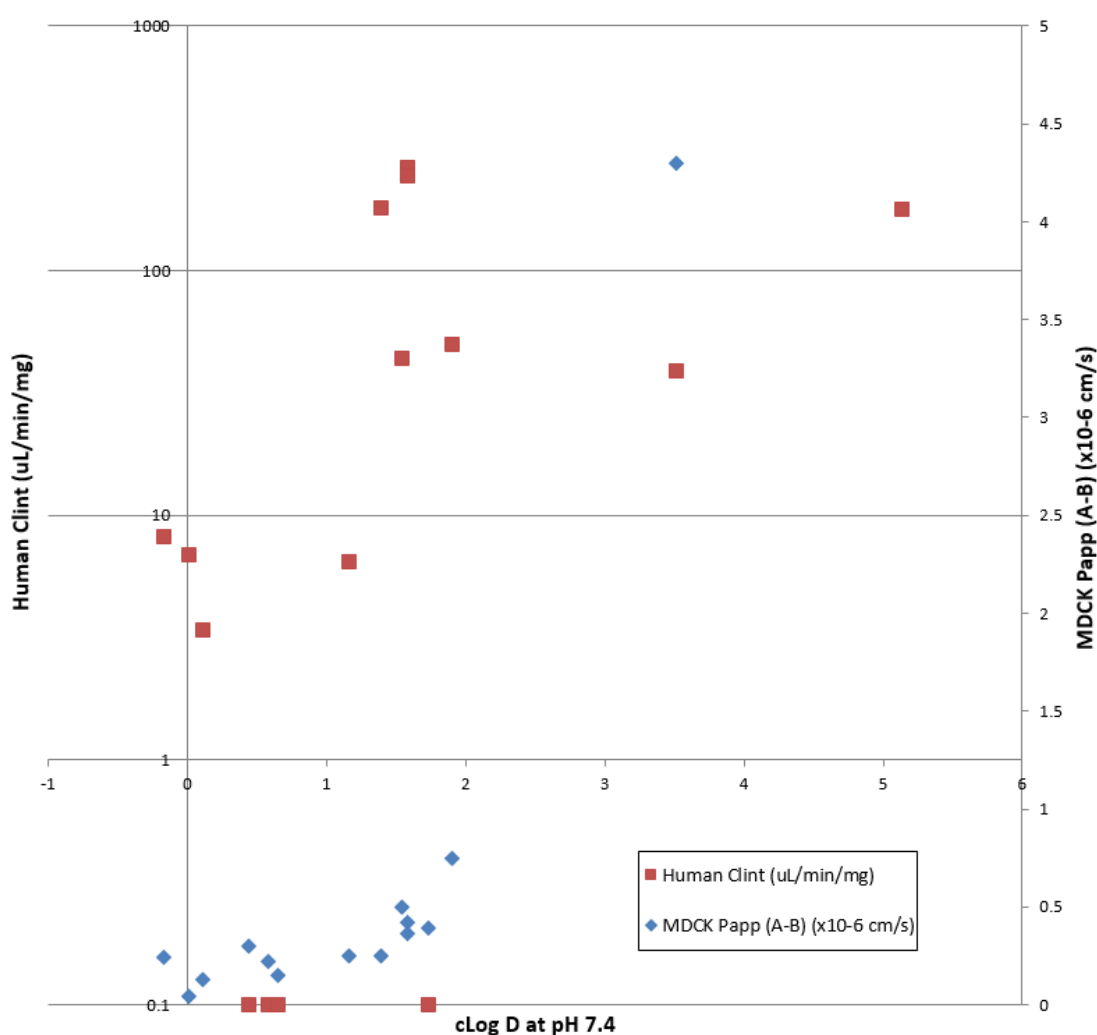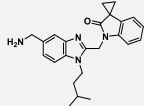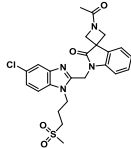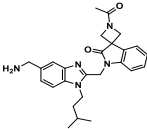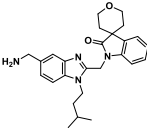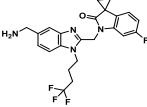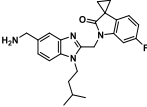
Figure 4.15. Human liver microsomes stability (left y-axis) and *MDR1*-MDCK P_{app} (A-B) (right y-axis) against $cLogD_{7.4}$ for selected compounds.

4.2.2 *In Vivo* Pharmacokinetics

It became apparent during the SAR exploration that, in this series, achieving the fine balance between good antiviral potency, metabolic stability, permeability and low P-gp efflux ratio in a single molecule would be difficult. Whilst recognising this difficulty in optimising the *in vitro* properties, a series of compounds that met the targeted antiviral activity and exhibiting low to moderate microsomal intrinsic clearance across species were selected for *in vivo* pharmacokinetic studies in rat (Table 4.9).

Table 4.9. *In vivo* pharmacokinetic studies in rat.

Compound	Structure	Cl[a] (mL/min/kg)	V_d (L/kg)	$T_{1/2}$ (hours)	F[b]
RV-39		98	34	3.3	4%
49a		48	1.1	0.42	<LLOQ[c]
49c		84	3.3	1.1	<LLOQ[c]
49i		108	19.7	2.3	74%
49j		164	22	1.8	42%
49k		174	54	7.3	25%

[a]iv clearance in mL/min/kg determined from a 1 mg/kg dose (n = 3 per dose group); [b]Oral bioavailability following administration at 10 mg/kg (n = 3 per dose group); [c]<LLOQ: below limit of quantification.

Compound **49a** is the only analogue from the chloro benzimidazole sub-series that was profiled in *in vivo* pharmacokinetic studies at Pharmidex. The compound demonstrated about 70% of the

rat liver blood flow clearance (Sprague-Dawley rat liver blood flow Q_h = 72 mL/min/kg) and a low volume of distribution in line with the neutral nature of the molecule, leading to a short half-life and an oral bioavailability below the level of quantification.[335] The non-measurable oral bioavailability was probably due to high first pass metabolism non predicted by the *in vitro* rat microsome turnover or, as implied by the MDCK permeability assay, poor absorption and active efflux. Unfortunately, the first compound from the aminomethylene azetidine spirooxindole sub-series **49c** profiled in *in vivo* pharmacokinetic studies showed disappointing results. The exposure in rat for **49c** was poor as a result of high clearance (Cl = 84 mL/min/kg) and non-measurable bioavailability.

Similarly to **RV-39**, for these two compounds, the low turnover observed in the *in vitro* microsomal stability studies did not translate into improved *in vivo* clearance obtained in the rat pharmacokinetic studies. This confirmed the initial concern of the rat *in vitro* microsomal clearance not being predictive of the *in vivo* clearance in this series, likely due to extra non-cytochrome P450 mediated clearance mechanisms. The data was in line with increased *in vivo* clearance driven by poor permeability and active transporters as suggested by the high efflux observed in the *in vitro MDR1*- MDCK permeability assay.[226,227,320,336] However, it was unclear if the lack of *in vivo* exposure was mainly the result of efflux transporters. No further *in vivo* transporter experiments were performed such as genetic P-gp knockout or chemical knockdown (co-administration with GF120918, a potent inhibitor of P-gp transporter) studies.[337–339] such studies may have helped to understand the effect of transporter-mediated hepatic uptake and elimination contributing to the overall high clearance for these compounds. Additionally, no further rat plasma analysis was conducted to identity the potential metabolites formed or to understand the potential extrahepatic clearance mechanisms *via* for example plasma instability, amine oxidases or amidases.

A further selection of analogues (**49i-k**) from the aminomethylene sub-series were also profiled in rat pharmacokinetic studies (plasma concentrations are represented as an example in Figure 4.16 for compound **49j**). Similarly to compounds **RV-39**, **49a** and **49c**, high *in vivo* clearance was observed for all 3 compounds **49i-k**, supporting the lack of correlation between moderate *in vitro* microsomal turnover and *in vivo* clearance. The compounds **49i-k** were all rapidly cleared from the blood with clearance values greater than the rat liver blood flow. Despite this high *in vivo* clearance, the oxindole analogues **49i**, **49j** and **49k** showed an acceptable half-life of about 2 hours for **49i** and **49j** and over 7 hours for **49k**, driven by the high volume of distribution, in line with the presence of the basic centre of the aminomethylene moiety. Encouragingly,

following oral administration, all three analogues **49i-k** showed a much improved bioavailability compared to **RV-39**, **49a** and **49c**, ranging from moderate (25% for **49k**, 42% for **49j**) to excellent bioavailability (74% for **49i**).

Concentration of **49j** in Rat (SD, ♂) following iv administration at 1 mg/kg and po administration at 10 mg/kg
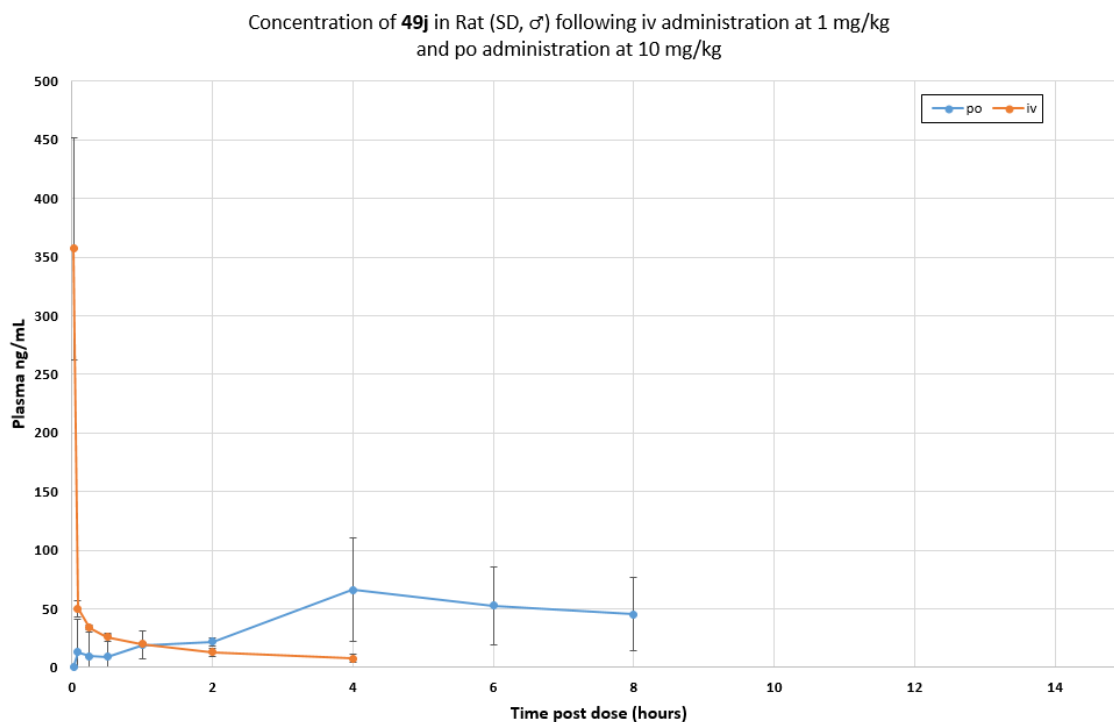
Figure 4.16. Plasma concentrations in rat (SD, ♂) following iv administration at 1 mg/kg and po administration at 10mg/kg of compound **49j** (mean ± SD, n = 3).

To understand the rapid clearance and the lack of correlation between the microsomal intrinsic clearance data and high *in vivo* blood clearance, compounds **49i**, **49j** and **49k** were further investigated in rat hepatocytes (Table 4.10). Both **49i** and **49k** showed a high rate of metabolism and compound **49j** also showed relatively high levels of hepatocyte turnover compared to the rat liver microsome data previously obtained, suggesting the involvement of non-P450 mediated clearance pathway across this series of compounds.

Table 4.10. *In vitro* hepatocyte stability assay in rat.

Compound	Structure	Cl_{hep} (µL/min/million cells)[a]
49i		70.5
49j		14.8
49k		43.1

[a]Classification band for categorising compound in rat: Low hepatocyte intrinsic clearance < 5.1 µL/min/million cells and high hepatocyte intrinsic clearance > 27.5 µL/min/million cells[315]

However, further studies would be necessary to establish a clear understanding of the high clearance results. Metabolite identification conducted from either the rat hepatocyte studies or the plasma samples following the iv and po dosing in rat would inform on the identity of the metabolites formed and, in particular, confirm the formation of metabolites resulting from phase II metabolism.

Chapter 5. Conclusion and Future Directions

The RSV fusion protein plays a critical role in the entry of the Respiratory Syncytial Virus into the respiratory tract host's cells. **RV-39** had previously been reported as a RSV fusion inhibitor, exhibiting excellent *in vitro* antiviral activity in both the fusion and plaque reduction assays. Although **RV-39** showed good stability in rat liver microsomes, the compound showed high clearance in human liver microsomes and a metabolite identification highlighted the potential vulnerability of the cyclopropyl oxindole moiety (Figure 5.1). Furthermore, **RV-39** showed high plasma clearance and low bioavailability when progressed to a rat pharmacokinetic study.
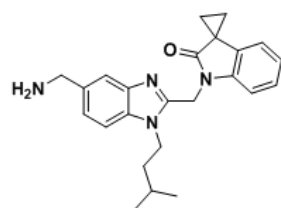
clogP 3.62, clogD$_{7.4}$ 1.75

Fusion IC$_{50}$ 0.5 ± 0.2 nM

PRA IC$_{50}$ 2.2 nM

Cl$_{int}$ (r/d/h) = 20.7/11.8/120 µL/min/mg

P$_{app}$ MDCK (A-B/B-A) = 0.42/49.1 x10^{-6} cm/s

Rat Pharmacokinetic Study

Cl = 98 mL/min/kg

V$_d$ = 34 L/kg; T$_{1/2}$ 3.3 h

F = 4%

Figure 5.1. Summary data of **RV-39**.

The overall aim of this thesis was to identify a novel and potent inhibitor of the RSV fusion protein with improved human liver microsomes and an improved pharmacokinetic profile over **RV-39** in rat.

The initial aim was to explore a novel series of 3,3'-spirocyclic oxindoles as potential replacement for the cyclopropyl oxindole moiety of **RV-39** and the previously reported imidazolones. The second objective of this thesis was to identify a strategy to block the potential instability observed for **RV-39** in human liver microsomes and incorporate fluorine atoms or nitrogens to the oxindole moiety. The preparation of 6-fluoro oxindoles, 3,3'-spirocyclic 5-aza-oxindoles and 3,3'-spirocyclic 6-aza-oxindoles was attempted.

The limitations of the *bis*-alkylation of oxindoles for the preparation of 3,3'-spirocyclic oxindoles and 3,3'-spirocyclic aza-oxindoles required the development of a new synthetic methodology that would allow for the rapid SAR exploration of the oxindole and aza-oxindole moieties. Initially, the formation of the 3,3'-spirooxindole, envisaged *via* a *bis*-electrophilic displacement, failed to access any of the spirocyclic oxindole chemotypes and none of the simple oxetane, azetidine or thietane (**28a-c**) could be prepared, mainly due to the lack of reactivity of the *bis*-mesylate intermediate **27** formed (Scheme 5.1).
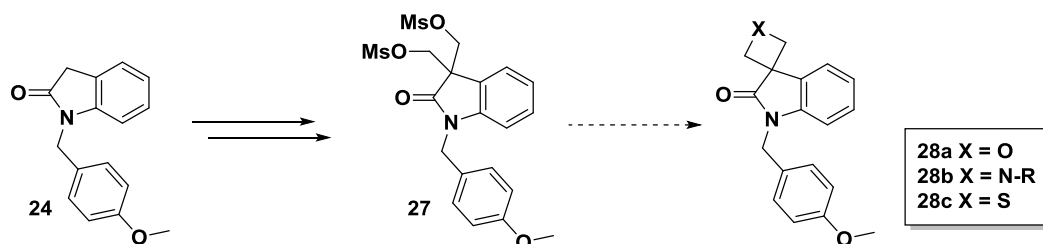
Scheme 5.1. Preparation of 3,3'-spirooxindoles *via bis*-electrophilic displacement.

Instead, a novel route was established *via* palladium-catalysed α-arylation of 2-bromo anilides to generate novel 3,3'-spirocyclic oxindoles (Scheme 5.2). The pre-requisite protected 2-bromo anilides **43** could be accessed from commercially available carboxylic acids and substituted 2-bromo anilines. The key arylation step led to the generation of the protected oxindoles **44** in good to excellent yield. However, the subsequent *para*-methoxybenzyl deprotection step proved problematic. In the case of the 3,3'-spirooxindoles, a series of conditions were investigated and cleavage of the PMB was achieved cleanly but only after harsh heating in trifluoroacetic acid. Encouragingly, milder conditions were also identified where the *para*-methoxybenzyl moiety could be removed at room temperature.
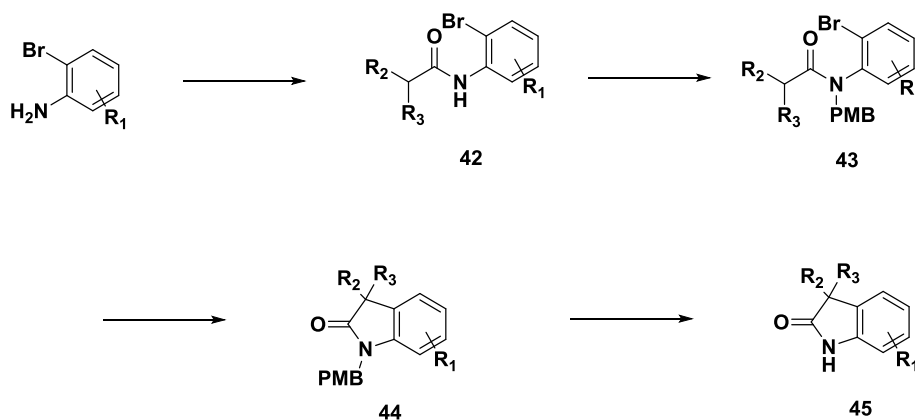
Scheme 5.2. Preparation of 3,3'-spirooxindoles *via* palladium-catalysed α-arylation.

The preparation of the spirocyclic 5-aza-oxindoles was also investigated and proved more challenging than the analogues from the spirooxindole series. Despite multiple attempts and changing the order of the synthetic sequence, the key protected amide **67** was obtained in less than optimal yield (Scheme 5.3). However, the 5-aza-oxindole **68** was isolated successfully under the palladium-catalysed α-arylation reaction conditions developed for the 3,3'-spirocyclic oxindole series. The *para*-methoxybenzyl deprotection also proved difficult and could only be achieved under high temperature and pressure conditions that were unfortunately not amenable to the preparation of a wider range of analogues.

X = Cl, NH₂

67

68

74
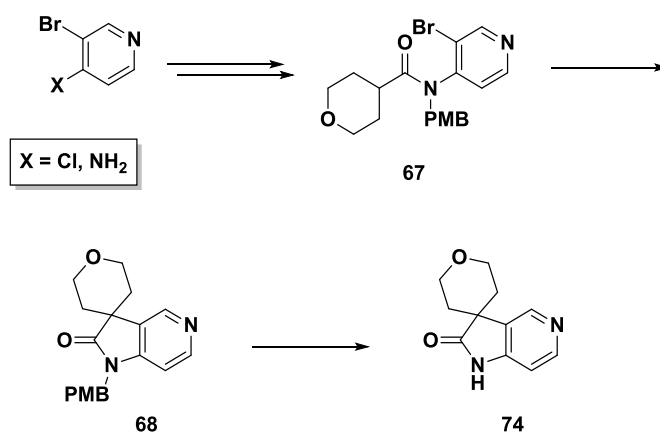
Scheme 5.3. Preparation of 5-aza-oxindole *via* palladium-catalysed α-arylation.

Although it was initially expected that the palladium-catalysed α-arylation would also allow the preparation of the spirocyclic 6-aza-oxindoles, the PMB deprotection under high pressure and temperature led to safety concerns and a review of the synthetic route. An alternative synthetic route was sought after for the preparation of the 3,3'-cyclopropyl-6-aza-oxindole *via* a double alkylation of the non-protected 6-aza-oxindole **82** under lithiation conditions, leading to the required product **77** but in very low yield (Scheme 5.4).

79

82

77
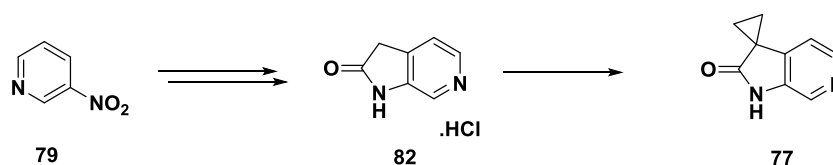
Scheme 5.4. Preparation of 6-aza-oxindole *via bis*-alkylation.

The synthetic work presented in this thesis has highlighted that the palladium-catalysed α-arylation of substituted anilides proved a very versatile and robust route and has enabled the synthesis of a range of novel 3,3'-spirocyclic oxindoles and aza-oxindoles. The initial methodology explored *via* a *bis*-electrophilic displacement failed to deliver the oxetane and

thiooxetane oxindoles but it is anticipated that these templates should also be accessible *via* the palladium-catalysed α-arylation of the corresponding anilides. The route developed is also amenable to the scale up of any analogues within this spirooxindole series. Future work should however focus on extending the scope of the palladium-catalysed α-arylation of spirooxindoles to assess the versatility of the reaction. Additionally, the removal of the *para*-methoxybenzyl protecting group remains a significant limitation to the exploration of the aza-spirooxindole series and future work in this series should focus on the optimisation of a suitable protecting group that could be removed under mild and safe conditions. In turn, this could allow for the efficient preparation of the 4-aza, 6-aza and 7-aza-spirooxindoles *via* palladium-catalysed α-arylation.
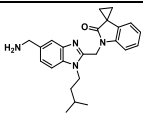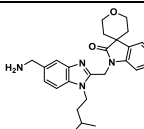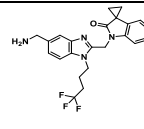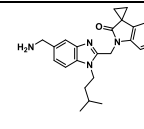
The last objective of this thesis was to combined the prepared spirocyclic oxindoles and aza-oxindoles with a range of substituted chloro and aminomethylene benzimidazoles with the aim of balancing the overall lipophilicity and polarity of the molecules, whilst retaining the RSV antiviral activity observed with **RV-39**. To this effect, the novel synthetic methodology presented in this work has allowed to extend the SARs around the oxindole and aza-oxindole moieties.

All the spirooxindole and spiro-aza-oxindole compounds prepared retained excellent antiviral activity in the RSV fusion assay irrespectively of the size of the spirocycle ring introduced. However, introduction of the 5-chloro benzimidazole moiety led to a significant loss of antiviral activity in the RSV plaque reduction assay. The compounds from the aminomethylene sub-series had excellent antiviral activity in the plaque reduction assay and improved microsomal clearance both in rat and human. A reduction in the lipophilicity of the compounds led to an increase in human microsomal stability but unfortunately also led to a decrease of membrane permeability in the MDCK assay. Overall, reducing the lipophilicity had a significant impact on improving the LiPE. This was demonstrated with the aza-oxindoles **87a** and **87b** with LiPE respectively of 6.65 and 6.80. All the derivatives prepared retained a very high efflux ratio and unfortunately the analysis of the data did not allow to identify any molecular property patterns responsible for the efflux. A selection of the compounds prepared (**49i-k**) were profiled in rat pharmacokinetic studies (Table 5.1).

These preliminary results suggest that whilst the plasma clearance remains high in rat, good half-life and bioavailability can be achieved across this series of compounds. The three compounds **49i**, **49j** and **49k** highlighted in table 5.1 all demonstrated a significant improvement in bioavailability compared to **RV-39**, whilst retaining or improving on the half-life.

This selection of compounds confirms that the initial objectives of this work of developing novel and potent RSV fusion inhibitors with an improved pharmacokinetic profile over **RV-39** have been achieved. An extension of this work would be to understand the regions of the molecule susceptible to non-microsome mediated enzymes that can often be involved in metabolic clearance pathways such as *N*-acetylation of the aminomethylene or aldehyde oxidase substrate recognition for example.[319,340] Furthermore, the aza-oxindoles **87a** and **87b** showed significantly improved LiPE and very low turnover in both the rat and human liver microsomes. Profiling those aza-oxindoles into rat pharmacokinetic studies would further inform on the suitability of this series of compounds for progression in the animal models of the disease.

Table 5.1. Profile summary of **RV-39**, **49i**, **49j** and **49k**

	RV-39	49i	49j	49k
Physicochemical properties				
Molecular weight	388	433	446	406
clogP^a/clogD$_{7.4}$^{b}	3.62/1.75^c	3.26/1.39	3.66	1.54^c
Solubility, pH$_{7.4}$ (μM)	156	300	417	172
LiPE	5.34	5.90	5.44	5.46
RSV Fusion IC$_{50}$ (nM)^d	0.5 ± 0.2	0.7 ± 0.3	0.8 ± 0.3	0.6 ± 0.2
RSV PRA IC$_{50}$ (nM)^e	2.2 (n = 1)	3.4 ± 3.2	3.2 ± 3.6	4.6 ± 5.2
P$_{app}$ MDCK (A-B/B-A) (x 10^{-6} m/s)	0.42/49.1	0.27/55.5	0.50/73.1	0.75/65.6
Human liver microsomes (μL/min/mg)^f	120	180	43.5	50.7
Rat Pharmacokinetics				
Cl (mL/min/kg)^g	98	108	164	174
V$_d$ (L/Kg)	34	19.7	22	54
T$_{1/2}$ (h)	3.3	2.3	1.8	7.3
F (%)^h	4^i	74	42	25

^{a}cLogP was calculated using ChemAxon; ^{b}measured logD at pH 7.4 in octanol/neutral buffer; ^{c}calculated clogD at pH 7.4 using ChemAxon calculator plugins; ^{d}RSV Fusion assay (nM). Determinations ± standard deviation from mean of n = two or more determinations; ^{e}RSV Plaque Reduction Assay (nM). Determinations ± standard deviation from mean of n = two or more determinations or data obtained from a single determination (n = 1); ^{f}Intrinsic clearance from liver microsomal stability assay; ^{g}iv clearance determined from a 1 mg/kg dose in Sprague-Dawley male rats (n = 3); ^{h}Bioavailability following oral administration of 10 mg/kg in Sprague-Dawley male rats (n = 3); ^{i}Bioavailability following oral administration of 5 mg/kg in Sprague-Dawley male rats (n = 3).

Chapter 6. Experimental Section

6.1 Summary of Generic Reactions, Analytical and Chromatographic Conditions

6.1.1   Chemicals and Solvents

All commercial reagents were purchased from Sigma-Aldrich, Alfa Aesar, Apollo Scientific, Fisher Scientific, Fluorochem, Manchester Organics or Tokyo Chemical Industry and of the highest available purity. Unless otherwise stated, chemicals were used as supplied without further purification. Anhydrous solvents were purchased from Acros (AcroSeal™) or Sigma-Aldrich (SureSeal™) and were stored under nitrogen. Anhydrous solvents and reagents were used as purchased. Petroleum ether refers to the fraction with a boiling point between 40 °C and 60 °C.

6.1.2   Reactions

All reactions were carried out under a nitrogen atmosphere, unless otherwise specified. Reactions were magnetically stirred and monitored by LCMS or thin layer chromatography (TLC) using aluminium-supported thin layer chromatography sheets with Merck silica gel 60 F_{254}. For TLC, the eluent was as stated (where this consisted of more than one solvent, the ratio is stated as volume: volume). Visualisation was by absorption of UV light (λ_{max} 254 or 365 nm) or by thermal development after dipping in an aqueous solution of potassium permanganate or an ethanolic solution of phosphomolybdic acid (PMA).

6.1.3   Chromatography

Flash column chromatography was carried out using either: **a**) commercial pre-packed silica columns from Biotage (SNAP and Zip), Isco (RediSep) or Grace (Reveleris); **b)** C18 silica (Biotage SNAP KP-C18-HS, Grace Reveleris C18) on an ISCO Combiflash Rf or a Biotage Isolera Prime.

6.1.4   Microwave Reactions

All microwave reactions were conducted using a Biotage Initiator 8+ microwave reactor.

6.1.5   Analytical Techniques

^{1}H NMR spectra were recorded at 500 MHz on a Varian VNMRS 500 MHz spectrometer (at 30 °C), using residual isotopic solvent as an internal reference. The chemical shift data for each signal are given as δ_H in units of parts per million (ppm). Each spectrum is corrected to the appropriate solvent reference; δ (CDCl$_3$) = 7.27 ppm, δ (DMSO-d_6) = 2.50 ppm or δ (CD$_3$OD) = 3.31 ppm. The multiplicity of each signal is indicated by: s (singlet); br s (broad singlet); d (doublet); t (triplet); q (quartet); dd (doublet of doublets); ddd (doublet of doublet of doublets); dddd (doublet of doublet of doublet of doublets); dt (doublet of triplets); ddt (doublet of doublet of triplets); or m (multiplet). The number of protons (n) for a given resonance signal is indicated by nH. Coupling constants (*J*) are quoted in Hz and are recorded to the nearest 0.1 Hz. Identical proton coupling constants (*J*) are averaged in each spectrum and reported to the nearest 0.1 Hz. The coupling constants are determined by analysis using MestReNova version 10 software.

^{13}C NMR spectra were recorded at 126 MHz on a Varian 500 MHz spectrometer and are proton decoupled. The chemical shift data for each signal are given as δ_C in units of parts per million (ppm). Each spectrum is corrected to the appropriate solvent reference; δ_C (CDCl$_3$) = 77.16 ppm, δ (DMSO-d_6) = 39.52 ppm or δ (CD$_3$OD) = 49.00 ppm.

^{1}H and ^{13}C spectra were assigned using 1D and when necessary using 2D NMR experiments including gDQCOSY, gHSQCAD, gHMBCAD and NOESY.

Melting points were determined using an OptiMelt apparatus and are uncorrected. The solvent(s) from which the sample is crystallised is given in parentheses.

High resolution mass spectrometry: data (ESI) was recorded on Bruker Daltonics, Apex III, ESI source: Apollo ESI with methanol as spray solvent. Only molecular ions, fractions from molecular ions and other major peaks are reported as mass/charge (*m/z*) ratios.

LCMS (LCQ) data was recorded on a Waters 2695 HPLC using a Waters 2487 UV detector and a Thermo LCQ ESI-MS or APCI-MS. Samples were eluted through a Phenomenex Luna 3 μm C18

50 mm × 4.6 mm column, using water and acetonitrile acidified by 0.1% formic acid at 1.5 mL/min and detected at 254 nm.

Method 1: 4 minute method

The gradient employed was:

Time (minutes)	% Water + 0.1% formic acid	% MeCN + 0.1% formic acid
0.0	65	35
3.5	10	90
3.9	10	90
4.0	65	35

Method 2: 7 minute method

The gradient employed was:

Time (minutes)	% Water + 0.1% formic acid	% MeCN + 0.1% formic acid
0.0	70	30
5.0	10	90
6.0	10	90
6.5	70	30
7.0	70	30

Method 3: 10 minute method

The gradient employed was:

Time (minutes)	% Water + 0.1% formic acid	% MeCN + 0.1% formic acid
0.0	95	5
8.0	5	95
8.5	5	95
9.0	95	5
9.5	95	5

LCMS (MDAP) data was recorded on a Shimadzu Prominence Series coupled to a LCMS-2020 ESI and APCI mass spectrometer. Samples were eluted through a Phenomenex Gemini 5 μm C18 110 Å 250 mm × 4.6 mm column, using water and acetonitrile acidified by 0.1% formic acid at 1 mL/min and detected at 254 nm.

Method 4: Analytical 5-95

The gradient employed was:

Time (minutes)	% Water + 0.1% formic acid	% MeCN + 0.1% formic acid
0.0	95	5
1.0	95	5
21.0	5	95
25.0	5	95
30.0	70	30

Method 5: Analytical 30-90

The gradient employed was:

Time (minutes)	% Water + 0.1% formic acid	% MeCN + 0.1% formic acid
0.0	70	30
1.0	70	30
21.0	10	90
25.0	10	90
30.0	70	30

Mass Directed Purification was performed on a Shimadzu Prominence Series coupled to a LCMS-2020 ESI and APCI mass spectrometer using a Phenomenex Gemini 5 μm C18 250 mm × 21.2 mm column, using water and acetonitrile acidified by 0.1% formic acid at 15 mL/min and detected at 254 nm.

The gradient employed was:

Time (minutes)	% Water + 0.1% formic acid	% MeCN + 0.1% formic acid
0.0	95	5
1.0	95	5
21.0	5	95
25.0	5	95
30.0	70	30

HPLC 1100 Preparative purification: HPLC purification was performed on an Agilent 1100 series HPLC spectrometer, using a Phenomenex Luna 10 μm C18 150 mm × 15 mm column, eluted using water and acetonitrile at 15 mL/min and detected at 254 nm.

The gradient employed was:

Time (minutes)	% Water + 0.1% formic acid	% MeCN + 0.1% formic acid
0	95	5
20	0	100
24	0	100
25	95	5
27	95	5

All reported yields refer to chromatographically and spectroscopically pure compounds, unless otherwise specified.

6.2 Compound Synthesis

1-[(4-Methoxyphenyl)methyl]indoline-2,3-dione (24)[341–343]
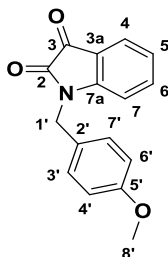
Sodium hydride (60% dispersion in mineral oil) (2.99 g, 74.70 mmol) was added portionwise to an ice cold solution of isatin (**23**) (10.0 g, 68.00 mmol) in anhydrous *N,N*-dimethylformamide (70 mL). The cold bath was removed and the solution was stirred for 15 minutes at room temperature. After this time, 1-(chloromethyl)-4-methoxy-benzene (9.67 mL, 71.13 mmol) was added and the resulting mixture was heated to 70 °C for 4 hours. After this time, the mixture was poured onto ice/water (200 mL) and the suspension formed was stirred vigorously for 15 minutes until a granular precipitate was formed. The orange precipitate was collected by filtration, rinsing with water and was dried at 50 °C under vacuum to give 1-[(4-methoxyphenyl)methyl]indoline-2,3-dione **(24)** as an orange solid (18.87 g, >99% yield): m.p. 170 – 171 °C [Lit.[342] 161 – 162 °C, Lit.[344] 169 – 171 °C, Lit.[343] 169 – 171 °C]; ^{1}H NMR (500 MHz, DMSO-*d$_6$*) δ_H 7.63 – 7.51 (m, 2H, H-4 and H-6), 7.35 (d, *J* = 8.2 Hz, 2H, H-3' and H-7'), 7.10 (t, *J* = 7.6 Hz, 1H, H-5), 6.99 (d, *J* = 7.6 Hz, 1H, H-7), 6.89 (d, *J* = 8.2 Hz, 2H, H-4' and H-6'), 4.83 (s, 2H, H-1'), 3.72 (s, 3H, H-8'); ^{13}C NMR (126 MHz, DMSO-*d$_6$*) δ_C 183.6 (C-3), 159.2 (C-2), 158.7 (C-5'), 150.8 (C-7a), 138.4 (C-4), 129.3 (C-3' and C-7'), 127.8 (C-2'), 124.9 (C-6), 123.7 (C-5), 118.1 (C-3a), 114.5 (C-4' and C-6'), 111.6 (C-7), 55.5 (C-8'), 42.9 (C-1'); LCMS (MDAP): Rt = 16.0 min (Method 5); m/z 268.0 [M+H]$^+$; HRMS (ESI) calcd for $C_{16}H_{13}NO_3Na$ 290.0788, found 290.0792.

1-[(4-Methoxyphenyl)methyl]indolin-2-one (25)[342,345,346]
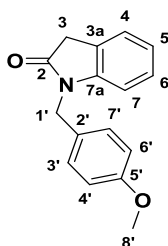
Hydrazine hydrate (7.86 mL, 161.0 mmol) was added to a suspension of 1-[(4-methoxyphenyl)methyl]indoline-2,3-dione (24) (10.77 g, 40.29 mmol) in 1-butanol (150 mL). The suspension turned rapidly to a solution. The reaction mixture was heated to 80 °C for 3 hours. Triethylamine (5.62 mL, 40.3 mmol) was added and the temperature was raised to 100 °C and left stirring at 100 °C for 48 hours. After this time, the volatiles were removed under reduced pressure. The oily residue was diluted with EtOAc (150 mL) and washed with saturated NaHCO$_3$ (150 mL) and brine (150 mL). The organic layers were dried over MgSO$_4$ and concentrated under reduced pressure to give 1-[(4-methoxyphenyl)methyl]indolin-2-one (25) as a colourless solid (9.79 g, 96% yield): m.p. 105 – 107 °C [Lit.[342] 105 – 106 °C, Lit.[346] 103 – 104 °C]; ^{1}H NMR (500 MHz, DMSO-d_6) δ$_H$ 7.29 – 7.22 (m, 3H, H-4, H-3' and H-7'), 7.17 (app. t, J = 7.6 Hz, 1H, H-6), 6.97 (app. t, J = 7.6 Hz, 1H, H-5), 6.90 – 6.84 (m, 3H, H-7, H-4' and H-6'), 4.80 (s, 2H, H-1'), 3.70 (s, 3H, H-8'), 3.63 (s, 2H, H-3); ^{13}C NMR (126 MHz, DMSO-d_6) δ$_C$ 174.9 (C- 2), 159.0 (C-5'), 144.4 (C-7a), 129.2 (C-3' and C-7'), 128.9 (C-3a), 127.8 (C-6), 125.2 (C-2'), 124.7 (C-4 or C-5), 122.3 (C-4 or C-5), 114.4 (C-4' and C-6'), 109.3 (C-7), 55.5 (C-8'), 42.4 (C-1'), 35.6 (C-3); LCMS (MDAP): Rt = 19.0 min (Method 4); m/z 254.1 [M+H]$^+$; HRMS (ESI) calcd for C$_{16}$H$_{15}$NNaO$_2$ 276.0995, found 276.0993.

3,3-*bis*(Hydroxymethyl)-1-[(4-methoxyphenyl)methyl]indolin-2-one (26)
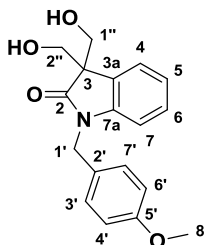
A solution of 1-[(4-methoxyphenyl)methyl]indolin-2-one (25) (9.79 g, 38.65 mmol) in tetrahydrofuran (194 mL) was treated with potassium carbonate (16.03 g, 115.95 mmol) and paraformaldehyde (27.86 g, 927.6 mmol). Upon completion of the addition, the obtained suspension was stirred at room temperature for 16 hours. After this time, the suspension was

diluted with saturated NaHCO$_3$ (500 mL) and extracted with EtOAc (2 x 200 mL). The organic layers were dried over MgSO$_4$ and evaporated under reduced pressure. The crude residue was purified by flash column chromatography (Biotage SNAP 100 g, CH$_2$Cl$_2$: MeOH: NH$_3$, 99: 1: 0.1 to 90: 10: 1) to give 3,3-*bis*(hydroxymethyl)-1-[(4-methoxyphenyl)methyl]indolin-2-one **(26)** as a colourless solid (6.32 g, 52% yield): ^{1}H NMR (500 MHz, Chloroform-*d*) δ$_H$ 7.34 (dd, *J* = 7.6, 1.0 Hz, 1H, H-4), 7.26 – 7.20 (m, 3H, H-6, H-3' and H-7'), 7.07 (dt, *J* = 7.6, 1.0 Hz, 1H, H-5), 6.87 – 6.82 (m, 2H, H-4' and H-6'), 6.78 (d, *J* = 7.6 Hz, 1H, H-7), 4.88 (s, 2H, H-1'), 4.06 (d, *J* = 11.4 Hz, 2H, H-1'' or H-2''), 4.00 (d, *J* = 11.4 Hz, 2H, H-1'' or H-2''), 3.77 (s, 3H, H-8').^{13}C NMR (126 MHz, Chloroform-*d*) δ$_C$ 178.2 (C-2), 159.1 (C-5'), 143.3 (C-7a), 128.7 (C-6), 128.4 (C-3' and C-7'), 128.2 (C-3a), 127.4 (C-2'), 123.6 (C-4), 122.9 (C-5), 114.2 (C-4' and C-6'), 109.6 (C-7), 64.2 (C-1'' and C-2''), 55.5 (C-3), 55.2 (C-8'), 43.1 (C-1'); LCMS (LCQ): Rt = 1.1 min (Method 2), m/z 314 [M+H]$^+$; HRMS (ESI) calcd for C$_{18}$H$_{19}$NNaO$_4$ 336.1206, found 336.1198.

[1-[(4-Methoxyphenyl)methyl]-3-(methylsulfonyloxymethyl)-2-oxo-indolin-3-yl]methyl methanesulfonate (27)
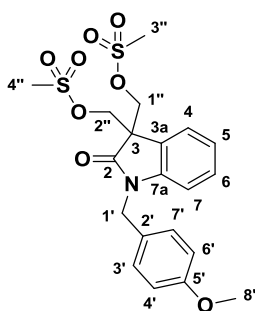
Triethylamine (11.24 mL, 80.68 mmol) was added to an ice cold suspension of 3,3-*bis*(hydroxymethyl)-1-[(4-methoxyphenyl)methyl]indolin-2-one **(26)** (6.32 g, 20.17 mmol) in dichloromethane (100 mL), followed by methanesulfonyl chloride (3.2 mL, 41.35 mmol) added dropwise. Upon completion of the addition, the reaction mixture was left stirring at room temperature for 4 days. After this time, the mixture was concentrated under reduced pressure and the crude residue was purified by flash column chromatography (Biotage SNAP 100 g, petroleum ether: EtOAc, 90: 10 to 0: 100) to give [1-[(4-methoxyphenyl)methyl]-3-(methylsulfonyloxymethyl)-2-oxo-indolin-3-yl]methyl methanesulfonate **(27)** as a colourless oil (7.76 g, 82% yield): ^{1}H-NMR (500 MHz, Chloroform-*d*) δ$_H$ 7.44 (dd, *J* = 7.8, 1.0 Hz, 1H, H-4), 7.30 (dt, *J* = 7.8, 1.0 Hz, 1H, H-6), 7.25 – 7.21 (d, *J* = 7.6 Hz, 2H, H-3' and H-7'), 7.13 (dt, *J* = 7.8, 1.0 Hz, 1H, H-5), 6.86 (d, *J* = 7.6 Hz, 2H, H-4' and H-6'), 6.83 (dd, *J* = 7.8, 1.0 Hz, 1H, H-7), 4.89 (s, 2H, H-1'), 4.66 (d, *J* = 10.0 Hz, 2H, H-1'' or H-2''), 4.49 (d, *J* = 10.0 Hz, 2H, H-1'' or H-2''), 3.78 (s, 3H, H-8'), 2.83 (s, 6H, H-3'' and H-4''); ^{13}C-NMR (126 MHz, Chloroform-*d*) δ$_C$ 172.9 (C-2), 159.3 (C-5'),

143.1 (C- 7a), 130.0 (C-6), 128.5 (C-3' and C-7'), 126.9 (C-3a), 125.2 (C-2'), 124.6 (C-4 or C-5), 123.3 (C-4 or C-5), 114.3 (C-4' and C-6'), 109.9 (C-7), 69.1 (C-1'' and C-2''), 55.2 (C-8'), 51.9 (C-3), 43.5 (C-1'), 37.4 (C-3'' and C-4''); LCMS (LCQ): Rt = 3.5 min (Method 2); m/z 492 [M+Na]$^+$; LCMS (MDAP): Rt = 19.6 min (Method 4); m/z 492 [M+Na$^+$].

Note: Unable to obtain any ionisation under HRMS.

tert-Butyl 3-[(2-bromophenyl)carbamoyl]azetidine-1-carboxylate (34)[179]
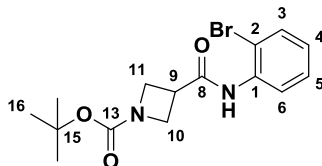
4-(Dimethylamino)pyridine (4.87 g, 39.9 mmol) was added in one portion to a solution of 2-bromoaniline (**33**) (5.28 g, 30.69 mmol) and 1-*tert*-butoxycarbonylazetidine-3-carboxylic acid (6.18 g, 30.69 mmol) in dichloromethane (150 mL), followed by EDCI.HCl (7.65 g, 39.9 mmol). The resulting reaction mixture was left stirring at room temperature for 4 days. After this time, the solvent was removed under reduced pressure. The residue was taken up in EtOAc (100 mL) and the organic layer was washed successively with 2 N HCl (50 mL), water (50 mL), a saturated solution of Na$_2$CO$_3$ (50 mL) then brine (50 mL). The organic layers were dried over MgSO$_4$ and concentrated to dryness under reduced pressure. The crude residue was purified by flash column chromatography (Isco RediSep 80g, petroleum ether: EtOAc, 95: 5 to 70: 30) to give *tert*-butyl 3-[(2-bromophenyl)carbamoyl]azetidine-1-carboxylate **(34)** as a colourless oil (8.77 g, 80% yield): ^{1}H NMR (500 MHz, Chloroform-*d*) δ$_H$ 8.36 (d, *J* = 8.2 Hz, 1H, H-6), 7.66 (br s, 1H, NH), 7.55 (d, *J* = 8.0 Hz, 1H, H-3), 7.34 (dd, *J* = 8.2, 7.8 Hz, 1H, H-5), 7.02 (dd, *J* = 8.0, 7.8 Hz, 1H, H-4), 4.26 − 4.13 (m, 4H, H-10 and H-11), 3.44 − 3.37 (m, 1H, H-9), 1.46 (s, 9H, H-16); ^{13}C NMR (126 MHz, Chloroform-*d*) δ$_C$ 169.8 (C-8), 156.1 (C-13), 135.2 (C-1), 132.3 (C-3), 128.5 (C-5), 125.6 (C-6), 122.1 (C-4), 113.5 (C-2), 79.9 (C-15); 51.9 (C-10 and C-11), 34.8 (C-9), 28.4 (C-16); LCMS (MDAP) Rt = 16.5 min (Method 5); m/z 254.9 [M(^{79}Br)H-Boc]$^+$, 256.9 [M(^{81}Br)H-Boc]$^+$; HRMS (ESI) calcd for C$_{15}$H$_{19}$BrN$_2$NaO$_3$ 377.0471, found 377.0466.

***tert*-Butyl 3-[(2-bromophenyl)-[(4-methoxyphenyl)methyl]carbamoyl]azetidine-1-carboxylate (35)**[179]
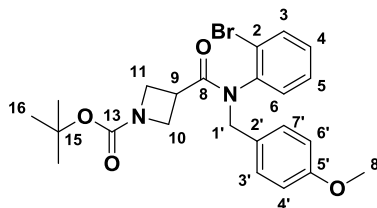
An ice cold solution of *tert*-butyl 3-[(2-bromophenyl)carbamoyl]azetidine-1-carboxylate (**34**) (7.77 g, 21.87 mmol) in anhydrous *N,N*-dimethylformamide (110 mL) was treated with sodium hydride (60 % dispersion in mineral oil) (0.34 g, 24.06 mmol). Upon completion of the addition, the reaction mixture was stirred at 0 °C for 1 hour. After this time, 1-(chloromethyl)-4-methoxy-benzene (3.26 mL, 24.06 mmol) was added and the resulting mixture was left to warm up to room temperature and left stirring at this temperature. After 16 hours, the solution was quenched with water (50 mL) and diluted with EtOAc (150 mL). The layers were separated and the organic layer was washed with sat. NaHCO$_3$ (100 mL) then brine (100 mL). The organic layer was dried over MgSO$_4$ and concentrated to dryness under reduced pressure. The crude was purified by flash column chromatography (Biotage SNAP 100 g, petroleum ether: EtOAc, 90: 10 to 60: 40) to give *tert*-butyl 3-[(2-bromophenyl)-[(4-methoxyphenyl) methyl]carbamoyl]azetidine-1-carboxylate (**35**) as a colourless oil (8.31 g, 80% yield): ^{1}H NMR (500 MHz, Chloroform-*d*) δ$_H$ 7.69 (dd, *J* = 7.5, 2.0 Hz, 1H, H-3), 7.25 − 7.16 (m, 2H, H-4 and H-5), 7.10 (d, *J* = 8.6 Hz, 2H, H-3' and H-7'), 6.79 (d, *J* = 8.6 Hz, 2H, H-4' and H-5'), 6.66 (dd, J = 7.2, 2.0 Hz, 1H, H-6), 5.55 (d, *J* = 14.2 Hz, 1H, H-1'), 4.30 (dd, *J* = 7.3 Hz, 1H, H-10 or H-11), 4.01 − 3.96 (m, 2H, H-1' and H-11 or H-10), 3.79 (s, 3H, H-8'), 3.71 (dd, *J* = 8.6 Hz, 1H, H-10 or H-11), 3.56 (dd, *J* = 8.6 Hz, 1H, H-10 or H-11), 3.11 − 3.02 (m, 1H, H-9), 1.41 (s, 9H, H-16); ^{13}C NMR (126 MHz, Chloroform-*d*) δ$_C$ 171.0 (C-8), 159.1 (C-5'), 139.6 (C-1), 133.9 (C-3), 131.6 (C-6), 130.6 (C-3' and C-7'), 130.0 (C-4), 128.8 (C-2'), 128.3 (C-5), 123.8 (C-2), 113.8 (C-4' and C-6'), 79.5 (C-15), 55.2 (C-8'), 51.1 (C-1'), 31.9 (C-9), 28.3 (C-16); LCMS (MDAP): Rt = 22.0 min (Method 5); m/z 497.1 [M(^{79}Br)+Na]$^+$, 498.9 [M(^{81}Br)+Na]$^+$; HRMS (ESI) calcd for C$_{23}$H$_{27}$BrN$_2$NaO$_4$ 497.1046, found 497.1051.

Note: Unable to visualise all carbon signals by NMR.

tert-Butyl 1'-[(4-methoxyphenyl)methyl]-2'-oxo-spiro[azetidine-3,3'-indoline]-1-carboxylate (36)[179]
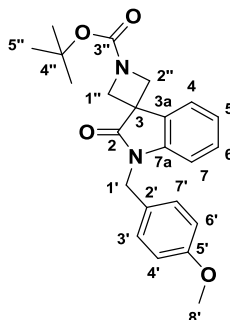
A ReactiVial™ was loaded with tert-butyl 3-[(2-bromophenyl)-[(4-methoxyphenyl)methyl]carbamoyl]azetidine-1-carboxylate (**35**) (480.0 mg, 1.02 mmol), palladium(II) acetate (22.9 mg, 0.10 mmol), tricyclohexylphosphine tetrafluoroborate (37.5 mg, 0.10 mmol) and sodium tert-butoxide (147.0 mg, 1.53 mmol). The vial was sealed and flushed with nitrogen/vacuum cycles. Anhydrous 1,4-dioxane (5 mL) was added and the resulting solution was evacuated with a vacuum/nitrogen cycle for 10 minutes before heating the reaction mixture to 80 °C. After 5 hours the reaction mixture was cooled to room temperature, diluted with ethyl acetate (20 mL) and saturated $NaHCO_3$ (15 mL). The layers were separated and the organic layer was washed with brine (20 mL), dried over $MgSO_4$ and concentrated under reduced pressure. The crude oil was purified by flash column chromatography (Biotage SNAP 25 g, petroleum ether: EtOAc, 95: 5 to 75: 25) to give tert-butyl 1'-[(4-methoxyphenyl)methyl]-2'-oxo-spiro[azetidine-3,3'-indoline]-1-carboxylate (**36**) as a pale yellow oil (315 mg, 78% yield): ^{1}H NMR (500 MHz, Chloroform-d) δ_H 7.55 (d, J = 7.5 Hz, 1H, H-4), 7.26 – 7.20 (m, 1H, H-6), 7.23 (d, J = 7.9 Hz, 2H, H-3' and H-7'), 7.11 (app. t, J = 7.8 Hz, 1H, H-5), 6.86 (d, J = 7.9 Hz, 2H, H-4' and H-6'), 6.78 (d, J = 7.8 Hz, 1H, H-7), 4.84 (s, 2H, H-1'), 4.43 (d, J = 8.2 Hz, 2H, H-1'' and H-2''), 4.09 (d, J = 8.2 Hz, 2H, H-1'' and H-2''), 3.78 (s, 3H, H-8'), 1.51 (s, 9H, H-5''); ^{13}C NMR (126 MHz, Chloroform-d) δ_C 176.9 (C-2), 159.2 (C-5'), 156.1 (C-3''), 142.7 (C-7a), 130.5 (C-3a), 128.9 (C-6), 128.8 (C-3' and C-7'), 123.1 (C-5), 122.9 (C-4), 114.2 (C-4' and C-6'), 109.1 (C-7), 80.2 (C-4''), 55.2 (C-8'), 43.5 (C-1'), 42.4 (C-3), 28.4 (C-5''); LCMS (MDAP): Rt = 20.6 min (Method 5); m/z 295.0 [M+H-BOC]$^+$; 417.0 [M+Na]$^+$; HRMS (ESI) calcd for $C_{23}H_{26}N_2NaO_4$ 417.1785, found 417.1789.

Note: Unable to visualise all carbon signals by NMR.

Scale up conditions:

A 500 mL 3 neck flask was loaded with tricyclohexylphosphine tetrafluoroborate (0.63 g, 1.72 mmol), palladium(II) acetate (0.38 g, 1.72 mmol) and sodium *tert*-butoxide (2.48 g, 25.87 mmol). The flask was evacuated with nitrogen/vacuum cycles before a solution of *tert*-butyl 3-[(2-bromophenyl)-[(4-methoxyphenyl)methyl]carbamoyl]azetidine-1-carboxylate (**35**) (8.20 g, 17.25 mmol) in anhydrous 1,4-dioxane (86 mL) was added. The flask was evacuated again with nitrogen/vacuum cycles before heating to 80 °C for 16 hours. After this time, the reaction mixture was cooled to room temperature, diluted with ethyl acetate (150 mL) and washed successively with sat. sodium bicarbonate (100 mL) and brine (100 mL). The organic layer was dried over MgSO$_4$ and concentrated under reduced pressure. The crude material was purified by flash column chromatography (Biotage SNAP 100 g, eluting petroleum ether: EtOAc, 95: 5 to 75: 25) to give (**36**) and (**36a**):

***tert*-Butyl 1'-[(4-methoxyphenyl)methyl]-2'-oxo-spiro[azetidine-3,3'-indoline]-1-carboxylate (36)** (1.36 g, 20% yield) as a glassy solid: ^{1}H NMR (500 MHz, Chloroform-*d*) δ$_H$ 7.55 (d, *J* = 7.5 Hz, 1H, H-4), 7.26 – 7.20 (m, 1H, H-6), 7.23 (d, *J* = 7.9 Hz, 2H, H-3' and H-7'), 7.11 (app. t, *J* = 7.8 Hz, 1H, H-5), 6.86 (d, *J* = 7.9 Hz, 2H, H-4' and H-6'), 6.78 (d, *J* = 7.8 Hz, 1H, H-7), 4.84 (s, 2H, H-1'), 4.43 (d, *J* = 8.2 Hz, 2H, H-1'' and H-2''), 4.09 (d, *J* = 8.2 Hz, 2H, H-1'' and H-2''), 3.78 (s, 3H, H-8'), 1.51 (s, 9H, H-5''); ^{13}C NMR (126 MHz, Chloroform-*d*) δ$_C$ 176.9 (C-2), 159.2 (C-5'), 156.1 (C-3''), 142.7 (C-7a), 130.5 (C-3a), 128.9 (C-6), 128.8 (C-3' and C-7'), 123.1 (C-5), 122.9 (C-4), 114.2 (C-4' and C-6'), 109.1 (C-7), 80.2 (C-4''), 55.2 (C-8'), 43.5 (C-1'), 42.4 (C-3), 28.4 (C-5''); LCMS (MDAP): Rt = 20.6 min (Method 5); m/z 295.0 [M+H-BOC]$^+$; 417.0 [M+Na]$^+$; HRMS (ESI) calcd for C$_{23}$H$_{26}$N$_2$NaO$_4$ 417.1785, found 417.1789.

Note: Unable to visualise all carbon signals by NMR.

***tert*-Butyl 3-[(4-methoxyphenyl)methyl-phenyl-carbamoyl]azetidine-1-carboxylate (36a)**

(3.27 g, 48% yield) as a brown gum.
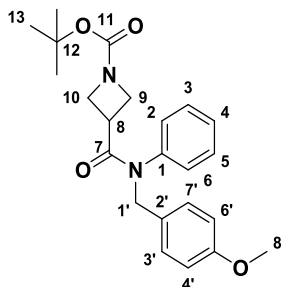
^{1}H NMR (500 MHz, Chloroform-*d*) δ$_H$ 7.38 – 7.30 (m, 3H, H-2, H-6 and H-4), 7.10 (d, *J* = 8.6 Hz, 2H, H-3' and H-7'), 6.92 – 6.84 (m, 2H, H-3 and H-5), 6.79 (d, *J* = 8.6 Hz, 2H, H-4' and H-6'), 4.83 (s, 2H, H-1'), 4.11 (app. t, *J* = 6.3 Hz, 2H, H-9 or H-10), 3.79 (s, 3H, H-8'), 3.62 (app. t, *J* = 8.6 Hz, 2H, H-9 or H-10), 3.25 – 3.12 (m, 1H, H-8), 1.41 (s, 9H, H-13); ^{13}C NMR (126 MHz, Chloroform-*d*) δ$_C$ 171.0 (C-2), 159.0 (C-5'), 156.1 (C-11), 141.1 (C-1), 130.2 (C-3 and C-5), 129.7 (C-2 and C-6), 129.3 (C-2'), 128.4 (C-3' and C-7'), 128.3 (C-4), 113.8 (C-4' and C-6'), 79.5 (C-12), 55.2 (C-8'), 52.6 (C-9 and C-10), 51.7 (C-1'), 32.1 (C-8), 28.3 (C-13); LCMS (MDAP): Rt = 20.1 min (Method 5), m/z 297.1 [M+H-BOC]$^+$, 419.0 [M+Na]$^+$; HRMS (ESI) calcd for $C_{23}H_{28}N_2NaO_4$ 419.1941, found 419.1944.

Note: Unable to visualise all carbon signals by NMR.

1'-[(4-Methoxyphenyl)methyl]spiro[azetidine-3,3'-indoline]-2'-one (37)
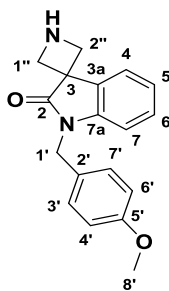
An ice cold solution of *tert*-butyl 1'-[(4-methoxyphenyl)methyl]-2'-oxo-spiro[azetidine-3,3'-indoline]-1-carboxylate (**36**) (315 mg, 0.80 mmol) in dichloromethane (5 mL) was treated with trifluoroacetic acid (1 mL, 0.80 mmol) and left stirring at 0 °C. After 2 hours, the solution was concentrated under reduced pressure and the residue was diluted with methanol (2 mL) before loading onto a SCX-2 cartridge. The column was rinsed with methanol (5 mL) before eluting the product with a solution of 2 N ammonia in methanol (2 x 5 mL). The elute was concentrated under reduced pressure to give 1'-[(4-methoxyphenyl)methyl]spiro[azetidine-3,3'-indoline]-2'-

one **(37)** as a colourless oil (152 mg, 65% yield): ^{1}H NMR (500 MHz, Chloroform-*d* + D$_2$O) δ$_H$ 7.77 (d, *J* = 7.6 Hz, 1H, H-4), 7.22 (d, *J* = 8.6 Hz, 2H, H-3' and H-7'), 7.22 − 7.17 (m, 1H, H-6), 7.11 (app. t, *J* = 7.6 Hz, 1H, H-5), 6.83 (d, *J* = 8.6 Hz, 2H, H-4' and H-6'), 6.74 (d, *J* = 7.6 Hz, 1H, H-7), 4.83 (s, 2H, H-1'), 4.27 (d, *J* = 8.0 Hz, 2H, H-1'' or H-2''), 3.78 (d, *J* = 8.0 Hz, 2H, H-1'' or H-2''), 3.76 (s, 3H, H-8'); ^{13}C NMR (126 MHz, Chloroform-*d*) δ$_C$ 177.7 (C-2), 159.1 (C-5'), 142.3 (C-7a), 131.6 (C-3a), 128.7 (C-3' and C-7'), 128.4 (C-6), 123.1 (C-4 or C-5), 123.0 (C-4 or C-5), 114.2 (C-4' or C-6'), 108.9 (C-7), 55.3 (C-8'), 55.2 (C-1'' and C-2''), 48.4 (C-3), 43.4 (C-1'); LCMS (MDAP): Rt = 10.9 min (Method 4); m/z 295.0 [M+H]$^+$; HRMS (ESI) calcd for C$_{18}$H$_{19}$N$_2$O$_2$ 295.1441, found 295.1442.

Note: Unable to visualise all carbon signals by NMR.

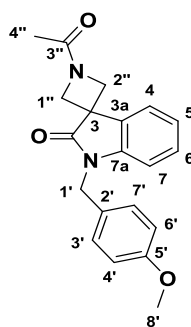**1-Acetyl-1'-[(4-methoxyphenyl)methyl]spiro[azetidine-3,3'-indoline]-2'-one (38)**

To a solution of 1'-[(4-methoxyphenyl)methyl]spiro[azetidine-3,3'-indoline]-2'-one (**37**) (146 mg, 0.50 mmol) in dichloromethane (5 mL) was added triethylamine (83 μL, 0.60 mmol) followed by acetyl chloride (39 μL, 0.55 mmol). Upon completion of the addition, the solution was left stirring at room temperature for 16 hours. After this time, the solution was washed with water (5 mL), followed by a saturated solution of sodium bicarbonate (5 mL) and brine (5 mL). The organic layer was dried over MgSO$_4$ and concentrated under reduced pressure to give 1-acetyl-1'-[(4-methoxyphenyl)methyl]spiro[azetidine-3,3'-indoline]-2'-one **(38)** as a colourless oil (158 mg, 95% yield): ^{1}H NMR (500 MHz, Chloroform-*d*) δ$_H$ 7.50 (d, *J* = 7.6 Hz, 1H, H-4), 7.27 − 7.22 (m, 3H, H-6, H-3' and H-7'), 7.11 (app. t, *J* = 7.6 Hz, 1H, H-5), 6.85 (d, *J* = 6.8 Hz, 2H, H-4' and H-6'), 6.80 (d, *J* = 7.6 Hz, 1H, H-7), 4.87 (d, *J* = 15.2 Hz, 1H, H-1'), 4.83 (d, *J* = 15.2 Hz, 1H, H-1'), 4.60 (d, *J* = 8.0 Hz, 1H, H-1'' or H-2''), 4.46 (d, *J* = 9.4 Hz, 1H, H-1'' or H-2''), 4.28 (d, *J* = 8.0 Hz, 1H, H-1'' or H-2''), 4.19 (d, *J* = 9.4 Hz, 1H, H-1'' or H-2''), 3.77 (s, 3H, H-8'), 1.99 (s, 3H, H-3''); ^{13}C NMR (126 MHz, Chloroform-*d*) δ$_C$ 176.7 (C-2), 170.7 (C-3''), 159.2 (C-5'), 142.8 (C-7a), 129.9 (C-6), 128.8 (C-3' and C-7'), 123.3 (C-4 or C-5), 122.8 (C-4 or C-5), 114.2 (C-4' and C-6'), 109.3 (C-7), 58.7 (C-1'' or C-2''), 56.6 (C-1'' or C-2''), 55.2 (C-8'), 43.6 (C-1'), 41.7 (C-3), 18.8 (C-4''); LCMS

(MDAP) Rt = 13.0 min (Method 5); m/z 337.0 [M+H]$^+$, 359.0 [M+Na]$^+$; HRMS (ESI) calcd for C$_{20}$H$_{21}$N$_2$O$_3$ 337.1547, found 337.1553.

Note: Unable to visualise all carbon signals by NMR.

1-Acetylspiro[azetidine-3,3'-indoline]-2'-one (39)
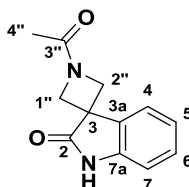
To a solution of 1-acetyl-1'-[(4-methoxyphenyl)methyl]spiro[azetidine-3,3'-indoline]-2'-one (**38**) (1.08 g, 3.21 mmol) in trifluoroacetic acid (12.29 mL, 160.53 mmol) was added anisole (2.44 mL, 22.47 mmol) and the resulting solution was heated to 150 °C under microwave irradiation for 2.5 hours. After this time, the solution was concentrated under reduced pressure, the residue was diluted with dichloromethane (30 mL) and neutralised with saturated NaHCO$_3$ (50 mL). The layers were separated, the organic layer was washed with brine (20 mL), dried over MgSO$_4$ and concentrated under reduced pressure to a brown oil. The crude material was purified by flash column chromatography (Biotage SNAP 10g, CH$_2$Cl$_2$: MeOH: NH$_3$, 99: 1: 0.1 to 90:10:1) to give 1-acetylspiro[azetidine-3,3'-indoline]-2'-one (**39**) as a pale yellow oil (318 mg, 46% yield): ^{1}H NMR (500 MHz, Chloroform-*d*) δ_H 8.27 (s, 1H, NH), 7.51 (d, *J* = 7.8 Hz, 1H, H-4), 7.30 (app. t, *J* = 7.8 Hz, 1H, H-6), 7.15 (app. t, *J* = 7.8 Hz, 1H, H-5), 6.94 (d, *J* = 7.8 Hz, 1H, H-7), 4.58 (d, *J* = 8.1 Hz, 1H, H-1'' or H-2''), 4.45 (d, *J* = 9.4 Hz, 1H, H-1'' or H-2''), 4.29 (d, *J* = 8.1 Hz, 1H, H-1'' or H-2''), 4.20 (d, *J* = 9.4 Hz, 1H, H-1'' or H-2''), 1.99 (s, 3H, 4''); ^{13}C NMR (126 MHz, Chloroform-*d*) δ_C 178.6 (C-2), 170.8 (C-3''), 140.8 (C-7a), 130.2 (C-3a), 129.4 (C-6), 123.3 (C-4 or C-5) 123.2 (C-4 or C-5), 110.1 (C-7), 58.6 (C-1'' or C-2''), 56.6 (C-1'' or C-2''), 42.1 (C-3), 18.8 (C-4''); LCMS (MDAP) Rt = 11.6 min (Method 4); m/z 217.0 [M+H]$^+$, 239.0 [M+Na]$^+$; HRMS (ESI) calcd for C$_{12}$H$_{13}$N$_2$O$_2$ 217.0972, found 217.0972.

Intermediate for the preparation of (40): ***N*-[(4-Methoxyphenyl)methyl]-*N*-phenyl-azetidine-3-carboxamide**
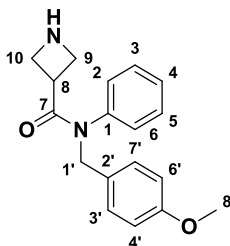
Trifluoroacetic acid (12.63 mL, 164.95 mmol) in dichloromethane (5 mL) was added dropwise to an ice cold solution of *tert*-butyl 3-[(4-methoxyphenyl)methyl-phenyl-carbamoyl]azetidine-1-carboxylate (**36a**) (3.32 g, 8.25 mmol) in dichloromethane (15 mL) and the solution was left to warm up and stir at room temperature for 16 hours. After this time, the solution was concentrated under reduced pressure. The residue was neutralised with saturated NaHCO$_3$ (20 mL) and extracted with dichloromethane (2 x 20 mL). The combined organic layers were dried over MgSO$_4$ and concentrated under reduced pressure to give *N*-[(4-methoxyphenyl)methyl]-*N*-phenyl-azetidine-3-carboxamide as a pale brown oil (2.37 g, 97% yield): ^{1}H NMR (500 MHz, Chloroform-*d*) δ_H 7.35 – 7.30 (m, 3H, H-2, H-4 and H-6), 7.09 (d, *J* = 8.6 Hz, 2H, H-3' and H-7'), 6.88 – 6.84 (m, 2H, H-3 and H-5), 6.79 (d, *J* = 8.6 Hz, 2H, H-4' and H-6'), 4.81 (s, 2H, H-1'), 4.18 (br s, 1H, NH), 4.00 (app. t, *J* = 8.2 Hz, 2H, H-9 or H-10), 3.78 (s, 3H, H-8'), 3.53 – 3.41 (m, 1H, H-8), 3.32 (app. t, *J* = 8.2 Hz, 2H, H-9 or H-10); ^{13}C NMR (126 MHz, Chloroform-*d*) δ_C 171.3 (C-7), 159.0 (C-5'), 141.1 (C-1), 130.2 (C-3 and C-5), 129.6 (C-2 and C-6), 129.3 (C-2'), 128.3 (C-3' and C-7'), 128.2 (C-4), 113.8 (C-4' and C-6'), 55.3 (C-8'), 52.5 (C-9 and C-10), 49.6 (C-1'), 37.4 (C-8); LCMS (MDAP) Rt = 3.8 min (Method 5); m/z 297.0 [M+H]$^+$. HRMS calcd for C$_{18}$H$_{21}$N$_2$O$_2$ 297.1598, found 297.1595.

1-Acetyl-*N*-[(4-methoxyphenyl)methyl]-*N*-phenyl-azetidine-3-carboxamide (40)
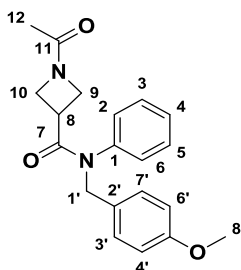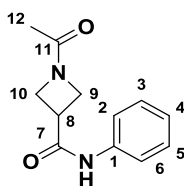

To an ice cold solution of *N*-[(4-methoxyphenyl)methyl]-*N*-phenyl-azetidine-3-carboxamide (2.37 g, 8 mmol) in dichloromethane (32 mL) was added triethylamine (1.45 mL, 10.4 mmol) followed by acetyl chloride (0.63 mL, 8.8 mmol) and the solution was left to warm up to room

temperature and stirred at this temperature for 16 hours. After this time, the solution was washed successively with water (50 mL), saturated citric acid (50 mL) and brine (50 mL). The organic layer was dried over MgSO$_4$ and concentrated under reduced pressure to give 1-acetyl-*N*-[(4-methoxyphenyl)methyl]-*N*-phenyl-azetidine-3-carboxamide **(40)** as a pale amber oil (2.67 g, 99% yield): ^{1}H NMR (500 MHz, Chloroform-*d*) δ$_H$ 7.38 – 7.32 (m, 3H, H-2, H-4 and H-6), 7.10 (d, *J* = 8.5 Hz, 2H, H-3' and H-7'), 6.91 – 6.85 (m, 2H, H-3 and H-5), 6.80 (d, *J* = 8.5 Hz, 2H, H-4' and H-6'), 4.86 (d, *J* = 14.5 Hz, 1H, H-1'), 4.80 (d, *J* = 14.5 Hz, 1H, H-1'), 4.52 – 4.43 (m, 1H, H-9 or H-10), 4.07 – 3.98 (m, 1H, H-9 or H-10), 3.93 – 3.85 (m, 1H, H-9 or H-10), 3.79 (s, 3H, H-8'), 3.70 – 3.59 (m, 1H, H-9 or H-10), 3.31 – 3.20 (m, 1H, H-8), 1.82 (s, 3H, H-12); ^{13}C NMR (126 MHz, Chloroform-*d*) δ$_C$ 170.6 (C-7 or C-11), 170.5 (C-7 or C-11), 159.1 (C-5'), 140.9 (C-1), 130.2 (C-3 and C-5), 129.8 (C-2 and C-6), 129.1 (C-2'), 128.5 (C-4), 128.4 (C-3' and C-7'), 113.8 (C-4' and C-6'), 55.2 (C-8'), 52.7 (C-1'), 52.1 (C-9 or C-10), 51.0 (C-9 or C-10), 31.5 (C-8), 18.5 (C-12); LCMS (MDAP): Rt = 12.1 min (Method 5); m/z 339.0 [M+H]$^+$, 361.0 [M+Na]$^+$.

Note: Unable to obtain any ionisation under HRMS.

1-Acetyl-*N*-phenyl-azetidine-3-carboxamide (41)

Anisole (0.32 mL, 2.96 mmol) was added to a solution of 1-acetyl-*N*-[(4-methoxyphenyl)methyl]-*N*-phenyl-azetidine-3-carboxamide (**40**) (250 mg, 0.74 mmol) in trifluoroacetic acid (1.13 mL, 14.78 mmol) and the solution was heated to 150 °C for 2.5 hours under microwave irradiation. After this time, the solution was concentrated under reduced pressure, the residue was diluted with dichloromethane (30 mL) and neutralised with saturated NaHCO$_3$ (50 mL). The layers were separated, the organic layer was washed with brine (20 mL), dried over MgSO$_4$ and concentrated under reduced pressure. The crude compound was purified by flash column chromatography (Biotage SNAP 10g, CH$_2$Cl$_2$:MeOH :NH$_3$, 99: 1: 0.1 to 90: 10: 1) to give 1-acetyl-*N*-phenyl-azetidine-3-carboxamide **(41)** as a pale amber oil (89 mg, 55% yield): ^{1}H NMR (500 MHz, Chloroform-*d*) δ$_H$ 8.31 (s, 1H, NH), 7.56 (d, *J* = 7.9 Hz, 2H, H-2 and H-6), 7.32 (dd, *J* = 7.9, 7.4 Hz, 2H, H-3 and H-5), 7.12 (t, *J* = 7.4 Hz, 1H, H-4), 4.49 (app. t, *J* = 8.4 Hz, 1H, H-9 or H-10), 4.24 (app. t, *J* = 8.4 Hz, 1H, H-9 or H-10), 4.19 (d, *J* = 7.5 Hz, 2H, H-9 or H-10), 3.51 – 3.38 (m, 1H, H-8), 1.88 (s, 3H, H-12); ^{13}C NMR (126 MHz, Chloroform-*d*) δ$_C$ 170.8 (C-7 or C-11), 169.6 (C-7 or C-11), 137.8 (C-1), 129.0 (C-3 and C-5), 124.6 (C-4), 120.0 (C-2 and C-6), 52.5 (C-9 or C-10), 50.9 (C-9 or C-10),

33.5 (C-8), 18.6 (C-12); LCMS (MDAP): Rt = 12.5 min (Method 4); m/z 219.0 [M+H]+, 241.0 [M+Na]+; HRMS (ESI) calcd for $C_{12}H_{15}N_2O_2$ 219.1128, found 219.1127.

tert-Butyl 4-[(2-bromophenyl)carbamoyl]piperidine-1-carboxylate (42a)[347,348]
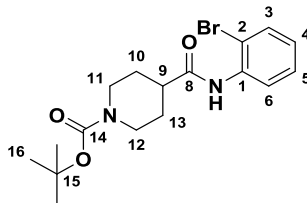
(Dimethylamino)pyridine (3.46 g, 28.34 mmol) and EDCI.HCl (5.43 g, 28.34 mmol) were added to a stirred solution of 2-bromoaniline (3.75 g, 21.8 mmol) and 1-tert-butoxycarbonylpiperidine-4-carboxylic acid (5.0 g, 21.8 mmol) in dichloromethane (110 mL) and the reaction was left to stir at room temperature. After 16 hours, water (150 mL) was added to the reaction and the layers were separated. The organic layer was washed with brine (100 mL), dried over $MgSO_4$ and concentrated under reduced pressure. The crude oil was purified by flash column chromatography (Biotage SNAP 100 g, petroleum ether: EtOAc, 90: 10 to 75: 25) to give tert-butyl 4-[(2-bromophenyl)carbamoyl]piperidine-1-carboxylate **(42a)** as a colourless oil (7.17 g, 86% yield): ^{1}H NMR (500 MHz, Chloroform-d) δ 8.30 (d, J = 7.8 Hz, 1H, H-6), 7.72 (s, 1H, NH), 7.51 (d, J = 7.8 Hz, 1H, H-3), 7.28 (d, J = 7.8 Hz, 1H, H-5), 6.96 (app. t, J = 7.8 Hz, 1H, H-4), 4.30 – 4.06 (m, 2H, H-11 and H-12), 2.91 – 2.71 (m, 2H, H-11 and H-12), 2.53 – 2.37 (m, 1H, H-9), 2.02 – 1.86 (m, 2H, H-10 and H-13), 1.83 – 1.66 (m, 2H, H-10 and H-13), 1.45 (s, 9H, H-16); ^{13}C NMR (126 MHz, Chloroform-d) δ 172.5 (C-8), 154.6 (C-14), 135.4 (C-1), 132.2 (C-3), 128.4 (C-5), 125.3 (C-4), 122.1 (C-6), 113.6 (C-2), 79.7 (C-15), 44.4 (C-9), 43.0 (C-11 and C-12), 28.6 (C-10 and C-13), 28.4 (C-16); LCMS (MDAP): Rt = 18.4 min (Method 5); m/z 404.9 [M(^{79}Br)+Na]+, 406.8 [M(^{81}Br)+Na]+; HRMS (ESI) calcd for $C_{17}H_{23}BrN_2NaO_3$ 405.0784, found 405.0779.

N-(2-Bromophenyl)tetrahydrofuran-3-carboxamide (42b)
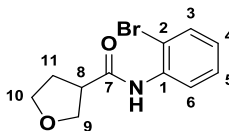
4-(Dimethylamino)pyridine (1.38 g, 11.29 mmol) and EDCI.HCl (2.16 g, 11.29 mmol) were added to a solution of 2-bromoaniline (0.89 mL, 8.68 mmol) and tetrahydrofuran-3-carboxylic acid (1.08 g, 8.68 mmol) in dichloromethane (20 mL) and the resulting mixture was stirred at 20 °C for 4 days. After this time, the solution was diluted with dichloromethane (30 mL) and washed

successively with 1 N HCl (50 mL), a saturated NaHCO₃ solution (50 mL) and brine (50 mL). The organic layer was dried over MgSO₄ and concentrated under reduced pressure to a colourless oil. The crude mixture was purified by column chromatography (Biotage SNAP 50 g, petroleum ether: EtOAc (90: 10 to 60: 40) to give *N*-(2-bromophenyl)tetrahydrofuran-3-carboxamide **(42b)** as a colourless solid (1.47 g, 63% yield): m.p. 84 – 87 °C; ^{1}H NMR (600 MHz, Chloroform-*d*) δ$_H$ 8.31 (d, *J* = 7.9 Hz, 1H, H-6), 7.95 (s, 1H, NH), 7.53 (d, *J* = 7.9 Hz, 1H, H-3), 7.32 (app. t, *J* = 7.9 Hz, 1H, H-5), 6.98 (app. t, *J* = 7.9 Hz, 1H, H-4), 4.14 (dd, *J* = 4.6 Hz, 1 H, H-9); 4.07 (dd, *J* = 7.4 Hz, 1 H, H-9), 3.95 (dd, *J* = 7.0 Hz, 1 H, H-10), 3.86 (dd, *J* = 7.5 Hz, 1 H, H-10), 3.15 – 3.09 (m, 1H, H-8), 2.36 – 2.23 (m, 2H, H-11); ^{13}C NMR (126 MHz, Chloroform-*d*) δ 172.1 (C-7), 135.6 (C-1), 132.2 (C-3), 128.3 (C-5), 125.3 (C-4), 122.1 (C-6), 113.5 (C-2), 70.8 (C-9), 66.0 (C-10), 46.9 (C-11), 30.5 (C-8); LCMS (LCQ): Rt = 2.2 min (Method 2); m/z 269.9 [M($^{79}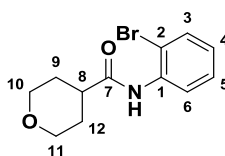$Br)+H]$^+$, 271.9 [M(^{81}Br)+H]$^+$; LCMS (MDAP): Rt = 11.5 min (Method 5); m/z 269.9 [M(^{79}Br)+H]$^+$, 271.9 [M(^{81}Br)+H]$^+$; HRMS (ESI) calcd for C₁₁H₁₃BrNO₂ 270.0124, found 270.0123.

N-(2-Bromophenyl)tetrahydropyran-4-carboxamide (42c)

Propylphosphonic acid (11.1 mL, 17.44 mmol) (50% in ethyl acetate) was added dropwise to a solution of 2-bromoaniline (1.5 g, 8.72 mmol), tetrahydro-2*H*-pyran-4-carboxylic acid (1.25 g, 9.59 mmol) and pyridine (2.12 mL, 26.16 mmol) in ethyl acetate (21 mL) kept at -10 °C. Once added, the reaction mixture was left stirring at room temperature for 16 hours. After this time, the solution was cooled with an ice bath and 1 N HCl (30 mL) was added dropwise. The mixture was left stirring for 10 minutes and the layers were separated. The organic layer was washed with brine (30 mL), dried over MgSO₄ and concentrated under reduced pressure to give *N*-(2-bromophenyl)tetrahydropyran-4-carboxamide **(42c)** as a colourless solid (2.17 g, 88% yield): m.p. 116 – 118 °C; ^{1}H NMR (500 MHz, DMSO-*d*₆) δ$_H$ 9.37 (s, 1H, NH), 7.64 (dd, *J* = 8.0, 1.4 Hz, 1H, H-6), 7.55 (dd, *J* = 8.0, 1.4 Hz, 1H, H-3), 7.35 (app. dt, *J* = 7.7, 1.4 Hz, 1H, H-5), 7.13 (app. dt, *J* = 7.7, 1.4 Hz, 1H, H-4), 3.93 – 3.87 (m, 2H, H-10 and H-12), 3.36 (app. td, *J* = 11.6, 2.4 Hz, 2H, H-10 and H-11), 2.76 – 2.65 (m, 1H, H-8), 1.80 – 1.61 (m, 4H, H-9 and H-12); ^{1}H NMR (500 MHz, Chloroform-*d*) δ 8.32 (d, *J* = 7.7 Hz, 1H, H-6), 7.72 (s, 1H, NH), 7.51 (dd, *J* = 7.7, 1.4 Hz, 1H, H-3), 7.29 (app. dt, *J* = 7.7, 1.4 Hz, 1H, H-5), 6.96 (app. dt, *J* = 7.7, 1.4 Hz, 1H, H-4), 4.05 (dt, *J* = 14.5, 3.4 Hz, 2H, H-10 and H-11), 3.46 (ddd, *J* = 14.2, 7.5, 5.1 Hz, 2H, H-10 and H-11), 2.56 (m, 1H, H-8), 1.89 (m, 4H, H-9 and H-12); ^{13}C NMR (126 MHz, Chloroform-*d*) δ 172.3 (C-7), 135.4 (C-1), 132.2(C-

3), 128.4 (C-5), 125.3 (C-4), 122.0 (C-6), 113.6 (C-2), 67.1 (C-10 and C-11), 43.3 (C-8), 29.2 (C-9 and C-12); LCMS (MDAP): Rt = 11.5 min (Method 5); m/z 283.9 [M(^{79}Br)+H]$^+$, 285.9 [M(^{81}Br)+H]$^+$; HRMS (ESI) calcd for C$_{12}$H$_{15}$BrNO$_2$ 284.0281, found 284.0289.

tert-Butyl 3-[(2-bromo-5-fluoro-phenyl)carbamoyl]azetidine-1-carboxylate (42d)
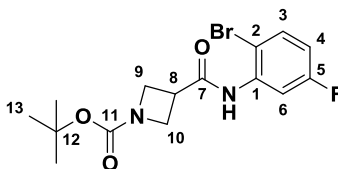
4-(Dimethylamino)pyridine (1.67 g, 13.68 mmol) and EDCI.HCl (2.62 g, 13.68 mmol) were added to a solution of 2-bromo-5-fluoro-aniline (2.0 g, 10.53 mmol) and 1-*tert*-butoxycarbonylazetidine-3-carboxylic acid (2.12 g, 10.53 mmol) in dichloromethane (26 mL). The resulting reaction mixture was left stirring at room temperature for 48 hours. After this time, the solution was washed successively with a saturated solution of citric acid (30 mL), a solution of saturated sodium bicarbonate (30 mL) and brine (50 mL). The organic layer was dried over MgSO$_4$ and concentrated under reduced pressure to a brown oil. The crude oil was purified by flash column chromatography (Biotage SNAP 50 g, petroleum ether: EtOAc, 95: 5 to 80: 20) to give *tert*-butyl 3-[(2-bromo-5-fluoro-phenyl)carbamoyl]azetidine-1-carboxylate **(42d)** as a colourless solid (1.75 g, 45% yield): m.p. 133 – 139 °C; ^{1}H NMR (500 MHz, Chloroform-*d*) δ$_H$ 8.25 (d, *J* = 10.2 Hz, 1H, H-6), 7.71 (br s, 1H, NH), 7.49 (dd, *J* = 8.9, 5.7 Hz, 1H, H-3), 6.80 – 6.73 (m, 1H, H-4), 4.24 – 4.14 (m, 4H, H-9 and H-10), 3.45 – 3.34 (m, 1H, H-8), 1.46 (s, 9H, H-13); ^{13}C NMR (126 MHz, Chloroform-*d*) δ$_C$ 170.0 (C-7), 162.1 (d, *J*$_{CF}$ = 253.4 Hz, C-5), 156.1 (C-11), 136.3 (d, *J*$_{CF}$ = 13.1 Hz, C-1), 132.8 (d, *J*$_{CF}$ = 8.4 Hz, C-3). 112.5 (d, *J*$_{CF}$ = 20.5 Hz, C-4), 110.0 (C-2), 109.4 (d, *J*$_{CF}$ = 29.6 Hz, C-6), 80.0 (C-12), 51.6 (C-9 and C-10, weak), 34.9 (C-8), 28.3 (C-13); LCMS (MDAP): Rt = 17.9 min (Method 5); m/z 272.9 [M(^{79}Br)H-Boc]$^+$, 274.8 [M(^{81}Br)H-Boc]$^+$; HRMS (ESI) calcd for C$_{15}$H$_{18}$BrFN$_2$NaO$_3$ 395.0377, found 395.0382.

N-(2-Bromo-5-fluoro-phenyl)cyclopropanecarboxamide (42e)
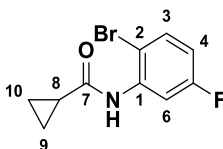
Propylphosphonic acid (50% in ethyl acetate) (13.3 mL, 21.05 mmol) was added dropwise to a solution of 2-bromo-5-fluoroaniline (2.0 g, 10.53 mmol), cyclopropanecarboxylic acid (1.0 g, 11.58 mmol) and pyridine (2.55 mL, 31.58 mmol) kept at -10 °C. Once added, the reaction mixture was left stirring at room temperature for 16 hours. After this time, the solution was

cooled with an ice bath and 1 N HCl (30 mL) was added dropwise. The mixture was left stirring for 10 minutes and the layers were separated. The organic layer was washed with brine (30 mL), dried over $MgSO_4$ and concentrated under reduced pressure to give *N*-(2-bromo-5-fluoro-phenyl)cyclopropanecarboxamide **(42e)** as a colourless solid (2.67 g, 98% yield): m.p. 101 – 102 °C; ^{1}H NMR (500 MHz, Chloroform-*d*) δ_H 8.27 (dd, *J* = 8.4, 2.9 Hz, 1H, H-6), 7.87 (br s, 1H), 7.48 (dd, *J* = 9.0, 5.8 Hz, 1H, H-3), 6.74 - 6.68 (m, 1H, H-4), 1.65 – 1.50 (m, 1H, H-8), 1.17 – 1.11 (m, 2H, H-9 and H-10), 0.97 – 0.90 (m, 2H, H-9 and H-10); ^{13}C NMR (126 MHz, Chloroform-*d*) δ_C 171.9 (C-7), 162.2 (d, J_{CF} = 247.5 Hz, C-5), 137.1 (d, J_{CF} = 11.2 Hz, C-1), 111.6 (d, J_{CF} = 23.4 Hz, C-4 or C-6), 109.0 (d, J_{CF} = 29.8 Hz, C-4 or C-6), 16.2 (C-8), 8.5 (C-9 and C-10); LCMS (MDAP): Rt = 16.5 min (Method 5); m/z 257.9 [M(^{79}Br)+H]$^+$, 259.9 [M(^{81}Br)+H]$^+$; HRMS (ESI) calcd for $C_{10}H_9BrFNONa$ 279.9744, found 279.9755.

tert-Butyl 4-[(2-bromophenyl)-[(4-methoxyphenyl)methyl]carbamoyl]piperidine-1-carboxylate (43a)[348]
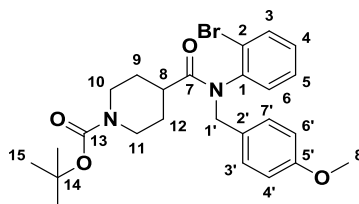
Sodium hydride (60% dispersion in oil) (0.823 g, 20.58 mmol) was added to an ice cold solution of *tert*-butyl 4-[(2-bromophenyl)carbamoyl]piperidine-1-carboxylate (**42a**) (7.17 g, 18.71 mmol) in anhydrous *N,N*- dimethylformamide (62 mL) and the reaction mixture was stirred cold for 1 hour before adding 1-(chloromethyl)-4-methoxy-benzene (2.79 mL, 20.58 mmol). The cold bath was removed and the mixture was left stirring at room temperature for 16 hours. After this time, the solution was quenched with water (100 mL) and the product was extracted with ethyl acetate (2 x 150 mL). The combined organic layers were washed successively with saturated citric acid (50 mL), saturated $NaHCO_3$ (100 mL) then brine (100 mL). The organic layer was dried over $MgSO_4$ and concentrated under reduced pressure. The crude residue was purified by flash column chromatography (Biotage SNAP 50 g, petroleum ether: EtOAc, 95: 5 to 70: 30) to give *tert*-butyl 4-[(2-bromophenyl)-[(4-methoxyphenyl)methyl]carbamoyl]piperidine-1-carboxylate **(43a)** as a colourless oil (6.99 g, 74% yield). ^{1}H NMR (500 MHz, Chloroform-d) δ_H 7.71 (dd, *J* = 7.4, 2.1 Hz, 1H, H-3), 7.25 – 7.17 (m, 2H, H-4 and H-5), 7.08 (d, *J* = 9.3 Hz, 2H, H-3' and H-7'), 6.79 (d, *J* = 8.1 Hz, 2H, H-4' and H-6'), 6.75 (dd, *J* = 7.2, 2.2 Hz, 1H, H-6), 5.55 (d, *J* = 14.2 Hz, 1H, H-1'), 4.12 – 3.99 (m, 2H, H-10 and H-11), 3.96 (d, *J* = 14.2 Hz, 1H, H-1'), 3.79 (s, 3H, H-8'), 2.59 – 2.46 (m, 1H, H-10 or H-11), 2.44 – 2.29 (m, 1H, H-10 or H-11), 2.05 (m, 1H, H-8), 1.93 – 1.80 (m, 1H,

H-9 or H-12), 1.77 – 1.61 (m, 3H, H-9 and H-11), 1.44 (s, 9H, H-15); ^{13}C NMR (126 MHz, Chloroform-d) δ_C 174.4 (C-7), 159.0 (C-5'), 154.6 (C-13), 140.4 (C-1), 134.2 (C-3), 131.2 (C-6), 130.5 (C-3' and C-7'), 129.7 (C-4), 129.1 (C-2'), 128.2 (C-5), 113.7 (C-4' and C-6'), 79.4 (C-14), 55.2 (C-8'), 50.8 (C-1'), 43.1 (C-10 and C-11), 40.4 (C-8), 28.4 (C-15); LCMS (MDAP): Rt = 24.0 min (Method 4); m/z 525.3 [M(^{79}Br)+Na]$^+$, 527.0 [M(^{81}Br)+Na]$^+$; HRMS (ESI) calcd for $C_{25}H_{31}BrN_2O_4Na$ 525.1359, found 525.1339.

Note: Unable to visualise all carbon signals by NMR.

N-(2-Bromophenyl)-*N*-[(4-methoxyphenyl)methyl]tetrahydrofuran-3-carboxamide (43b)
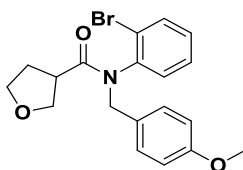
Sodium hydride (60% dispersion in oil) (0.239 g, 5.99 mmol) was added to an ice cold solution of *N*-(2-bromophenyl)tetrahydrofuran-3-carboxamide (**42b**) (1.47 g, 5.44 mmol) in anhydrous *N,N*-dimethylformamide (22 mL). Upon completion of the addition, the reaction mixture was stirred cold for 1 hour before adding 1-(chloromethyl)-4-methoxy-benzene (0.81 mL, 5.99 mmol). The cold bath was removed and the mixture was left stirring at room temperature for 16 hours. After this time, the solution was quenched with water (50 mL) and the product was extracted with ethyl acetate (2 x 50 mL). The combined organic layers were washed successively with 1 N HCl (50 mL) and brine (50 mL), dried over MgSO$_4$ and concentrated under reduced pressure to give *N*-(2-bromophenyl)-*N*-[(4-methoxyphenyl)methyl]tetrahydrofuran-3-carboxamide (**43b**) as a colourless oil that was used as is into the next step (1.81 g, 85% yield).

N-(2-Bromophenyl)-*N*-[(4-methoxyphenyl)methyl]tetrahydropyran-4-carboxamide (43c)
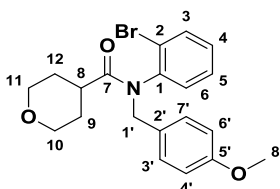
Sodium hydride (60% dispersion in oil) (0.339 g, 8.87 mmol) was added to an ice cold solution of *N*-(2-bromophenyl)tetrahydropyran-4-carboxamide (**42c**) (2.1 g, 7.39 mmol) in anhydrous *N,N*-dimethylformamide (25 mL). Upon completion of the addition, the cold bath was removed and the suspension was stirred at room temperature for 30 minutes. After this time, the suspension was cooled again with an ice bath and 4-methoxybenzyl chloride (1.1 mL, 8.13 mmol) was added

dropwise. The cold bath was removed and the solution was left stirring at room temperature for 4 hours. After this time, water (50 mL) was added and the reaction mixture was extracted with ethyl acetate (2 x 50 mL). The combined organic layers were washed with brine (2 x 50 mL), dried over MgSO$_4$ and concentrated under reduced pressure. The crude material was purified by flash column chromatography (Redisep 40 g, petroleum ether: EtOAc, 95: 5 to 70: 30) to give *N*-(2-bromophenyl)-*N*-[(4-methoxyphenyl)methyl]tetrahydropyran-4-carboxamide **(43c)** as a colourless oil that crystallised on standing to a colourless solid (2.13 g, 71% yield): m.p. 112 – 116 °C; ^{1}H NMR (500 MHz, DMSO-*d*$_6$) δ$_H$ 7.79 (dd, *J* = 7.6, 1.9 Hz, 1H, H-3), 7.37 – 7.28 (m, 2H, H-4 and H-5), 7.05 (d, *J* = 9.0 Hz, 2H, H-3' and H-7'), 6.97 (dd, *J* = 7.0, 2.4 Hz, 1H, H-6), 6.82 (d, *J* = 9.0 Hz, 2H, H-4' and H-6'), 5.27 (d, *J* = 14.4 Hz, 1H, H-1'), 4.05 (d, *J* = 14.4 Hz, 1H, H-1'), 3.84 – 3.73 (m, 2H, H-10 and H-11), 3.70 (s, 3H, H-8'), 3.04 (app. dt, *J* = 12.0, 2.3 Hz, 1H, H-10 or H11), 2.93 (app. dt, *J* = 11.8, 2.3 Hz, 1H, H-10 or H-11), 2.11 (m, 1H, H-8), 1.85 – 1.70 (m, 1H, H-11 or H-12), 1.64 – 1.53 (m, 1H, H-9 or H-12), 1.52 – 1.40 (m, 2H, H-9 and H-12); ^{13}C NMR (126 MHz, DMSO-*d*$_6$) δ$_C$ 173.8 (C-7), 159.0 (C-5'), 140.5 (C-1), 134.1 (C-3), 131.6 (C-5), 130.7 (C-6), 130.4 (C-3' and C-7'), 129.3 (C-4) 129.2 (C-2'), 123.9 (C-2), 114.1 (C-4' and C-6'), 66.5 (C-10 or C-11), 66.4 (C-10 or C-11), 55.4 (C-8'), 50.7 (C-1'), 39.1 (C-8), 29.6 (C-9 or C-12), 28.8 (C-9 or C-12); LCMS (LCQ): Rt = 2.6 min (Method 1); m/z 404.1 [M(^{79}Br)+H]$^+$, 406.1 [M(^{81}Br)+H]$^+$; HRMS (ESI) calcd for C$_{20}$H$_{23}$BrNO$_3$ 404.0856, found 404.0854.

tert-Butyl 3-[(2-bromo-5-fluoro-phenyl)-[(4-methoxyphenyl)methyl]carbamoyl]azetidine-1-carboxylate (43d)
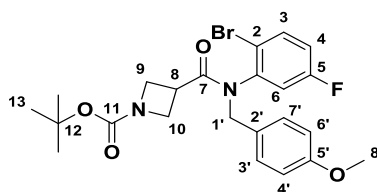
Sodium hydride (60% dispersion in oil) (0.206 g, 5.16 mmol) was added in one portion to an ice cold solution of *tert*-butyl 3-[(2-bromo-5-fluoro-phenyl)carbamoyl]azetidine-1-carboxylate **(42d)** (1.75 g, 4.69 mmol) in anhydrous *N,N*-dimethylformamide (19 mL) and the cloudy solution was left to stir at room temperature for 1 hour. After this time, the solution was cooled with an ice bath and 1-(chloromethyl)-4-methoxy-benzene (0.70 mL, 5.16 mmol) was added dropwise. The solution was left to stir at room temperature for 16 hours. After this time, the reaction mixture was quenched with water (50 mL) and extracted with ethyl acetate (2 x 50 mL). The combined organic layers were washed successively with a saturated solution of sodium bicarbonate (50 mL) and brine (100 mL), dried over MgSO$_4$ and concentrated under reduced

pressure. The crude oil was purified by flashed column chromatography (Biotage SNAP 50 g, petroleum ether: EtOAc (95: 5 to 70: 30) to give *tert*-butyl 3-[(2-bromo-5-fluoro-phenyl)-[(4-methoxyphenyl)methyl]carbamoyl]azetidine-1-carboxylate **(43d)** as a colourless oil (1.85 g, 79% yield): ^{1}H NMR (500 MHz, Chloroform-*d*) δ_H 7.64 (dd, *J* = 8.9, 5.6 Hz, 1H, H-3), 7.09 (d, *J* = 8.3 Hz, 2H, H-3' and H-7'), 6.99 (ddd, *J* = 8.9, 7.5, 2.8 Hz, 1H, H-4), 6.80 (d, *J* = 8.5 Hz, 2H, H-4' and H-6'), 6.43 (dd, *J* = 8.9, 2.8 Hz, 1H, H-6), 5.51 (d, *J* = 14.3 Hz, 1H, H-1'), 4.28 (dd, *J* = 8.5 Hz, 1H, H-9 or H-10), 4.03 (d, *J* = 14.3 Hz, 1H, H-1'), 4.05 – 4.00 (m, 1H, H-9 or H-10), 3.79 (s, 3H, H-8'), 3.74 (app. t, *J* = 8.5 Hz, 1H, H-9 or H-10), 3.63 (app. t, *J* = 8.5 Hz, 1H, H-9 or H-10), 3.10 – 3.02 (m, 1H, H-8), 1.41 (s, 9H, H-13); ^{13}C NMR (126 MHz, Chloroform-*d*) δ_C 170.8 (C-7), 161.4 (d, J_{CF} = 251.6 Hz, C-5), 159.3 (C-5'), 156.1 (C-13), 140.8 (d, J_{CF} = 9.6 Hz, C-1), 134.6 (d, J_{CF} = 8.4 Hz, C-3), 130.6 (C-3' and C-7'), 128.3 (C-2'), 118.8 (d, J_{CF} = 22.3 Hz, C-6), 117.5 (d, J_{CF} = 23.3 Hz, C-4), 114.0 (C-2), 113.9 (C-4' or C-6'), 79.6 (C-12), 55.2 (C-9 and C-10), 55.1 (C-8'), 51.1 (C-1'), 31.8 (C-8), 28.3 (C-13); LCMS (MDAP): Rt = 21.8 min (Method 5); m/z 515.1 [M([79]Br)+Na]$^+$, 517.0 [M([81]Br)+Na]$^+$; HRMS (ESI) calcd for $C_{23}H_{26}BrFN_2NaO_4$ 515.0952, found 515.0963.

N-(2-Bromo-5-fluoro-phenyl)-*N*-[(4-methoxyphenyl)methyl]cyclopropanecarboxamide (43e)
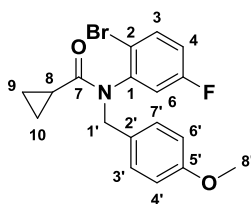
Sodium hydride (60% dispersion in oil) (0.475 g, 12.41 mmol) was added to an ice cold solution of *N*-(2-bromo-5-fluoro-phenyl)cyclopropanecarboxamide (**42e**) (2.67 g, 10.35 mmol) in anhydrous *N*,*N*-dimethylformamide (25 mL). Upon completion of the addition, the cold bath was removed and the suspension was stirred at room temperature for 30 minutes. After this time, the suspension was cooled again with an ice bath and 4-methoxylbenzyl chloride (1.54 mL, 11.38 mmol) was added dropwise. The cold bath was removed and the solution was left stirring at room temperature for 4 hours. After this time, water (50 mL) was added and the reaction mixture was extracted with ethyl acetate (2 x 50 mL). The combined organic layers were washed with brine (2 x 50 mL), dried over MgSO$_4$ and concentrated under reduced pressure. The crude material was purified by flash column chromatography (Redisep 40 g, petroleum ether: EtOAc, 95: 5 to 70: 30) to give *N*-(2-bromo-5-fluoro-phenyl)-*N*-[(4-methoxyphenyl)methyl] cyclopropanecarboxamide **(43e)** as a colourless oil that solidified on standing to a crystalline colourless solid (3.48 g, 89% yield): m.p. 59 – 63 °C; ^{1}H NMR (500 MHz, DMSO-*d*$_6$) δ_H 7.80 (dd,

J = 8.9, 5.8 Hz, 1H, H-3), 7.22 (app. dt, *J* = 8.9, 3.0 Hz, 1H, H-4), 7.08 (d, *J* = 8.6 Hz, 2H, H-3' and H-7'), 6.99 (dd, *J* = 9.2, 3.0 Hz, 1H, H-6), 6.82 (d, *J* = 8.6 Hz, 2H, H-4' and H-6'), 5.13 (d, *J* = 14.4 Hz, 1H, H-1'), 4.29 (d, *J* = 14.4 Hz, 1H, H-1'), 3.71 (s, 3H, H-8'), 1.15 − 1.06 (m, 1H, H-8), 0.91 − 0.77 (m, 2H, H-9 and H-10), 0.71 − 0.57 (m, 2H, H-9 and H-10); ^{13}C NMR (126 MHz, DMSO-*d₆*) δ$_C$ 172.4 (C-7), 161.6 (d, J_{CF} = 248.1 Hz, C-5), 159.1 (C-5'), 142.2 (d, J_{CF} = 9.2 Hz, C-1), 135.1 (d, J_{CF} = 9.2 Hz, C-3), 130.6 (C-3' and C-7'), 129.0 (C-2'), 119.4 (d, J_{CF} = 3.5 Hz, C-2), 119.1 (d, J_{CF} = 23.3 Hz, C-6), 118.5 (d, J_{CF} = 22.4 Hz, C-4), 114.1 (C-4' and C-6'), 55.4 (C-8'), 50.8 (C-1'), 12.8 (C-8), 8.7 (C-9 or C-10), 8.5 (C-9 or C-10); LCMS (LCQ): Rt = 22.2 min (Method 4); m/z 378.0 [M(^{79}Br)+H]$^+$, 380.0 [M(^{81}Br)+H]$^+$; HRMS (ESI) calcd for $C_{18}H_{17}BrFNNaO_2$ 400.0319, found 400.0334.

tert-Butyl 1-[(4-methoxyphenyl)methyl]-2-oxo-spiro[indoline-3,4'-piperidine]-1'-carboxylate (44a)[348,349]
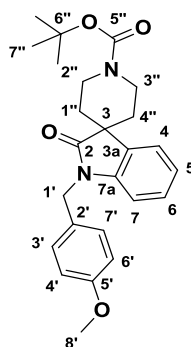
A flame dried three neck flask was loaded with tricyclohexylphosphine tetrafluoroborate (0.500 g, 1.36 mmol), palladium(II) acetate (0.305 g, 1.36 mmol) and sodium *tert*-butoxide (1.95 g, 20.38 mmol). The flask was purged with nitrogen/vacuum cycles (3 times) before a solution of *tert*-butyl 4-[(2-bromophenyl)-[(4-methoxyphenyl)methyl]carbamoyl]piperidine-1-carboxylate (**43a**) (6.84 g, 13.59 mmol) in anhydrous 1,4-dioxane (68 mL) was added. The resulting solution was purged with nitrogen/vacuum cycles (3 times) before heating to 80 °C. After 16 hours, the reaction mixture was cooled to room temperature, diluted with ethyl acetate (150 mL) and washed successively with a saturated solution of sodium hydrogen carbonate (2 x 100 mL) and brine (100 mL). The organic layer was dried over MgSO₄ and concentrated under reduced pressure. The crude oil was purified by flash column chromatography (Biotage SNAP 50 g, petroleum ether: EtOAc, 95: 5 to 75: 25) to give *tert*-butyl 1-[(4-methoxyphenyl)methyl]-2-oxo-spiro[indoline-3,4'-piperidine]-1'-carboxylate (**44a**) as a yellow solid (2.93 g, 51% yield): m.p. 143 − 145 °C; ^{1}H NMR (500 MHz, Chloroform-*d*) δ$_H$ 7.29 (d, *J* = 7.6 Hz, 1H, H-4), 7.21 (d, *J* = 8.6 Hz, 2H, H-3' and H-7'), 7.18 (app. dt, *J* = 7.6, 1.1 Hz, 1H, H-6), 7.03 (app. dt, *J* = 7.6, 1.1 Hz, 1H, H-5), 6.85 (d, *J* = 8.6 Hz, 2H, H-4' and H-6'), 6.77 (d, *J* = 7.6 Hz, 1H, H-

7), 4.85 (s, 2H, H-1'), 3.96 – 3.86 (m, 2H, H-2'' and H-3''), 3.86 – 3.79 (m, 2H, H-2'' and H-3''), 3.76 (s, 3H, H-8'), 1.94 – 1.86 (m, 2H, H-1'' and H-4''), 1.85 – 1.76 (m, 2H, H-1'' and H-4''), 1.52 (s, 9H, H-7''); ^{13}C NMR (126 MHz, Chloroform-d) δ_C 179.5 (C-2), 159.0 (C-5'), 155.0 (C-5''), 141.9 (C-7a), 133.6 (C-3a), 128.5 (C-3' and C-7'), 128.0 (C-2'), 127.9 (C-6), 123.1 (C-4), 122.4 (C-5), 114.2 (C-4' and C-6'), 109.1 (C-7), 79.6 (C-6''), 55.2 (C-8'), 45.0 (C-3), 42.9 (C-1'), 39.2 (C-2'' and C-3'', weak), 32.7 (C-2'' and C-3''), 28.5 (C-7''); LCMS (MDAP): Rt = 22.5 min (Method 5); m/z 323.0 [MH-Boc]$^+$, 445.1 [M+Na]$^+$; HRMS (ESI) calcd for $C_{25}H_{30}N_2NaO_4$ 445.2098, found 445.2103.

1-[(4-Methoxyphenyl)methyl]spiro[indoline-3,3'-tetrahydrofuran]-2-one (44b)
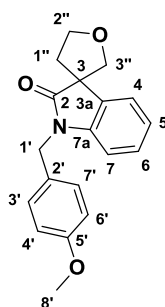
A flame dried three neck flask was loaded with *N*-(2-bromophenyl)-*N*-[(4-methoxyphenyl)methyl]tetrahydrofuran-3-carboxamide **(43b)** (1.02 g, 2.61 mmol), tricyclohexylphosphine tetrafluoroborate (0.096 g, 0.26 mmol) , palladium(II) acetate (0.059 g, 0.26 mmol) and sodium *tert*-butoxide (0.376 g, 3.92 mmol). The flask was purged with nitrogen/vacuum cycles before adding anhydrous 1,4-dioxane (20 mL) and the solution was purged with vacuum/nitrogen cycles before heating to 90 °C for 16 hours. After this time, the solution was cooled to room temperature, diluted with ethyl acetate (50 mL) and washed successively with saturated sodium bicarbonate (50 mL) and brine (50 mL). The organic layer was dried over MgSO$_4$ and concentrated under reduced pressure. The crude oil was purified by flash column chromatography (Biotage SNAP 40 g, petroleum ether: EtOAc, 90: 10 to 65: 35) to give 1-[(4-methoxyphenyl)methyl]spiro[indoline-3,3'-tetrahydrofuran]-2-one **(44b)** as a colourless oil (0.650 g, 80% yield): ^{1}H NMR (500 MHz, Methanol-d_4) δ_H 7.33 (dd, J = 7.5, 1.1 Hz, 1H, H-4), 7.23 (d, J = 8.1 Hz, 2H, H-3' and H-7'), 7.20 (app. dt, J = 7.5, 1.1 Hz, 1H, H-6), 7.07 (app. dt, J = 7.5, 1.1 Hz, 1H, H-5), 6.89 (d, J = 7.5 Hz, 1H, H-7), 6.87 (d, J = 8.1 Hz, 2H, H-4' and H-6'), 4.90 (d, J = 15.6 Hz, 1H, H-1'), 4.86 (d, J = 15.6 Hz, 1H, H-1'), 4.30 – 4.15 (m, 2H, H-2''), 4.02 (d, J = 8.5 Hz, 1H, H-3''), 3.91 (d, J = 8.5 Hz, 1H, H-3''), 3.75 (s, 3H, H-8'), 2.51 – 2.45 (m, 1H, H-1''), 2.23 – 2.17 (m, 1H, H-1''); ^{13}C NMR (126 MHz, Chloroform-d) δ_C 178.3 (C-2), 159.1 (C-5'), 142.1 (C-7a), 128.7 (C-3' and C-7'), 127.9 (C-6), 123.0 (C-4 or C-5), 122.7 (C-4 or C-5), 114.2 (C-4' and C-6'), 109.0 (C-7), 69.1 (C-3''), 55.2 (C-8'), 54.3 (C-2''), 43.4 (C-1'), 38.8 (C-1''); LCMS (MDAP):

Rt = 19.44 min (Method 4); m/z 310.0 [M+H]$^+$; HRMS (ESI) cacld for $C_{19}H_{19}NNaO_3$ 332.1257, found 332.1260.

Note: Unable to visualise all carbon signals by NMR.

1-[(4-Methoxyphenyl)methyl]spiro[indoline-3,4'-tetrahydropyran]-2-one (44c)
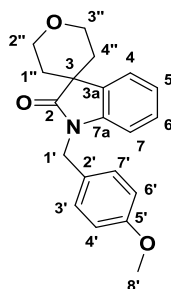
A pressure vessel was loaded with palladium (II) acetate (27.8 mg, 0.12 mmol), sodium *tert*-butoxide (178.3 mg, 1.86 mmol), tricyclohexylphosphine tetrafluoroborate (45.5 mg, 0.12 mmol) and *N*-(2-bromophenyl)-*N*-[(4-methoxyphenyl)methyl]tetrahydropyran-4-carboxamide (**43c**) (500 mg, 1.24 mmol). The vessel was sealed and evacuated with a vacuum/nitrogen cycle for 10 minutes. Anhydrous 1,4-dioxane (10 mL) was added and the vessel was further evacuated with a vacuum/nitrogen cycle before heating the solution to 90 °C for 16 hours. After this time, the reaction mixture was diluted with water (10 mL) and extracted with ethyl acetate (2 x 15 mL). The combined organic layers were washed with brine (20 mL), dried over MgSO$_4$ and concentrated under reduced pressure. The crude material was purified by flash column chromatography (Biotage SNAP 10 g, petroleum ether: EtOAc, 90: 10 to 70: 30) to give 1-[(4-methoxyphenyl)methyl]spiro[indoline-3,4'-tetrahydropyran]-2-one **(44c)** as a colourless foam (260 mg, 65% yield): ^{1}H NMR (500 MHz, Chloroform-*d*) δ$_H$ 7.38 (dd, *J* = 7.8, 1.2 Hz, 1H, H-4), 7.21 (d, *J* = 8.6 Hz, 2H, H-3' and H-7'), 7.18 (app. dt, *J* = 7.8, 1.2 Hz, 1H, H-6), 7.05 (app. dt, *J* = 7.8, 1.2 Hz, 1H, H-5), 6.85 (d, *J* = 8.6 Hz, 2H, H-4' and H-6'), 6.78 (d, *J* = 7.8 Hz, 1H, H-7), 4.85 (s, 2H, H-1'), 4.31 (dt, *J* = 12.0, 6.1 Hz, 2H, H-2'' and H-3''), 3.96 (dt, *J* = 12.0, 4.8 Hz, 2H, H-2'' and H-3''), 3.78 (s, 3H, H-8'), 1.91 (app. dd, *J* = 6.1, 4.8 Hz, 4H, H-1'' and H-4''); ^{13}C NMR (126 MHz, Chloroform-*d*) δ$_C$ 179.7 (C-2), 159.0 (C-5'), 141.8 (C-7a), 134.1 (C-3a), 128.5 (C-2'), 128.1 (C-3' and C-7'), 127.9 (C-6), 123.1 (C-4 or C-5), 122.4 (C-4 or C-5), 114.2 (C-4' and C-6'), 109.1 (C-7), 63.0 (C-2'' and C-3''), 55.2 (C-8'), 44.2 (C-1'), 42.9 (C-3), 33.1 (C-1'' and C-4''); LCMS (MDAP): Rt = 17.1 min (Method 5); m/z 324.1 [M+H]$^+$; HRMS (ESI) calcd for $C_{20}H_{21}NO_3Na$ 346.1414, found 346.1429.

***tert*-Butyl   6'-fluoro-1'-[(4-methoxyphenyl)methyl]-2'-oxo-spiro[azetidine-3,3'-indoline]-1-carboxylate (44d)**[179]
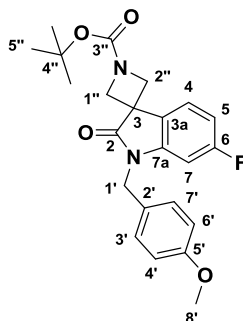
Palladium(II) acetate (0.083 g, 0.37 mmol), tricyclohexylphosphine tetrafluoroborate (0.136 g, 0.37 mmol) and sodium *tert*-butoxide (0.534 g, 5.56 mmol) were loaded in a microwave vial. The vial was sealed and nitrogen/vacuum flushed for 5 minutes before a solution of *tert*-butyl 3-[(2-bromo-5-fluoro-phenyl)-[(4-methoxyphenyl)methyl]carbamoyl]azetidine-1-carboxylate   (**43d**) (1.83 g, 3.71 mmol) in anhydrous 1,4-dioxane (19 mL) was added. The solution was nitrogen/vacuum flushed for 5 minutes and heated to 130 °C under microwave irradiation for 4 minutes. After this time, the reaction was diluted with ethyl acetate (15 mL) and washed successively with a saturated solution of sodium bicarbonate (10 mL) and brine (10 mL). The organic layer was dried over $MgSO_4$ and concentrated under reduced pressure to a pale yellow oil. The crude oil was purified by flash column chromatography (Biotage SNAP 25 g, petroleum ether: EtOAc, 90: 10 to 60: 40) to give *tert*-butyl 6'-fluoro-1'-[(4-methoxyphenyl)methyl]-2'-oxo-spiro[azetidine-3,3'-indoline]-1-carboxylate **(44d)** as a pale yellow oil (1.33 g, 87% yield): ^{1}H NMR (500 MHz, Chloroform-*d*) δ_H 7.47 (dd, *J* = 8.2, 5.2 Hz, 1H, H-4), 7.22 (d, *J* = 8.1 Hz, 2H, H-3' and H-7'), 6.86 (d, *J* = 8.1 Hz, 2H, H-4' and H-6'), 6.78 (ddd, *J* = 9.3, 8.2, 2.3 Hz, 1H, H-5), 6.50 (dd, *J* = 8.9, 2.3 Hz, 1H, H-7), 4.81 (s, 2H, H-1'), 4.42 (d, *J* = 8.2 Hz, 2H, H-1'' and H-2''), 4.06 (d, *J* = 8.2 Hz, 2H, H-1'' and H-2''), 3.79 (s, 3H, H-8'), 1.50 (s, 9H, H-5''); ^{13}C NMR (126 MHz, Chloroform-*d*) δ_C 177.2 (C-2), 163.3 (d, J_{CF} = 252.0 Hz, C-6), 159.3 (C-5'), 156.0 (C-3''), 144.2 (d, J_{CF} = 11.8 Hz, C-7a), 128.8 (C-3' and C-7'), 127.1 (C-2'), 125.8 (d, J_{CF} = 3.3 Hz, C-3a), 123.9 (d, J_{CF} = 10.4 Hz, C-4), 114.3 (C-4' and C-6'), 109.1 (d, *J* = 23.2 Hz, C-5), 98.1 (d, J_{CF} = 28.4 Hz, C-7), 80.3 (C-4''), 55.3 (C-8'), 43.7 (C-1'), 42.0 (C-1'' and C-2''), 28.4 (C-5''); LCMS (MDAP): Rt = 21.1 min (Method 5); m/z 313.0 [M+H-Boc]$^+$, 435.2 [M+Na]$^+$; HRMS (ESI) calcd for $C_{23}H_{25}FN_2NaO_4$ 435.1691, found 435.1681.

Note: Unable to visualise all carbon signals by NMR.

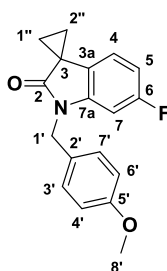**6'-Fluoro-1'-[(4-methoxyphenyl)methyl]spiro[cyclopropane-1,3'-indoline]-2'-one (44e)**

A pressure vessel was loaded with palladium (II) acetate (0.079 g, 0.35 mmol), sodium *tert*-butoxide (0.510 g, 5.31 mmol), tricyclohexylphosphine tetrafluoroborate (0.130 g, 0.35 mmol) and *N*-(2-bromo-5-fluoro-phenyl)-*N*-[(4-methoxyphenyl)methyl]cyclopropanecarboxamide (**43e**) (1.34 g, 3.54 mmol). The vessel was sealed and evacuated with a vacuum/nitrogen cycle for 10 minutes. Anhydrous 1,4-dioxane (18 mL) was added and the vessel was further evacuated with a vacuum/nitrogen cycle before heating the solution to 90 °C for 16 hours. After this time, the reaction mixture was diluted with water (10 mL) and extracted with ethyl acetate (2 x 15 mL). The combined organic layers were washed with brine (20 mL), dried over MgSO$_4$ and concentrated under reduced pressure. The crude material was purified by flash column chromatography (Biotage SNAP 10 g, petroleum ether: EtOAc, 90: 10 to 70: 30) to give 6'-fluoro-1'-[(4-methoxyphenyl)methyl] spiro[cyclopropane-1,3'-indoline]-2'-one **(44e)** as a colourless oil (0.732 g, 69% yield): ^{1}H NMR (500 MHz, Chloroform-*d*) δ$_H$ 7.26 (d, *J* = 8.7 Hz, 2H, H-3' and H-7'), 6.87 (d, *J* = 8.7 Hz, 2H, H-4' and H-6'), 6.74 (dd, *J* = 8.2, 5.2 Hz, 1H, H-4), 6.66 (app. dt, *J* = 8.2, 2.3 Hz, 1H, H-5), 6.57 (dd, *J* = 9.1, 2.3 Hz, 1H, H-7), 4.90 (s, 2H, H-1'), 3.79 (s, 3H, H-8'), 1.81 – 1.77 (m, 2H, H-1'' and H-2''), 1.54 – 1.51 (m, 2H, H-1'' and H-2''); ^{13}C NMR (126 MHz, Chloroform-*d*) δ$_C$ 177.4 (C-2), 162.2 (d, *J*$_{CF}$ = 244.5 Hz, C-6), 159.2 (C-5'), 143.9 (d, *J*$_{CF}$ = 11.8 Hz, C-7a), 128.7 (C-3' and C-7'), 127.8 (C-2'), 126.0 (d, *J*$_{CF}$ = 2.6 Hz, C-3a), 118.9 (d, *J*$_{CF}$ = 9.5 Hz, C-4), 114.2 (C-4' and C-6'), 108.0 (d, *J*$_{CF}$ = 25.9 Hz, C-5), 97.8 (d, *J*$_{CF}$ = 29.0 Hz, C-7), 55.2 (C-8'), 43.8 (C-1'), 26.6 (C-3), 19.2 (C-1'' and C-2''); LCMS (LCQ): Rt = 2.8 min (Method 1); m/z 298.1 [M+H]$^+$; HRMS (ESI) calcd for C$_{18}$H$_{16}$FNO$_2$Na 320.1057, found 320.1046.

Spiro[indoline-3,4'-piperidine]-2-one (45a)[179,348]
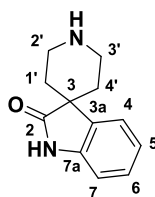
Anisole (5.04 mL, 46.39 mmol) was added to a solution of *tert*-butyl 1-[(4-methoxyphenyl)methyl]-2-oxo-spiro[indoline-3,4'-piperidine]-1'-carboxylate (**44a**) (2.80 g, 6.63 mmol) in trifluoroacetic acid (25.37 mL, 331.35 mmol) and the resulting solution was heated to 150 °C for 2 hours under microwave irradiation. After this time, the solution was concentrated under reduced pressure and the brown mixture was loaded onto a SCX-2 cartridge, washing with methanol (3 x 30 mL) and eluting the product with a 2 N solution of ammonia in methanol (100 mL). The elute was concentrated under reduced pressure to give spiro[indoline-3,4'-piperidine]-2-one (**45a**) as a colourless solid (1.34 g, 100% yield): m.p. 182 − 186 °C [Lit.[350] 184 − 186 °C]; ^{1}H NMR (500 MHz, Chloroform-*d*) δ_H 8.00 (br s, 1H, NH), 7.42 (d, *J* = 7.5 Hz, 1H, H-4), 7.23 (app. dt, *J* = 7.5, 1.1 Hz, 1H, H-6), 7.06 (app. dt, *J* = 7.5, 1.1 Hz, 1H, H-5), 6.90 (d, *J* = 7.5 Hz, 1H, H-7), 3.43 − 3.35 (m, 2H, H-2' and H-3'), 3.14 − 3.05 (m, 2H, H-2' and H-3'), 1.95 − 1.85 (m, 2H, H-1' and H-4'), 1.82 − 1.71 (m, 2H, H-1' and H-4'); ^{13}C NMR (126 MHz, Chloroform-*d*) δ_C 182.0 (C-2), 139.8 (C-7a), 135.1 (C-3a), 127.7 (C-6), 123.8 (C-4), 122.2 (C-5), 109.5 (C-7), 46.0 (C-3), 41.3 (C-2' and C-3'), 33.4 (C-1' and C-4'); LCMS (MDAP): Rt = 5.0 min (Method 4); m/z 203.0 [M+H]$^+$; HRMS (ESI) calcd for $C_{12}H_{15}N_2O$ 203.1179; found 203.1178.

Spiro[indoline-3,3'-tetrahydrofuran]-2-one (45b)[351]
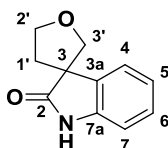
Anisole (1.45 mL, 13.33 mmol) was added to a solution of 1-[(4-methoxyphenyl)methyl]spiro[indoline-3,3'-tetrahydrofuran]-2-one (**44b**) (589 mg, 1.9 mmol) in trifluoroacetic acid (7.30 mL, 95.2 mmol) and the resulting solution was heated to 100 °C under microwave irradiation for 2 hours, followed by further irradiation at 150 °C for 4 hours. After this time, the volatiles were removed under reduced pressure. The residue was diluted with ethyl acetate (10 mL) and neutralised with a saturated solution of sodium bicarbonate (10 mL), then washed with brine (10 mL). The organic layer was dried over MgSO$_4$ and concentrated under reduced pressure. The crude oil was purified by flash column chromatography (Biotage

Flash SNAP 10 g, CH$_2$Cl$_2$: MeOH: NH$_3$, 99: 1: 0.1 to 93: 7: 0.7) to give spiro[indoline-3,3'-tetrahydrofuran]-2-one **(45b)** as a pale brown solid (284 mg, 79% yield): ^{1}H NMR (500 MHz, Chloroform-*d*) δ$_H$ 8.14 (br s, 1H), 7.30 (d, *J* = 7.7 Hz, 1H, H-4), 7.24 (app. dt, *J* = 7.7, 1.3 Hz, 1H, H-6), 7.08 (app. dt, *J* = 7.7, 1.3 Hz, 1H, H-5), 6.92 (d, *J* = 7.7 Hz, 1H, H-7), 4.29 – 4.18 (m, 2H, H-2'), 4.08 (d, *J* = 8.5 Hz, 1H, H-3'), 3.98 (d, *J* = 8.5 Hz, 1H, H-3'), 2.62 – 2.52 (m, 1H, H-1'), 2.24 – 2.15 (m, 1H, H-1'); ^{13}C NMR (126 MHz, Chloroform-*d*) δ$_C$ 180.5 (C-2), 140.0 (C-7a), 134.2 (C-3a), 128.1 (C-6), 123.1 (C-4 or C-5), 123.0 (C-4 or C-5), 109.7 (C-7), 69.0 (C-3'), 54.6 (C-2'), 38.7 (C-1'); LCMS (MDAP): Rt = 8.4 min, 80% purity by UV (254 nm) (Method 5); m/z 189.9 [M+H]$^+$.

Note: Unable to visualise all carbon signals by NMR; Unable to obtain any ionisation under HRMS.

Spiro[indoline-3,4'-tetrahydropyran]-2-one (45c)[292,352,353]
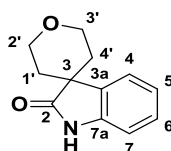
Anisole (0.61 mL, 5.63 mmol) was added to a solution of 1-[(4-methoxyphenyl)methyl]spiro[indoline-3,4'-tetrahydropyran]-2-one **(44c)** (260 mg, 0.80 mmol) in trifluoroacetic acid (4.7 mL, 61.76 mmol) and the resulting solution was heated to 150 °C for 2 hours under microwave irradiations. After this time, the volatiles were removed under reduced pressure and the residue was purified by flash column chromatography (Redisep 25 g, CH$_2$Cl$_2$: MeOH: NH$_3$, 100: 0: 0 to 95: 5: 0.5) to give spiro[indoline-3,4'-tetrahydropyran]-2-one **(45c)** as a colourless solid (155 mg, 95% yield): m.p. 232 – 236 °C [lit.[292] 238 – 240 °C]; ^{1}H NMR (500 MHz, Chloroform-*d*) δ$_H$ 7.64 (br s, 1H, NH), 7.37 (d, *J* = 7.6 Hz, 1H, H-4), 7.26 – 7.22 (app. dt, *J* = 7.6, 1.1 Hz, 1H, H-6), 7.09 – 7.05 (app. dt, *J* = 7.6, 1.1 Hz, 1H, H-5), 6.90 (d, *J* = 7.6 Hz, 1H, H-7), 4.30 – 4.22 (m, 2H, H-2' and H-3'), 3.98 – 3.91 (m, 2H, H-2' and H-3'), 1.93 – 1.88 (m, 4H, H-1' and H-4'); ^{13}C NMR (126 MHz, Chloroform-*d*) δ$_C$ 181.3 (C-2), 139.6 (C-7a), 134.6 (C-3a), 127.9 (C-6), 123.4 (C-4 or C-5), 122.4 (C-4 or C-5), 109.5 (C-7), 62.5 (C-2' and C-3'), 44.5 (C-3), 32.9 (C-1' and C-4'); LCMS (MDAP): Rt = 9.1 min (Method 5); m/z 204.1 [M+H]$^+$; HRMS (ESI) calcd for C$_{12}$H$_{13}$NO$_2$Na 226.0838, found 226.0843.

6'-Fluorospiro[azetidine-3,3'-indoline]-2'-one (45d)
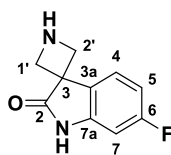
Trifluoromethanesulfonic acid (0.85 mL, 9.63 mmol) was added to a solution of *tert*-butyl 6'-fluoro-1'-[(4-methoxyphenyl)methyl]-2'-oxo-spiro[azetidine-3,3'-indoline]-1-carboxylate (**44d**) (1.32 g, 3.21 mmol) in trifluoroacetic acid (12.3 mL, 160.54 mmol) and the resulting solution was stirred at room temperature for 16 hours. After this time, the solution was concentrated under reduced pressure and the black residue was purified by SCX-2 ion exchange column, washing with methanol (3 x 10 mL) and eluting the product with a solution of ammonia in methanol (15 mL). The elute was concentrated under reduced pressure to give 6'-fluorospiro[azetidine-3,3'-indoline]-2'-one (**45d**) as a colourless solid (447 mg, 72% yield): m.p. 238 – 242 °C; ^{1}H NMR (500 MHz, DMSO-d_6) δ_H 10.41 (br s, 1H, NH), 7.65 (dd, J = 8.2, 5.6 Hz, 1H, H-4), 6.82 (ddd, J = 10.3, 8.2, 2.5 Hz, 1H, H-5), 6.61 (dd, J = 9.4, 2.5 Hz, 1H, H-7), 3.89 (d, J = 7.3 Hz, 2H, H-1' and H-2'), 3.46 (d, J = 7.3 Hz, 2H, H-1' and H-2'); ^{13}C NMR (126 MHz, DMSO-d_6) δ_C 179.4 (C-2), 162.6 (d, J_{CF} = 242.9 Hz, C-6), 129.2 (d, J_{CF} = 3.0 Hz, C-3a), 124.6 (d, J_{CF} = 10.5 Hz, C-4), 108.3 (d, J_{CF} = 24.3 Hz, C-5), 97.9 (d, J_{CF} = 28.2 Hz, C-7), 54.8 (C-1' and C-2'), 48.0 (C-3); LCMS (MDAP) Rt = 2.8 min (Method 5); m/z 193.2 [M+H]$^+$; HRMS (ESI) calcd for $C_{10}H_{10}FN_2O$ 193.0772, found 193.0766.

Note: Unable to visualise all carbon signals by NMR.

6'-Fluorospiro[cyclopropane-1,3'-indoline]-2'-one (45e)
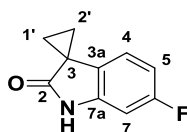
Anisole (1.84 mL, 16.95 mmol) was added to a solution of 6'-fluoro-1'-[(4-methoxyphenyl)methyl]spiro[cyclopropane-1,3'-indoline]-2'-one (**44e**) (720 mg, 2.42 mmol) in trifluoroacetic acid (9.27 mL, 121.08 mmol) and the resulting solution was heated to 150 °C for 2 hours under microwave irradiation. After this time, the volatiles were removed under reduced pressure and the residue was purified by flash column chromatography (Redisep 25 g, CH$_2$Cl$_2$: MeOH: NH$_3$, 100: 0: 0 to 95: 5: 0.5) to give 6'-fluorospiro[cyclopropane-1,3'-indoline]-2'-one (**45e**) as a white foam (375 mg, 87% yield): ^{1}H NMR (500 MHz, Chloroform-*d*) δ_H 9.37 (br s, 1H),

6.79 – 6.66 (m, 3H, H-4, H-5 and H-7), 1.76 (app. q, J = 4.2 Hz, 2H, H-1' and H-2'), 1.53 (app. q, J = 4.2 Hz, 2H, H-1' and H-2'); ^{13}C NMR (126 MHz, Chloroform-d) δ_C 180.1 (C-2), 162.1 (d, J_{CF} = 242.3 Hz, C-6), 141.8 (d, J_{CF} = 12.2 Hz, C-7a), 126.5 (d, J_{CF} = 2.5 Hz, C-3a), 119.2 (d, J_{CF} = 10.5 Hz, C-4), 108.3 (d, J_{CF} = 22.9 Hz, C-5), 98.6 (d, J_{CF} = 27.9 Hz, C-7), 27.2 (C-3), 19.3 (C-1' and C-2'); LCMS (LCQ): Rt = 1.2 min (Method 1); m/z 178.4 [M+H]$^+$; HRMS (ESI) calcd for $C_{10}H_9FNO$ 178.0663, found 178.0662.

tert-Butyl 2-oxospiro[indoline-3,4'-piperidine]-1'-carboxylate (46)[179,348,350]
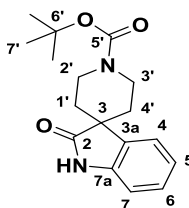
Di-_tert_-butyl dicarbonate (1.59 g, 7.28 mmol) was added to an ice cold suspension of spiro[indoline-3,4'-piperidine]-2-one (**45a**) (1.34 g, 6.62 mmol) and triethylamine (1.01 mL, 7.28 mmol) in dichloromethane (33 mL). Upon addition, a solution was obtained and was left to warm up to room temperature and stirred at this temperature for 16 hours. After this time, the solution was washed successively with a saturated solution of sodium bicarbonate (50 mL), saturated citric acid (50 mL) and brine (50 mL). The organic layer was dried over $MgSO_4$ and concentrated under reduced pressure to give _tert_-butyl 2-oxospiro[indoline-3,4'-piperidine]-1'-carboxylate (**46**) as a colourless solid (1.56 g, 78% yield): m.p. 138 – 141 °C [lit.[350] 138 – 140 °C]; ^{1}H NMR (500 MHz, Chloroform-d) δ_H 7.85 (br s, 1H, NH), 7.29 (d, J = 7.8 Hz, 1H, H-4), 7.24 (app. dt, J = 7.8, 1.1 Hz, 1H, H-6), 7.06 (app. dt, J = 7.8, 1.1 Hz, 1H, H-5), 6.91 (d, J = 7.8 Hz, 1H, H-7), 3.92 – 3.83 (m, 2H, H-2' and H-3'), 3.83 – 3.75 (m, 2H, H-2' and H-3'), 1.94 – 1.86 (m, 2H, H-1' and H-4'), 1.83 – 1.75 (m, 2H, H-1' and H-4'), 1.52 (s, 9H, H-7'); ^{13}C NMR (126 MHz, Chloroform-d) δ_C 181.4 (C-2), 155.0 (C-5'), 139.7 (C-7a), 134.3 (C-3a), 128.0 (C-6), 123.4 (C-4), 122.4 (C-5), 109.6 (C-7), 79.7 (C-6'), 45.4 (C-3), 32.6 (C-2' and C-3'), 28.5 (C-7'), 27.4 (C-1' and C-4'); LCMS (MDAP): Rt = 19.1 min (Method 4); m/z 325.0 [M+Na]$^+$; HRMS (ESI) calcd for $C_{17}H_{22}N_2NaO_3$ 325.1523, found 325.1525.

1-Acetyl-6'-fluoro-spiro[azetidine-3,3'-indoline]-2'-one (47)
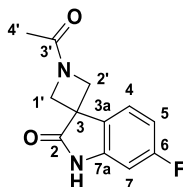
Acetyl chloride (0.18 mL, 2.57 mmol) was added to an ice cold solution of 6'-fluorospiro[azetidine-3,3'-indoline]-2'-one (**45d**) (412 mg, 2.14 mmol) and triethylamine (0.45 mL, 3.22 mmol) in dichloromethane (10 mL) and the resulting solution was left to warm up to room temperature and stirred at this temperature for 16 hours. After this time, the reaction mixture was washed with saturated sodium bicarbonate (2 x 10 mL), then brine (10 mL). The organic layer was dried over $MgSO_4$ and concentrated under reduced pressure. The crude material was purified by flash column chromatography (Isco Redisep 25 g, CH_2Cl_2: MeOH: NH_3, 100: 0: 0 to 95: 5: 0.5) to give 1-acetyl-6'-fluoro-spiro[azetidine-3,3'-indoline]-2'-one **(47)** as a colourless oil (316 mg, 63% yield): ^{1}H NMR (600 MHz, Chloroform-d) δ_H 8.86 (s, 1H, NH), 7.43 (dd, J = 8.3, 5.1 Hz, 1H, H-4), 6.81 (ddd, J = 9.3, 8.3, 2.3 Hz, 1H, H-5), 6.69 (dd, J = 8.5, 2.3 Hz, 1H, H-7), 4.54 (d, J = 7.7 Hz, 1H, H-1' or H-2'), 4.42 (d, J = 9.4 Hz, 1H, H-1' or H-2'), 4.25 (d, J = 7.7 Hz, 1H, H-1' or H-2'), 4.16 (d, J = 9.4 Hz, 1H, H-1' or H-2'), 1.98 (s, 3H, H-4'); ^{13}C NMR (126 MHz, Chloroform-d) δ_C 179.0 (C-2), 170.9 (C-3'), 163.2 (d, J_{CF} = 248.6 Hz, C-6), 142.3 (d, J_{CF} = 11.8 Hz, C-7a), 125.5 (d, J_{CF} = 3.2 Hz, C-3a), 124.3 (d, J_{CF} = 10.4 Hz, C-4), 109.7 (d, J_{CF} = 22.4 Hz, C-5), 99.0 (d, J_{CF} = 27.2 Hz, C-7), 58.6 (C-1' or C-2'), 56.6 (C-1' or C-2'), 41.8 (C-3), 18.8 (C-4'); LCMS (MDAP): Rt = 6.8 min (Method 5); m/z 235.1 [M+H]$^+$.

Note: Unable to obtain any ionisation under HRMS.

1-Acetyl-1'-[[5-chloro-1-(3-methylsulfonylpropyl)benzimidazol-2-yl]methyl]spiro[azetidine-3,3'-indoline]-2'-one (49a)[179]
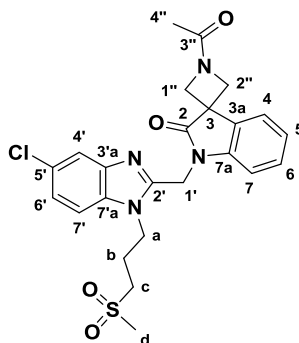
Sodium hydride (60% dispersion in oil) (58.2 mg, 1.46 mmol) was added to an ice cold solution of 1-acetylspiro[azetidine-3,3'-indoline]-2'-one (**39**) (314.7 mg, 1.46 mmol) in anhydrous *N,N*-dimethylformamide (10 mL). The cold bath was removed and the cloudy solution was stirred at room temperature for 1 hour. To this solution was added 5-chloro-2-(chloromethyl)-1-(3-methylsulfonylpropyl)benzimidazole (425.0 mg, 1.32 mmol) and the resulting reaction mixture was left stirring at room temperature for 48 hours. After this time, the reaction was quenched with water (15 mL) and extracted with ethyl acetate (2 x 15 mL). The combined organic layers were washed with brine (20 mL), dried over $MgSO_4$ and concentrated under reduced pressure. The crude material was purified by flash column chromatography (Biotage SNAP 25 g, CH_2Cl_2: MeOH: NH_3, 100: 0: 0 to 93: 7: 0.7) to give 1-acetyl-1'-[[5-chloro-1-(3-methylsulfonylpropyl) benzimidazol-2-yl]methyl]spiro[azetidine-3,3'-indoline]-2'-one (**49a**) as a colourless solid (518 mg, 78% yield): ^{1}H NMR (500 MHz, Chloroform-*d*) δ_H 7.77 (d, *J* = 1.9 Hz, 1H, H-4'), 7.55 – 7.51 (m, 2H, H-4 and H-7), 7.40 – 7.33 (m, 2H, H-6 and H-6'), 7.30 (d, *J* = 8.6 Hz, 1H, H-7'), 7.19 (app. dt, *J* = 7.6, 1.9 Hz, 1H, H-5), 5.25 (d, *J* = 20.2 Hz, 1H, H-1'), 5.20 (d, *J* = 20.2 Hz, 1H, H-1'), 4.59 (d, J = 8.2 Hz, 1H, H-1'' or H-2''), 4.59 – 4.45 (m, 2H, H-a), 4.42 (d, *J* = 9.4 Hz, 1H, H-1'' or H-2''), 4.31 (d, *J* = 8.2 Hz, 1H, H-1'' or H-2''), 4.20 (d, *J* = 9.4 Hz, 1H, H-1'' or H-2''), 3.22 – 3.09 (m, 2H, H-c), 2.98 (s, 3H, H-d), 2.36 – 2.23 (m, 2H, H-b), 2.00 (s, 3H, H-4''); ^{13}C NMR (126 MHz, Chloroform-*d*) δ_C 177.0 (C-2), 170.8 (C-3''), 148.8 (C-2'), 143.1 (C-3'a), 142.1 (C-7a), 133.6 (C-7'a), 129.8 (C-6), 129.3 (C-3a), 128.5 (C-5'), 124.3 (C-4 or C-5), 124.2 (C-4 or C-5), 122.8 (C-6'), 120.0 (C-4'), 110.8 (C-7 or C-7'), 110.6 (C-7 or C-7'), 58.7 (C-1'' or C-2''), 56.7 (C-1'' or C-2''), 51.2 (C-c), 42.4 (C-3), 41.9 (C-a), 41.4 (C-d), 37.8 (C-1'), 22.6 (C-b), 18.8 (C-4''); LCMS (MDAP): Rt = 11.2 min (Method 5); m/z 501.1 [M+H]$^+$; HRMS (ESI) calcd for $C_{24}H_{26}ClN_4O_4S$ 501.1358, found 501.1371.

1-Acetyl-1'-[[5-(aminomethyl)-1-(4,4,4-trifluorobutyl)benzimidazol-2-yl]methyl]spiro[azetidine-3,3'-indoline]-2'-one (49b)
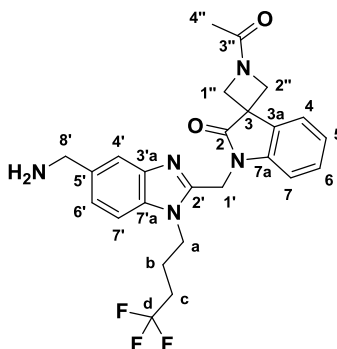
Sodium hydride (60% dispersion in oil) (19.8 mg, 0.50 mmol) was added to an ice cold solution of 1-acetylspiro[azetidine-3,3'-indoline]-2'-one (**39**) (107.3 mg, 0.50 mmol) in anhydrous *N,N*-dimethylformamide (5 mL). The cold bath was removed and the reaction mixture was left stirring at room temperature for 1 hour. *tert*-Butyl *N*-[[2-(chloromethyl)-1-(4,4,4-trifluorobutyl)benzimidazol-5-yl]methyl]carbamate (183.0 mg, 0.45 mmol) was added and the mixture was left stirring at room temperature for 16 hours. After this time, the reaction was quenched with water (10 mL) and the product was extracted with acetate (2 x 10 mL). The combined organic layers were dried over $MgSO_4$ and concentrated under reduced pressure. The crude oil was purified by reverse phase HPLC to give *tert*-butyl *N*-[[2-[(1-acetyl-2'-oxo-spiro[azetidine-3,3'-indoline]-1'-yl)methyl]-1-(4,4,4-trifluorobutyl)benzimidazol -5-yl]methyl]carbamate: LCMS (MDAP): Rt = 17.1 min (Method 4); m/z 586.2 [M+H]$^+$; HRMS (ESI) calcd for $C_{30}H_{35}F_3N_5O_4$ 586.2636, found 586.2660.

The intermediate was suspended in diethyl ether (5 mL) and treated with 1 M HCl in diethyl ether (1 mL). The resulting cloudy suspension was left stirring for 16 hours at room temperature. After this time, the solution was concentrated under reduced pressure, the residue was dissolved in methanol (2 mL) and loaded onto a SCX-2 cartridge, rinsing with methanol (2 x 6 mL) and eluting the product with a 2 M solution of ammonia in methanol (2 x 6 mL). The elute was concentrated under reduced pressure to give 1-acetyl-1'-[[5-(aminomethyl)-1-(4,4,4-trifluorobutyl)benzimidazol-2-yl]methyl]spiro[azetidine-3,3'-indoline]-2'-one **(49b)** as a colourless oil (10.8 mg, 5% yield): ^{1}H NMR (500 MHz, Methanol-*d₄*) δ$_H$ 7.68 (d, *J* = 7.4 Hz, 1H, H-7'), 7.57 (s, 1H, H-4'), 7.54 (d, *J* = 7.4 Hz, 1H, H-6'), 7.35 (d, *J* = 7.8 Hz, 1H, H-4), 7.28 (app. t, *J* = 7.8 Hz, 1H, H-6), 7.19 (app. t, *J* = 7.8 Hz, 1H, H-5), 7.03 (d, *J* = 7.8 Hz, 1H, H-7), 5.29 (s, 2H, H-1'), 4.60 (d, *J* = 8.7 Hz,1H ,H-1'' or H-2''), 4.51 − 4.43 (m, 3H, H-1'' or H-2'' and H-a), 4.39 (d, *J* = 9.8 Hz, 1H, H-1'' or H-2''), 4.22 (d, *J* = 9.8 Hz, 1H, H-1'' or H-2''), 3.92 (s, 2H, H-8'), 2.41 − 2.26

(m, 2H, H-c), 2.15 – 2.04 (m, 2H, H-b), 2.00 (s, 3H, H-4''); LCMS (MDAP): Rt = 10.4 min (Method 4); m/z 486.0 [M+H]⁺.

Note: No carbon NMR obtained.

Compound intermediate to (**49c**): *tert*-**Butyl** *N*-**[[2-[(1-acetyl-2'-oxo-spiro[azetidine-3,3'-indoline]-1'-yl)methyl]-1-isopentyl-benzimidazol-5-yl]methyl]carbamate**
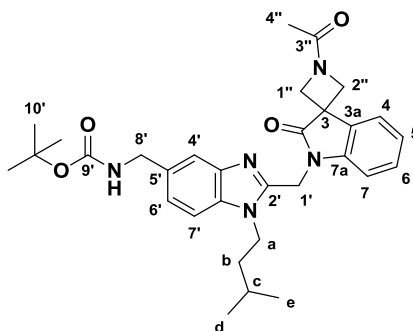
To an ice cold solution of 1-acetylspiro[azetidine-3,3'-indoline]-2'-one (**39**) (26 mg, 0.12 mmol) in anhydrous *N*,*N*-dimethylformamide (3 mL) was added sodium hydride (60% dispersion in oil) (4.8 mg, 0.12 mmol) and the suspension was stirred at 0 °C for 45 minutes before *tert*-butyl *N*-[[2-(chloromethyl)-1-isopentyl-benzimidazol-5-yl]methyl]carbamate (41.8 mg, 0.11 mmol) was added in one portion. The resulting mixture was left stirring at room temperature for 48 hours. After this time, the solution was quenched with water (10 mL) and extracted with dichloromethane (10 mL). The organic layer was dried over MgSO₄ and concentrated under reduced pressure. The crude residue was purified by flash column chromatography (Biotage SANP 10 g, CH₂Cl₂: MeOH: NH₃, 100: 0: 0 to 93: 7: 0.7) to give *tert*-butyl *N*-[[2-[(1-acetyl-2'-oxo-spiro[azetidine-3,3'-indoline]-1'-yl)methyl]-1-isopentyl-benzimidazol-5-yl]methyl]carbamate as a colourless oil (28 mg, 66% yield): ¹H NMR (500 MHz, Chloroform-d) δ_H 7.66 (s, 1H, H-4'), 7.52 – 7.44 (m, 2H, H-4 and H-7), 7.33 – 7.21 (m, 3H, H-6, H-6' and H-7), 7.15 (dt, *J* = 7.7, 1.1 Hz, 1H, H-5), 5.25 (d, *J* = 15.5 Hz, 1H, H-1'), 5.17 (d, *J* = 15.5 Hz, 1H, H-1'), 4.89 (s, 1H, NH), 4.58 (d, *J* = 8.0 Hz, 1H, H-1'' or H-2''), 4.44 (m, 3H, H-1'' or H-2'' and H-a), 4.32 – 4.23 (m, 3H, H-1'' or H-2'' and H-8'), 4.19 (d, *J* = 9.3 Hz, 1H, H-1'' or H-2''), 1.99 (s, 3H, H-4''), 1.71 (m, 1H, H-c), 1.60 – 1.52 (m, 2H, H-b), 1.47 (s, 9H, H-10'), 1.00 (d, *J* = 6.6 Hz, 6H, H-d and H-e); LCMS (MDAP): Rt = 13.2 min (Method 5); m/z 546.3 [M+H]⁺; HRMS (ESI) calcd for C₃₁H₄₀N₅O₄ 546.3075, found 546.3079.

Note: No carbon NMR obtained.

1-Acetyl-1'-[[5-(aminomethyl)-1-isopentyl-benzimidazol-2-yl]methyl]spiro[azetidine-3,3'-indoline]-2'-one (49c)

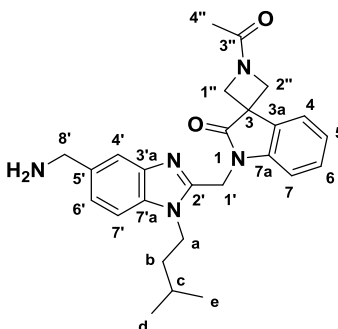Trifluoroacetic acid (1.09 mL, 14.28 mmol) was added to a solution of *tert*-butyl *N*-[[2-[(1-acetyl-2'-oxo-spiro[azetidine-3,3'-indoline]-1'-yl)methyl]-1-isopentyl-benzimidazol-5-yl]methyl] carbamate (26 mg, 0.05 mmol) in dichloromethane (3 mL) and the resulting solution was left stirring at room temperature for 16 hours. After this time, the reaction mixture was concentrated under reduced pressure, the residue was dissolved in methanol (6 mL) and loaded onto a SCX-2 cartridge, rinsing with methanol (2 x 6 mL) and eluting the product with a 2 M solution of ammonia in isopropyl alcohol (2 x 6 mL). The elute was concentrated under reduced pressure and purified by flash column chromatography (Biotage SNAP 10g, CH_2Cl_2: MeOH: NH_3, 98: 2: 0.2 to 90: 10: 1) to give 1-acetyl-1'-[[5-(aminomethyl)-1-isopentyl-benzimidazol-2-yl] methyl]spiro[azetidine-3,3'-indoline]-2'-one **(49c)** as a colourless oil (15.4 mg, 73% yield): ^{1}H NMR (500 MHz, Methanol-d_4) δ_H 8.04 (d, *J* = 8.7 Hz, 1H, H-7'), 7.92 (s, 1H, H-4'), 7.79 (app. dd, *J* = 8.7, 7.8 Hz, 2H, H-6' and H-4), 7.41 (dt, *J* = 7.8, 1.2 Hz, 1H, H-6), 7.30 (dt, *J* = 7.8, 1.2 Hz, 1H, H-5), 7.12 (d, *J* = 7.8 Hz, 1H, H-7), 5.65 (d, *J* = 16.7 Hz, 1H, H-1'), 5.60 (d, *J* = 16.7 Hz, 1H, H-1'), 4.63 (m, 2H, H-a), 4.62 (d, *J* = 8.8 Hz, 1H, H-1'' or H-2''), 4.55 (d, *J* = 8.8 Hz, 1H, H-1'' or H-2''), 4.39 (d, *J* = 9.7 Hz, 1H, H-1'' or H-2''), 4.35 (s, 2H, H-8'), 4.26 (d, *J* = 9.7 Hz, 1H, H-1'' or H-2''), 2.01 (s, 3H, H-4''), 1.92 – 1.82 (m, 3H, H-b and H-c), 1.07 (d, *J* = 5.9 Hz, 6H, H-d and H-e); ^{13}C NMR (126 MHz, DMSO-d_6) δ_C 177.8 (C-2), 170.4 (C-3''), 149.5 (C-2'), 142.7 (C-7a or C-3'a), 130.4 (C-6 or C-6'), 129.2 (C-6 or C-6'), 124.0 (C-4 or C-5), 123.8 (C-4 or C-5), 110.0 (C-7 or C-7'), 109.7 (C-7 or C-7'), 58.8 (C-1'' or C-2''), 56.8 (C-1'' or C-2''), 43.7 (C-8'), 42.6 (C-a), 42.0 (C-3), 37.9 (C-1'), 36.9 (C-b), 26.0 (C-c), 22.7 (C-d and C-e), 19.2 (C-4''); LCMS (MDAP): Rt = 11.0 min (Method 4); m/z 446.2 [M+H]$^+$; HRMS (ESI) calcd for $C_{26}H_{32}N_5O_2$ 446.2551, found 446.2563.

Note: Unable to visualise all carbon signals by NMR.

1-Acetyl-1'-[[5-chloro-1-(4-hydroxybutyl)benzimidazol-2-yl]methyl]spiro[azetidine-3,3'-indoline]-2'-one (49d)
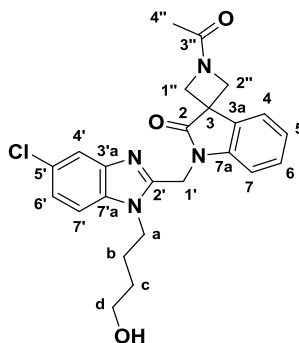
Potassium carbonate (63.2 mg, 0.46 mmol) was added to a solution of 4-[5-chloro-2-(chloromethyl)benzimidazol-1-yl]butan-1-ol (50 mg, 0.18 mmol) and 1-acetylspiro[azetidine-3,3'-indoline]-2'-one (**39**) (39.6 mg, 0.18 mmol) in acetonitrile (10 mL) and the resulting reaction mixture was heated to 80°C for 16 hours. After this time, the solution was cooled to room temperature and concentrated under reduced pressure. The residue was partitioned between a saturated solution of sodium bicarbonate (5 mL) and dichloromethane (10 mL). The layers were separated, the organic layer was dried over MgSO$_4$ and concentrated under reduced pressure. The crude residue was purified by flash column chromatography (Biotage SNAP 10 g, CH$_2$Cl$_2$: MeOH: NH$_3$, 100: 0: 0 to 90: 10: 1) to give 1-acetyl-1'-[[5-chloro-1-(4-hydroxybutyl) benzimidazol-2-yl]methyl]spiro[azetidine-3,3'-indoline]-2'-one **(49d)** as a colourless solid (43 mg, 52% yield): m.p. 230 − 233 °C; ^{1}H NMR (500 MHz, Methanol-d_4) δ$_H$ 7.68 (d, J = 7.8 Hz, 1H, H-4), 7.56 (d, J = 8.7 Hz, 1H, H-7'), 7.54 (d, J = 2.0 Hz, 1H, H-4'), 7.33 − 7.26 (m, 2H, H-6 and H-6'), 7.19 (app. t, J = 7.8 Hz, 1H, H-5), 7.00 (d, J = 7.8 Hz, 1H, H-7), 5.31 (d, J = 16.9 Hz, 1H, H-1'), 5.27 (d, J = 16.9 Hz, 1H, H-1'), 4.61 (d, J = 8.8 Hz, 1H, H-1'' or H-2''), 4.50 (d, J = 8.8 Hz, 1H, H-1'' or H-2''), 4.44 − 4.37 (m, 3H, H-1'' or H-2'' and H-a), 4.22 (d, J = 9.8 Hz, 1H, H-1'' or H-2''), 3.60 (t, J = 6.2 Hz, 2H, H-d), 2.01 (s, 3H, H-4''), 1.96 − 1.84 (m, 2H, H-b), 1.69 − 1.55 (m, 2H, H-c); ^{13}C NMR (126 MHz, Methanol-d_4) δ$_C$ 177.6 (C-2), 171.9 (C-3''), 150.2 (C-2'), 142.5 (C-7a), 142.2 (C-3'a), 134.0 (C-7'a), 129.7 (C-3a), 128.8 (C-4), 127.9 (C-5'), 123.5 (C-5), 123.2 (C-6'), 122.8 (C-4), 117.9 (C-4'), 111.3 (C-7'), 110.0 (C-7), 60.8 (C-d), 58.8 (C-1'' or C-2''), 56.6 (C-1'' or C-2''), 43.6 (C-a), 42.1 (C-3), 36.9 (C-1'), 29.2 (C-c), 26.2 (C-b), 17.2 (C-4''); LCMS (MDAP): Rt = 10.4 min (Method 5); m/z 453.1 [M+H]$^+$; HRMS (ESI) calcd for C$_{24}$H$_{25}$ClN$_4$O$_3$Na 475.1507, found 475.1520.

1-Acetyl-*N*-[[5-chloro-1-(3-methylsulfonylpropyl)benzimidazol-2-yl]methyl]-*N*-phenyl-azetidine-3-carboxamide (49e)
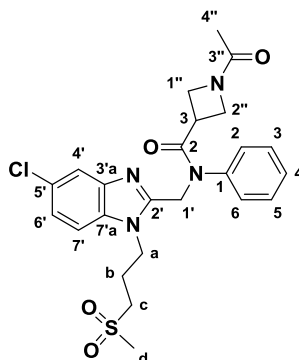
Sodium hydride (60% dispersion in oil) (13.2 mg, 0.33 mmol) was added to an ice cold solution of 1-acetyl-*N*-phenyl-azetidine-3-carboxamide (**41**) (72 mg, 0.33 mmol) in anhydrous *N,N*-dimethylformamide (2 mL). The cold bath was removed and the reaction mixture was stirred at room temperature for 1 hour. After this time, 5-chloro-2-(chloromethyl)-1-(3-methylsulfonylpropyl)benzimidazole (**48**) (106 mg, 0.33 mmol) was added and the reaction mixture was left stirring at room temperature for 16 hours. After this time, the reaction was diluted with water (10 mL) and ethyl acetate (10 mL). The layers were separated and the aqueous layer was further extracted with ethyl acetate (5 mL). The combined organic layers were washed with brine (15 mL), dried over MgSO$_4$ and concentrated under reduced pressure. The crude material was purified by flash column chromatography (Biotage SNAP 10 g, CH$_2$Cl$_2$: MeOH: NH$_3$, 100: 0: 0 to 95: 5: 0.5) to give 1-acetyl-*N*-[[5-chloro-1-(3-methylsulfonylpropyl) benzimidazol-2-yl]methyl]-*N*-phenyl-azetidine-3-carboxamide (**49e**) as a colourless oil (78 mg, 47% yield): ^{1}H NMR (500 MHz, Chloroform-*d*) δ$_H$ 7.69 (d, *J* = 1.8 Hz, 1H, H-4'), 7.46 - 7.37 (m, 2H, H-3, H-5), 7.34 − 7.25 (m, 5H, H-2, H-4, H-6, H-6' and H-7'), 5.23 (d, *J* = 15.5 Hz, 1H, H-1'), 5.06 (d, *J* = 15.5 Hz, 1H, H-1'), 4.55 − 4.44 (m, 2H, H-a), 4.36 (dd, *J* =8.5, 6.1 Hz, 1H, H-1'' or H-2''), 4.08 (dd, *J* = 9.3, 6.1 Hz, 1H, H-1'' or H-2''), 3.89 (t, *J* = 8.5 Hz, 1H, H-1'' or H-2''), 3.73 (t, *J* = 9.3 Hz, 1H, H-1'' or H-2''), 3.37 (m, 1H, H-3), 3.21 − 3.09 (m, 2H, H-c), 2.99 (s, 3H, H-d), 2.48 − 2.37 (m, 2H, H-b), 1.80 (s, 3H, H-4''); ^{13}C-NMR (126 MHz, Chloroform-*d*) δ$_C$ 171.5 (C-2), 170.5 (C-4''), 150.9 (C-2'), 140.8 (C-1), 133.3 (C-7'a), 130.1 (C-3 and C-5), 129.1 (C-4), 128.3 (C-5'), 128.1 (C-2 and C-6), 123.7 (C-6'), 119.9 (C-4'), 110.3 (C-7'), 52.3 (C-1'' and C-2''), 50.6 (C-c), 46.1 (C-1'), 42.2 (C-a), 41.3 (C-d), 31.3 (C-3), 22.2 (C-b), 18.5 (C-4''); LCMS (MDAP): Rt = 9.7 min (Method 5); m/z 503.1 [M+H]$^+$; HRMS (ESI) calcd for C$_{24}$H$_{28}$ClN$_4$O$_4$S 503.1514, found 503.1524.

1-Acetyl-1'-[[5-chloro-1-(3-methylsulfonylpropyl)benzimidazol-2-yl]methyl]-6'-fluoro-spiro[azetidine-3,3'-indoline]-2'-one (49f)
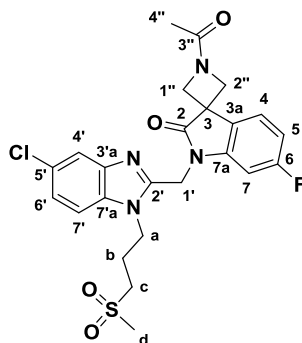
Sodium hydride (60% dispersion in oil) (12.6 mg, 0.31 mmol) was added to an ice cold solution of 1-acetyl-6'-fluoro-spiro[azetidine-3,3'-indoline]-2'-one (**47**) (67 mg, 0.29 mmol) in anhydrous *N,N*-dimethylformamide (4 mL). Upon completion of the addition, the cold bath was removed and the suspension was stirred at room temperature for 30 minutes. After this time, the suspension was cooled again and 5-chloro-2-(chloromethyl)-1-(3-methylsulfonylpropyl) benzimidazole (**48**) (91.9 mg, 0.29 mmol) was added in one portion and the resulting reaction mixture was left stirring at room temperature for 16 hours. After this time, the solution was diluted with water (10 mL) and extracted with ethyl acetate (2 x 15 mL). The combined organic layers were washed with brine (10 mL), dried over MgSO$_4$ and concentrated under reduced pressure. The crude material was purified by flash column chromatography (Biotage Zip 5 g, CH$_2$Cl$_2$: MeOH: NH$_3$, 100: 0: 0 to 95: 5: 0.5) to give 1-acetyl-1'-[[5-chloro-1-(3-methylsulfonylpropyl)benzimidazol-2-yl]methyl]-6'-fluoro-spiro[azetidine-3,3'-indoline]-2'-one (**49f**) as a white foam (119 mg, 80% yield): ^{1}H NMR (500 MHz, Chloroform-*d*) δ_H 7.75 (d, *J* = 1.9 Hz, 1H, H-4'), 7.44 (dd, *J* = 8.2, 5.0 Hz, 1H, H-4), 7.35 – 7.27 (m, 3H, H-7, H-6' and H-7'), 6.85 (ddd, *J* = 9.0, 8.2, 2.3 Hz, 1H, H-5), 5.20 (d, *J* = 15.3 Hz, 1H, H-1'), 5.13 (d, *J* = 15.3 Hz, 1H, H-1'), 4.61 – 4.44 (m, 3H, H-1'' or H-2'' and H-a), 4.39 (d, *J* = 9.5 Hz, 1H, H-1'' or H-2''), 4.27 (d, *J* = 8.2 Hz, 1H, H-1'' or H-2''), 4.16 (d, *J* = 9.5 Hz, 1H, H-1'' or H-2''), 3.15 (t, *J* = 7.2 Hz, 2H, H-c), 2.98 (s, 3H, H-d), 2.35 – 2.21 (m, 2H, H-b), 1.98 (s, 3H, H-4''); ^{13}C NMR (126 MHz, Chloroform-*d*) δ_C 177.4 (C-2), 170.8 (C-3''), 163.6 (d, *J*$_{CF}$ = 247.7 Hz, C-6), 148.5 (C-2'), 143.7 (d, *J* = 12.1 Hz, C-7a), 143.1 (C-3'a), 133.6 (C-7'a), 128.6 (C-5'), 124.7 (d, *J*$_{CF}$ = 3.1 Hz, C-3a), 124.3 (C-6'), 123.9 (d, *J*$_{CF}$ = 10.1 Hz, C-4), 120.1 (C-4'), 110.6 (C-7'), 110.3 (d, *J*$_{CF}$ = 23.3 Hz, C-5), 100.1 (d, *J*$_{CF}$ = 28.8 Hz, C-7), 58.8 (C-1'' or C-2''), 56.7 (C-1'' or C-2''), 51.1 (C-c), 42.4 (C-a), 41.6 (C-3), 41.4 (C-d), 37.7 (C-1'), 22.6 (C-b), 18.8 (C-4''); LCMS (MDAP): Rt = 12.2 min (Method 5); m/z 519.2 [M+H]$^+$; HRMS (ESI) calcd for C$_{24}$H$_{24}$ClFN$_4$O$_4$SNa 541.1083, found 541.1096.

Compound intermediate to (**49g**): *tert*-**Butyl 1-[[5-chloro-1-(3-methylsulfonylpropyl) benzimidazol-2-yl]methyl]-2-oxo-spiro[indoline-3,4'-piperidine]-1'-carboxylate**
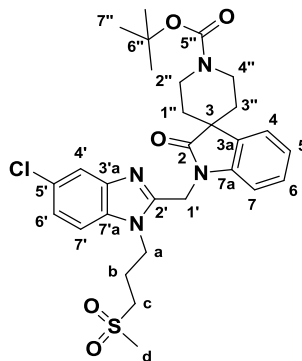
Sodium hydride (60% dispersion in oil) (58.9 mg, 1.47 mmol) (60% dispersion in oil) was added to an ice cold solution of *tert*-butyl 2-oxospiro[indoline-3,4'-piperidine]-1'-carboxylate (**46**) (445 mg, 1.47 mmol) in anhydrous *N*,*N*-dimethylformamide (8 mL). Upon completion of the addition, the cold bath was removed and the solution was stirred at room temperature for 1 hour. After this time, the solution was cooled with an ice bath and 5-chloro-2-(chloromethyl)-1-(3-methylsulfonylpropyl)benzimidazole (**48**) (430 mg, 1.34 mmol) was added portionwise. The cold bath was removed and the reaction mixture was left stirring at room temperature for 24 hours. After this time, the solution was quenched with water (5 mL) and extracted with ethyl acetate (2 x 15 mL). The combined organic layers were washed with brine (2 x 10 mL), dried over MgSO$_4$ and concentrated under reduced pressure. The crude oil was purified by flash column chromatography (Biotage SNAP 10g, CH$_2$Cl$_2$: MeOH: NH$_3$, 100: 0: 0 to 94: 6: 0.6) to give *tert*-butyl 1-[[5-chloro-1-(3-methylsulfonylpropyl)benzimidazol-2-yl]methyl]-2-oxo-spiro[indoline-3,4'-piperidine]-1'-carboxylate as a colourless solid (733 mg, 93% yield): ^{1}H NMR (500 MHz, Chloroform-*d*) δ$_H$ 7.77 (s, 1H, H-4'), 7.51 (d, *J* = 7.9 Hz, 1H, H-7), 7.35 (d, *J* = 7.9 Hz, 1H, H-6'), 7.33 – 7.28 (m, 3H, H-4, H-6 and H-7'), 7.09 (app. t, *J* = 7.7 Hz, 1H, H-5), 5.21 (s, 2H, H-1'), 4.51 (t, *J* = 7.5 Hz, 2H, H-a), 3.92 – 3.75 (m, 4H, H-2'' and H-4''), 3.12 (t, *J* = 7.1 Hz, 2H, H-c), 2.97 (s, 3H, H-d), 2.35 – 2.26 (m, 2H, H-b), 1.92 – 1.73 (m, 4H, H-1'' and H-3''), 1.52 (s, 9H, H-7''); ^{13}C NMR (126 MHz, Chloroform-*d*) δ$_C$ 179.6 (C-2), 154.9 (C-5''), 149.2 (C-2'), 143.1 (C-3'a), 141.1 (C-7a), 133.6 (C-7'a), 133.2 (C-3a), 128.6 (C-5'), 128.5 (C-6), 124.3 (C-6'), 123.3 (C-4 or C-5), 123.1 (C-4 or C-5), 119.9 (C-4'), 110.7 (C-7 or C-7'), 110.6 (C-7 or C-7'), 79.9 (C-6''), 51.2 (C-c), 45.3 (C-2'' and C-4''), 42.3 (C-a), 41.4 (C-d), 37.5 (C-1'), 32.7 (C-1'' and C-3''), 28.5 (C-7''), 22.7 (C-b); LCMS (MDAP) Rt = 9.7 min (Method 5); m/z 587.1 [M+H]$^+$; HRMS (ESI) calcd for C$_{29}$H$_{35}$ClN$_4$O$_5$S 587.2094, found 587.2090.

1-[[5-Chloro-1-(3-methylsulfonylpropyl)benzimidazol-2-yl]methyl]spiro[indoline-3,4'-piperidine]-2-one (49g)[179]
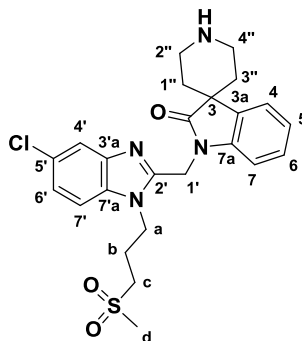
Trifluoroacetic acid (4.73 mL, 61.74 mmol) in dichloromethane (6 mL) was added dropwise to an ice cold solution of *tert*-butyl 1-[[5-chloro-1-(3-methylsulfonylpropyl)benzimidazol-2-yl]methyl]-2-oxo-spiro[indoline-3,4'-piperidine]-1'-carboxylate (725 mg, 1.23 mmol) in dichloromethane (6 mL). The cold bath was removed and the solution was left to stir at room temperature for 5 hours. After this time, the volatiles were removed under reduced pressure. The crude mixture was neutralised with a saturated solution of sodium bicarbonate (20 mL) and the product was extracted with dichloromethane (2 x 20 mL). The combined organic layers were washed with brine (20 mL), dried over MgSO$_4$ and concentrated under reduced pressure. The residue was purified by flash column chromatography (Biotage SNAP 25 g, CH$_2$Cl$_2$: MeOH: NH$_3$, 98: 2: 0.2 to 90:10:1) to give 1-[[5-chloro-1-(3-methylsulfonylpropyl)benzimidazol-2-yl]methyl]spiro[indoline-3,4'-piperidine]-2-one **(49g)** as a colourless solid (399 mg, 66% yield): m.p. 121 – 124 °C; ^{1}H NMR (500 MHz, Chloroform-d) δ_H 7.76 (d, *J* = 1.9 Hz, 1H, H-4'), 7.48 (d, *J* = 7.8 Hz, 1H, H-7), 7.42 (d, *J* = 7.6 Hz, 1H, H-4), 7.33 (d, *J* = 8.6 Hz, 1H, H-7'), 7.30 – 7.25 (m, 2H, H-6 and H-6'), 7.08 (app. t, *J* = 7.6 Hz, 1H, H-5), 5.20 (s, 2H, H-1'), 4.53 – 4.44 (m, 2H, H-a), 3.42 – 3.29 (m, 2H, H-2'' and H-4''), 3.18 – 3.04 (m, 4H, H-2'' and H-4'' and H-c), 2.95 (s, 3H, H-d), 2.35 – 2.21 (m, 2H, H-b), 1.96 – 1.84 (m, 2H, H-1'' and H-3''), 1.81 – 1.68 (m, 2H, H-1'' and H-3''); ^{13}C NMR (126 MHz, Chloroform-*d*) δ_C 180.0 (C-2) , 149.4 (C-2'), 143. (C-3'a), 141.0 (C-7a), 134.0 (C-3a), 133.6 (C-7'a), 128.4 (C-5'), 128.2 (C-6), 124.1 (C-6'), 123.4 (C-5), 123.2 (C-5), 120.0 (C-4'), 110.6 (C-7 or C-7'), 110.4 (C-7 or C-7'), 51.3 (C-c), 45.8 (C-3), 42.3 (C-a), 41.4 (C-d), 41.3 (C-2'' and C-4''), 37.6 (C-1'), 33.5 (C-1'' and C-3''), 22.7 (C-b); LCMS (MDAP): Rt = 3.8 min (Method 5); m/z 487.1 [M+H]$^+$; HRMS (ESI) calcd for C$_{24}$H$_{28}$ClN$_4$O$_3$S 487.1565, found 487.1567.

1-[[5-Chloro-1-(3-methylsulfonylpropyl)benzimidazol-2-yl]methyl]spiro[indoline-3,3'-tetrahydrofuran]-2-one (49h)
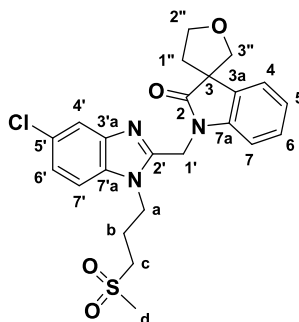
Sodium hydride (60% dispersion in oil) (60.3 mg, 1.51 mmol) added in one portion to an ice cold solution of spiro[indoline-3,3'-tetrahydrofuran]-2-one (**45b**) (284 mg, 1.51 mmol) in anhydrous *N,N*-dimethylformamide (10 mL). The cold bath was removed and the cloudy solution was stirred at room temperature for 1 hour. 5-Chloro-2-(chloromethyl)-1-(3-methylsulfonylpropyl) benzimidazole (**48**) (440 mg, 1.37 mmol) was added and the solution was left stirring at room temperature for 16 hours. After this time, the solution was diluted with water (25 mL) and ethyl acetate (25 mL) and the layers were separated. The organic layer was washed with brine (2 x 20 mL), dried over $MgSO_4$ and concentrated under reduced pressure. The crude yellow oil was purified by flash column chromatography (Biotage SNAP 10 g, eluting CH_2Cl_2: MeOH: NH_3, 100: 0: 0 to 93: 7: 0.7) to give 1-[[5-chloro-1-(3-methylsulfonylpropyl)benzimidazol-2-yl]methyl]spiro [indoline-3,3'-tetrahydrofuran]-2-one **(49h)** as a pale yellow solid (470 mg, 72% yield): m.p. 81 – 87 °C; ^{1}H NMR (500 MHz, Chloroform-*d*) δ_H 7.78 (d, *J* = 1.9 Hz, 1H, H-4'), 7.51 (d, *J* = 7.5 Hz, 1H, H-7), 7.35 – 7.28 (m, 4H, H-4, H-6, H-7' and H-6'), 7.11 (dt, *J* = 7.5, 1.1 Hz, 1H, H-5), 5.25 (d, *J* = 15.6 Hz, 1H, H-1'), 5.21 (d, *J* = 15.6 Hz, 1H, H-1'), 4.56 – 4.49 (m, 2H, H-a), 4.25 (t, *J* = 7.1 Hz, 2H, H-2''), 4.06 (d, *J* = 8.6 Hz, 1H, H-3''), 3.96 (d, *J* = 8.6 Hz, 1H, H-3''), 3.12 (t, *J* = 7.3 Hz, 2H, H-c), 2.95 (s, 3H, H-d), 2.58 – 2.50 (m, 1H, H-1''), 2.36 – 2.15 (m, 3H, H-1'' and H-b); ^{13}C NMR (126 MHz, Chloroform-*d*) δ_C 178.7 (C-2), 149.1 (C-2'), 143.0 (C-3'a), 141.4 (C-7a), 133.6 (C-7'a), 132.9 (C-3a), 128.6 (C-5'), 124.3 (C-6'), 123.9 (C-5), 122.6 (C-4), 120.0 (C-4'), 110.7 (C-7 or C-7'), 110.5 (C-7 or C-7'), 77.0 (C-3''), 69.1 (C-2''), 54.3 (C-3), 51.3 (C-c), 42.3 (C-a), 41.3 (C-d), 38.9 (C-1''), 37.8 (C-1'), 22.7 (C-b); LCMS (MDAP): Rt = 17.9 min (Method 4); m/z 474.1 [M+H]$^+$; HRMS (ESI) calcd for $C_{23}H_{25}ClN_3O_4S$ 474.1249, found 474.1255.

1-[[5-(Aminomethyl)-1-isopentyl-benzimidazol-2-yl]methyl]spiro[indoline-3,4'-tetrahydropyran]-2-one (49i)
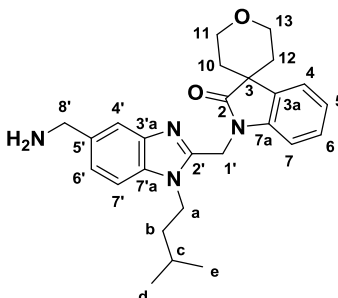
Sodium hydride (60% dispersion in oil) (6.3 mg, 0.16 mmol) was added to an ice cold solution of spiro[indoline-3,4'-tetrahydropyran]-2-one (**45c**) (30.5 mg, 0.15 mmol) in anhydrous *N,N*-dimethylformamide (3 mL). The cold bath was removed and the reaction mixture was stirred at room temperature for 1 hour. After this time, a solution of *tert*-butyl *N*-[[2-(chloromethyl)-1-isopentyl-benzimidazol-5-yl]methyl]carbamate (**48**) (50 mg, 0.14 mmol) in anhydrous *N,N*-dimethylformamide (3 mL) was added and the resulting mixture was left stirring at room temperature for 16 hours. After this time, the solution was quenched with a saturated solution of sodium bicarbonate (10 mL) and the aqueous layer was extracted with ethyl acetate (2 x 15 mL). The combined organic layers were washed with brine (10 mL), dried over MgSO$_4$ and concentrated under reduced pressure. The crude material was dissolved in dichloromethane (5 mL), treated with trifluoroacetic acid (2 mL, 0.14 mmol) and left stirring at room temperature. After 2 hours, the volatiles were removed under reduced pressure. The crude residue was purified by SCX-2 ion exchange column, rinsing with methanol (2 x 3 mL) and eluting the product with a 2 M solution of ammonia in methanol (2 x 3 mL). The elutes were concentrated under reduced pressure and further purified by flash column chromatography (Isco Redisep 4 g, CH$_2$Cl$_2$: MeOH: NH$_3$, 100: 0: 0 to 95: 5: 0.5) to give 1-[[5-(aminomethyl)-1-isopentyl-benzimidazol-2-yl]methyl]spiro[indoline-3,4'-tetrahydropyran]-2-one **(49i)** as a pale yellow oil (35 mg, 59% yield): ^{1}H NMR (500 MHz, Methanol-*d$_4$*) δ$_H$ 7.86 (s, H-4'), 7.84 (d, *J* = 8.8 Hz, H-7'), 7.63 (d, *J* = 8.8 Hz, H-6'), 7.55 (d, *J* = 7.5 Hz, 1H, H-4), 7.30 (app. t, *J* = 7.7 Hz, H-6), 7.22 – 7.10 (m, 2H, H-5 and H-7), 5.45 (s, H-1'), 4.53 (t, *J* = 7.6 Hz, 2H, H-a), 4.29 (s, 1H, H-8'), 4.20 (ddd, *J* = 12.2, 9.0, 4.2 Hz, 2H, H-11 and H-13), 3.93 (ddd, *J* = 12.2, 4.2 Hz, 2H, H-11 and H-13), 1.98 (m, 2H, H-10 and H-12), 1.90 (m, 2H, H-10 and H-12), 1.80 – 1.72 (m, 3H, H-b and H-c), 1.02 (d, *J* = 5.7 Hz, 6H, H-d and H-e); ^{13}C NMR (126 MHz, Methanol-*d$_4$*) δ$_C$ 180.2 (C-2), 149.9 (C-2'), 140.7 (C-7a), 133.9 (C-3a or C-7'a), 133.7 (C-3a or C-7'a), 127.9 (C-6), 126.0 (C-6'), 123.4 (C-4 or C-5), 123.3 (C-4 or C-5), 115.5 (C-4'), 112.4 (C-7'), 108.6 (C-7), 62.4 (C-11 and C-13), 44.2 (C-3),

43.7 (C-a), 42.8 (C-8'), 37.7 (C-b), 36.0 (C-1'), 32.6 (C-10 and C-12), 26.0 (C-c), 21.2 (C-d and C-e); LCMS (MDAP): Rt = 11.5 min (Method 4); m/z 433.2 [M+H]$^+$; HRMS (ESI) calcd for $C_{26}H_{33}N_4O_2$ 433.2598, found 433.2600.

Note: Unable to visualise all carbon signals by NMR.

1'-[[5-(Aminomethyl)-1-(4,4,4-trifluorobutyl)benzimidazol-2-yl]methyl]-6'-fluoro-spiro [cyclopropane-1,3'-indoline]-2'-one (49j)

Sodium hydride (60% dispersion in oil) (6.3 mg, 0.16 mmol) was added to an ice cold solution of 6'-fluorospiro[cyclopropane-1,3'-indoline]-2'-one (**45e**) (26.6 mg, 0.15 mmol) in anhydrous *N,N*-dimethylformamide (3 mL). The cold bath was removed and the reaction mixture was stirred at room temperature for 1 hour. After this time, a solution of *tert*-butyl *N*-[[2-(chloromethyl)-1-(4,4,4-trifluorobutyl)benzimidazol-5-yl]methyl]carbamate (**48**) (50 mg, 0.14 mmol) in anhydrous *N,N*-dimethylformamide (3 mL) was added and the resulting mixture was left stirring at room temperature. After 16 hours, the solution was quenched with a saturated solution of sodium bicarbonate (10 mL) and the aqueous layer extracted with ethyl acetate (2 x 15 mL). The combined organic layers were washed with brine (10 mL), dried over MgSO$_4$ and concentrated under reduced pressure. The crude material was dissolved in dichloromethane (5 mL), treated with trifluoroacetic acid (0.52 mL, 6.83 mmol) and left stirring at room temperature for 2 hours. After this time, the volatiles were removed under reduced pressure. The residue was purified by SCX-2 ion exchange column, rinsing with methanol (2 x 3 mL) and eluting the product with a 2 M solution of ammonia in methanol (2 x 3 mL). The elutes were concentrated under reduced pressure and further purified by flash column chromatography (Isco Redisep 4 g, CH$_2$Cl$_2$: MeOH: NH$_3$, 100: 0: 0 to 95: 5: 0.5) to give 1'-[[5-(aminomethyl)-1-(4,4,4-trifluorobutyl)benzimidazol-2-yl]methyl]-6'-fluoro-spiro[cyclopropane-1,3'-indoline]-2'-one **(49j)** as a pale yellow solid (38 mg, 61% yield): m.p. 271 – 279 °C; ^{1}H NMR (500 MHz, Methanol-*d*$_4$) δ 7.82 (d, *J* = 1.8 Hz, 1H, H-4'), 7.72 (d, *J* = 8.4 Hz, 1H, H-7'), 7.50 (dd, *J* = 8.4, 1.8 Hz, 1H, H-6'), 7.06 (dd, *J* = 9.2, 2.2 Hz, 1H, H-7), 7.00 (dd, *J* = 8.3, 5.1 Hz, 1H, H-4), 6.83 – 6.75 (m, 1H, H-5), 5.41 (s, 2H, H-1'), 4.50 (t, *J* = 7.9 Hz,

2H, H-a), 4.27 (s, 2H, H-8'), 2.40 – 2.19 (m, 2H, H-c), 2.04 – 1.93 (m, 2H, H-b), 1.79 – 1.72 (m, 2H, H-1'' and H-2''), 1.72 – 1.66 (m, 2H, H-1'' and H-2''); ^{13}C NMR (126 MHz, Methanol-d_4) δ 177.9 (C-2), 162.2 (d, J_{CF} = 242.1 Hz, C-6), 150.2 (C-2'), 143.0 (d, J_{CF} = 12.0 Hz, C-7a), 139.9 (C-3'a), 135.1 (C-7'a), 128.4 (C-5'), 125.9 (d, J_{CF} = 2.5 Hz, C-3a), 124.7 (C-6'), 119.7 (d, J_{CF} = 9.39 Hz, C-4), 119.0 (C-4'), 111.1 (C-7'), 108.6 (d, J_{CF} = 22.9 Hz, C-5), 97.8 (d, J_{CF} = 28.7 Hz, C-7), 43.2 (C-8'), 42.7 (C-a), 37.1 (C-1'), 30.6 (q, $^2J_{CF}$ = 29.4 Hz, C-c), 26.4 (C-3), 22.1 (C-b), 18.8 (C-1'' and C-2''); LCMS (MDAP): Rt = 12.1 min (Method 4); m/z 447.1 [M+H]$^+$; HRMS (ESI) calcd for $C_{23}H_{23}F_4N_4O$ 447.1803, found 447.1803.
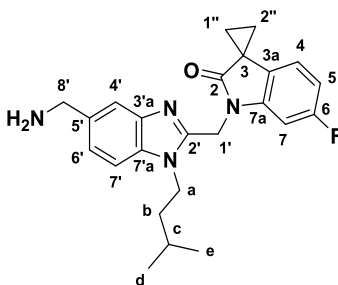
1'-[[5-(Aminomethyl)-1-isopentyl-benzimidazol-2-yl]methyl]-6'-fluoro-spiro[cyclopropane-1,3'-indoline]-2'-one (49k)

Sodium hydride (60% dispersion in oil) (6.3 mg, 0.16 mmol) was added to an ice cold solution of 6'-fluorospiro[cyclopropane-1,3'-indoline]-2'-one (**45e**) (26.6 mg, 0.15 mmol) in anhydrous *N,N*-dimethylformamide (3 mL). The cold bath was removed and the reaction mixture was stirred at room temperature for 1 hour. After this time, a solution of *tert*-butyl *N*-[[2-(chloromethyl)-1-isopentyl-benzimidazol-5-yl]methyl]carbamate (**48**) (50 mg, 0.14 mmol) in anhydrous *N,N*-dimethylformamide (3 mL) was added and the resulting mixture was left stirring at room temperature. After 16 hours, the solution was quenched with a saturated solution of sodium bicarbonate (10 mL) and the aqueous were extracted with ethyl acetate (2 x 15 mL). The combined organic layers were washed with brine (10 mL), dried over MgSO$_4$ and concentrated under reduced pressure. The crude material was dissolved in dichloromethane (5 mL), treated with trifluoroacetic acid (0.52 mL, 6.83 mmol) and left stirring at room temperature for 2 hours. After this time, the volatiles were removed under reduced pressure. The residue was purified by SCX-2 ion exchange column, rinsing with methanol (2 x 3 mL) and eluting the product with a 2 M solution of ammonia in methanol (2 x 3 mL). The elutes were concentrated under reduced pressure and further purified by flash column chromatography (Isco Redisep 4 g, CH$_2$Cl$_2$: MeOH: NH$_3$, 100: 0: 0 to 95: 5: 0.5) to give 1'-[[5-(aminomethyl)-1-isopentyl-benzimidazol-2-yl]methyl]-6'-fluoro-spiro[cyclopropane-1,3'-indoline]-2'-one **(49k)** as a colourless solid (32 mg, 56% yield):

m.p. 125 – 129 °C; ^{1}H NMR (500 MHz, Methanol-d_4) δ$_H$ 7.67 (d, J = 1.6 Hz, 1H, H-4'), 7.45 (d, J = 8.4 Hz, 1H, H-7'), 7.34 (dd, J = 8.4, 1.6 Hz, 1H, H-6'), 7.04 – 6.93 (m, 2H, H-4 and H-7a), 6.75 (ddd, J = 10.3, 8.3, 2.3 Hz, 1H, H-5), 5.32 (s, 2H, H-1'), 4.36 – 4.24 (t, J = 8.2 Hz, 2H, H-a), 3.94 (s, 2H, H-8'), 1.80 – 1.66 (m, 5H, H-1'' and H-2'' and H-c), 1.56 – 1.41 (m, 2H, H-b), 0.96 (d, J = 6.6 Hz, 6H, H-d and H-e); ^{13}C NMR (126 MHz, Methanol-d_4) δ$_C$ 177.6 (C-2), 162.1 (d, J_{CF} = 244.6 Hz, C-6), 148.8 (C-2'), 143.2 (d, J_{CF} = 11.3 Hz, C-7a), 141.7 (C-3'a), 136.3 (C-7'a), 134.3 (C-5'), 125.8 (d, J_{CF} = 2.8 Hz, C-3a), 123.2 (C-6'), 119.5 (d, J_{CF} = 10.2 Hz, C-4), 117.4 (C-4'), 110.0 (C-7'), 108.4 (d, J_{CF} = 23.2 Hz, C-5), 97.9 (d, J_{CF} = 28.5 Hz, C-7), 45.3 (C-8'), 42.4 (C-a), 38.2 (C-b), 37.4 (C-1'), 26.3 (C-3), 26.0 (C-c), 21.4 (C-d and C-e), 18.7 (C-1'' and C-2''); LCMS (MDAP): Rt = 12.3 min (Method 4); m/z 407.2 [M+H]$^+$; HRMS (ESI) calcd for $C_{24}H_{28}FN_4O$ 407.2242, found 407.2249.

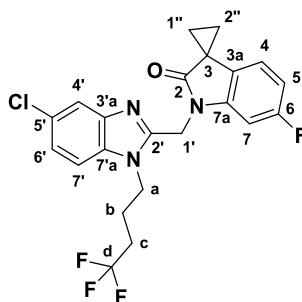**1'-[[5-Chloro-1-(4,4,4-trifluorobutyl)benzimidazol-2-yl]methyl]-6'-fluoro-spiro[cyclopropane-1,3'-indoline]-2'-one (49l)**

Sodium hydride (60% dispersion in oil) (6.3 mg, 0.16 mmol) was added to an ice cold solution of 6'-fluorospiro[cyclopropane-1,3'-indoline]-2'-one (**45e**) (26.6 mg, 0.15 mmol) in anhydrous *N,N*-dimethylformamide (3 mL). The cold bath was removed and the reaction mixture was stirred at room temperature for 1 hour. After this time, a solution of 5-chloro-2-(chloromethyl)-1-(4,4,4-trifluorobutyl)benzimidazole (**48**) (42.5 mg, 0.14 mmol) in anhydrous *N,N*-dimethylformamide (3 mL) was added and the resulting mixture was left stirring at room temperature. After 16 hours, the solution was quenched with a saturated solution of sodium bicarbonate (10 mL) and the aqueous layer was extracted with ethyl acetate (2 x 15 mL). The combined organic layers were washed with brine (10 mL), dried over MgSO$_4$ and concentrated under reduced pressure. The crude material was purified by flash column chromatography (Isco Redisep 4 g, CH$_2$Cl$_2$: MeOH: NH$_3$, 100: 0: 0 to 95: 5: 0.5) to give 1'-[[5-chloro-1-(4,4,4-trifluorobutyl)benzimidazol-2-yl]methyl]-6'-fluoro-spiro[cyclopropane-1,3'-indoline]-2'-one (**49l**) as a colourless solid (46 mg, 75% yield): m.p. 161 – 164 °C; ^{1}H NMR (500 MHz, Methanol-d_4) δ$_H$ 7.66 (d, J = 1.9 Hz, 1H, H-4'), 7.54 (d, J = 8.7 Hz, 1H, H-7'), 7.33 (dd, J = 8.7, 2.0 Hz, 1H, H-6'), 7.07 (dd, J = 9.2, 2.3 Hz, 1H, H-7), 6.97 (dd, J = 8.2, 5.1 Hz, 1H, H-4), 6.77 (ddd, J = 9.7, 8.2, 2.3 Hz, 1H, H-5), 5.33 (s, 2H, H-1'), 4.42

(d, J = 8.0 Hz, 2H, H-a), 2.36 – 2.21 (m, 2H, H-c), 1.99 – 1.85 (m, 2H, H-b), 1.79 – 1.71 (m, 2H, H-1'' and H-2''), 1.70 – 1.63 (m, 2H, H-1'' and H-2''); ^{13}C NMR (126 MHz, Methanol-d_4) δ_C 177.8 (C-2), 162.2 (d, J_{CF} = 242.2 Hz, C-6), 150.3 (C-2'), 143.1 (d, J_{CF} = 11.7 Hz, C-7a), 142.3 (C-3'a), 133.8 (C-7'a), 128.2 (C-5'), 125.8 (d, J_{CF} = 3.0 Hz, C-3a), 123.6 (C-6'), 119.6 (d, J_{CF} = 9.7 Hz, C-4), 118.4 (C-4'), 111.0 (C-7'), 108.5 (d, J_{CF} = 22.7 Hz, C-5), 97.9 (d, J_{CF} = 28.8 Hz, C-7), 42.4 (C-a), 37.2 (C-1'), 30.5 (q, $^2J_{CF}$ = 29.5 Hz, C-c) 26.4 (C-3), 22.1 (C-b), 18.7 (C-1'' and C-2''); LCMS (MDAP): Rt = 22.0 min (Method 5); m/z 452.0 [M+H]$^+$; HRMS (ESI) calcd for $C_{22}H_{18}ClF_4N_3ONa$ 474.0967, found 474.0990.

Note: Unable to visualise all carbon signals by NMR

1'-[[5-Chloro-1-(4-hydroxybutyl)benzimidazol-2-yl]methyl]-6'-fluoro-spiro[cyclopropane-1,3'-indoline]-2'-one (49m)
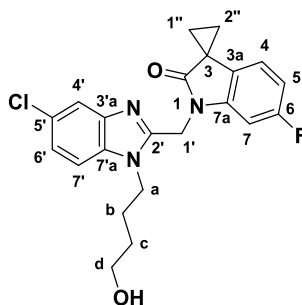
Potassium carbonate (28.3 mg, 0.20 mmol) was added to an ice cold solution of 6'-fluorospiro[cyclopropane-1,3'-indoline]-2'-one (**45e**) (26.6 mg, 0.15 mmol) in acetonitrile (1 mL). The cold bath was removed and the reaction mixture was stirred at room temperature for 1 hour. After this time, a solution of 4-[5-chloro-2-(chloromethyl)benzimidazol-1-yl]butan-1-ol (**48**) (37.3 mg, 0.14 mmol) in acetonitrile (1 mL) was added and the resulting mixture was left stirring at room temperature. After 16 hours, the solution was quenched with a saturated solution of sodium bicarbonate (5 mL) and the aqueous layer was extracted with ethyl acetate (2 x 5 mL). The combined organic layers were washed with brine (5 mL), dried over MgSO$_4$ and concentrated under reduced pressure. The crude material was purified by flash column chromatography (Isco Redisep 4 g, CH$_2$Cl$_2$: MeOH: NH$_3$, 100: 0: 0 to 95: 5: 0.5) to give 1'-[[5-chloro-1-(4-hydroxybutyl)benzimidazol-2-yl]methyl]-6'-fluoro-spiro[cyclopropane-1,3'-indoline]-2'-one (**49m**) as a colourless solid (42 mg, 74% yield): m.p. 209 – 212 °C; ^{1}H NMR (500 MHz, Methanol-d_4) δ_H 7.64 (d, J = 1.9 Hz, 1H, H-4'), 7.54 (d, J = 8.7 Hz, 1H, H-7'), 7.30 (dd, J = 8.7, 2.0 Hz, 1H, H-6'), 7.01 (dd, J = 9.2, 2.3 Hz, 1H, H-7), 6.97 (dd, J = 8.3, 5.2 Hz, 1H, H-4), 6.76 (ddd, J = 9.8, 8.3, 2.3 Hz, 1H, H-5), 5.34 (s, 2H, H-1'), 4.36 (t, J = 7.9 Hz, 2H, H-a), 3.55 (t, J = 6.3 Hz,

2H, H-d), 1.79 – 1.66 (m, 6H, H-b and H-1'' and H-2''), 1.63 – 1.51 (m, 2H, H-c); ^{1}H NMR (500 MHz, DMSO-d_6) δ_H 7.67 (s, 1H, H-4'), 7.58 (d, J = 8.6 Hz, 1H, H-7'), 7.25 (d, J = 8.4 Hz, 1H, H-6'), 7.09 – 7.00 (m, 2H, H-4 and H-7), 6.79 (app. t, J = 8.8 Hz, 1H, H-5), 5.27 (s, 2H, H-1'), 4.50 (s, 1H, OH), 4.28 (t, J = 7.5 Hz, 3H, H-a), 3.39 – 3.33 (m, 2H, H-d), 1.70 – 1.53 (m, 6H, H-1'' and H-2'' and H-b), 1.48 – 1.33 (m, 2H, H-c); ^{13}C NMR (126 MHz, DMSO-d_6) δ_C 176.7 (C-2), 161.9 (d, J_{CF} = 239.5 Hz, C-6) 150.9 (C-2'), 144.0 (d, J_{CF} = 12.2 Hz, C-7a), 143.2 (C-3'a), 134.6 (C-7'a), 126.7 (C-5'), 126.1 (d, J_{CF} = 2.5 Hz, C-3a), 123.0 (C-6'), 120.7 (d, J_{CF} = 9.5 Hz, C-4), 119.0 (C-4'), 112.3 (C-7'), 108.4 (d, J_{CF} = 24.2 Hz, C-5), 98.5 (d, J_{CF} = 28.6 Hz, C-7), 60.7 (C-d), 43.9 (C-a), 37.6 (C-1'), 29.9 (C-c), 26.8 (C-b), 26.7 (C-3), 19.4 (C-1'' and C-2''); LCMS (MDAP): Rt = 18.8 min (Method 4); m/z 414.3 [M+H]$^+$; HRMS (ESI) calcd for $C_{22}H_{22}ClFN_3O_2$ 414.1379, found 414.1388.

1-[[5-Chloro-1-(3-methylsulfonylpropyl)benzimidazol-2-yl]methyl]spiro[indoline-3,3'-tetrahydrofuran]-2-one (49n) and (49o) as single enantiomers
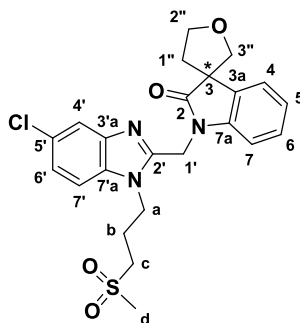
1-[[5-Chloro-1-(3-methylsulfonylpropyl)benzimidazol-2-yl]methyl]spiro[indoline-3,3'-tetrahydrofuran]-2-one (**49h**) (350 mg, 0.74 mmol) was purified by SFC on a ChiralPak AD (250 mm x 20 mm, 5 μm) column eluting with 45% methanol at a flow of 50 mL/min. The peaks were detected at a wavelength of 215 nm. The fraction collected were concentrated under reduced pressure and dried in a vacuum oven at 40 °C to give isomer (**49n**) as a colourless solid (148.5 mg) and isomer (**49o**) as a colourless solid (135.6 mg). The final purity analysis was performed by SFC using a ChiralPak AD (250 mm x 4.6 mm, 5 μm), using 45% methanol as the eluent and a flow rate of 4 mL/min.

Isomer (**49n**): ^{1}H NMR (500 MHz, Chloroform-d) δ_H 7.78 (d, J = 1.9 Hz, 1H, H-4'), 7.51 (d, J = 7.5 Hz, 1H, H-7), 7.35 – 7.28 (m, 4H, H-4, H-6, H-7' and H-6'), 7.11 (dt, J = 7.5, 1.1 Hz, 1H, H-5), 5.25 (d, J = 15.6 Hz, 1H, H-1'), 5.21 (d, J = 15.6 Hz, 1H, H-1'), 4.56 - 4.49 (m, 2H, H-a), 4.25 (t, J = 7.1 Hz, 2H, H-2''), 4.06 (d, J = 8.6 Hz, 1H, H-3''), 3.96 (d, J = 8.6 Hz, 1H, H-3''), 3.12 (t, J = 7.3 Hz, 2H, H-c), 2.95 (s, 3H, H-d), 2.58 – 2.50 (m, 1H, H-1''), 2.36 – 2.15 (m, 3H, H-1'' and H-b); ^{13}C NMR (126 MHz, Chloroform-d) δ_C 178.7 (C-2), 149.1 (C-2'), 143.0 (C-3'a), 141.4 (C-7a), 133.6 (C-7'a), 132.9 (C-3a),

128.6 (C-5'), 124.3 (C-6'), 123.9 (C-5), 122.6 (C-4), 120.0 (C-4'), 110.7 (C-7 or C-7'), 110.5 (C-7 or C-7'), 77.0 (C-3''), 69.1 (C-2''), 54.3 (C-3), 51.3 (C-c), 42.3 (C-a), 41.3 (C-d), 38.9 (C-1''), 37.8 (C-1'), 22.7 (C-b); ChiralPak AD: Rt = 4.03 min; 100% ee, 93.9% pure by UV detection at 220 nm; LCMS (MDAP): Rt = 17.9 min (Method 4); m/z 474.1 [M+H]⁺.

Isomer (**49o**): ¹H NMR (500 MHz, Chloroform-*d*) δ$_H$ 7.78 (d, *J* = 1.9 Hz, 1H, H-4'), 7.51 (d, *J* = 7.5 Hz, 1H, H-7), 7.35 - 7.28 (m, 4H, H-4, H-6, H-7' and H-6'), 7.11 (dt, *J* = 7.5, 1.1 Hz, 1H, H-5), 5.25 (d, *J* = 15.6 Hz, 1H, H-1'), 5.21 (d, *J* = 15.6 Hz, 1H, H-1'), 4.56 – 4.49 (m, 2H, H-a), 4.25 (t, *J* = 7.1 Hz, 2H, H-2''), 4.06 (d, *J* = 8.6 Hz, 1H, H-3''), 3.96 (d, *J* = 8.6 Hz, 1H, H-3''), 3.12 (t, *J* = 7.3 Hz, 2H, H-c), 2.95 (s, 3H, H-d), 2.58 – 2.50 (m, 1H, H-1''), 2.36 – 2.15 (m, 3H, H-1'' and H-b); ¹³C NMR (126 MHz, Chloroform-*d*) δ$_C$ 178.7 (C-2), 149.1 (C-2'), 143.0 (C-3'a), 141.4 (C-7a), 133.6 (C-7'a), 132.9 (C-3a), 128.6 (C-5'), 124.3 (C-6'), 123.9 (C-5), 122.6 (C-4), 120.0 (C-4'), 110.7 (C-7 or C-7'), 110.5 (C-7 or C-7'), 77.0 (C-3''), 69.1 (C-2''), 54.3 (C-3), 51.3 (C-c), 42.3 (C-a), 41.3 (C-d), 38.9 (C-1''), 37.8 (C-1'), 22.7 (C-b); ChiralPak AD: Rt = 4.84 min; 99.2% ee, 97.9% pure by UV detection at 220 nm; LCMS (MDAP): Rt = 17.9 min (Method 4); m/z 474.1 [M+H]⁺.

1-[[5-Chloro-1-(3-methylsulfonylpropyl)benzimidazol-2-yl]methyl]-1'-methylsulfonyl-spiro[indoline-3,4'-piperidine]-2-one (49p)

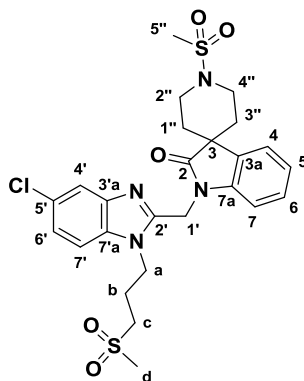Triethylamine (0.04 mL, 0.31 mmol) and methanesulfonyl chloride (0.02 mL, 0.23 mmol) were successively added to a solution of 1-[[5-chloro-1-(3-methylsulfonylpropyl)benzimidazol-2-yl]methyl]spiro[indoline-3,4'-piperidine]-2-one (**49g**) (100 mg, 0.21 mmol) in dichloromethane (2 mL) and the solution was left stirring at room temperature for 16 hours. After this time, the solution was washed with a saturated solution of sodium bicarbonate (5 mL), then brine (5 mL). The organic layer was dried over MgSO₄ and concentrated under reduced pressure. The crude material was purified by flash column chromatography (Biotage SNAP 10 g, CH₂Cl₂: MeOH: NH₃, 99: 1: 0.1 to 93: 7: 0.7) to give 1-[[5-chloro-1-(3-methylsulfonylpropyl)benzimidazol-2-yl]methyl]-1'-methylsulfonyl-spiro[indoline-3,4'-piperidine]-2-one **(49p)** as a colourless solid

(97 mg, 84% yield): m.p. 135–140 °C; ^{1}H NMR (500 MHz, Chloroform-*d*) δ_H 7.75 (d, *J* = 1.8 Hz, 1H, H-4'), 7.46 (d, *J* = 7.9 Hz, 1H, H-7), 7.35 − 7.26 (m, 3H, H-6, H-7', H-6'), 7.23 (d, *J* = 7.6 Hz, 1H, H-4), 7.12 (app. t, *J* = 7.6 Hz, 1H, H-5), 5.18 (s, 2H, H-1'), 4.50 (t, *J* = 7.5 Hz, 2H, H-a), 3.75 − 3.60 (m, 4H, H-2'' and H-4''), 3.11 (t, *J* = 7.3 Hz, 2H, H-c), 2.95 (s, 3H, H-d), 2.92 (s, 3H, H-5''), 2.41 − 2.26 (m, 2H, H-b), 2.20 − 2.04 (m, 2H, H-1'' and H-3''), 2.00 − 1.88 (m, 2H, H-1'' and H-3''); ^{13}C NMR (126 MHz, Chloroform-*d*) δ_C 179.3 (C-2), 149.2 (C-2'), 143.2 (C-3'a), 141.2 (C-7a), 133.7 (C-7'a), 132.7 (C-3a), 128.7 (C-6), 128.5 (C-5'), 124.2 (C-6'), 123.6 (C-5), 122.7 (C-4), 120.1 (C-4'), 110.6 (C-7 or C-7'), 110.5 (C-7 or C-7'), 51.3 (C-c), 44.2 (C-3), 42.2 (C-a), 41.3 (C-d), 41.2 (C-2'' and C-4''), 37.4 (C-1'), 35.3 (C-5''), 32.8 (C-1'' and C-3''), 22.8 (C-b); LCMS (MDAP): Rt = 15.4 min (Method 5); m/z 565.1 [M+H]$^+$; HRMS (ESI) calcd for $C_{25}H_{30}ClN_4O_5S_2$ 565.1341, found 565.1333.
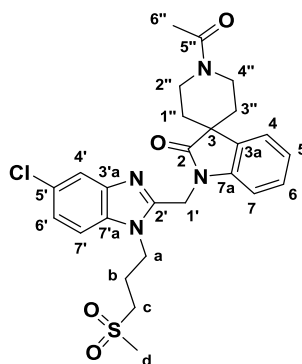
1'-Acetyl-1-[[5-chloro-1-(3-methylsulfonylpropyl)benzimidazol-2-yl]methyl]spiro[indoline-3,4'-piperidine]-2-one (49q)[179]

Triethylamine (0.08 mL, 0.58 mmol) and acetyl chloride (0.03 mL, 0.42 mmol) were successively added to a solution of 1-[[5-chloro-1-(3-methylsulfonylpropyl)benzimidazol-2-yl]methyl]spiro[indoline-3,4'-piperidine]-2-one (**49g**) (188 mg, 0.39 mmol) in dichloromethane (2 mL) and the resulting mixture was stirred at room temperature for 24 hours. After this time, the solution was diluted with further dichloromethane (5 mL) and washed successively with a saturated solution of sodium bicarbonate (5 mL) and brine (5 mL). The organic layer was dried over MgSO$_4$ and concentrated under reduced pressure. The crude material was purified by flash column chromatography (Biotage SNAP 10 g, CH$_2$Cl$_2$: MeOH: NH$_3$, 99: 1: 0.1 to 93: 7: 0.7) to give 1'-acetyl-1-[[5-chloro-1-(3-methylsulfonylpropyl)benzimidazol-2-yl]methyl]spiro[indoline-3,4'-piperidine]-2-one **(49q)** as a colourless solid (110 mg, 54% yield): ^{1}H NMR (500 MHz, Chloroform-*d*) δ_H 7.75 (s, 1H, H-4'), 7.49 (d, *J* = 7.9 Hz, 1H, H-7), 7.34 − 7.23 (m, 4H, H-4, H-5, H-6 and H-6'), 7.09 (d, *J* = 7.5 Hz, 1H, H-7'), 5.30 (s, 2H, H-1'), 4.63 − 4.50 (m, 2H, H-a), 4.19 − 4.12 (m, 1H, H-2'' or H-4''), 4.04 − 3.94 (m,1H, H-2'' or H-4''), 3.92 − 3.83 (m, 1H, H-2'' or H-4''), 3.79 − 3.69 (m, 1H, H-2'' or H-4''), 3.15 (t, *J* = 7.0 Hz, 2H, H-c), 2.98 (s, 3H, H-d), 2.40 − 2.25 (m, 2H, H-b), 2.19 (s, 3H,

H-6''), 2.00 – 1.79 (m, 4H, H-1'' and H-3''); ^{13}C NMR (126 MHz, Chloroform-d) δ_C 179.4 (C-2), 169.2 (C-5''), 149.2 (C-2'), 143.1 (C-3'a), 141.1 (C-7a), 133.6 (C-7'a), 132.8 (C-3a), 128.6 (C-6), 128.5 (C-5'), 124.2 (C-6'), 123.5 (C-5), 122.9 (C-4), 120.0 (C-4'), 110.6 (C-7 or C-7'), 110.5 (C-7 or C-7'), 51.2 (C-c), 45.1 (C-3), 42.3 (C-a), 41.9 (C-2'' and C-4''); 41.4 (C-d), 37.5 (C-1'), 33.2 (C-1'' or C-3''), 32.6 (C-1'' or C-3''), 22.6 (C-b), 21.6 (C-6''); LCMS (MDAP) Rt = 16.9 min (Method 4); 529.2 [M+H]$^+$; HRMS (ESI) calcd for $C_{26}H_{30}ClN_4O_4S$ 529.1671, found 529.1671.

N-(3-Bromo-4-pyridyl)tetrahydropyran-4-carboxamide (71)
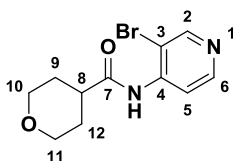
To a solution of 3-bromopyridin-4-amine (**70**) (2.16 g, 12.52 mmol) and triethylamine (3.49 mL, 25.04 mmol) in dichloromethane (19 mL) stirred at 0 °C was added dropwise a solution of tetrahydropyran-4-carbonyl chloride (1.86 g, 12.52 mmol) in dichloromethane (19 mL). Upon completion of the addition, the reaction was left to warm up to room temperature and stirred at this temperature for 16 hours. After this time, the solution was washed with a solution of saturated sodium bicarbonate (20 mL), then brine (20 mL). The organic layer was dried over MgSO$_4$ and concentrated under reduced pressure. The crude material was purified by flash column chromatography (Biotage SNAP 50 g, petroleum ether: EtOAc, 70: 30 to 20: 80) to give *N*-(3-bromo-4-pyridyl)tetrahydropyran-4-carboxamide (**71**) as a colourless solid (2.73 g, 76% yield): m.p. 134 – 136 °C; ^{1}H NMR (500 MHz, DMSO-d_6) δ_H 9.46 (s, 1H, NH), 8.69 (s, 1H, H-2), 8.42 (d, J = 5.4 Hz, 1H, H-6), 7.92 (d, J = 5.4 Hz, 1H, H-5), 3.96 – 3.84 (m, 2H, H-10 and H-11), 3.35 (td, J = 11.7, 2.3 Hz, 2H, H-10 and H-11), 2.95 – 2.83 (m, 1H, H-8), 1.80 – 1.71 (m, 2H, H-9 and H-12), 1.70 – 1.51 (m, 2H, H-9 and H-12); ^{13}C NMR (126 MHz, DMSO-d_6) δ_C 174.4 (C-7), 152.5 (C-2), 149.4 (C-6), 143.7 (C-4), 118.7 (C-5), 113.2 (C-3), 66.7 (C-10 and C-11), 41.6 (C-8), 29.2 (C-9 and C-12); LCMS (MDAP): Rt = 5.4 min (Method 5); m/z 284.90 [M(^{79}Br)+H]$^+$, 286.9 [M(^{81}Br)+H]$^+$; HRMS (ESI) calcd for $C_{11}H_{14}BrN_2O_2$ 285.0233, found 285.0235.

N-(3-Bromo-4-pyridyl)-N-[(4-methoxyphenyl)methyl]tetrahydropyran-4-carboxamide (67)
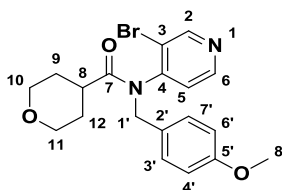
Sodium hydride (60% dispersion in oil) (0.400 g, 9.95 mmol) was added to an ice cold solution of N-(3-bromo-4-pyridyl)tetrahydropyran-4-carboxamide (**71**) (2.58 g, 9.05 mmol) in anhydrous N,N- dimethylformamide (30 mL). Upon completion of the addition, the cold bath was removed and the mixture was stirred at room temperature for 1 hour. After this time, the reaction mixture was cooled again with an ice bath and 1-(chloromethyl)-4-methoxy-benzene (1.35 mL, 9.95 mmol) was added. The resulting reaction mixture was left stirring at room temperature for 16 hours. After this time, the reaction mixture was diluted with water (50 mL) and extracted with ethyl acetate (2 x 50 mL). The combined organic layers were washed successively with a saturated solution of sodium bicarbonate (50 mL) then brine (50 mL). The organic layer was dried over MgSO$_4$ and concentrated under reduced pressure. The crude material was purified by flash column chromatography (Biotage SNAP 50 g, petroleum ether: EtOAc, 90: 10 to 75: 25) to give a partially crystalline solid. The solid was triturated with methanol and collected by filtration to give N-(3-bromo-4-pyridyl)-N-[(4-methoxyphenyl)methyl]tetrahydropyran-4-carboxamide **(67)** as a colourless solid (0.589 g, 16% yield): m.p. 168 – 171 °C; ^{1}H NMR (500 MHz, DMSO-d_6) δ$_H$ 8.89 (s, 1H, H-2), 8.53 (d, J = 5.1 Hz, 1H, H-6), 7.17 (d, J = 5.1 Hz, 1H, H-5), 7.06 (d, J = 8.1 Hz, 2H, H-3' and H-7'), 6.81 (d, J = 8.1 Hz, 2H, H-4' and H-6'), 5.11 (d, J = 14.5 Hz, 1H, H-1'), 4.30 (d, J = 14.5 Hz, 1H, H-1'), 3.84 – 3.71 (m, 2H, H-10 and H-11), 3.70 (s, 3H, H-8'), 3.09 (app. t, J = 11.1 Hz, 1H, H-10 or H-11), 3.00 (app. t, J = 11.1 Hz, 1H, H-10 or H-11), 2.21 – 2.08 (m, 1H, H-8), 1.84 – 1.70 (m, 1H, H-9 or H-12), 1.63 – 1.41 (m, 3H, H-9 and H-12); ^{13}C NMR (126 MHz, DMSO-d_6) δ$_C$ 173.3 (C-7), 159.1 (C-5'), 153.6 (C-2), 150.6 (C-6), 148.1 (C-4), 130.5 (C-3' and C-7'), 128.6 (C-2'), 126.4 (C-5), 122.3 (C-3), 114.2 (C-4' and C-6'), 66.4 (C-10 and C-11), 66.2 (C-10 and C-11), 55.5 (C-8'), 50.5 (C-1'), 29.6 (C-9 and C-12), 28.8 (C-9 and C-12); LCMS (MDAP): Rt = 13.8 min (Method 5); m/z 404.9 [M(^{79}Br)+H]$^+$, 406.8 [M(^{81}Br)+H]$^+$; HRMS (ESI) calcd for C$_{19}$H$_{21}$BrN$_2$NaO 427.0628, found 427.0629.

1-[(4-Methoxyphenyl)methyl]spiro[pyrrolo[3,2-c]pyridine-3,4'-tetrahydropyran]-2-one (68)
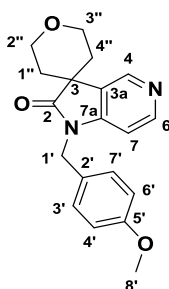
A microwave vial was charged with *N*-(3-bromo-4-pyridyl)-*N*-[(4-methoxyphenyl)methyl]tetrahydropyran-4-carboxamide (**67**) (314 mg, 0.77 mmol), palladium(II) acetate (17.4 mg, 0.08 mol), tricyclohexylphosphine tetrafluoroborate (28.5 mg, 0.08 mmol), and sodium *tert*-butoxide (111.7 mg, 1.16 mmol). The vial was sealed and evacuated with a vacuum/nitrogen cycle. Anhydrous 1,4-dioxane (8 mL) was added and the solution was again evacuated with a nitrogen/vacuum cycle before heating the reaction to 150 °C for 4 hours under microwave irradiation. After this time, the reaction was diluted with ethyl acetate (15 mL) and washed successively with a saturated solution of sodium bicarbonate (15 mL) then brine (10 mL). The organic layer was dried over MgSO$_4$ and concentrated under reduced pressure. The crude material was purified by flash column chromatography (Biotage SNAP 25 g, CH$_2$Cl$_2$: MeOH: NH$_3$, 99: 1: 0.1 to 95: 5: 0.5) to give 1-[(4-methoxyphenyl)methyl]spiro[pyrrolo[3,2-c]pyridine-3,4'-tetrahydropyran]-2-one (**68**) as a colourless oil (156 mg, 62% yield): ^{1}H NMR (500 MHz, Chloroform-*d*) δ_H 8.57 (s, 1H, H-4), 8.37 (d, *J* = 5.3 Hz, 1H, H-6), 7.17 (d, *J* = 8.4 Hz, 2H, H-3' and H-7'), 6.83 (d, *J* = 8.4 Hz, 2H, H-4' and H-6'), 6.73 (d, *J* = 5.3 Hz, 1H, H-7), 4.81 (s, 2H, H-1'), 4.29 – 4.19 (m, 2H, H-2'' and H-3''), 3.97 – 3.89 (m, 2H, H-2'' and H-3''), 3.76 (s, 3H, H-8'), 2.04 – 1.96 (m, 2H, H-1'' and H-4''), 1.86 – 1.77 (m, 2H, H-1'' and H-4''); ^{13}C NMR (126 MHz, Chloroform-*d*) δ_C 179.1 (C-2), 159.3 (C-5'), 149.6 (C-4 or C-6), 149.2 (C-7a), 143.3 (C-4 or C-6), 129.7 (C-2' or C-3a), 128.6 (C-3' and C-7'), 127.0 (C-2' or C-3a), 114.4 (C-4' and C-6'), 104.7 (C-7), 62.9 (C-2'' and C-3''), 55.2 (C-8'), 43.7 (C-3), 43.1 (C-1'), 32.6 (C-1'' and 4''); LCMS (MDAP): Rt = 10.4 min (Method 4); m/z 325.1 [M+H]$^+$; HRMS (ESI) calcd for C$_{19}$H$_{21}$N$_2$O$_3$ 325.1547, found 325.1547.

Spiro[1*H*-pyrrolo[3,2-c]pyridine-3,4'-tetrahydropyran]-2-one (74)[179]
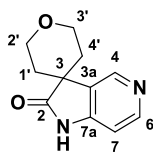
Anisole (0.36 mL, 3.34 mmol) was added to a solution of 1-[(4-methoxyphenyl)methyl]spiro[pyrrolo[3,2-c]pyridine-3,4'-tetrahydropyran]-2-one (**68**) (155 mg, 0.48 mmol) in trifluoroacetic acid (1.83 mL, 23.89 mmol) and the solution was heated under microwave irradiation at 200 °C for 4.5 hour After this time, the volatiles were removed under reduced pressure. The residue was diluted with ethyl acetate (10 mL) and neutralised with a saturated solution of sodium bicarbonate (10 mL). The layers were separated and the organic layer was dried over MgSO$_4$ and concentrated under reduced pressure to a black oil. The crude oil was purified by flash column chromatography (Biotage SNAP 10 g, CH$_2$Cl$_2$: MeOH: NH$_3$, 99: 1: 0.1 to 93: 7: 0.7) to give spiro[1*H*-pyrrolo[3,2-c]pyridine-3,4'-tetrahydropyran]-2-one (**74**) as a pale brown oil (11 mg, 11% yield): ^{1}H NMR (500 MHz, Chloroform-*d*) δ$_H$ 8.63 (s, 1H, H-4), 8.47 (d, *J* = 5.3 Hz, 1H, H-6), 6.95 (d, *J* = 5.3 Hz, 1H, H-7), 4.27 – 4.16 (m, 2H, H-2' and H-3'), 3.99 – 3.89 (m, 2H, H-2' and H-3'), 2.07 – 1.96 (m, 2H, H-1' and H-4'), 1.91 – 1.82 (m, 2H, H-1' and H-4'); LCMS (MDAP): Rt = 4.3 min (Method 4); m/z 205.0 [M+H]$^+$; HRMS (ESI) calcd for C$_{11}$H$_{13}$N$_2$O$_2$ 205.0972, found 205.0974.

Note: No ^{13}C NMR could be acquired on this sample.

1-[[5-Chloro-1-(3-methylsulfonylpropyl)benzimidazol-2-yl]methyl]spiro[pyrrolo[3,2-*c*] pyridine-3,4'-tetrahydropyran]-2-one (76)[179]
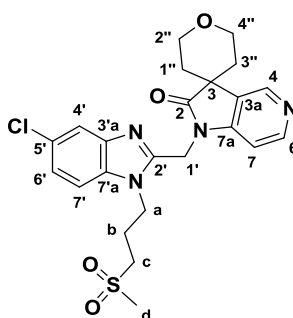
Sodium hydride (60% dispersion in oil) (14.2 mg, 0.37 mmol) added in one portion to an ice cold solution of spiro[1*H*-pyrrolo[3,2-c]pyridine-3,4'-tetrahydropyran]-2-one (**74**) (62.9 mg, 0.31 mmol) in anhydrous *N,N*- dimethylformamide (6 mL). The cold bath was removed and the cloudy solution was stirred at room temperature for 1 hour. 5-Chloro-2-(chloromethyl)-1-(3-

methylsulfonylpropyl)benzimidazole **(75)** (99 mg, 0.31 mmol) was added and the resulting solution was left stirring at room temperature for 16 hours. After this time, the solution was diluted with water (5 mL) and ethyl acetate (5 mL) and the layers were separated. The organic layer was washed with brine (2 x 5 mL), dried over MgSO$_4$ and concentrated under reduced pressure. The crude material was purified by mass directed HPLC (MDAP) to give 1-[[5-chloro-1-(3-methylsulfonylpropyl)benzimidazol-2-yl]methyl]spiro[pyrrolo[3,2-*c*]pyridine-3,4'-tetrahydropyran]-2-one **(76)** as the *bis*-formate salt and colourless oil (52 mg, 35% yield): ^{1}H NMR (500 MHz, Methanol-d_4) δ_H 8.66 (s, 1H, H-4), 8.44 (d, J = 5.6 Hz, 1H, H-6), 8.12 (s, 2H, formate salt), 7.61 (d, J = 8.7 Hz, 1H, H-7'), 7.57 (d, J = 1.9 Hz, 1H, H-4'), 7.34 – 7.31 (m, 2H, H-7 and H-6'), 5.33 (s, 2H, H-1'), 4.58 (t, J = 7.7 Hz, 2H, H-a), 4.20 (m, 2H, H-2'' and H-4''), 3.94 (m, 2H, H-2'' and H-4''), 3.32 – 3.27 (m, 2H, H-c), 3.03 (s, 3H, H-d), 2.45 – 2.34 (m, 2H, H-b), 2.09 – 1.95 (m, 4H, H-1'' and H-3''); ^{13}C NMR (126 MHz, Chloroform-d) δ_C 179.1 (C-2), 148.3 (C-2'), 143.1 (C-4 or C-6), 141.4 (C-4 or C-6), 133.5 (C-7a or C-3'a), 128.8 (C-5'), 124.4 (C-6'), 120.1 (C-4'), 110.6 (C-7'), 106.2 (C-7), 62.7 (C-2'' and C-4''), 50.9 (C-c), 44.1 (C-3), 42.3 (C-a), 41.5 (C-d), 37.3 (C-1'), 32.4 (C-1'' and C-3''), 22.6 (C-b); LCMS (MDAP): Rt = 3.3 min (Method 5); m/z 489.2 [M+H]$^+$; HRMS (ESI) calcd for C$_{23}$H$_{26}$ClN$_4$O$_4$S 489.1358, found 489.1345.

Note: Unable to visualise all carbon signals by NMR.

Ethyl 2-(3-nitro-4-pyridyl)acetate (80)[309,354,355]
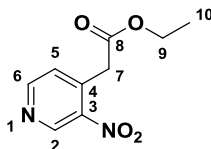
To a slurry of potassium *tert*-butoxide (77.76 g, 692.99 mmol) in anhydrous tetrahydrofuran (300 mL) stirred at 0 °C was added a solution of 3-nitropyridine (8.6 g, 69.3 mmol) and ethyl 2-chloroacetate (12.39 mL, 115.73 mmol) in tetrahydrofuran (200 mL) added dropwise over 2 hours whilst maintaining the reaction temperature between 5 °C and 10 °C. Upon completion of the addition, the cold bath was removed and the dark red-purple solution was stirred at room temperature for 1 hour. After this time, the reaction mixture was cooled with an ice bath and saturated ammonium chloride (500 mL) was added dropwise, keeping the temperature below 20 °C. The resulting mixture was stirred for 20 min before the product was extracted with ethyl acetate (500 mL). The aqueous layer was extracted with further ethyl acetate (200 mL). The combined organic layers were washed with brine (2 x 500 mL), dried over MgSO$_4$ and concentrated under reduced pressure to give ethyl 2-(3-nitro-4-pyridyl)acetate **(80)** as a dark

red-orange oil (7.22 g, 50% yield): ^{1}H NMR (500 MHz, DMSO-d$_6$) δ$_H$ 9.23 (s, 1H, H-2), 8.84 (d, J = 5.0 Hz, 1H, H-6), 7.65 (d, J = 5.0 Hz, 1H, H-5), 4.15 (s, 2H, H-7), 4.09 (q, J = 7.1 Hz, 2H, H-9), 1.16 (t, J = 7.1 Hz, 3H, H-10); ^{13}C NMR (126 MHz, DMSO-d$_6$) δ$_C$ 169.3 (C-8), 154.4 (C-6), 146.1 (C-2), 139.3 (C-4), 128.3 (C-5), 61.3 (C-9), 38.5 (C-7), 14.4 (C-10); LCMS (MDAP): Rt = 15.9 min (Method 4); m/z 211.0 [M+H]$^+$; HRMS (ESI) calcd for $C_9H_{11}N_2O_4$ 211.0713, found 211.0713.

Ethyl 2-(3-amino-4-pyridyl)acetate (81)[354,355]
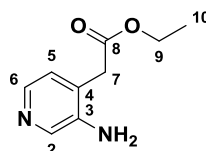
A suspension of ethyl 2-(3-nitro-4-pyridyl)acetate (**80**) (7.22 g, 34.35 mmol) and 10% palladium on carbon (0.720 g, 6.79 mmol) in methanol (150 mL) was hydrogenated at 20 °C under 1 atmosphere of hydrogen for 24 hours. After this time, the catalyst was removed by filtration through a pad of celite and the filtrate was concentrated under reduced pressure to give ethyl 2-(3-amino-4-pyridyl)acetate **(81)** as a dark brown oil that was taken crude into the next step without further purification (5.82 g, 94% yield): ^{1}H NMR (500 MHz, Chloroform-d) δ$_H$ 8.10 (s, 1H, H-2), 7.99 (d, J = 4.9 Hz, 1H, H-6), 7.00 (d, J = 4.9 Hz, 1H, H-5), 4.17 (q, J = 7.1 Hz, 2H, H-9), 3.55 (s, 2H, H-7), 1.26 (t, J = 7.1 Hz, 3H, H-10); ^{13}C NMR (126 MHz, Chloroform-d) δ$_C$ 170.5 (C-8), 141.9 (C-4), 140.2 (C-2 or C-6), 138.5 (C-2 or C-6), 127.2 (C-3), 125.2 (C-5), 61.5 (C-9), 37.9 (C-7), 14.1 (C-10); LCMS (MDAP): Rt = 5.3 min (Method 4); m/z 181.1 [M+H]$^+$; HRMS (ESI) calcd for $C_9H_{13}N_2O_2$ 181.0972, found 181.0973.

1,3-Dihydropyrrolo[2,3-c]pyridin-2-one hydrochloride (82)[299,355]
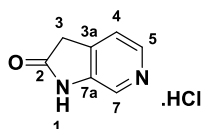
A solution of ethyl 2-(3-amino-4-pyridyl)acetate (**81**) (5.82 g, 32.3 mmol) in diethyl ether (170 mL) and HCl (1.4 M) (170 mL, 238 mmol) was stirred at room temperature for 16 hours. After this time, the layers were separated. The organic layer was extracted with water (100 mL) and the combined aqueous were further washed with dichloromethane (100 mL) and concentrated under reduced pressure. The solid was dried under reduced pressure at 40 °C for 16 hours to give 1,3-dihydropyrrolo[2,3-c]pyridin-2-one hydrochloride **(82)** as a colourless solid (4.53 g, 82% yield): m.p. 220 – 223 °C [lit.[299] 225 °C] ^{1}H NMR (500 MHz, DMSO-d$_6$) δ$_H$ 14.06 (s,

1H, NH), 12.53 (s, 1H, OH), 8.48 (s, 1H, H-7), 8.08 – 7.95 (d, J = 6.5 Hz, 1H, H-5), 7.58 (d, *J* = 6.5 Hz, 1H, H-4), 5.93 (s, 1H, H-3); ^{13}C NMR (126 MHz, DMSO-d_6) δ_C 163.2 (C-2), 139.7 (C-7a), 129.2 (C-5 or C-7), 127.0 (C-3a), 121.8 (C-5 or C-7), 112.5 (C-4), 83.6 (C-3); LCMS (MDAP): Rt = 2.8 min (Method 5); m/z 135.1 [M+H]$^+$; HRMS (ESI) calcd for $C_7H_7N_2O$ 135.0553, found 135.0553.

Spiro[1*H*-pyrrolo[2,3-*c*]pyridine-3,1'-cyclopropane]-2-one (77)
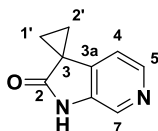
To a suspension of 1,3-dihydropyrrolo[2,3-*c*]pyridin-2-one hydrochloride (**82**) (1.0 g, 5.86 mmol) and diisopropylamine (3.28 mL, 23.45 mmol) in anhydrous tetrahydrofuran (60 mL) cooled to - 40 °C (ice/acetonitrile bath) was added dropwise n-butyl lithium (2.5 M solution in hexanes) (14.06 mL, 35.17 mmol) over 90 minutes. Upon completion of the addition, the reaction temperature was allowed to raise to 0 °C over a 2 hour period. A solution of 1,2-dibromoethane (1.95 mL, 12.31 mmol) in tetrahydrofuran (10 mL) was added dropwise over 2 hours. Upon completion of the addition, the reaction mixture was left to warm up to room temperature and left stirring for 16 hours. The reaction was quenched with a solution of ammonium chloride (50 mL) and the layers were separated. The aqueous layer was extracted with ethyl acetate (3 x 20 mL). The combined organic layers were washed with brine (50 mL), dried over MgSO$_4$ and concentrated under reduced pressure. The crude material was purified by flash column chromatography (Biotage SNAP 25 g, CH$_2$Cl$_2$: MeOH: NH$_3$, 100: 0: 0 to 90: 10: 1) to give spiro[1*H*-pyrrolo[2,3-*c*]pyridine-3,1'-cyclopropane]-2-one **(77)** as a colourless solid (105 mg, 11% yield): ^{1}H NMR (500 MHz, DMSO-d_6) δ_H 10.70 (s, 1H, NH), 8.17 (d, *J* = 4.9 Hz, 1H, H-5), 8.15 (s, 1H, H-7), 7.06 (d, *J* = 4.9 Hz, 1H, H-4), 1.69 (t, *J* = 3.9 Hz, 2H, H-1' and H-2'), 1.57 (t, *J* = 3.9 Hz, 2H, H-1' and H-2'); LCMS (LCQ) Rt = 0.4 min (Method 2); m/z 161.3 [M+H]$^+$.

1'-[[5-(Aminomethyl)-1-isopentyl-benzimidazol-2-yl]methyl]spiro[cyclopropane-1,3'-pyrrolo[2,3-c]pyridine]-2'-one (87a)
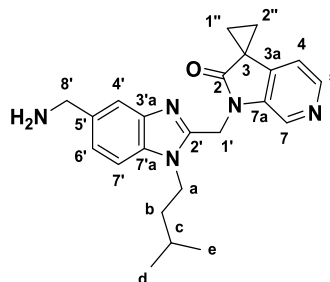
Sodium hydride (60% dispersion in oil) (26.3 mg, 0.69 mmol) was added to an ice cold solution of spiro[1*H*-pyrrolo[2,3-*c*]pyridine-3,1'-cyclopropane]-2-one (**77**) (100 mg, 0.62 mmol) in anhydrous *N,N*-dimethylformamide (3 mL). The cold bath was removed and the reaction mixture was stirred at room temperature for 1 hour. After this time, a solution of *tert*-butyl *N*-[[2-(chloromethyl)-1-isopentyl-benzimidazol-5-yl]methyl]carbamate (**48**) (251.3 mg, 0.69 mmol) in anhydrous *N,N*-dimethylformamide (3 mL) was added and the resulting reaction mixture was left stirring at room temperature for 16 hours. After this time, the solution was quenched with a saturated solution of sodium bicarbonate (10 mL) and the aqueous layer was extracted with ethyl acetate (2 x 15 mL). The combined organic layers were washed with brine (10 mL), dried over MgSO$_4$ and concentrated under reduced pressure. The crude material was dissolved in dichloromethane (5 mL) and was treated with trifluoroacetic acid (1 mL, 0.62 mmol) and left stirring at room temperature for 2 hours. After this time, the volatiles were removed under reduced pressure. The residue was purified by SCX-2 ion exchange column, rinsing with methanol (2 x 3 mL) and eluting the product with 2 M solution of ammonia in methanol (2 x 3 mL). The elutes were concentrated under reduced pressure and further purified by flash column chromatography (Isco Redisep 4 g, CH$_2$Cl$_2$: MeOH: NH$_3$, 100: 0: 0 to 95: 5: 0.5) to give 1'-[[5-(aminomethyl)-1-isopentyl-benzimidazol-2-yl]methyl]spiro[cyclopropane-1,3'-pyrrolo[2,3-*c*]pyridine]-2'-one **(87a)** as a colourless foam (43 mg, 18% yield): ^{1}H NMR (500 MHz, Methanol-*d$_4$*) δ_H 8.33 (s, 1H, H-7), 8.24 (d, *J* = 4.9 Hz, 1H, H-5), 7.64 (d, *J* = 1.5 Hz, 1H, H-4'), 7.49 (d, *J* = 8.4 Hz, 1H, H-7'), 7.35 (dd, *J* = 8.4, 1.5 Hz, 1H, H-6'), 7.15 (d, *J* = 4.9 Hz, 1H, H-4), 5.40 (s, 2H, H-1'), 4.41 – 4.31 (m, 2H, H-a), 3.97 (s, 2H, H-8'), 1.94 – 1.85 (m, 4H, H-1'' and H-2''), 1.77 – 1.66 (m, 1H, H-c), 1.57 (m, 2H, H-b), 0.99 (d, *J* = 6.6 Hz, 6H, H-d and H-e); LCMS (MDAP): Rt = 2.7 min (Method 5); m/z 390.0 [M+H]$^+$; HRMS (ESI) calcd for C$_{23}$H$_{28}$N$_5$O 390.2294, found 390.2299.

1'-[[5-(Aminomethyl)-1-(4,4,4-trifluorobutyl)benzimidazol-2-yl]methyl]spiro[cyclopropane-1,3'-pyrrolo[2,3-*c*]pyridine]-2'-one (87b)
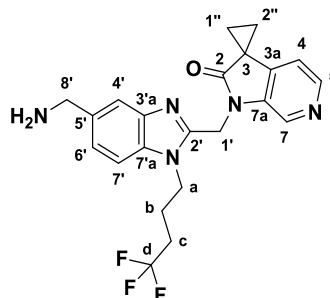
Sodium hydride (60% dispersion in oil) (10.4 mg, 0.27 mmol) was added to an ice cold solution of spiro[1*H*-pyrrolo[2,3-*c*]pyridine-3,1'-cyclopropane]-2-one (**77**) (43.4 mg, 0.27 mmol) in anhydrous *N*,*N*-dimethylformamide (3 mL). The cold bath was removed and the reaction mixture was stirred at room temperature for 1 hour. After this time, a solution of *tert*-butyl *N*-[[2-(chloromethyl)-1-(4,4,4-trifluorobutyl)benzimidazol-5-yl]methyl]carbamate (**48**) (100 mg, 0.25 mmol) in anhydrous *N*,*N*-dimethylformamide (3 mL) was added and the resulting reaction mixture was left stirring at room temperature for 16 hours. After this time, the solution was quenched with a saturated solution of sodium bicarbonate (10 mL) and the aqueous layer was extracted with ethyl acetate (2 x 5 mL). The combined organic layers were washed with brine (10 mL), dried over MgSO$_4$ and concentrated under reduced pressure. The crude material was dissolved in dichloromethane (3 mL), treated with trifluoroacetic acid (1 mL) and left stirring at room temperature for 2 hours. After this time, the volatiles were removed under reduced pressure. The residue was purified by SCX-2 ion exchange column, rinsing with methanol (2 x 3 mL) and eluting the product with 2 M solution of ammonia in methanol (2 x 3 mL). The elutes were concentrated under reduced pressure and further purified by flash column chromatography (Isco Redisep 4 g, CH$_2$Cl$_2$: MeOH: NH$_3$, 100: 0: 0 to 95: 5: 0.5) to give 1'-[[5-(aminomethyl)-1-(4,4,4-trifluorobutyl)benzimidazol-2-yl]methyl]spiro[cyclopropane-1,3'-pyrrolo[2,3-*c*]pyridine]-2'-one (**87b**) as a colourless solid (25 mg, 24% yield): m.p. 348 °C (decomposition); ^{1}H NMR (500 MHz, Methanol-*d₄*) δ$_H$ 8.41 (s, 1H, H-7), 8.25 (d, *J* = 4.9 Hz, 1H, H-5), 7.63 (s, 1H, H-4'), 7.53 (d, *J* = 8.4 Hz, 1H, H-7'), 7.36 (dd, *J* = 8.4, 1.6 Hz, 1H, H-6'), 7.15 (d, *J* = 4.9 Hz, 1H, H-4), 5.41 (s, 2H, H-1'), 4.51 – 4.36 (m, 2H, H-a), 3.91 (s, 2H, H-8'), 2.40 – 2.19 (m, 2H, H-c), 2.04 – 1.93 (m, 2H, H-b), 1.92 – 1.85 (m, 4H, H-1'' and H-2''); ^{13}C NMR (126 MHz, Methanol-*d₄*) δ$_C$ 176.0 (C-2), 148.8 (C-2'), 143.6 (C-5),141.7 (C-3'a), 141.2 (C-3a), 139.8 (C-7a), 134.2 (C-7'a), 129.0 (C-7), 125.8 (C-5'), 123.4 (C-6'), 117.5 (C-4'), 114.3 (C-4), 109.9 (C-7'), 45.3 (C-8'), 42.3 (C-a), 37.2 (C-1'), 30.3 (q, $^2J_{CF}$ = 29.6 Hz, C-c), 27.0 (C-3), 22.2 (C-b), 20.2 (C-1'' and C-

2''); LCMS (MDAP): Rt = 8.7 min (Method 4); m/z 430.2 [M+H]$^+$; HRMS (ESI) calcd for C$_{22}$H$_{23}$F$_3$N$_5$O 430.1849, found 430.1830.

References

1.   Nair, H. *et al.* Global burden of acute lower respiratory infections due to respiratory syncytial virus in young children: a systematic review and meta-analysis. *Lancet* **375,** 1545–1555 (2010).

2.   Blount, R., Morris, J. & Savage, R. Recovery of cytopathogenic agent from chimpanzees with coryza. *Proc. Soc. Exp. Biol. Med.* **92,** 544–549 (1956).

3.   Chanock, R., Roizman, B. & Myers, R. Recovery from infants with respiratory illness of a virus related to chimpanzee coryza agent (CCA). I. Isolation, properties and characterization. *Am. J. Hyg.* **66,** 281–290 (1957).

4.   Afonso, C. L., Amarasinghe, G. K. & Bányai, K. Taxonomy of the order Mononegavirales: update 2016. *Arch. Virol.* **161,** 2351–2360 (2016).

5.   Graham, B. S., Modjarrad, K. & McLellan, J. S. Novel antigens for RSV vaccines. *Curr. Opin. Immunol.* **35,** 30–38 (2015).

6.   Hall, C. B. *et al.* The burden of Respiratory Syncytial Virus infection in young children. *N. Engl. J. Med.* **360,** 588–598 (2009).

7.   Falsey, A. R., Treanor, J. J., Betts, R. F. & Walsh, E. E. Viral respiratory infections in the institutionalized elderly: clinical and epidemiologic findings. *J. Am. Geriatr. Soc.* **40,** 115–119 (1992).

8.   Thompson, W. W. Mortality associated with influenza and Respiratory Syncytial Virus in the United States. *JAMA* **289,** 179 (2003).

9.   Cianci, C. *et al.* Orally active fusion inhibitor of Respiratory Syncytial Virus. *Antimicrob. Agents Chemother.* **48,** 413–422 (2004).

10.   Elliot, A. J. & Fleming, D. M. Influenza and respiratory syncytial virus in the elderly. *Expert Rev. Vaccines* **7,** 249–258 (2008).

11.   Leader, S. & Kohlhase, K. Respiratory syncytial virus-coded pediatric hospitalizations, 1997 to 1999. *Pediatr. Infect. Dis. J.* **21,** 629–632 (2002).

12.   Shay, D. K. Bronchiolitis-associated hospitalizations among US children, 1980-1996. *JAMA* **282,** 1440 (1999).

13.   Simoes, E. A. F. Respiratory syncytial virus infection. *Lancet* **354,** 847 (1999).

14. Diagnosis and management of bronchiolitis. *Pediatrics* **118,** 1774–1793 (2006).

15. Taylor, S. *et al.* Modelling estimates of the burden of respiratory syncytial virus infection in children in the UK. *BMJ Open* **6,** e009337 (2016).

16. Glezen, W., Taber, L., Frank, A. & Kasel, J. Risk of primary infection and reinfection with respiratory syncytial virus. *Am. J. Dis. Child.* **140,** 543–546 (1986).

17. Piñeros, J. G. *et al.* Respiratory syncytial virus infection as a cause of hospitalization in population under 1 year in Colombia. *J. Pediatr. (Rio. J).* **89,** 544–548 (2013).

18. Sigurs, N. *et al.* Severe Respiratory Syncytial Virus Bronchiolitis in Infancy and Asthma and Allergy at Age 13. *Am. J. Respir. Crit. Care Med.* **171,** 137–141 (2005).

19. Knudson, C. J. & Varga, S. M. The relationship between Respiratory Syncytial Virus and asthma. *Vet. Pathol.* **52,** 97–106 (2015).

20. Simoes, E. A. F. *et al.* Palivizumab prophylaxis, Respiratory Syncytial Virus, and subsequent recurrent wheezing. *J. Pediatr.* **151,** 34–42.e1 (2007).

21. Falsey, A. R. *et al.* Respiratory Syncytial Virus infection in elderly and high-risk adults. *N. Engl. J. Med.* **352,** 1749–1759 (2005).

22. O'Caoimh, R. *et al.* Risk prediction in the community: A systematic review of case-finding instruments that predict adverse healthcare outcomes in community-dwelling older adults. *Maturitas* **82,** 3–21 (2015).

23. Whimbey, E. & Englund, J. Community respiratory virus infections in immunocompromised patients with cancer. *Am. J. Med.* **102,** 10–8; Discussion 25–6 (1997).

24. Bowden, R. Respiratory virus infections after marrow transplant: the Fred Hutchinson Cancer Research Center experience. *Am. J. Med.* **102,** 27–30; Discussion 42–3 (1997).

25. Zambon, M., Stockton, J., Clewley, J. & Fleming, D. Contribution of influenza and respiratory syncytial virus to community cases of influenza-like illness: an observational study. *Lancet* **358,** 1410–1416 (2001).

26. Walsh, E. E., Peterson, D. R. & Falsey, A. R. Is clinical recognition of Respiratory Syncytial Virus infection in hospitalized elderly and high-risk adults possible? *J. Infect. Dis.* **195,** 1046–1051 (2007).

27. Dawson-Caswell, M. & Muncie, H. Respiratory Syncytial Virus infection in children. *Am. Fam. Physician* **83,** 141–146 (2011).

28. Perkins, S. M. *et al.* Comparison of a Real-Time Reverse Transcriptase PCR assay and a culture technique for quantitative assessment of viral load in children naturally infected with Respiratory Syncytial Virus. *J. Clin. Microbiol.* **43,** 2356–2362 (2005).

29. Duncan, C. B., Walsh, E. E., Peterson, D. R., Lee, F. E. & Falsey, A. R. Risk factors for respiratory failure associated with Respiratory Syncytial Virus infection in adults. *J. Infect. Dis.* **200,** 1242–1246 (2009).

30. Simões, E. A. F. *et al.* Challenges and opportunities in developing Respiratory Syncytial Virus therapeutics. *J. Infect. Dis.* **211,** S1–S20 (2015).

31. Ginocchio, C. C. & McAdam, A. J. Current best practices for respiratory virus testing. *J. Clin. Microbiol.* **49,** S44–S48 (2011).

32. Falsey, A. Respiratory Syncytial Virus infection in adults. *Semin. Respir. Crit. Care Med.* **28,** 171–181 (2007).

33. Weisshaar, M., Cox, R. & Plemper, R. K. Blocking Respiratory Syncytial Virus entry: A story with twists. *DNA Cell Biol.* **34,** 505–510 (2015).

34. Peret, T. C. T. *et al.* Circulation patterns of group A and B human Respiratory Syncytial Virus genotypes in 5 communities in north America. *J. Infect. Dis.* **181,** 1891–1896 (2000).

35. Collins, P. L. & Graham, B. S. Viral and host factors in human Respiratory Syncytial Virus pathogenesis. *J. Virol.* **82,** 2040–2055 (2008).

36. Scott, P. D. *et al.* Molecular analysis of Respiratory Syncytial Virus reinfections in infants from coastal Kenya. *J. Infect. Dis.* **193,** 59–67 (2006).

37. Mangtani, P., Hajat, S., Kovats, S., Wilkinson, P. & Armstrong, B. The association of Respiratory Syncytial Virus infection and influenza with emergency admissions for respiratory disease in London: An analysis of routine surveillance data. *Clin. Infect. Dis.* **42,** 640–646 (2006).

38. Brief report: Respiratory Syncytial Virus activity , United States, July 2007-December 2008. (2008). Available at: https://www.cdc.gov/mmwr/preview/mmwrhtml/mm5750a3.htm.

39. Respiratory Syncytial Virus Infection (RSV): Trends and Surveillance. (2009). Available at: https://www.cdc.gov/rsv/research/us-surveillance.html.

40. Zlateva, K. T., Vijgen, L., Dekeersmaeker, N., Naranjo, C. & Van Ranst, M. Subgroup prevalence and genotype circulation patterns of human Respiratory Syncytial Virus in

Belgium during ten successive epidemic seasons. *J. Clin. Microbiol.* **45,** 3022–3030 (2007).

41.　White, L. J. *et al.* Understanding the transmission dynamics of respiratory syncytial virus using multiple time series and nested models. *Math. Biosci.* **209,** 222–239 (2007).

42.　Meerhoff, T. J., Paget, J. W., Kimpen, J. L. & Schellevis, F. Variation of Respiratory Syncytial Virus and the relation with meteorological factors in different winter seasons. *Pediatr. Infect. Dis. J.* **28,** 860–866 (2009).

43.　Medscape, anatomical line drawings. Available at: http://www.medscape.com/features/ald/resp.

44.　Johnson, J. E., Gonzales, R. A., Olson, S. J., Wright, P. F. & Graham, B. S. The histopathology of fatal untreated human respiratory syncytial virus infection. *Mod. Pathol.* **20,** 108–119 (2007).

45.　Pickles, R. J. & DeVincenzo, J. P. Respiratory syncytial virus (RSV) and its propensity for causing bronchiolitis. *J. Pathol.* **235,** 266–276 (2015).

46.　Schroeder, A. R. & Mansbach, J. M. Recent evidence on the management of bronchiolitis. *Curr. Opin. Pediatr.* **26,** 328–333 (2014).

47.　Homaira, N., Rawlinson, W., Snelling, T. L. & Jaffe, A. Effectiveness of Palivizumab in preventing RSV hospitalization in high risk children: A real-world perspective. *Int. J. Pediatr.* **2014,** 1–13 (2014).

48.　Byington, C. L. & Munoz, F. M. Palivizumab prophylaxis for healthy preterm infants: More data supporting American Academy of Pediatrics guidelines. *Pediatrics* **138,** e20161494–e20161494 (2016).

49.　The IMpact-RSV Study Group. Palivizumab, a Humanized Respiratory Syncytial Virus Monoclonal Antibody, Reduces Hospitalization From Respiratory Syncytial Virus Infection in High-risk Infants. *Pediatrics* **102,** 531–537 (1998).

50.　Meissner, H. C. *et al.* The role of immunoprophylaxis in the reduction of disease attributable to Respiratory Syncytial Virus. *Pediatrics* **124,** 1676–1679 (2009).

51.　Feltes, T. F. *et al.* Palivizumab prophylaxis reduces hospitalization due to respiratory syncytial virus in young children with hemodynamically significant congenital heart disease. *J. Pediatr.* **143,** 532–540 (2003).

52.　Sanchez, P. Immunoprophylaxis of respiratory syncytial virus disease. *Pediatr. Infect. Dis. J.* **19,** 791–801 (2000).

53. Wang, D., Bayliss, S. & Meads, C. Palivizumab for immunoprophylaxis of respiratory syncitial virus (RSV) bronchiolitis in high-risk infants and young children: a systematic review and additional economic modelling of subgroup analyses. *Health Technol. Assess. (Rockv).* **15,** (2011).

54. Smart, K. A., Lanctôt, K. L. & Paes, B. A. The cost effectiveness of palivizumab: a systematic review of the evidence. *J. Med. Econ.* **13,** 453–463 (2010).

55. Hampp, C., Kauf, T. L., Saidi, A. S. & Winterstein, A. G. Cost-effectiveness of Respiratory Syncytial Virus prophylaxis in various indications. *Arch. Pediatr. Adolesc. Med.* **165,** (2011).

56. Turner, T. *et al.* Respiratory syncytial virus: current and emerging treatment options. *Clin. Outcomes Res.* 217 (2014). doi:10.2147/CEOR.S60710

57. Rodriguez, W. *et al.* Respiratory syncytial virus (RSV) immune globulin intravenous therapy for RSV lower respiratory tract infection in infants and young children at high risk for severe RSV infections: Respiratory Syncytial Virus Immune Globulin Study Group. *Pediatrics* **99,** 454–461 (1997).

58. Veerman, M., Reuman, P., Burchfield, D. & Sherman, J. Cost-effectiveness of RespiGam at a University Teaching Hospital. *Pediatrics* **100,** 160–160 (1997).

59. Randall, G., Jensen, D. & Te, H. Mechanism of action of Ribavirin in the treatment of chronic Hepatitis C. *Gastroenterol. Hepatol.* **3,** 218–225 (2007).

60. Leyssen, P., Balzarini, J., De Clercq, E. & Neyts, J. The predominant mechanism by which Ribavirin exerts its antiviral activity in vitro against Flaviviruses and Paramyxoviruses is mediated by inhibition of IMP Dehydrogenase. *J. Virol.* **79,** 1943–1947 (2005).

61. Ventre, K. & Randolph, A. in *Cochrane Database of Systematic Reviews* (ed. Ventre, K.) (John Wiley & Sons, Ltd, 2010). doi:10.1002/14651858.CD000181.pub4

62. Kielian, M. & Rey, F. A. Virus membrane-fusion proteins: more than one way to make a hairpin. *Nat. Rev. Microbiol.* **4,** 67–76 (2006).

63. Mufson, M. A., Orvell, C., Rafnar, B. & Norrby, E. Two distinct subtypes of human Respiratory Syncytial Virus. *J. Gen. Virol.* **66,** 2111–2124 (1985).

64. Sullender, W. M. Respiratory Syncytial Virus genetic and antigenic diversity. *Clin. Microbiol. Rev.* **13,** 1–15 (2000).

65. Gilca, R. *et al.* Distribution and clinical impact of human Respiratory Syncytial Virus genotypes in hospitalized children over 2 winter seasons. *J. Infect. Dis.* **193,** 54–58

(2006).

66. Imaz, M., Sequeira, M., Carballal, G. & Cociglio, R. Clinical and epidemiologic characteristics of respiratory syncytial virus subgroups A and B infections in Santa Fe, Argentina. *J. Med. Virol.* **61,** 76–80 (2000).

67. Wu, W., Macdonald, A., Hiscox, J. A. & Barr, J. N. Different NF-κB activation characteristics of human respiratory syncytial virus subgroups A and B. *Microb. Pathog.* **52,** 184–191 (2012).

68. Collins, P. L., Fearns, R. & Graham, B. S. in *Current Topics in Microbiology and Immunology* 3–38 (2013). doi:10.1007/978-3-642-38919-1_1

69. Sun, Z., Pan, Y., Jiang, S. & Lu, L. Respiratory syncytial virus entry inhibitors targeting the F protein. *Viruses* **5,** 211–25 (2013).

70. Mastrangelo, P. & Hegele, R. G. RSV fusion: time for a new model. *Viruses* **5,** 873–85 (2013).

71. Borchers, A. T., Chang, C., Gershwin, M. E. & Gershwin, L. J. Respiratory Syncytial Virus—A comprehensive review. *Clin. Rev. Allergy Immunol.* **45,** 331–379 (2013).

72. Liu, P. *et al.* Retinoic acid-inducible gene I mediates early antiviral response and Toll-Like Receptor 3 expression in Respiratory Syncytial Virus-infected airway epithelial cells. *J. Virol.* **81,** 1401–1411 (2007).

73. Akira, S., Uematsu, S. & Takeuchi, O. Pathogen recognition and innate immunity. *Cell* **124,** 783–801 (2006).

74. MacLellan, K., Loney, C., Yeo, R. P. & Bhella, D. The 24-angstrom structure of Respiratory Syncytial Virus nucleocapsid protein-RNA decameric rings. *J. Virol.* **81,** 9519–9524 (2007).

75. Bakker, S. E. *et al.* The respiratory syncytial virus nucleoprotein-RNA complex forms a left-handed helical nucleocapsid. *J. Gen. Virol.* **94,** 1734–1738 (2013).

76. Cowton, V. M. & Fearns, R. Unravelling the complexities of respiratory syncytial virus RNA synthesis. *J. Gen. Virol.* **87,** 1805–1821 (2006).

77. Collins, P., Huang, Y. & Wertz, G. Identification of a tenth mRNA of respiratory syncytial virus and assignment of polypeptides to the 10 viral genes. *J. Virol.* **49,** 572–578 (1984).

78. Fearns, R. & Deval, J. New antiviral approaches for respiratory syncytial virus and other mononegaviruses: Inhibiting the RNA polymerase. *Antiviral Res.* **134,** 63–76 (2016).

79. Tiong-Yip, C.-L. *et al.* Characterization of a Respiratory Syncytial Virus L protein inhibitor. *Antimicrob. Agents Chemother.* **58,** 3867–3873 (2014).

80. Fuentes, S. M., Sun, D., Schmitt, A. P. & He, B. Phosphorylation of paramyxovirus phosphoprotein and its role in viral gene expression. *Future Microbiol.* **5,** 9–13 (2010).

81. Lu, B., Ma, C.-H., Brazas, R. & Jin, H. The Major phosphorylation sites of the Respiratory Syncytial Virus phosphoprotein are dispensable for virus replication in vitro. *J. Virol.* **76,** 10776–10784 (2002).

82. Castagne, N. Biochemical characterization of the respiratory syncytial virus P-P and P-N protein complexes and localization of the P protein oligomerization domain. *J. Gen. Virol.* **85,** 1643–1653 (2004).

83. Asenjo, A., González-Armas, J. C. & Villanueva, N. Phosphorylation of human respiratory syncytial virus P protein at serine 54 regulates viral uncoating. *Virology* **380,** 26–33 (2008).

84. Bailly, B. *et al.* Targeting human respiratory syncytial virus transcription anti-termination factor M2-1 to inhibit in vivo viral replication. *Sci. Rep.* **6,** 25806 (2016).

85. Tanner, S. J. *et al.* Crystal structure of the essential transcription antiterminator M2-1 protein of human respiratory syncytial virus and implications of its phosphorylation. *Proc. Natl. Acad. Sci.* **111,** 1580–1585 (2014).

86. Li, D. *et al.* Association of Respiratory Syncytial Virus M protein with viral nucleocapsids is mediated by the M2-1 protein. *J. Virol.* **82,** 8863–8870 (2008).

87. Collin, P. & Fearns, R. Role of the M2-1 Transcription Antitermination Protein of Respiratory Syncytial Virus in Sequential Transcription. *J. Virol.* **73,** 5852–5864 (1999).

88. Bermingham, A. & Collins, P. L. The M2-2 protein of human respiratory syncytial virus is a regulatory factor involved in the balance between RNA replication and transcription. *Proc. Natl. Acad. Sci.* **96,** 11259–11264 (1999).

89. Swedan, S., Andrews, J., Majumdar, T., Musiyenko, A. & Barik, S. Multiple functional domains and complexes of the two nonstructural proteins of human Respiratory Syncytial Virus contribute to interferon suppression and cellular location. *J. Virol.* **85,** 10090–10100 (2011).

90. Lo, M. S., Brazas, R. M. & Holtzman, M. J. Respiratory Syncytial Virus nonstructural proteins NS1 and NS2 mediate inhibition of Stat2 expression and alpha/beta interferon responsiveness. *J. Virol.* **79,** 9315–9319 (2005).

91. Spann, K. M., Tran, K. C. & Collins, P. L. Effects of nonstructural Proteins NS1 and NS2 of human Respiratory Syncytial Virus on interferon regulatory factor 3, NF- B, and proinflammatory cytokines. *J. Virol.* **79,** 5353–5362 (2005).

92. Bitko, V. *et al.* Nonstructural proteins of Respiratory Syncytial Virus suppress premature apoptosis by an NF- B-dependent, interferon-independent mechanism and facilitate virus growth. *J. Virol.* **81,** 1786–1795 (2007).

93. Bossert, B. & Conzelmann, K.-K. Respiratory Syncytial Virus (RSV) nonstructural (NS) proteins as host range determinants: a chimeric bovine RSV with NS genes from human RSV is attenuated in interferon-competent bovine cells. *J. Virol.* **76,** 4287–4293 (2002).

94. Hendry, R., Beeler, J. & Feldman, S. Identification of a linear heparin binding domain for human respiratory syncytial virus attachment glycoprotein G. *J. Virol.* **73,** 6610–6617 (1999).

95. Harcourt, J. L., Karron, R. A. & Tripp, R. A. Anti–G protein antibody responses to Respiratory Syncytial Virus infection or vaccination are associated with inhibition of G protein CX3C-CX3CR1 binding and leukocyte chemotaxis. *J. Infect. Dis.* **190,** 1936–1940 (2004).

96. Harcourt, J. L., Henderson, C. & Tripp, R. Respiratory syncytial virus G protein and G protein CX3C motif adversely affect CX3CR1+ T cell responses. *J. Immunol.* **176,** 1600–1608 (2006).

97. Marr, N. & Turvey, S. E. Role of human TLR4 in respiratory syncytial virus-induced NF-κB activation, viral entry and replication. *Innate Immun.* **18,** 856–865 (2012).

98. Collins, P., Hallak, L., Spillmann, D. & Peeples, M. Glycosaminoglycan sulfation requirements for respiratory syncytial virus infection. *J. Virol.* **74,** 10508–10513 (2000).

99. Tripp, R. A. *et al.* CX3C chemokine mimicry by respiratory syncytial virus G glycoprotein. *Nat. Immunol.* **2,** 732–738 (2001).

100. Wertz, G., Krieger, M. & Ball, L. Structure and cell surface maturation of the attachment glycoprotein of human respiratory syncytial virus in a cell line deficient in O glycosylation. *J. Virol.* **63,** 4767–4776 (1989).

101. Teng, M. N., Whitehead, S. S. & Collins, P. L. Contribution of the Respiratory Syncytial Virus G glycoprotein and its secreted and membrane-bound forms to virus replication in vitro and in vivo. *Virology* **289,** 283–296 (2001).

102. Techaarpornkul, S., Barretto, N. & Peeples, M. E. Functional analysis of recombinant

Respiratory Syncytial Virus deletion mutants lacking the mmall hydrophobic and/or attachment glycoprotein gene. *J. Virol.* **75,** 6825–6834 (2001).

103. Carter, S. D. *et al.* Direct visualization of the small hydrophobic protein of human respiratory syncytial virus reveals the structural basis for membrane permeability. *FEBS Lett.* **584,** 2786–2790 (2010).

104. Collins, P., Murphy, B., Whitehead, S. & Bukreyev, A. Recombinant respiratory syncytial virus from which the entire SH gene has been deleted grows efficiently in cell culture and exhibits site-specific attenuation in the respiratory tract of the mouse. *J. Virol.* **71,** 8973–8982 (1997).

105. Karron, R., Whitehead, S. S. & Adamus, J. Respiratory syncytial virus (RSV) SH and G proteins are not essential for viral replication in vitro: Clinical evaluation and molecular characterization of a cold-passaged, attenuated RSV subgroup B mutant. *Proc Natl Acad Sci U S A* **94,** 13961–13966 (1997).

106. Batonick, M., Oomens, A. G. P. & Wertz, G. W. Human Respiratory Syncytial Virus glycoproteins are not required for apical targeting and release from polarized epithelial cells. *J. Virol.* **82,** 8664–8672 (2008).

107. Walsh, E. & Hruska, J. Monoclonal antibodies to respiratory syncytial virus proteins: identification of the fusion protein. *J. Virol.* **47,** 171–177 (1983).

108. Tajrishi, M. M., Tuteja, R. & Tuteja, N. Nucleolin. *Commun. Integr. Biol.* **4,** 267–275 (2011).

109. Koutsioumpa, M. & Papadimitriou, E. *Cell surface nucleolin as a target for anti-cancer therapies*. *Recent Patents on Anti-Cancer Drug Discovery* **9,** (2014).

110. DeVincenzo, J. P. The promise, pitfalls and progress of RNA-interference-based antiviral therapy for respiratory viruses. *Antivir. Ther.* **17,** 213–225 (2012).

111. Challa, S. *et al.* Mechanism of action for Respiratory Syncytial Virus inhibitor RSV604. *Antimicrob. Agents Chemother.* **59,** 1080–1087 (2015).

112. Chapman, J. *et al.* RSV604, a novel inhibitor of Respiratory Syncytial Virus replication. *Antimicrob. Agents Chemother.* **51,** 3346–3353 (2007).

113. Schibli, D. J. & Weissenhorn, W. Class I and class II viral fusion protein structures reveal similar principles in membrane fusion (Review). *Mol. Membr. Biol.* **21,** 361–371 (2004).

114. White, J. M., Delos, S. E., Brecher, M. & Schornberg, K. Structures and mechanisms of viral membrane fusion proteins: Multiple variations on a common theme. *Crit. Rev.*

Biochem. Mol. Biol. **43,** 189–219 (2008).

115. Melero, J. A. & Mas, V. The Pneumovirinae fusion (F) protein: A common target for vaccines and antivirals. *Virus Res.* **209,** (2015).

116. Colman, P. M. & Lawrence, M. C. The structural biology of type I viral membrane fusion. *Nat. Rev. Mol. Cell Biol.* **4,** 309–319 (2003).

117. Calder, L. J. *et al.* Electron microscopy of the human Respiratory Syncytial Virus fusion protein and complexes that it forms with monoclonal antibodies. *Virology* **271,** 122–131 (2000).

118. Collins, P., Huang, Y. & Wertz, G. W. Nucleotide sequence of the gene encoding the fusion (F) glycoprotein of human respiratory syncytial virus. *Proc Natl Acad Sci U S A* **81,** 7683–7687 (1984).

119. McLellan, J. S. *et al.* Structure of RSV fusion glycoprotein trimer bound to a prefusion-specific neutralizing antibody. *Science* **340,** (2013).

120. Baker, K., Dutch, R. E., Lamb, R. a & Jardetzky, T. S. Structural basis for paramyxovirus-mediated membrane fusion. *Mol. Cell* **3,** 309–319 (1999).

121. Cianci, C. *et al.* Targeting a binding pocket within the trimer-of-hairpins: small-molecule inhibition of viral fusion. *Proc. Natl. Acad. Sci. U. S. A.* **101,** 15046–51 (2004).

122. Roymans, D. *et al.* Binding of a potent small-molecule inhibitor of six-helix bundle formation requires interactions with both heptad-repeats of the RSV fusion protein. *Proc. Natl. Acad. Sci.* **107,** 308–313 (2010).

123. Battles, M. B. *et al.* Molecular mechanism of respiratory syncytial virus fusion inhibitors. *Nat. Chem. Biol.* **12,** 87–93 (2015).

124. Samuel, D. *et al.* GS-5806 inhibits pre- to postfusion conformational changes of the Respiratory Syncytial Virus fusion protein. *Antimicrob. Agents Chemother.* **59,** 7109–7112 (2015).

125. Yu, K.-L., Civiello, R. L., Krystal, M., Kadow, K. F. & Meanwell, N. a. WO00/004900: Substituted benzimidazole antiviral agents. (2000).

126. Yu, K.-L., Civiello, R. L., Combrink, K. D. & Meanwell, N. a. WO01/95910: Imidazopyridine and imidazopyrimidine antiviral agents. (2001).

127. Yu, K.-L., Civiello, R. L., Meanwell, N. a & Combrink, K. D. WO02/26228: Benzimidazolone antiviral agents. (2002).

128. Civiello, R. L., Yu, K.-L., Combrink, K. D., Meanwell, N. a & Cianci, C. W. WO03/053344: Substituted 2-methyl benzimidazole RSV antiviral agents. (2003).

129. Yu, K. *et al.* Respiratory syncytial virus inhibitors. Part 2: Benzimidazol-2-one derivatives. *Bioorg. Med. Chem. Lett.* **14,** 1133–7 (2004).

130. Yu, K.-L. *et al.* Respiratory syncytial virus fusion inhibitors. Part 3: Water-soluble benzimidazol-2-one derivatives with antiviral activity in vivo. *Bioorg. Med. Chem. Lett.* **16,** 1115–1122 (2006).

131. Yu, K.-L. L. *et al.* Respiratory syncytial virus fusion inhibitors. Part 4: optimization for oral bioavailability. *Bioorg. Med. Chem. Lett.* **17,** 895–901 (2007).

132. Wang, X. A. *et al.* Respiratory syncytial virus fusion inhibitors. Part 5: Optimization of benzimidazole substitution patterns towards derivatives with improved activity. *Bioorg. Med. Chem. Lett.* **17,** 4592–8 (2007).

133. Combrink, K. D. *et al.* Respiratory syncytial virus fusion inhibitors. Part 6: an examination of the effect of structural variation of the benzimidazol-2-one heterocycle moiety. *Bioorg. Med. Chem. Lett.* **17,** 4784–90 (2007).

134. Sin, N. *et al.* Respiratory syncytial virus fusion inhibitors. Part 7: Structure–activity relationships associated with a series of isatin oximes that demonstrate antiviral activity in vivo. *Bioorg. Med. Chem. Lett.* **19,** 4857–4862 (2009).

135. Yu, K.-L. L. *et al.* Fundamental structure–activity relationships associated with a new structural class of respiratory syncytial virus inhibitor. *Bioorg. Med. Chem. Lett.* **13,** 2141–2144 (2003).

136. Cianci, C. *et al.* Oral efficacy of a Respiratory Syncytial Virus inhibitor in rodent models of infection. *Antimicrob. Agents Chemother.* **48,** 2448–2454 (2004).

137. Janssens, F. *et al.* WO01/00611: Respiratory syncytial virus replication inhibitors. (2000).

138. Janssens, F., Meersman, K., Sommen, F. & Andries, K. WO01/00612: Respiratory syncytial virus replication inhibitors. (2000).

139. Janssens, F., Lacrampe, J., Guillemont, J. & Venet, M. WO00/100615: Respiratory syncytial virus replication inhibitors. (2001).

140. Wyde, P. R., Andries, K. & Gilbert, B. E. Short duration aerosols of JNJ 2408068 (R170591) administered prophylactically or therapeutically protect cotton rats from experimental respiratory syncytial virus infection. *Antiviral Res.* **60,** 221–231 (2003).

141. Wyde, P. R., Janssens, F., Lacrampe, J. & Andries, K. Substituted benzimidazoles with nanomolar activity against respiratory syncytial virus. *Antiviral Res.* **60,** 209–219 (2003).

142. Bonfanti, J.-F. *et al.* Selection of a respiratory syncytial virus fusion inhibitor clinical candidate, part 1: improving the pharmacokinetic profile using the structure-property relationship. *J. Med. Chem.* **50,** 4572–84 (2007).

143. Bonfanti, J.-F. *et al.* Selection of a respiratory syncytial virus fusion inhibitor clinical candidate. 2. Discovery of a morpholinopropylaminobenzimidazole derivative (TMC353121). *J. Med. Chem.* **51,** 875–96 (2008).

144. Olszewska, W. *et al.* Antiviral and lung protective activity of a novel respiratory syncytial virus fusion inhibitor in a mouse model. *Eur. Respir. J.* **38,** 401–408 (2011).

145. Nikitenko, a a, Raifeld, Y. E. & Wang, T. Z. The discovery of RFI-641 as a potent and selective inhibitor of the respiratory syncytial virus. *Bioorg. Med. Chem. Lett.* **11,** 1041–1044 (2001).

146. Razinkov, V., Huntley, C. & Ellestad, G. RSV entry inhibitors block F-protein mediated fusion with model membranes. *Antiviral Res.* **55,** 189–200 (2002).

147. Huntley, C. C. *et al.* RFI-641, a potent respiratory syncytial virus inhibitor. *Antimicrob. Agents Chemother.* **46,** 841–847 (2002).

148. Weiss, W. J. *et al.* Inhalation efficacy of RFI-641 in an African green monkey model of RSV infection. *J. Med. Primatol.* **32,** 82–88 (2003).

149. Bond, S., Sanford, V., Lambert, J. & Draffan, A. G. WO05/061513: polycyclic agents for the treatment of respiratory syncytial virus infections. (2005).

150. Bond, S. *et al.* 1,2,3,9b-Tetrahydro-5H-imidazo[2,1-a]isoindol-5-ones as a new class of respiratory syncytial virus (RSV) fusion inhibitors. Part 2: Identification of BTA9881 as a preclinical candidate. *Bioorg. Med. Chem. Lett.* **25,** 976–981 (2015).

151. Wyde, P. R. *et al.* Antiviral efficacy of VP14637 against respiratory syncytial virus in vitro and in cotton rats following delivery by small droplet aerosol. *Antiviral Res.* **68,** 18–26 (2005).

152. Douglas, J. L., Panis, M. L. & Lin, K. Inhibition of respiratory syncytial virus fusion by the small molecule VP-14637 via specific interactions with F protein. *J. Virol.* **77,** 5054–5064 (2003).

153. Roymans, D. & Koul, A. in *Human Respiratory Syncytial Virus Infection* (InTech, 2011). doi:10.5772/26528

154. van Bleek, G. M., Osterhaus, A. D. M. E. & de Swart, R. L. RSV 2010: Recent advances in research on respiratory syncytial virus and other pneumoviruses. *Vaccine* **29,** 7285–7291 (2011).

155. Blade, H. *et al.* WO2010/103306: Benzimidazole derivatives and their use as antiviral agents. (2010).

156. Cockerill, S., Pilkington, C., Lumley, J., Angell, R. & Mathews, N. WO2013/068769: Pharmaceutical compounds. (2013).

157. Paradowski, M. *et al.* WO2016/055780: Spiro-indolines for the treatment and prophylaxis of respiratory syncytial virus infection (RSV). (2016).

158. Cockerill, S. *et al.* The preclinical characterisation of RV-521, an orally bioavailable inhibitor of RSV. in *RSV 16, 10th International Respiratory Syncytial Virus Symposium* (2016).

159. ReViral initiates Phase 1 clinical trial of potent oral inhibitor against Respiratory Syncytial Virus. (2016). Available at: http://www.reviral.co.uk/news/23/79/ReViral-initiates-Phase-1-clinical-trial-of-potent-oral-inhibitor-against-Respiratory-Syncytial-Virus.html.

160. Chungen Liang, Lisha Wang, HongYing Yun, X. Z. US2013/0090328: Compounds for the treatment and prophylaxis of Respiratory Syncytial Virus disease. (2013).

161. Chen, L. *et al.* WO2013/020993: Compounds for the treatment and prophylaxis of Respiratory Syncytial Virus disease. (2013).

162. Feng, S. *et al.* Discovery of imidazopyridine derivatives as highly potent Respiratory Syncytial Virus fusion inhibitors. *ACS Med. Chem. Lett.* **6,** 359–362 (2015).

163. Feng, S., Hong, D., Wang, L., Yun, H. & Zhao, S. WO2014/009302: Novel indazoles for the treatment and prophylaxis of respiratory syncytial virus infection.

164. Feng, S. *et al.* WO2014/184163: Preparation of aza-oxo-indoles for the treatment and prophylaxis of respiratory syncytial virus infection. (2014).

165. Gao, L. *et al.* WO2015/022263: Novel aza-oxo-indoles for the treatment and prophylaxis of Syncytial Virus Infection. (2015).

166. Wang, L., Yun, H., Zhan, W. & Zhen, X. WO2015/022301: Novel aza-oxo-indoles for the treatment and prophylaxis of Syncytial Virus Infection. (2015).

167. Siegel, D., Sperandio, D., Parrish, J. P., Yang, H. & Sangi, M. WO2013/158776:

Compounds and methods for antiviral treatment. (2013).

168. Babaoglu, K. *et al.* WO2011/163518: Pyrazolo[1,5-a] pyrimidines as antiviral agents. (2011).

169. Jansa, P., Mackman, R., Parrish, J. P., Siegel, D. & Sperandio, D. WO2013/096681: Pyrazolo[1,5-a] pyrimidines as antiviral agents. (2013).

170. Mackman, R. L. *et al.* Discovery of an oral respiratory syncytial virus (RSV) fusion inhibitor (GS-5806) and clinical proof of concept in a human RSV challenge study. *J. Med. Chem.* **58,** 1630–1643 (2015).

171. Xin, Y. *et al. IDWeek, San Diego, CA: Drug-Interaction profile of Presatovir (GS-5806).* (2015).

172. Eisenberg, E. J. *et al. IDWeek, San Diego, CA: Presatovir (GS-5806), a novel fusion inhibitor of Respiratory Syncytial Virus , delivers high respiratory tract levels in non-clinical species*. (2015).

173. Cooymans, L. P. *et al.* WO2012/080446: Preparation of benzimidazole derivatives for use as respiratory syncytial virus inhibitors. (2012).

174. Cooymans, L. P. *et al.* WO2012/080447: Preparation of indolylmethylimidazopyridinone derivatives and analogs for use as respiratory syncytial virus antiviral agents. (2012).

175. Demin, S. D., Jonkers, T. H. M., Raboisson, P. J.-M. B., Tahri, A. & Vendeville, Sandrine, M. H. WO2012/080449: Azabenzimidazoles as respiratory syncytial virus antiviral agents. (2012).

176. Cooymans, L. P., Jonckers, tim hugo maria, Raboisson, P. J.-M. B., Tahri, A. & Vendeville, Sandrine, M. H. WO2012/080451: Preparation of imidazopyridine derivatives for use as respiratory syncytial virus antiviral agents. (2012).

177. Vendeville, Sandrine, M. H., Tahri, A., Jonkers, T. H. M. & Raboisson, P. J.-M. B. WO2013/186332: 4-substituted 1,3-dihydro-2H-benzimidazol-2-one derivatives substituted with benzimidazoles as respiratory syncytial virus antiviral agents. (2013).

178. Vendeville, Sandrine, M. H. *et al.* WO2013/186335: 1,3-dihydro-2H-benzimidazol-2-one derivatives substituted with heterocycles as respiratory syncytial virus antiviral agents. (2013).

179. Tahri, A. *et al.* WO2014/060411: Preparation of indolylmethylspiropiperidinepyrrolopyridinone derivatives and analogs for use as RSV inhibitors. (2014).

180. Ackermann, M., Rigaux, P., Gallup, J. & Roymans, D. Therapeutic efficacy of JNJ-53718678, a RSV fusion inhibitor in neonatal lambs. in *RSV16 10th International Respiratory Syncytial Virus Symposium,* (2016).

181. Mayes, P. A., Mitchell, J. P., Draffan, A. G., Pitt, G. & Andreson, K. WO2012/068622: Compounds for treating RSV infections. (2012).

182. Mitchell, J. P., Pitt, G., Draffan, A. G. & Mayes, P. A. WO2011/094823: Compounds for treating RSV infections. (2011).

183. Pitt, G., Mayes, P. A. & Andrau, L. WO2013/020164: Compounds for treating RSV infections. (2013).

184. Draffan, A. G., Mitchell, J. P., Pitt, G., Halim, R. & Vernachio, J. WO2016/133888: Compounds for treating RSV infections. (2016).

185. Brochu, C., Decor, A., Ghiro, E. & Pesant, M. WO2015/065336: RSV inhibitors. (2015).

186. Sturino, C., Halmos, T., Decor, A., Duplessis, M. & Deroy, P. WO2015/065338: Quinazoline based RSV inhibitors. (2015).

187. MIV-323 for the treatment of RSV infection. Available at: http://www.medivir.se/v5/en/RnD/proj_MIV-323.cfm.

188. Hunt, S., Onions, S., Fordyce, E. & Murray, P. WO2016/055792: Novel 5,6-dihydro-4H-benzo[b] thieno[2,3-d] azepine derivatives. (2016).

189. Hunt, S., Onions, S., Fordyce, E. & Murray, P. WO2016/055791: novel 5,6-dihydro-4H-benzo[b] thieno-[2,3-d] azepine derivatives. (2016).

190. Pryde, D. C. *et al.* Non-benzimidazole containing inhibitors of respiratory syncytial virus. *Bioorganic Med. Chem. Lett.* **23,** 827–833 (2013).

191. Zheng, X. *et al.* Discovery of piperazinylquinoline derivatives as novel Respiratory Syncytial Virus fusion inhibitors. *ACS Med. Chem. Lett.* **7,** 558–562 (2016).

192. DeVincenzo, J. P. *et al.* Oral GS-5806 activity in a respiratory syncytial virus challenge study. *N. Engl. J. Med.* **371,** (2014).

193. Ark Biosciences Initiates VICTOR Study. (2016). Available at: http://www.arkbiosciences.com/news.asp?ClassID=439.

194. Aviragen Therapeutics announces top-line Results from Phase 2a RSV challenge study of BTA585. (2017). Available at: http://investors.aviragentherapeutics.com/releasedetail.cfm?releaseid=1010067.

195. Modjarrad, K., Giersing, B., Kaslow, D. C., Smith, P. G. & Moorthy, V. S. WHO consultation on Respiratory Syncytial Virus vaccine development report from a World Health Organization meeting held on 23–24 March 2015. *Vaccine* **34,** 190–197 (2016).

196. Rudraraju, R., Jones, B., Sealy, R., Surman, S. & Hurwitz, J. Respiratory Syncytial Virus: Current progress in vaccine development. *Viruses* **5,** 577–594 (2013).

197. Anderson, L. J. *et al.* Strategic priorities for respiratory syncytial virus (RSV) vaccine development. *Vaccine* **31,** B209–B215 (2013).

198. Neuzil, K. M. Progress toward a Respiratory Syncytial Virus Vaccine. *Clin. Vaccine Immunol.* **23,** 186–188 (2016).

199. Chin, J., Magoffin, R. L., Shearer, L. A., Schieble, J. H. & Lennette, E. H. Field evaluation of a respiratory syncytial virus vaccine and a trivalent parainfluenza virus vaccine in a pediatric population. *Am. J. Epidemiol.* **89,** 449–63 (1969).

200. Graham, B. S. Biological challenges and technological opportunities for respiratory syncytial virus vaccine development. *Immunol. Rev.* **239,** 149–166 (2011).

201. Gregory, A. E., Titball, R. & Williamson, D. Vaccine delivery using nanoparticles. *Front. Cell. Infect. Microbiol.* **3,** (2013).

202. Hurwitz, J. L. Respiratory syncytial virus vaccine development. *Expert Rev. Vaccines* **10,** 1415–33 (2011).

203. Kim, E. *et al.* Development of an adenovirus-based Respiratory Syncytial Virus vaccine: preclinical evaluation of efficacy, immunogenicity, and enhanced disease in a cotton rat model. *J. Virol.* **88,** 5100–5108 (2014).

204. Carbonell-Estrany, X. *et al.* Motavizumab for prophylaxis of Respiratory Syncytial Virus in high-risk children: A non-inferiority trial. *Pediatrics* **125,** e35–e51 (2010).

205. Lo, J. & Charron, R. *Respiratory Syncytial Virus: High incidence + few interventions = large market opportunity*. *Therapeutic Markets: Opportunities and Pipeline Analysis* (2010).

206. *Respiratory Syncytial Virus (RSV) – Market size, share, analysis, growth, outlook, 2024: Acute market reports*. (2016).

207. Olszewska, W. & Openshaw, P. Emerging drugs for respiratory syncytial virus infection. *Expert Opin. Emerg. Drugs* **14,** 207–17 (2009).

208. Storey, S. Respiratory syncytial virus market. *Nat. Rev. Drug Discov.* **9,** 15–6 (2010).

209. Yu, K.-L. *et al.* WO01/95910A2: Preparation of imidazopyridine and imidazopyrimidine antiviral agents. (2001).

210. Bonfanti, J.-F. & Roymans, D. Prospects for the development of fusion inhibitors to treat human respiratory syncytial virus infection. *Curr. Opin. Drug Discov. Devel.* **12,** 479–87 (2009).

211. Wang, G. *et al.* Discovery of 4'-chloromethyl-2'-deoxy-3',5'-di- O -isobutyryl-2'-fluorocytidine (ALS-8176), a first-in-Class RSV polymerase inhibitor for treatment of human Respiratory Syncytial Virus infection. *J. Med. Chem.* **58,** 1862–1878 (2015).

212. Gleeson, M. P. Plasma protein binding affinity and its relationship to molecular structure: An in-silico analysis. *J. Med. Chem.* **50,** 101–112 (2007).

213. Gleeson, M. P. Generation of a set of simple, interpretable ADMET rules of thumb. *J. Med. Chem.* **51,** 817–834 (2008).

214. Hann, M. M. & Keserü, G. M. Finding the sweet spot: the role of nature and nurture in medicinal chemistry. *Nat. Rev. Drug Discov.* **11,** 355–365 (2012).

215. Hughes, J. D. *et al.* Physiochemical drug properties associated with in vivo toxicological outcomes. *Bioorg. Med. Chem. Lett.* **18,** 4872–4875 (2008).

216. Leeson, P. D. & Springthorpe, B. The influence of drug-like concepts on decision-making in medicinal chemistry. *Nat. Rev. Drug Discov.* **6,** 881–890 (2007).

217. Hopkins, A. L., Keserü, G. M., Leeson, P. D., Rees, D. C. & Reynolds, C. H. The role of ligand efficiency metrics in drug discovery. *Nat. Rev. Drug Discov.* **13,** 105–121 (2014).

218. Ryckmans, T. *et al.* Rapid assessment of a novel series of selective CB2 agonists using parallel synthesis protocols: A Lipophilic Efficiency (LiPE) analysis. *Bioorg. Med. Chem. Lett.* **19,** 4406–4409 (2009).

219. Tarcsay, Á., Nyíri, K. & Keserű, G. M. Impact of lipophilic efficiency on compound quality. *J. Med. Chem.* **55,** 1252–1260 (2012).

220. Hann, M. M. Molecular obesity, potency and other addictions in drug discovery. *Multifaceted Roles Crystallogr. Mod. Drug Discov.* **2,** 183–196 (2015).

221. Shultz, M. D. Setting expectations in molecular optimizations: Strengths and limitations of commonly used composite parameters. *Bioorg. Med. Chem. Lett.* **23,** 5980–5991 (2013).

222. Freeman-Cook, K. D., Hoffman, R. L. & Johnson, T. W. Lipophilic efficiency: the most

important efficiency metric in medicinal chemistry. *Future Med. Chem.* **5,** 113–115 (2013).

223. Wager, T. T. *et al.* Defining desirable central nervous system drug space through the alignment of molecular properties, in vitro ADME, and safety attributes. *ACS Chem. Neurosci.* **1,** 420–434 (2010).

224. Hopkins, A. L., Keserü, G. M., Leeson, P. D., Rees, D. C. & Reynolds, C. H. The role of ligand efficiency metrics in drug discovery. *Nat. Rev. Drug Discov.* **13,** 105–121 (2014).

225. Shultz, M. D. *et al.* Structure–Efficiency Relationship of [1,2,4]Triazol-3-ylamines as Novel Nicotinamide Isosteres that Inhibit Tankyrases. *J. Med. Chem.* **56,** 7049–7059 (2013).

226. Ward, S. E. & Davis, A. *The handbook of medicinal chemistry : Principles and practice*. (Royal Society of Chemistry, 2015).

227. Kerns, E. & Di, L. *Drug-like properties: Concepts, structure design and methods, from ADME to toxicity optimization*. (Academic Press).

228. Griebel, G. *et al.* Anxiolytic- and antidepressant-like effects of the non-peptide vasopressin V1b receptor antagonist, SSR149415, suggest an innovative approach for the treatment of stress-related disorders. *Proc. Natl. Acad. Sci.* **99,** 6370–6375 (2002).

229. Liu, X.-L. *et al.* A highly efficient and eco-friendly method for the synthesis of 1,3-indandione ring-fused 3-oxindoles bearing two contiguous quaternary stereocenters via an aldol reaction in aqueous media. *Org. Biomol. Chem.* **13,** 601–611 (2015).

230. Tan, Y. *et al.* Enantioselective synthesis of spirooxindole benzoquinolizines via organo-catalyzed cascade reactions. *Org. Biomol. Chem.* **4,** 1166–1169 (2016).

231. Kong, K. *et al.* An enantioselective total synthesis and stereochemical revision of (+)-citrinadin B. *J. Am. Chem. Soc.* **135,** 10890–3 (2013).

232. Zheng, Y., Tice, C. M. & Singh, S. B. The use of spirocyclic scaffolds in drug discovery. *Bioorg. Med. Chem. Lett.* **24,** 3673–3682 (2014).

233. Jossang, A., Jossang, P., Hadi, H. A., Sevenet, T. & Bodo, B. Horsfiline, an oxindole alkaloid from Horsfieldia superba. *J. Org. Chem.* **56,** 6527–6530 (1991).

234. Budovská, M., Kutschy, P., Kožár, T., Gondová, T. & Petrovaj, J. Synthesis of spiroindoline phytoalexin (S)-(−)-spirobrassinin and its unnatural (R)-(+)-enantiomer. *Tetrahedron* **69,** 1092–1104 (2013).

235. Cui, C.-B., Kakeya, H. & Osada, H. Novel mammalian cell cycle inhibitors, spirotryprostatins A and B, produced by Aspergillus fumigatus, which inhibit mammalian cell cycle at G2/M phase. *Tetrahedron* **52,** 12651–12666 (1996).

236. Rottmann, M. *et al.* Spiroindolones, a potent compound class for the treatment of malaria. *Science (80-.).* **329,** 1175–1180 (2010).

237. Zheng, M. *et al.* Efficacy of MDM2 inhibitor MI-219 against lung cancer cells alone or in combination with MDM2 knockdown, a XIAP inhibitor or etoposide. *Anticancer Res.* **30,** 3321–31 (2010).

238. Sosin, A. M. *et al.* HDM2 antagonist MI-219 (spiro-oxindole), but not Nutlin-3 (cis-imidazoline), regulates p53 through enhanced HDM2 autoubiquitination and degradation in human malignant B-cell lymphomas. *J. Hematol. Oncol.* **5,** 57 (2012).

239. Ball-Jones, N. R., Badillo, J. J. & Franz, A. K. Strategies for the enantioselective synthesis of spirooxindoles. *Org. Biomol. Chem.* **10,** 5165 (2012).

240. Pavlovska, T. L., Redkin, R. G., Lipson, V. V. & Atamanuk, D. V. Molecular diversity of spirooxindoles. Synthesis and biological activity. *Mol. Divers.* (2015). doi:10.1007/s11030-015-9629-8

241. Yu, B., Yu, D.-Q. & Liu, H.-M. Spirooxindoles: Promising scaffolds for anticancer agents. *Eur. J. Med. Chem.* **97,** 673–698 (2015).

242. Cao, Z.-Y. & Zhou, J. Catalytic asymmetric synthesis of polysubstituted spirocyclopropyl oxindoles: organocatalysis versus transition metal catalysis. *Org. Chem. Front.* **2,** 849–858 (2015).

243. Trost, B. & Brennan, M. Asymmetric syntheses of oxindole and indole spirocyclic alkaloid natural products. *Synthesis (Stuttg).* **2009,** 3003–3025 (2009).

244. Frost, J. R., Huber, S. M., Breitenlechner, S., Bannwarth, C. & Bach, T. Enantiotopos-selective C-H Oxygenation catalyzed by a supramolecular ruthenium complex. *Angew. Chemie Int. Ed.* **54,** 691–695 (2015).

245. Zhou, F. *et al.* Asymmetric copper(I)-catalyzed azide-alkyne cycloaddition to quaternary oxindoles. *J. Am. Chem. Soc.* **135,** 10994–10997 (2013).

246. Winter, B. Spirocyclic ethers related to ambrox: synthesis and structure-odor relationships. *Helv. Chim. Acta* **87,** 1616–1627 (2004).

247. Bernardinelli, G., Schneider, P., Aizenberg, M. & Winter, B. Synthesis and optical resolution of the floral odorant 2 , 3-dihydro-2 , 5- dimethyl-1 H -indene-2-methanol ,

and preparation of analogues. *Helv. Chim. Acta* **88,** 3109–3117 (2005).

248. Xu, R. *et al.* An improved synthesis of 2-oxa-7-azaspiro[3,5]nonane and analogs as novel reagents in medicinal chemistry. *Tetrahedron Lett.* **52,** 3266–3270 (2011).

249. Radchenko, D. S. *et al.* Cyclobutane-derived diamines: synthesis and molecular structure. *J. Org. Chem.* **75,** 5941–52 (2010).

250. Miller, R. A., Lang, F., Marcune, B., Zewge, D. & Song, Z. J. A practical process for the preparation of azetidine-3-carboxylic acid. *Synth. Commun.* **33,** 3347–3353 (2003).

251. Gonzalez-Lopez de Turiso, F. *et al.* Discovery and in vivo evaluation of dual PI3Kβ/δ inhibitors. *J. Med. Chem.* **55,** 7667–85 (2012).

252. Gentry, P. R. *et al.* Discovery of ML326: The first sub-micromolar, selective M5 PAM. *Bioorg. Med. Chem. Lett.* **23,** 2996–3000 (2013).

253. Roy, A., Achari, B. & Mandal, S. B. An easy access to spiroannulated glyco-oxetane, -thietane and -azetane rings: synthesis of spironucleosides. *Tetrahedron Lett.* **47,** 3875–3879 (2006).

254. Dong, J. & Xu, J. Facile synthesis of thietanes via ring expansion of thiiranes. *Org. Biomol. Chem.* **15,** 836–844 (2017).

255. Lee, S. & Hartwig, J. F. Improved catalysts for the palladium-catalyzed synthesis of oxindoles by amide α-arylation. Rate acceleration, use of aryl chloride substrates, and a new carbene ligand for asymmetric transformations. *J. Org. Chem.* **66,** 3402–3415 (2001).

256. De Carvalho, G. S. G., Fourrey, J. L., Dodd, R. H. & Da Silva, A. D. Synthesis of a 4',4'-spirothietane-2', N3-cycloadenosine as a highly constrained analogue of 5'-deoxy-5'-methylthioadenosine (MTA). *Tetrahedron Lett.* **50,** 463–466 (2009).

257. Alberico, D., Scott, M. E. & Lautens, M. Aryl-aryl bond formation by transition-metal-catalyzed direct arylation. *Chem. Rev.* **107,** 174–238 (2007).

258. Chen, X., Engle, K. M., Wang, D. H. & Jin-Quan, Y. Palladium(II)-catalyzed C-H activation/C-C cross-coupling reactions: Versatility and practicality. *Angew. Chemie - Int. Ed.* **48,** 5094–5115 (2009).

259. Ashenhurst, J. A. Intermolecular oxidative cross-coupling of arenes. *Chem. Soc. Rev.* **39,** 540–548 (2010).

260. Ackermann, L., Vicente, R. & Kapdi, A. R. Transition-metal-catalyzed direct arylation of

(hetero)arenes by C-H bond cleavage. *Angew. Chemie - Int. Ed.* **48,** 9792–9826 (2009).

261. Parella, R. & Babu, S. A. Regio- and Stereoselective Pd-Catalyzed Direct Arylation of Unactivated sp 3 C(3)–H Bonds of Tetrahydrofuran and 1,4-Benzodioxane Systems. *J. Org. Chem.* **80,** 2339–2355 (2015).

262. Jazzar, R., Hitce, J., Renaudat, A., Sofack-Kreutzer, J. & Baudoin, O. Functionalization of organic molecules by transition-metal-catalyzed C(sp3)-H activation. *Chem. - A Eur. J.* **16,** 2654–2672 (2010).

263. Ladd, C. L., Sustac Roman, D. & Charette, A. B. Silver-promoted, palladium-catalyzed direct arylation of cyclopropanes: Facile access to spiro 3,3'-cyclopropyl oxindoles. *Org. Lett.* **15,** 1350–1353 (2013).

264. Saget, T. & Cramer, N. Palladium(0)-catalyzed enantioselective C-H arylation of cyclopropanes: Efficient access to functionalized tetrahydroquinolines. *Angew. Chemie - Int. Ed.* **51,** 12842–12845 (2012).

265. Gutekunst, W. R., Gianatassio, R. & Baran, P. S. Sequential C sp3-H arylation and olefination: Total synthesis of the proposed structure of pipercyclobutanamide a. *Angew. Chemie - Int. Ed.* **51,** 7507–7510 (2012).

266. Saget, T., Perez, D. & Cramer, N. Synthesis of functionalized spiroindolines via palladium-catalyzed methine C-H arylation. *Org. Lett.* **15,** 1354–1357 (2013).

267. Roman, D. S. & Charette, A. B. C-H functionalization of cyclopropanes: A practical approach employing a picolinamide auxiliary. *Org. Lett.* **15,** 4394–4397 (2013).

268. Affron, D. P., Davis, O. A. & Bull, J. A. Regio- and stereospecific synthesis of C-3 functionalized proline derivatives by palladium catalyzed directed C(sp3)–H arylation. *Org. Lett.* **16,** 4956–4959 (2014).

269. Maison, W., Deppermann, N., Thomanek, H. & Prenzel, A. H. G. P. Pd-catalyzed assembly of spirooxindole natural products: A short synthesis of horsfiline. *J. Org. Chem.* **75,** 5994–6000 (2010).

270. Shore, G., Morin, S., Mallik, D. & Organ, M. G. Pd PEPPSI-iPr-mediated reactions in metal-coated capillaries under MACOS: The synthesis of indoles by sequential aryl amination/ Heck coupling. *Chem. - A Eur. J.* **14,** 1351–1356 (2008).

271. Chen, D. & Xu, M.-H. Zn-mediated asymmetric allylation of N-tert-butanesulfinyl ketimines: an efficient and practical access to chiral quaternary 3-aminooxindoles. *Chem. Commun. (Camb).* **49,** 1327–9 (2013).

272. Sano, D., Nagata, K. & Itoh, T. Catalytic asymmetric hydroxylation of oxindoles by molecular oxygen using a phase-transfer catalyst. *Org. Lett.* **10,** 1593–1595 (2008).

273. Chafeev, M. *et al.* WO 2010/045251: Spiro-oxindole compounds and their use as therapeutic agents in the treatment of sodium channel-mediated diseases and their preparationitle. (2010).

274. Jung, M. E. & Koch, P. Mild, selective deprotection of PMB ethers with triflic acid/1,3-dimethoxybenzene. *Tetrahedron Lett.* **52,** 6051–6054 (2011).

275. De Medeiros, E. F., Herbert, J. M. & Taylor, R. J. K. The synthesis and absolute configuration of the novel ichthyotoxic diacyiglycerols, umbraculumin A and umbraculumin C. *J. Chem. Soc. Perkin Trans. 1* 2725 (1991). doi:10.1039/p19910002725

276. Wuts, P. G. M. & Greene, T. W. *Greene's Protective Groups in Organic Synthesis*. (John Wiley & Sons, Inc., 2006). doi:10.1002/0470053488

277. Sarraf, D., Richy, N. & Vidal, J. Synthesis of lactams by isomerization of oxindoles substituted at C-3 by an ω-amino chain. *J. Org. Chem.* **79,** 10945–10955 (2014).

278. Stevens, F. C. *et al.* Potent oxindole based human β3 adrenergic receptor agonists. *Bioorg. Med. Chem. Lett.* **17,** 6270–6273 (2007).

279. Chandler, B. D., Roland, J. T., Li, Y. & Sorensen, E. J. Seebach's conjunctive reagent enables double cyclizations. *Org. Lett.* **12,** 2746–2749 (2010).

280. Arizpe, A., Sayago, F. J., Jiménez, A. I., Ordóñez, M. & Cativiela, C. Stereodivergent synthesis of two novel α-aminophosphonic acids characterised by a cis-fused octahydroindole system. *European J. Org. Chem.* **2011,** 3074–3081 (2011).

281. Escher, R. & Bünning, P. Synthesis of N-(1-carboxy-5-aminopentyl)dipeptides as inhibitors of angiotensin converting enzyme. *Angew. Chemie Int. Ed. English* **25,** 277–278 (1986).

282. Liu, L., Ishida, N., Ashida, S. & Murakami, M. Synthesis of chiral N-heterocyclic carbene ligands with rigid backbones and application to the palladium-catalyzed enantioselective intramolecular α-arylation of amides. *Org. Lett.* **13,** 1666–1669 (2011).

283. Würtz, S., Lohre, C., Fröhlich, R., Bergander, K. & Glorius, F. IBiox[(-)-menthyl]: A sterically demanding chiral NHC ligand. *J. Am. Chem. Soc.* **131,** 8344–8345 (2009).

284. Katayev, D. *et al.* Synthesis of 3,3-disubstituted oxindoles by palladium-catalyzed asymmetric intramolecular α-arylation of amides: Reaction development and mechanistic studies. *Chem. - A Eur. J.* **19,** 11916–11927 (2013).

285. Trillo, R. B., Leven, M., Neudörfl, J. M. & Goldfuss, B. Electronegativity governs enantioselectivity: Alkyl-aryl cross-coupling with fenchol-based palladium-phosphorus halide catalysts. *Adv. Synth. Catal.* **354,** 1451–1465 (2012).

286. Awata, A. & Arai, T. Catalytic asymmetric cyclopropanation with diazooxindole. *Synlett* **24,** 29–32 (2012).

287. Schwarzer, D. D., Gritsch, P. J. & Gaich, T. Mimicking dimethylallyltryptophan synthase: Experimental evidence for a biosynthetic Cope rearrangement process. *Angew. Chemie Int. Ed.* **51,** 11514–11516 (2012).

288. Marti, C. & Carreira, E. M. Total synthesis of (−)-spirotryprostatin B: Synthesis and related Sstudies. *J. Am. Chem. Soc.* **127,** 11505–11515 (2005).

289. Cheng, L. & Huang, F. WO 2011069298: Spiro-cyclopropane-indolinone derivatives as AMPK modulators and their preparation, pharmaceutical compositions and use in the treatment of diseases. (2011).

290. Trost, B. M., Bringley, D. a, Zhang, T. & Cramer, N. Rapid access to spirocyclic oxindole alkaloids: application of the asymmetric palladium-catalyzed [3 + 2] trimethylenemethane cycloaddition. *J. Am. Chem. Soc.* **135,** 16720–35 (2013).

291. El Bouakher, A. *et al.* A general and efficient method to access tetracyclic spirooxindole derivatives. *European J. Org. Chem.* **2015,** 556–569 (2015).

292. Hsieh, J.-C., Cheng, A.-Y., Fu, J.-H. & Kang, T.-W. Copper-catalyzed domino coupling reaction: an efficient method to synthesize oxindoles. *Org. Biomol. Chem.* **10,** 6404 (2012).

293. Efremov, I., Evrard, E., Brodney, M. & Rogers, B. WO2008/012623: Benzimidazolyl compounds as potentiators of mGluR2 subtype of glutamate receptor and their preparation, pharmaceutical compositions and use in the treatment of diseases. (2008).

294. Yu, K. *et al.* WO2003/053344: Preparation of 2-(heterocyclylmethyl) benzimidazoles as respiratory syncytial virus antiviral agents. (2003).

295. Blade, H. *et al.* WO2010/103306: Benzimidazole derivatives as RSV protein inhibitors and their preparation, pharmaceutical compositions and use in the treatment of respiratory syncytial virus infections. (2010).

296. Dey, C. & Kündig, E. P. Aza-oxindole synthesis by oxidative coupling of Csp2–H and Csp3–H centers. *Chemical Communications* **48,** 3064 (2012).

297. Storey, J. M. D. & Ladwa, M. M. Homolytic aromatic substitution: A radical approach

towards the synthesis of 5-azaoxindoles. *Tetrahedron Lett.* **47,** 381–383 (2006).

298. Saito, T., Furukawa, N. & Otani, T. A facile synthesis of pyrrolo[2,3-b]quinolines via a Rh(I)-catalyzed carbodiimide-Pauson-Khand-type reaction. *Org. Biomol. Chem.* **8,** 1126–1132 (2010).

299. Andreassen, E. J. & Bakke, J. M. Preparation of 6-azaoxindole (6-azaindol-2(3H)-one) and substituted derivatives. *J. Heterocycl. Chem.* **43,** 49–54 (2006).

300. Ackermann, L., Vicente, R. & Hofmann, N. Air-stable secondary phosphine oxide as preligand for palladium-catalyzed intramolecular a-arylations with chloroarenes. *Org. Lett.* **11,** 4274–4276 (2009).

301. Dey, C., Katayev, D., Ylijoki, K. E. O. & Kündig, E. P. Aza-oxindole synthesis via base promoted Truce–Smiles rearrangement. *Chem. Commun.* **48,** 10957 (2012).

302. Levy, A. A., Rains, H. C. & Smiles, S. The rearrangement of hydroxy-sulphones. Part I. *J. Chem. Soc.* 3264–3269 (1931). doi:10.1039/JR9310003264

303. Truce, W. E., Kreider, E. M. & Brand, W. W. in *Organic Reactions* 99–215 (John Wiley & Sons, Inc., 2011). doi:10.1002/0471264180.or018.02

304. Kosowan, J. R., W'Giorgis, Z., Grewal, R. & Wood, T. E. Truce–Smiles rearrangement of substituted phenyl ethers. *Org. Biomol. Chem.* **13,** 6754–6765 (2015).

305. Henderson, A. R. P., Kosowan, J. R. & Wood, T. E. The Truce–Smiles rearrangement and related reactions: a review. *Can. J. Chem.* **95,** 483–504 (2017).

306. Sasaki, K., Rouf, A. S. S. & Hirota, T. Polycyclic N -heterocyclic compounds. 48 . syntheses of furo[2,3- h]-[1,6]naphthyridine and imidazo(or pyrimido)[2,1- f]-[1,6]naphthyridines with rearrangement. *J. Heterocycl. Chem.* **33,** 49–52 (1996).

307. Abraham, R. J., Warne, A. & Gri, L. Proton chemical shifts in NMR . Part 12 . 1 Steric , electric fi eld and conformational e ff ects in acyclic and cyclic ethers. *J. Chem. Soc. Perkin Trans. 2* 1751–1758 (1998).

308. Alorati, A. D., Gibb, A. D., Mullens, P. R. & Stewart, G. W. An efficient process for the large-scale synthesis of a 2,3,6-trisubstituted indole. *Org. Process Res. Dev.* **16,** 1947–1952 (2012).

309. Jończyk, A. & Kowalkowska, A. Base-mediated reaction of quaternary ammonium salts with nitroarenes - Their useful functionalization via vicarious nucleophilic substitution (VNS). *Synthesis* **2002,** 674–680 (2002).

310. Andreassen, E. J., Bakke, J. M., Sletvold, I. & Svensen, H. Nucleophilic alkylations of 3-nitropyridines. *Org. Biomol. Chem.* **2,** 2671–2676 (2004).

311. Woolford, A. J.-A. *et al.* WO2012/143726: Preparation of bicyclic heterocycles as anticancer agents. (2012).

312. Santos, M. M. M. Recent advances in the synthesis of biologically active spirooxindoles. *Tetrahedron* **70,** 9735–9757 (2014).

313. *ReViral confidential information. Undisclosed assay conditions*.

314. Y, Y. & Y, K. A line of cells derived from African green monkey kidney. *Nippon Rinsho* **21,** 1209–1210 (1963).

315. Cyprotex in vitro ADMET assays. Available at: http://www.cyprotex.com/admepk.

316. Pharmidex in vitro ADMET assays. Available at: http://www.cyprotex.com/admepk.

317. Obach, R. S. Prediction of human clearance of twenty-nine drugs from hepatic microsomal intrinsic clearance data: An examination of in vitro half-life approach and nonspecific binding to microsomes. *Drug Metab. Dispos.* **27,** 1350–1359 (1999).

318. Sohlenius-Sternbeck, A.-K. *et al.* Intrinsic clearance from hepatocytes. *Xenobiotica* **42,** 841–853 (2012).

319. Zhang, D., Luo, G., Ding, X. & Lu, C. Preclinical experimental models of drug metabolism and disposition in drug discovery and development. *Acta Pharm. Sin. B* **2,** 549–561 (2012).

320. Rydzewski, R. *Real world drug discovery - A chemist's guide to biotech and pharmaceutical research*. (Elsevier).

321. Houston, J. B. Utility of in vitro drug metabolism data in predicting in vivo metabolic clearance. *Biochem. Pharmacol.* **47,** 1469–79 (1994).

322. Veber, D. F. *et al.* Molecular properties that influence the oral bioavailability of drug candidates. *J. Med. Chem.* **45,** 2615–2623 (2002).

323. Leeson, P. Drug discovery: Chemical beauty contest. *Nature* **481,** 455–456 (2012).

324. Ellens, H. *et al.* In vitro permeability screening for identification of orally bioavailable endothelin receptor antagonists. *Adv. Drug Deliv. Rev.* **23,** 99–109 (1997).

325. Manallack, D. T., Prankerd, R. J., Yuriev, E., Oprea, T. I. & Chalmers, D. K. The significance of acid/base properties in drug discovery. *Chem. Soc. Rev.* **42,** 485–496 (2013).

326. Giacomini, K. M. *et al.* Membrane transporters in drug development. *Nat. Rev. Drug Discov.* **9,** 215–236 (2010).

327. Hitchcock, S. A. Structural modifications that alter the P-glycoprotein efflux properties of compounds. *J. Med. Chem.* **55,** 4877–4895 (2012).

328. Seelig, A. A general pattern for substrate recognition by P-glycoprotein. *Eur. J. Biochem.* **251,** 252–261 (1998).

329. Stouch, T. R. & Gudmundsson, O. Progress in understanding the structure–activity relationships of P-glycoprotein. *Adv. Drug Deliv. Rev.* **54,** 315–328 (2002).

330. Cianchetta, G. *et al.* A pharmacophore hypothesis for P-glycoprotein substrate recognition using GRIND-based 3D-QSAR. *J. Med. Chem.* **48,** 2927–2935 (2005).

331. Didziapetris, R., Japertas, P., Avdeef, A. & Petrauskas, A. Classification analysis of P-glycoprotein substrate specificity. *J. Drug Target.* **11,** 391–406 (2003).

332. Blagg, J. *et al.* Discovery of potent, selective, and orally bioavailable small-molecule modulators of the mediator complex-associated kinases CDK8 and CDK19. *J. Med. Chem.* **59,** 1078–1101 (2016).

333. Di, L., Rong, H. & Feng, B. Demystifying brain penetration in central nervous system drug discovery. *J. Med. Chem.* **56,** 2–12 (2013).

334. Lu, K. *et al.* Strategies to lower the Pgp efflux liability in a series of potent indole azetidine MCHR1 antagonists. *Bioorganic Med. Chem. Lett.* **21,** 5310–5314 (2011).

335. Peters, S. A. *Physiologically-Based Pharmacokinetic (PBPK) Modeling and Simulations*. (John Wiley & Sons, Inc., 2012). doi:10.1002/9781118140291

336. Smith, D. a., Beaumont, K., Maurer, T. S. & Di, L. Volume of distribution in drug design. *J. Med. Chem.* **58,** 5691–5698 (2015).

337. Schinkel, A. H. *et al.* Disruption of the mouse mdr1a P-glycoprotein gene leads to a deficiency in the blood-brain barrier and to increased sensitivity to drugs. *Cell* **77,** 491–502 (1994).

338. Letrent, S. P., Pollack, G. M., Brouwer, K. R. & Brouwer, K. L. R. Effect of GF120918, a potent P-glycoprotein inhibitor, on morphine pharmacokinetics and pharmacodynamics in the rat. *Pharm. Res.* **15,** 599–605 (1998).

339. Polli, J. W. *et al.* Role of P-glycoprotein on the CNS disposition of amprenavir (141W94), an HIV protease inhibitor. *Pharm. Res.* **16,** 1206–12 (1999).

340. Pryde, D. C. *et al.* Aldehyde oxidase: An enzyme of emerging importance in drug discovery. *J. Med. Chem.* **53,** 8441–8460 (2010).

341. Vine, K. L., Locke, J. M., Ranson, M., Pyne, S. G. & Bremner, J. B. An investigation into the cytotoxicity and mode of action of some novel N -alkyl-substituted isatins. *J. Med. Chem.* **50,** 5109–5117 (2007).

342. Jensen, T. & Madsen, R. Ruthenium-catalyzed alkylation of oxindole with alcohols. *J. Org. Chem.* **74,** 3990–3992 (2009).

343. Wang, Y. *et al.* Ru(III)-mediated intramolecular ortho-C(sp2)–H activation/oxidative acylation: one-pot synthesis of isatins from α-hydroxy amides. *Tetrahedron* **72,** 3193–3197 (2016).

344. Zheng, Y. *et al.* Ferric(III) chloride catalyzed intramolecular cyclization of N-alkyl-2-oxo-acetanilides: a facile access to isatins. *Tetrahedron Lett.* **57,** 39–42 (2016).

345. Poondra, R. R. & Turner, N. J. Microwave-assisted sequential amide bond formation and intramolecular amidation: A rapid entry to functionalized oxindoles. *Org. Lett.* **7,** 863–866 (2005).

346. Lee, Y. R., Suk, J. Y. & Kim, B. S. Efficient synthesis of oxindoles by thermal and rhodium(II)-catalyzed Wolff rearrangement. *Tetrahedron Lett.* **40,** 8219–8221 (1999).

347. Ganguly, A. K., Wang, C. H., David, M., Bartner, P. & Chan, T. M. Synthesis of heterocyclic compounds using radical reactions. *Tetrahedron Lett.* **43,** 6865–6868 (2002).

348. Bignan, G. C. *et al.* Preparation of 3-spirocyclic indolin-2-ones as ligands for the ORL-1 receptor. *Bioorg. Med. Chem. Lett.* **15,** 5022–5026 (2005).

349. Tantry, S. J. *et al.* Whole cell screen based identification of spiropiperidines with potent antitubercular properties. *Bioorg. Med. Chem. Lett.* **25,** 3234–3245 (2015).

350. Hoffman, J., Wai, J. & Perlow, D. WO99/65494: Oxadiaza- and triazaspiro[4.5] decylmethylimidazoles and analogs as inhibitors of prenyl-protein transferase. (1999).

351. Mautino, M., Waldo, J. & Jaipuri, F. WO2009/073620: Preparation and disclosure of indoleamine 2,3-dioxygenase (IDO) inhibitors. (2009).

352. Tegley, C., Miller, L., Fensome, A. & Bender, R. WO2000/066167: Preparation of oxospiro[cycloalkane-1,3'-indoline] derivatives and analogs as progesterone receptor antagonists. (2000).

353. Fensome, A., Bender, R. & Miller, L. WO2000/066556: Preparation of indolinones as progesterone antagonists. (2000).

354. Badland, M. *et al.* Preparation of azaindolines and benzoyl substituted azaindolines: precursors of triazabenzo[cd]azulen-9-one PDE4 inhibitors. *Tetrahedron Lett.* **52,** 5292–5296 (2011).

355. Veal, J., Lakey, K. & Harris, P. WO2000/055159: Preparation of anilinomethylene aza-oxindoles and analogs as protein tyrosine kinase and protein serine/threonine kinase inhibitors. (2000).

Appendix

RSV fusion and cell toxicity assays

The primary biological RSV fusion and cell toxicity assays were carried out within the Sussex Drug Discovery Centre at the University of Sussex and the protocol for the assay is summarised below.

Cell culture

HEK 293T/17 cells were cultured in T75 culture flasks in Dulbecco's Modified Eagle Medium containing 10 % FBS (Foetal bovine serum, South American origin) and Penicillin-Streptomycin. The cells were passaged by washing briefly with 3 mL of PBS, followed by a 4 minutes incubation with TrypLE at 37 °C in a humidified 5% CO_2 atmosphere. Media (7 mL) was then added to the flask and the cells were dispersed *via* pipetting. Two further T75 flasks were each seeded with 2×10^6 cells in 15 mL of fresh media.

DAY 1

The cells were counted and diluted to 3×10^5 cells/mL in fresh media. Two T75 flasks were each seeded with 15.58 mL diluted cells.

DAY 2

The plasmid DNA to be transfected into the HEK cells was first prepared in serum free media (Dulbecco's Modified Eagle Medium containing Penicillin-Streptomycin) containing the transfection reagent FuGENE® 6. The transfections were set up as follows:

- Luc = pFR_Luc
- Gal4 = pcDNA3.1+_Gal4/NFκB
- A2_F = pcDNA3.1+_A2_F

Appendix Table 1.

Transfections:	
Cell population 1	Luc + A2_F_1
Cell population 2	Gal4

Appendix Table 2. Transfection constituents

Reagent	Cell Population 1	Cell population 2
Serum free media	779 µL	779 µL
FuGENE® 6	23.37 µL	23.37 µL
Luc (1 µg/mL)	7.79 µL	-
Gal4 (1 µg/mL)	-	7.79 µL
A2_F_1 (1 µg/mL)	7.79 µL	-

The transfection reagents were then added to the appropriate T75 flask and incubated overnight at 37 °C in a humidified 5% CO_2 atmosphere.

DAY 3

Compound preparation:

The compounds were diluted in a polypropylene round-bottomed 96 well plate in a twelve-point dilution curve to give top final concentration of 3.3 µM. 10 mM stocks of each of the compounds were made up with 100 % DMSO.

In an Eppendorf, 20 µL of a 10 mM stock was mixed with 80 µL of DMSO to give a 2 mM solution. 100 µL of DMSO was placed in each well of a row on a 96 well plate. 50 µL of a 2 mM solution was placed in column 1 and mixed. 50 µL of this solution was then placed in column 2 and mixed. This process of transferring and mixing was repeated for columns 2 – 12

For each compound 250 µL of media was placed in the appropriate numbers of rows of a 96 well plate. 2.5 µL of the dilution curves were then transferred into the media, giving 100-fold dilution of the compounds.

Cell preparation:

The transfected cells were dissociated as follows:

- The media was aspirated followed by a gentle wash with 5 mL of PBS
- The PBS was aspirated and 3 mL of TrypLE was added to each flask
- The plate was incubated at 37 °C for 4 minutes
- 7 mL of fresh media was added to each flask and the cells were re-suspended

The cells were counted and diluted to 4×10^5 cells/mL in fresh media. 50 µL of transfection 'cell population 1' was added to all the wells of the assay plates. 100 µL of diluted compound (2 rows per compound) and the controls (100 nM, 100 % inhibition, four wells and DMSO, 0 % inhibition, eight wells) were added to the appropriate wells as indicated in Appendix figure 1. 50 µL of the diluted (4×10^5 cells/mL) 'cell population 2' was subsequently added to all the wells. The plates were then incubated for 24 hr at 37 °C in a humidified 5% CO_2 atmosphere.
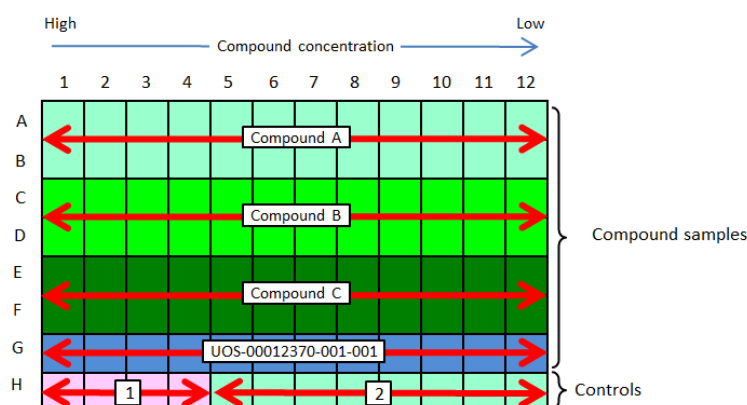
Appendix Figure 1. Plate layout

Day 4

In vitro cell based assay - RSV Fusion antiviral activity:

The luciferase plates were prepared for measurement as follows:

- The media was discarded into Virkon and the plates were washed with 100 µL PBS per well
- 20µL/well of lysis buffer (25 mM tris-phosphate, 8 mM $MgCl_2$, 1 mM DTT, 1% triton X-11, 15% glycerol) was added to each well and incubated, shaking for 5 min at room temperature.

- Luciferin (100 µL) was added to a luciferase assay activity buffer composed of 20mM tricine, 10 mM $MgSO_4$, 1mM EDTA and 10 mM DTT at a dilution of 1:49 to give a working luciferin buffer. The luciferin buffer was added to each well
- The luminescence was measured for the conversion of luciferin to oxyluciferin.

Cell viability - Resazurin Plates

- The media was discarded into Virkon and the plates were treated with 100 µL/well of SF media and 20 µL/well of Cell Titre Blue® solution
- The pates were incubated at 37 °C in a humidified 5% CO_2 atmosphere for 2 hours
- The fluorescence was measured at 590 nm

Results:

The data handling and analysis were performed using the Dotmatics database. The corresponding values of background levels for fluorescence (cell viability) and luminescence (Fusion antiviral activity) were subtracted. All the replicate wells were averaged and the percentage of control was calculated using the untreated cell-cell fusion wells as 100% reference. A standard four parameters non-linear regression analysis of the data obtained from each compound was then used to calculate the IC_{50}.

RSV plaque reduction assay

The RSV plaque reduction assay screening was conducted at the University of Queensland, Australia, within the laboratory of Professor Paul Young.

Vero cells were seeded in 96-well plates in a volume of 100 µL of Optimem supplemented with 3% FBS at a concentration of 4 x 104 cells per well. After an overnight incubation at 37 °C in a humidified 5% CO_2, the monolayer of cells should be 90% confluent. The compounds were titrated in pre-warmed Serum Free (SF) Optimem in a U-bottom 96 well plate. The compounds in a 10 mM stock solution, titration in 100% DMSO was performed first and each concentration added individually to a 2-fold concentration at 4% DMSO in SF media before mixing with the virus (2% final DMSO with virus). The media was then removed from the cells and replaced with

PBS (100 μL/well). RSV stock was thawed and diluted in SF Optimem media to 4000 PFU/mL. An equal volume of virus was added to the compounds on the titration plate. PBS was removed from the cells that where subsequently inoculated with the virus and compound solution (50 μL/well). The cells were incubated for 2 hours at 37 °C in a humidified 5% CO_2 to allow infection. The inoculum was removed and media (Optimem and 1% FBS) was added to the cells (100 μL/well). The cells were subsequently incubated for 48 hours at 37 °C in a humidified 5% CO_2.

Immunostaining procedure:

The media was removed from the cells and the monolayer was washed with PBS. The cells were fixed with ice and cold 80% acetone in PBS (100 μL/well) for 20 minutes at -20 °C. The fixative was removed and the cells were dried for 30 minutes with the plates inverted. A blocking solution (5% skim milk powder in PBS) was added to the cells (150 μL/well) and the plates were incubated for 30 minutes at room temperature. The blocking solution was removed and the plates were washed once with PBS. Primary antibody in blocking solution was added to the plates (50 μL/well) and incubated for 1 hour at 37 °C. The plates were then washed 3 times with PBS. A secondary antibody in blocking the solution was added to the plates (50 μL/well). And incubated for 1 hour at 37 °C in the dark. The plates were washed as above and dried for 10 minutes. The plates were scanned on the Odyssey Imager (Li-Cor Biosciences) at a resolution of 42 μM, medium quality and level 5 intensity in the 800 nM channel.

Data analysis:

The images obtained were saved and plaque counted with the aid of a computer imaging software. The IC50 values for the compounds were derived from dose response curves obtained using the Graphpad Prism software.
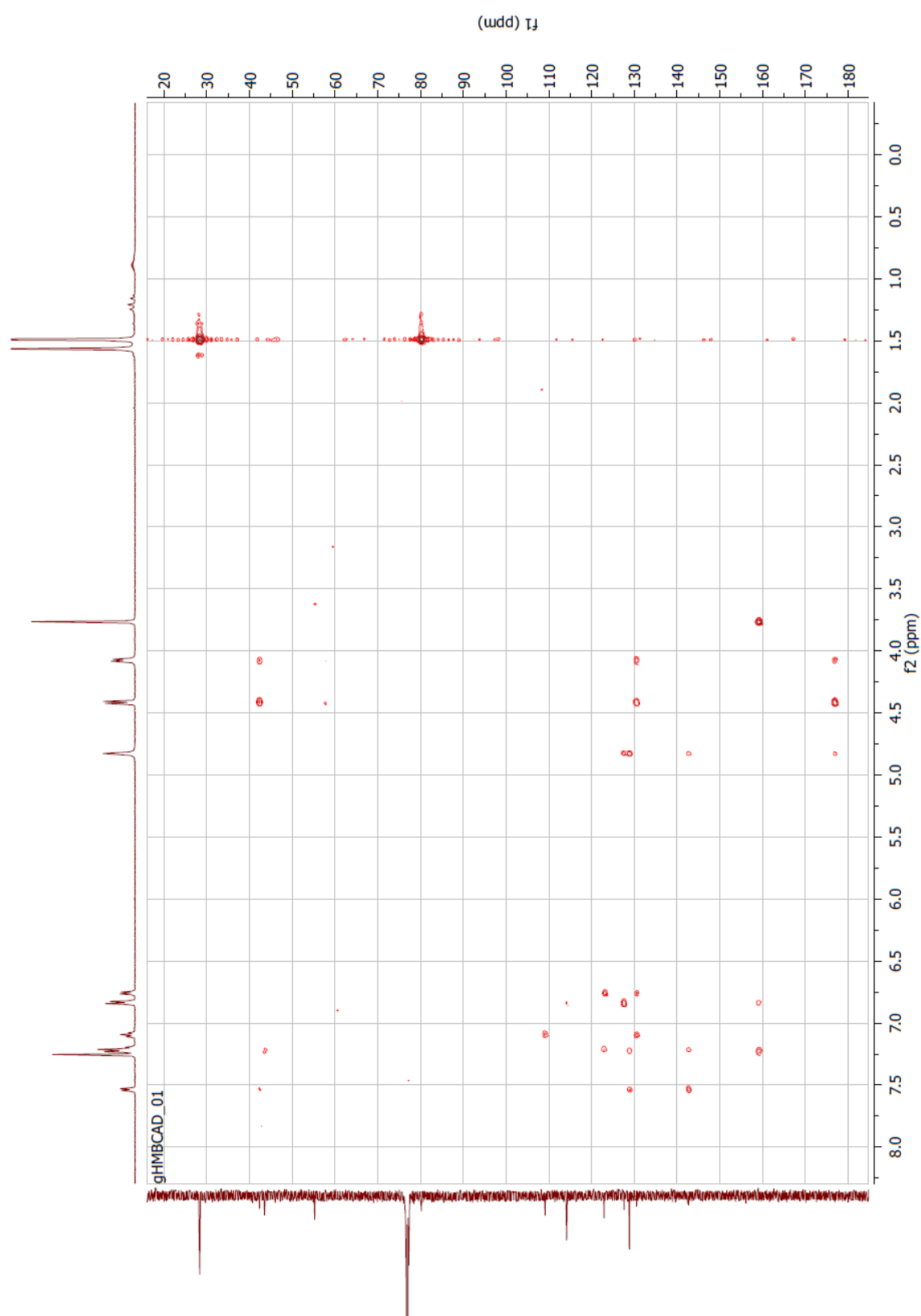
NMR Spectra

^{1}H NMR and 2D NMR (gHMBCAD and NOESY) spectra described in Chapter 3 have been summarised below for compounds **35, 36, 43e**, **44a** and **68**.
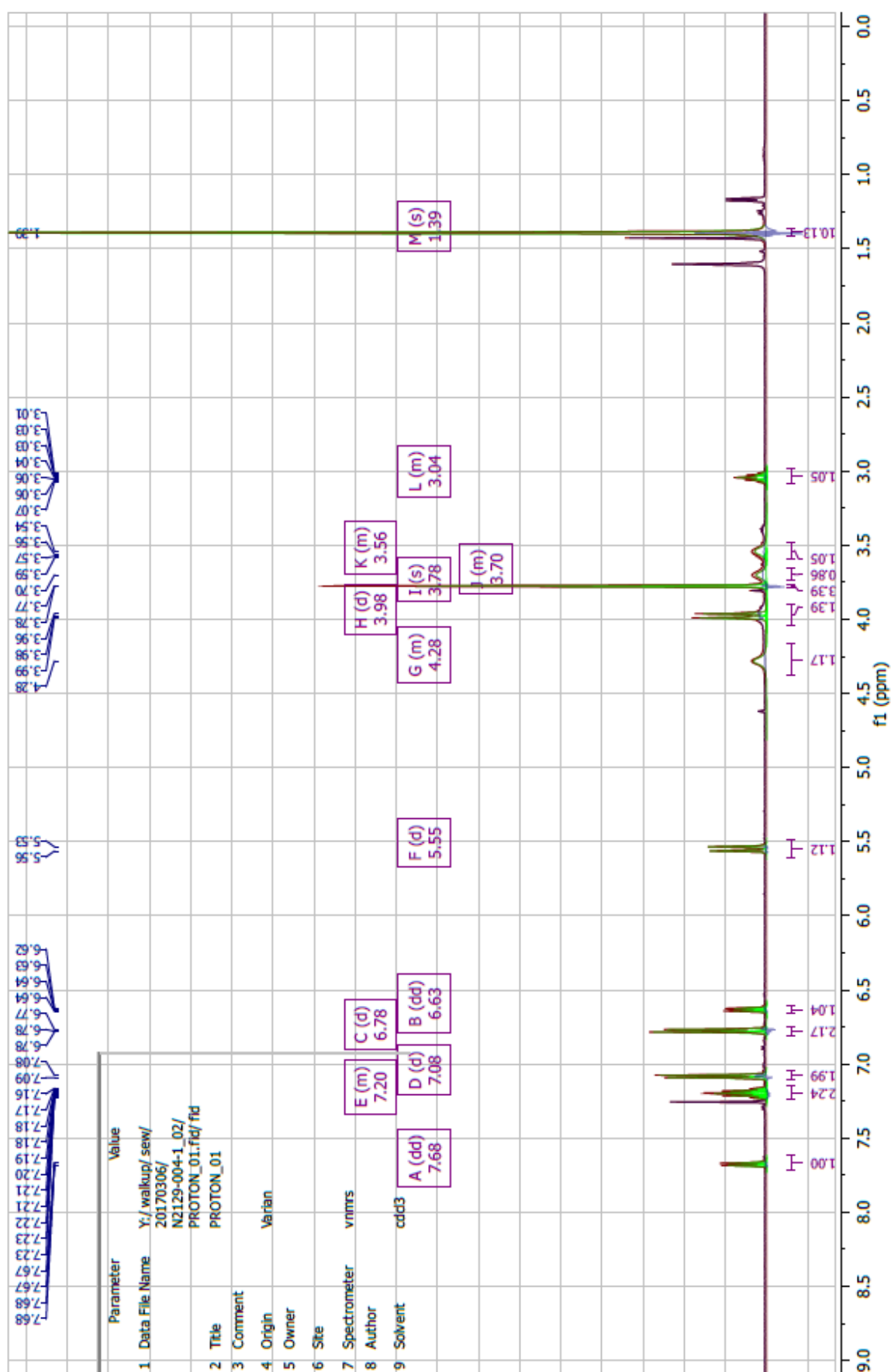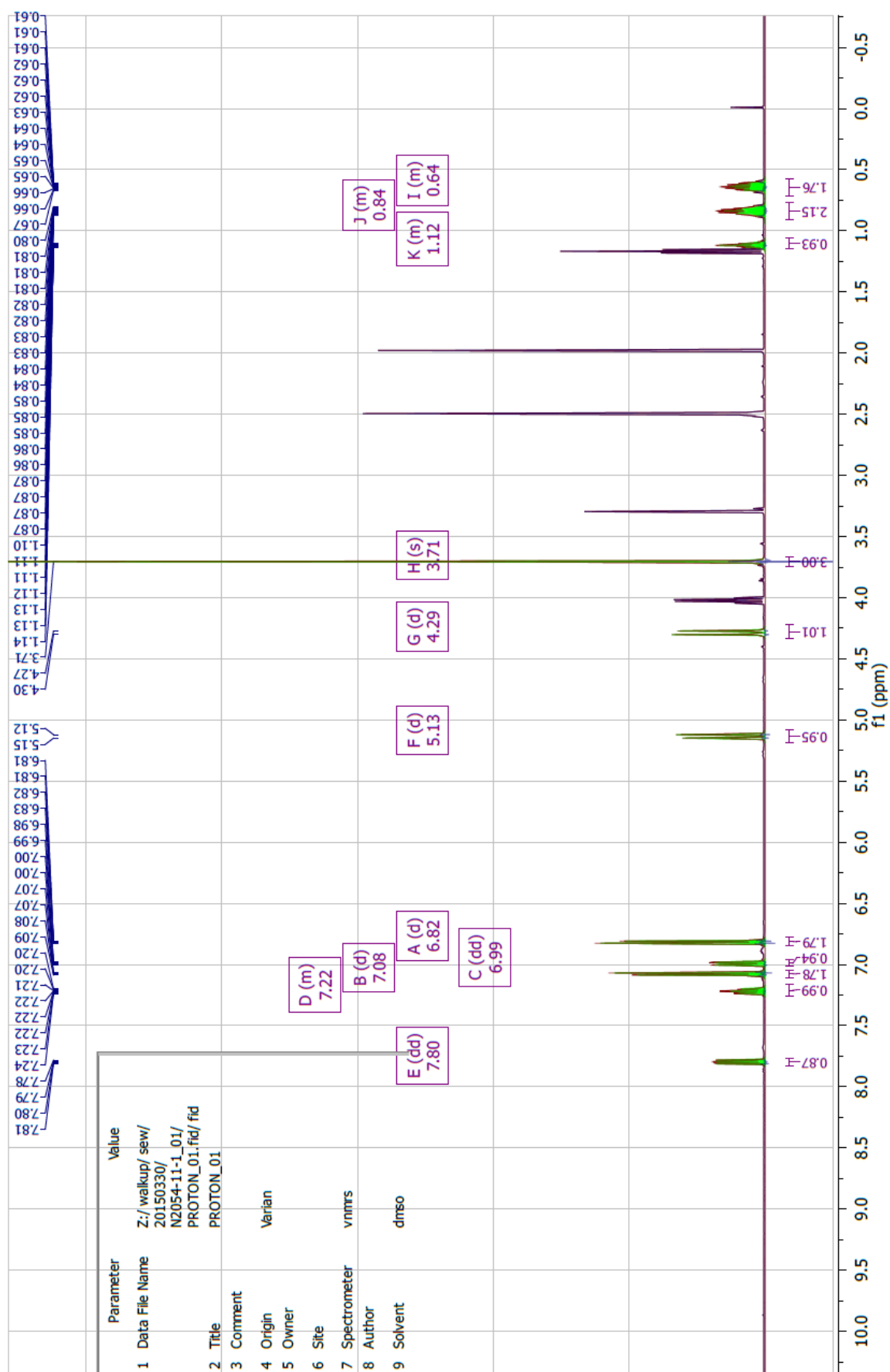
Appendix Figure 2. ^{1}H NMR spectrum of compound **35** in CDCl$_3$.
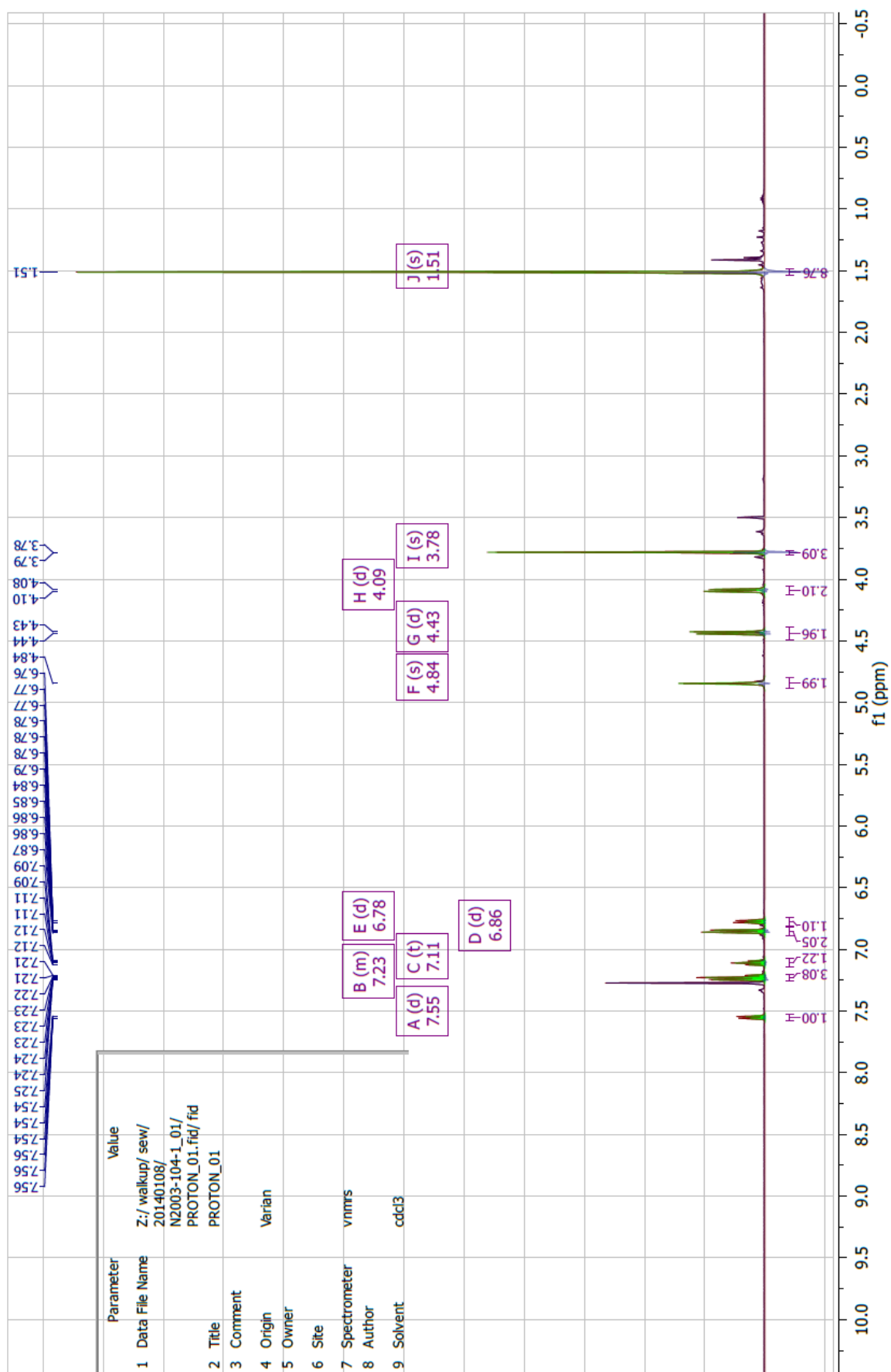
Appendix Figure 3. ¹H NMR spectrum of compound **36** in CDCl₃.
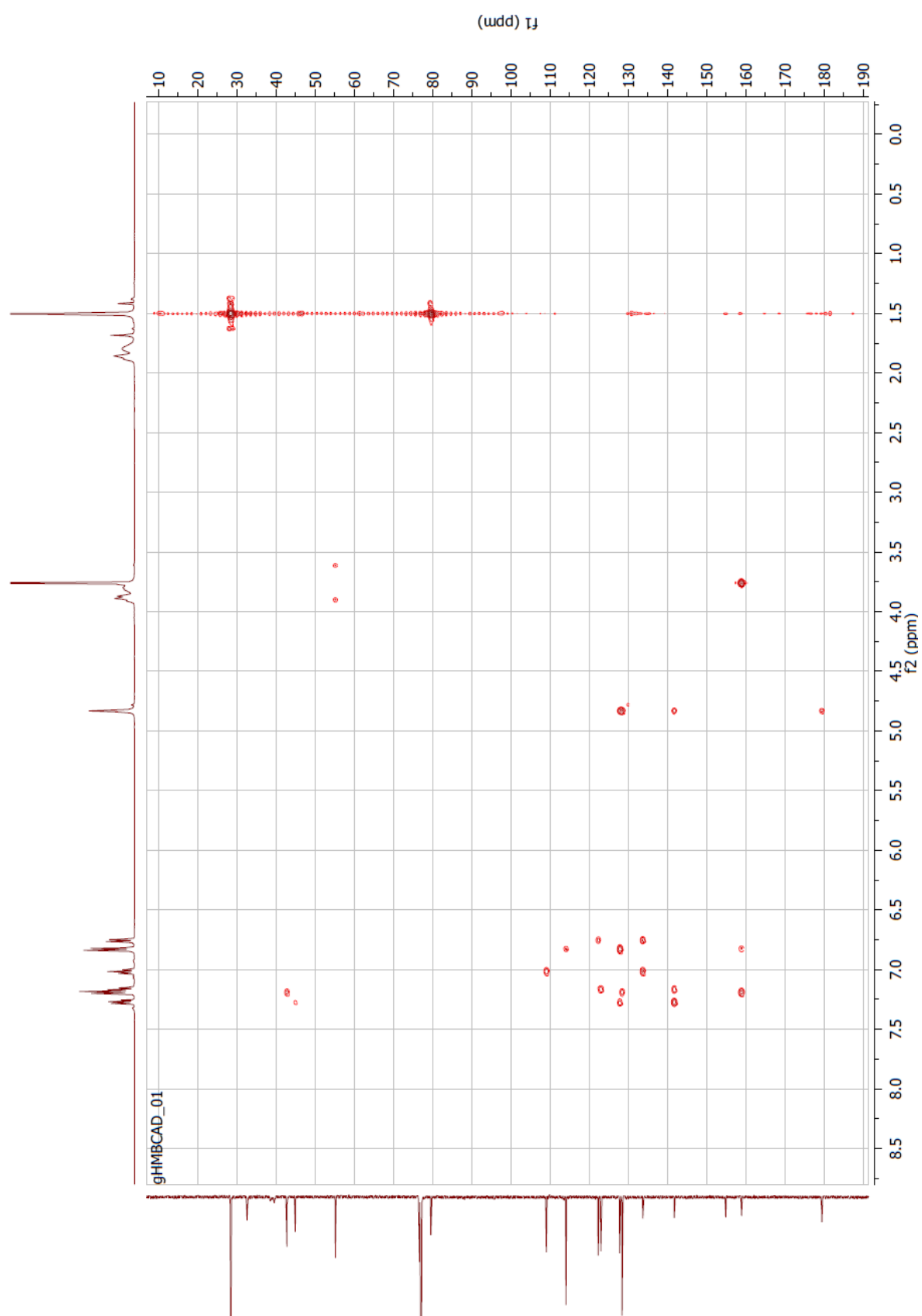
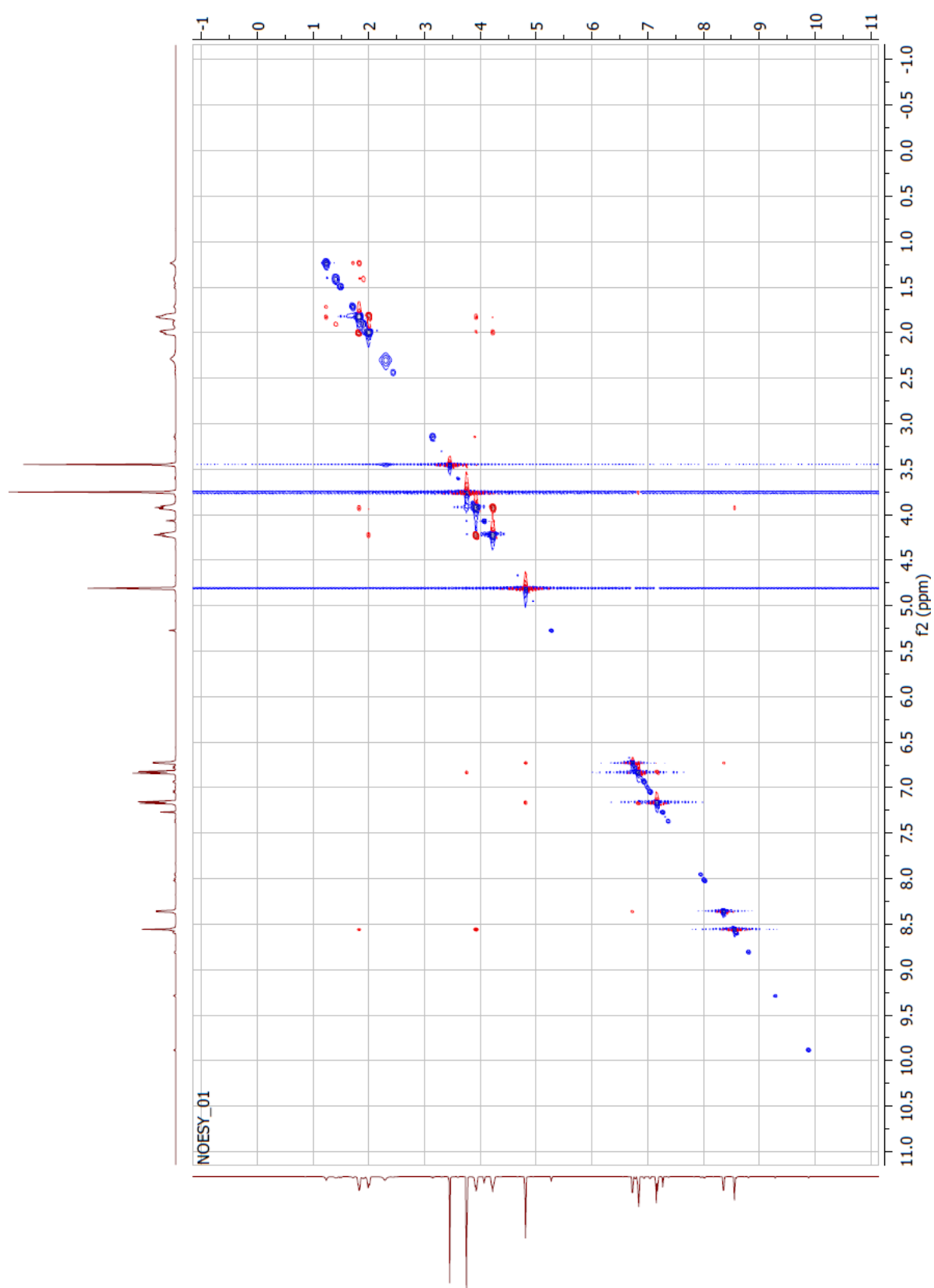**Appendix Figure 4**. Heteronuclear multiple-bond correlation spectroscopy of compound **36** in CDCl₃.

Appendix Figure 5. ^{1}H NMR spectrum of compound **43e** in DMSO-d_6.

Appendix Figure 6. ¹H NMR spectrum of compound **44a** in CDCl₃.

Appendix Figure 7. Heteronuclear multiple-bond correlation spectroscopy of compound **44a** in CDCl₃.

Appendix Figure 8. NOESY of compound **68** in CDCl₃.